ISSN 2458-973X

JSCMT

Journal of Sustainable Construction Materials and Technologies

Volume 9
Number 1
Year 2024

YTÜ PRESS

www.jscmt.yildiz.edu.tr

ISSN 2458-973X

JSCMT

Journal of Sustainable Construction Materials and Technologies

Volume 9 Number 1 Year 2024

ISSN 2458-973X

JSCMT

Journal of
Sustainable Construction
Materials and Technologies

Volume 9 Number 1 Year 2024

CONTENTS

Journal of Sustainable Construction Materials and Technologies
Web page info: https://jscmt.yildiz.edu.tr
DOI: 10.47481/jscmt.1404010

JSCMT
Journal of Sustainable Construction Materials and Technologies

Research Article

Preparation of calcite-precipitating bacteria-embedded magnesium phosphate cement for self-healing application

Deeksha PATIL[1], Alankar SAPKAL[1], Shreyas PRANAV[2], Mukund LAHOTI[2], Ashish GADEKAR[1], Anupama PABLE[1], Umesh U. JADHAV[*1]

[1]*Department of Microbiology, Savitribai Phule Pune University, Pune, Maharashtra, India*
[2]*Department of Civil Engineering, Birla Institute of Technology and Science, Pilani, India*

ARTICLE INFO

Article history
Received: 12 December 2023
Revised: 22 January 2024
Accepted: 01 February 2024

Key words:
Bacteria, calcite precipitation, magnesium phosphate cement, self-healing

ABSTRACT

The present study was undertaken to check the feasibility of magnesium phosphate cement (MPC) for the immobilization of calcite-precipitating bacteria. An aqueous route of MPC synthesis was followed using magnesium phosphate $Mg_3(PO_4)_2$ powder and ammonium phosphate solution. The Fourier-transform infrared spectroscopy (FTIR) and scanning electron microscopy (SEM) analysis confirmed the synthesis of MPC. The thermal decomposition analysis (TGA) showed decomposition of struvite between 50–60 °C - Paenibacillus sp. NCIM 5410 was used due to its urea hydrolysis ability. pH 9 was found to be optimum for urea hydrolysis. The urea hydrolysis steadily decreased with an increase in temperature from 30 °C to 60 °C. The hydrolysis was seen to increase with an incubation time of up to 72 h and subsequently reduced. The bacteria showed 90% urea hydrolysis at pH 9, 30 °C temperature, and after 72 h. The bacterial spores were incorporated during MPC synthesis, which helped their immobilization. The bacterial spore-containing MPC decomposed around 70 (±0.48)% of urea. Further, calcite precipitation was studied. The precipitate formed due to bacterial action in the MPC crack showed the presence of calcium. The calcite precipitation helped to reduce the water absorption by MPC specimens. The spore containing MPC specimens showed around 2.62 (±0.55) % water absorption. These results suggest that it is possible to synthesize bioactive MPC by immobilizing bacterial spores in MPC.

Cite this article as: Patil, D., Sapkal, A., Pranav, S., Lahoti, M., Gadekar, A., Pable, A., & Jadhav, U. U. (2024). Preparation of calcite-precipitating bacteria-embedded magnesium phosphate cement for self-healing application. *J Sustain Const Mater Technol*, 9(1), 1–10.

1. INTRODUCTION

Following the technological revolution and the increase in human population, the construction industry is growing rapidly [1]. Concrete is an inherent part of the construction industry, and it is the Earth's second most widely used material, after water. Besides all its advantages, a concrete structure is prone to deterioration. With time, small cracks appear in concrete structures. The water enters through these cracks, leading to durability issues such as corrosion, which may damage the structure [2]. Therefore, there is an increasing demand for rapid and durable repair material [3]. Magnesium phosphate cement (MPC) has recently emerged as a fast repair material for concrete structures [4]. It differs from ordinary Portland Cement (OPC) but bonds well to the old concrete substrate [5]. It is chemically bonded ceramic. It is a new binder material formed through acid-base reactions between magnesia and the alkali metal or ammonium phosphates [6]. It is a clinker-free binder with a quick-setting, high early compressive strength, good volume stability, strong bonding strength, minor shrinkage, and good abrasion resistance [7, 8].

***Corresponding author.**
*E-mail address: umeshjadhav02@gmail.com

With the rapid economic development, the need for basic infrastructure is increasing. This resulted in the construction of new roads. Currently, the roads are built mainly using cement concrete. The traditional maintenance method for roads involves the removal of the damaged part and then rebuilding it. In the case of cement-concrete roads, this method is not only expensive but also time-consuming. Hence, it requires quick repair options. MPC is known for its rapid setting and hardening characteristics. This makes it suitable for quick repairs, allowing faster turnaround times in concrete structure maintenance [9, 10]. It is an effective bonding agent for attaching new concrete to existing surfaces. The cement adheres well to various substrates, promoting a strong bond [11, 12]. Repairing concrete structures is paramount in natural disasters, accidents, and unforeseen situations. There might be situations where the structure needs to be repaired in a submerged or wet environment. The quick-setting nature of MPC makes it suitable for underwater repairs [7]. The corrosion resistance ability of MPC makes it the right choice for repairing structures in aggressive environments, such as those exposed to chemicals or marine conditions. MPC develops high early strength, allowing repaired structures to be returned to service sooner. This can be crucial in minimizing downtime for bridges, highways, and buildings [13, 14]. In cases where the structure's integrity has been compromised, MPC can be used as part of a comprehensive rehabilitation strategy, ensuring that the repaired sections meet the necessary structural requirements [15, 16]. To extend the applicability of MPC in concrete structure repairs, calcite-precipitating microorganisms can be embedded in the MPC matrix to achieve the self-healing phenomenon in the structures. Previously, geopolymers were used to immobilize calcite precipitation bacteria [17]. Producing geopolymer involves combining an alkaline solution that can trigger the geo-polymerization process with an aluminosilicate source, such as coal fly ash or other waste by-products [18]. The geopolymer material utilizes less carbon and is an energy-intensive process. Doctolero et al. [18] produced bio-geopolymers using alkali activation of coal fly ash mixed with self-healing agents using biochar-immobilized B. sphaericus and B. thuringiensis [18]. Ekinci and his colleagues [19] studied the microbial self-healing capacity of geopolymer binders. The Na_2SiO_3 activated GP samples were made from ground blast furnace slag (GBFS). Bacillus subtilis was used as the healing agent to produce GP samples. This resulted in geopolymer composites having self-healing mechanisms with good mechanical qualities and durability. Similarly, Soltmann et al. [20] showed that it is possible to immobilize Saccharomyces cerevisiae and Rhodococcus ruber in MPC. They produced MPC at low temperatures by mixing magnesium phosphate ($Mg_3(PO_4)_2$) powder and ammonium phosphate solution. They found the produced MPC had developed strength rapidly with low shrinkage and very good mechanical and chemical durability. The immobilization of microorganisms in the MPC matrix is promising since it follows an aqueous preparation route. Considering these benefits, the present study was undertaken to immobilize the calcite-precipitating bacteria in MPC. Such bioactive material can be used as cement plaster in sewers. The compatibility of MPC with concrete will open new paradigms for self-healing applications in concrete.

2. MATERIALS AND METHODS

2.1. The Microbial Culture and Chemicals

Paenibacillus sp. NCIM 5410 was procured from the National Collection of Industrial Microorganisms (NCIM), National Chemical Laboratory (NCL), Pune, India. Magnesium phosphate powder [$Mg_3(PO_4)_2$], urea, diammonium hydrogen phosphate [$(NH_4)_2HPO_4$], ammonium dihydrogen phosphate [$NH_4H_2PO_4$], potassium phosphate dibasic [K_2HPO_4], potassium phosphate monobasic [KH_2PO_4], Nessler's reagent was purchased from Sigma Aldrich. Luria Bertani (LB) was used as a growth medium. The composition of the precipitation medium was – 3 g/L Nutrient broth, 20 g/L urea, 1 g/L ammonium chloride [NH_4Cl], and 5.6 g/L calcium chloride [$CaCl_2$].

2.2. Bacterial Spore Formation

Cells of Paenibacillus sp. were grown in LB media containing $MnSO_4.H_2O$. The media was placed in a water bath at 80 °C for 10 minutes, followed by ice water treatment for 5 minutes. Media was centrifuged at 8000 rpm for 15 minutes, then the pellet was taken, and the supernatant was discarded. Saline wash was given to the pellet, and cells were stored at 4 °C. Endospore staining was performed for confirmation of spores. A clean glass slide was taken. The bacterial sample was spread on the slide and heat-fixed. The slide was flooded with a primary stain of malachite green solution and heated to steaming three or four times. The slide was allowed to cool, and the smear was rinsed with water to remove excess stains. The bacterial cells were counterstained with 0.5% safranin, contrasting the endospores. The glass slide was washed, dried, blotted, and observed under a light microscope. Lyophilization was carried out to obtain the spore powder.

2.3. Microbial Urea Hydrolysis

0.5 g spores of Paenibacillus sp. NCIM 5410 was inoculated in 50 ml LB media and incubated at 30 °C for 24 h. 200 µl grown culture was spread on a Luria Bertani agar plate and incubated at 30 °C for 24 h. Isolated colonies were picked and inoculated in a flask with 50 ml LB media and incubated at 30 °C for 24 h. The grown culture is taken and centrifuged at 8000 rpm for 15 minutes. Then, OD was adjusted to 1, and a 500 µl culture was inoculated in urea containing LB media (50 ml). It is incubated at 30 °C for 24 h. After 24 hours, the media is centrifuged at 8000 rpm for 15 minutes. The supernatant (free of bacterial cells) was collected by centrifugation. The urea hydrolysis was determined by NASH assay. NASH reagent method gives an idea about bacterial hydrolysis of urea to ammonia and carbon dioxide. Nessler's reagent and ammonia combine to form a yellow complex, and the complex's absorbance is directly proportional to the ammonia concentration. Consequently, it can be used to calculate urea hydrolysis. First, 0.1 ml supernatant was added to 1.9 ml buffer for the NASH assay. 0.5 ml 500 mM H_2SO_4

was added. Then 0.5 ml of Nessler's reagent was added and incubated at dark conditions for 30 minutes, and absorbance was recorded on a spectrophotometer at 480 nm. Readings were acquired, and ammonium content was determined by comparing them to a standard graph. For a standard graph, known concentrations of ammonium chloride are used [21].

2.4. Optimization of Bacterial Urea Hydrolysis

Various parameters were used to study bacterial urea hydrolysis. The parameters studied were pH (7–11), temperature (30–60 °C), and time duration (24–96 h).

2.5. MPC Synthesis

The MPC was synthesized as described by Soltmann [20] with slight modifications. Various combinations of ammonium phosphate solution (10–14 ml) are mixed with 5 g magnesium phosphate powder in a beaker. The content is mixed vigorously and poured into an ice-making tray with trapezoidal shape wells. The ice-making tray is used as a mold to form the specimen. The tray is kept at 37 °C for 24 h. After 24 h, specimens were removed from the tray. The specimens, 1.8 cm x 1.5 cm x 1.3 cm in size, were formed. They were kept in a hot oven at 60 °C for 36 h. Specimens are taken out from the oven for further analysis. The spore containing MPC was synthesized by taking a mixture of 0.5 g Paenibacillus sp. NCIM 5410 spores and 4.5 g magnesium phosphate powder. An ammonium phosphate solution was added to this mixture.

2.6. Analysis of Spore Leakage from MPC

The analysis of spore leakage was carried out as described by Jadhav et al. [17]. MPC specimens with and without spores were crushed. Both samples' powder (~ 0.15 g) was added into 20 ml sterile saline in two falcon tubes. The content of the falcon was vortexed for 2 minutes and then kept static for 15 minutes at room temperature. From this solution, ten-fold serial dilutions (a total of five dilutions) were prepared. After that, 100 µl suspension was taken from an appropriate dilution and was spread onto a urea-containing agar plate homogeneously. All agar plates were incubated upside down at static conditions at 30 °C for 48 h and monitored for the appearance of colonies.

2.7. Viability of Immobilized Spores Using Urea Hydrolysis

The viability of bacterial spores was determined by studying urea hydrolysis. The MPC specimens with and without spores were sterilized by Tyndallization [22]. The specimens were then immersed in urea containing 50 ml LB media. One flask with only urea-containing media was kept as control. In another flask, free spore powder was added and used as a positive control. All the flasks were incubated at 30 °C for 24 h. After 24 h, the specimens were taken out, and the media was centrifuged to collect the supernatant. The supernatant was used to study urea hydrolysis. NASH assay was performed to check the urea hydrolysis.

2.8. Calcite Precipitation and Self-healing

For crack healing of the specimen, precipitation media was prepared with 0.3 g nutrient broth, 1 g NH_4Cl, 2 g urea, and 0.56 g $CaCl_2$ in 100 ml distilled water. The cracks were generated in spores containing MPC specimens. Calcite precipitation and self-healing were studied by running wet and dry cycles. The specimens were immersed in a 100 ml precipitation medium. The flask was incubated at 30 °C for 24 h at static conditions. After 24 h, specimens were removed from the press and dried at room temperature for 24 h. Then, the specimens were again immersed in precipitation media. Such wet and dry cycles were performed for seven days.

2.9. Effect of Calcite Precipitation on Water Absorption by MPC Specimen

The MPC specimens with and without spores were immersed in precipitation media. The wet and dry cycles were carried out for 7 days. The specimens were dried in an oven at 60 °C. Afterward, these specimens were immersed in the beaker with 100 ml of distilled water. The specimens were kept in water overnight. Specimens were taken outside. The weight of the specimens was determined before (w) and after (w′) immersing them in water. The % water absorption was calculated as shown in the formula:

$$\%Absorption=(W'-W)x100/W$$

2.10. Analytical Techniques Used for Characterization

The functional groups present in magnesium phosphate powder, MPC, etc., were analyzed by Fourier-transform infrared spectroscopy (Jasco FT/IR-6100, Japan). The microstructure was investigated using scanning electron microscopy (SEM) (FEI Nova SEM 450, Netherlands). The thermal behavior of MPC was studied by thermogravimetric analysis.

2.11. Statistical Analysis

The data analysis was performed utilizing OriginPro 2020 SR19.7.0.188 statistical analysis software. The statistical significance of the differences between means was assessed using a one-way analysis of variance (ANOVA) followed by Tukey's test. All experiments were conducted thrice; the presented values represent the means ± standard deviation (SD). Symbols with different letters indicate significant differences ($p<0.05$) between the compared groups.

3. RESULTS

3.1. The Optimization of Bacterial Urea Hydrolysis

Paenibacillus sp. NCIM 5410 was used in the present study considering its halophilic nature, urea hydrolyzing, and spore-forming ability. The endospores protect ureolytic bacteria from death under adverse conditions [23]. This makes the application of Paenibacillus sp. NCIM 5410 is suitable for the bio-cementation process. The endospores can help survive the high pH conditions of Portland cement-based concrete. It also helps to overcome desiccation and pore size shrinkage in concrete environments. The urea hydrolysis at different pH, temperature, and incubation times was experimentally investigated. As shown in Figure 1, the urea hydrolysis increased with increasing pH. PH 9 was found to be optimum for urea hydrolysis.

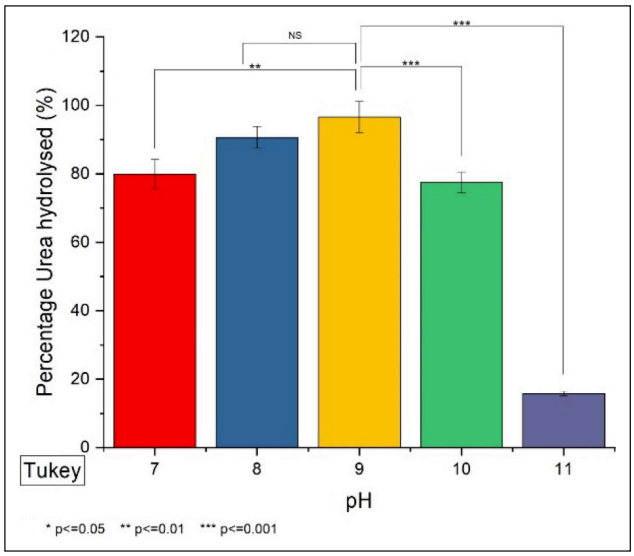

Figure 1. Effect of pH on urea hydrolysis by Paenibacillus sp. NCIM 5410.

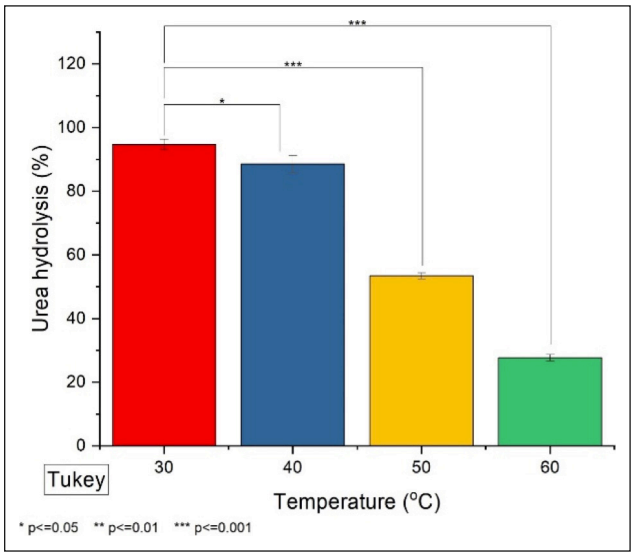

Figure 2. Effect of temperature on urea hydrolysis by Paenibacillus sp. NCIM 5410.

The urea hydrolysis decreased at higher pH values. Several researchers reported that pH 8–9 is ideal for bacterial calcite precipitation [23]. Bacterial hydrolysis of urea is important to achieve calcite precipitation [24]. Hence, the ability of Paenibacillus sp. NCIM 5410 to hydrolyze urea at pH 9 is advantageous. The effects of temperature on urea hydrolysis can be found in Figure 2. The urea hydrolysis steadily decreased and increased in temperature from 30 °C to 60 °C. The optimum temperature in the present study for Paenibacillus sp. 5410 was 30 °C. Some reports showed that 37 °C is the optimum temperature for B. sphaericus [25].

Similarly, the optimum pH in the present study was 9, whereas Singh et al. [25] got 7 for B. sphaericus [25]. Figure 3 shows the effect of incubation time on urea hydrolysis. The hydrolysis increased with incubation time up to 72 h and subsequently decreased. The increasing trend might be because of an increase in bacterial growth and an increase in bacterial production of urease enzyme. The exhaustion of nutrients, cell death, and enzyme degradation might be responsible for the decrease in urea hydrolysis after 72 h. A similar phenomenon of urea hydrolysis has been reported by several researchers [26]. Dhami et al. [27] said the urease activity to be around 650 U/ml for Bacillus megaterium S33, which was investigated at 37 °C for 96 h [27]. In the present study, the spores of Paenibacillus sp. NCIM 5410 was generated and used in further experiments to prepare bioactive MPC.

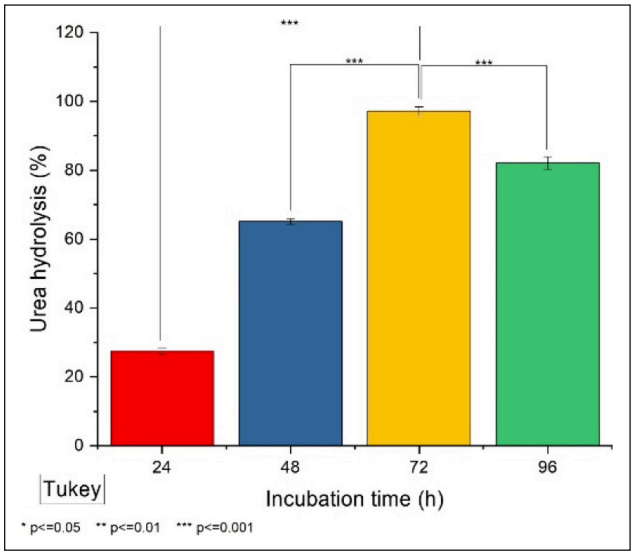

Figure 3. Effect of incubation time on urea hydrolysis by Paenibacillus sp. NCIM 5410.

3.2. Preparation and Characterization of Cements with Embedded Microorganisms

The MPC without bacterial spores was prepared as described by Soltmann et al. [20] with slight modifications using magnesium phosphate powder and ammonium phosphate solution. Adding 13 ml ammonium phosphate solution to 5 g magnesium phosphate powder gave a better consistency; hence, this combination was used in further experiments. The slurry system showed a fast setting caused by the formation of ammonium phosphate hexahydrate (Fig. 4). Soltmann et al. [20] also reported similar observations.

The reaction was carried out at neutral pH. This type of binder material is suitable for the immobilization of calcite-precipitating bacteria. MPC specimens with and without spores were not breaking after overnight treatment with water (data not shown). The MPC with bacterial spores is prepared by adding 0.5 g of spore powder to the reaction mixture. It is reported that ammonium magnesium phosphate hexahydrate [$(NH_4)MgPO_4.6H_2O$, Struvite] is formed as a primary reaction product when ammonium phosphate solution and magnesium phosphate powder are mixed [20, 28]. It is further confirmed by FTIR analysis. The functional groups are observed in the region of OH stretching vibrations of H_2O molecules at 3728, 3604, and 3532 cm^{-1}. A band at 2382 cm^{-1} corresponds to the stretching vibrations of the PO–H bond. The bands at 1643 and 1535 cm^{-1} correspond to in-plane H–O–H bending vibrations of at least two different types of water molecules (Fig. 5). The other

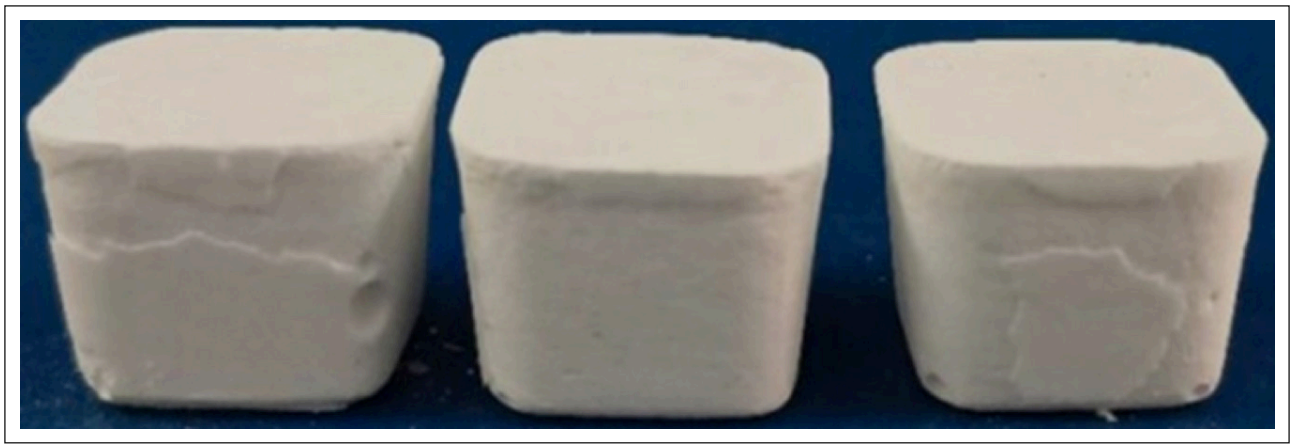

Figure 4. Magnesium phosphate cement specimen.

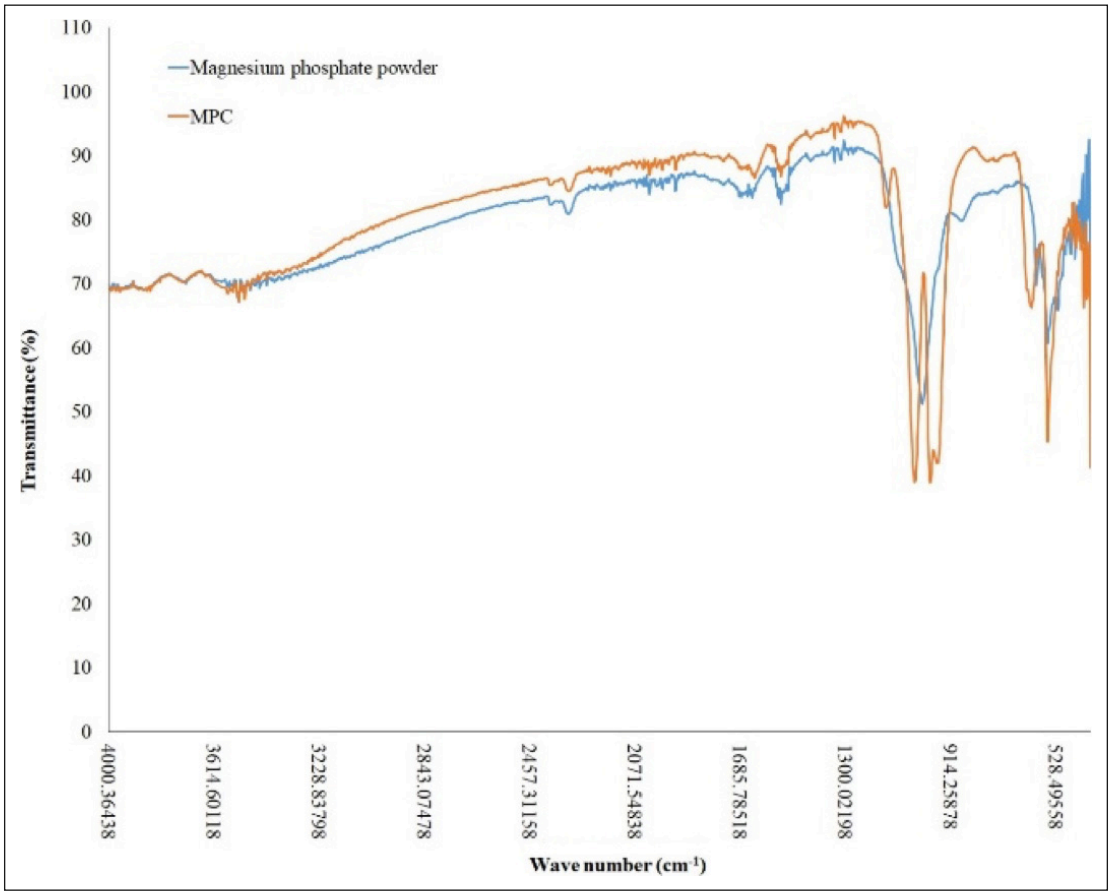

Figure 5. FTIR Spectrum of (a) $Mg_3(PO_4)_2$ (b) MPC.

bands are assigned to 1138 and 1012 cm^{-1} stretching vibrations of $(PO_4)^{3-}$ and bending vibrations at 680 cm^{-1} [29]. Meanwhile, Figure 4 shows structural vibrations of water occurring at 3847, 3604, and 3525 cm^{-1}. Also, at 1641 and 1535 cm^{-1}, bending vibrations of water occurred. The bands appeared at 752, 680, and 999 cm^{-1}, assigned to different modes of vibrations of $(PO_4)^3$. The band at 1427 cm^{-1} is attributed to NH_3. These results confirm the presence of the struvite [30]. The abrasion resistance of the as-prepared MPC specimen was tested by shaking the MPC specimen in water for 24 h. A minimal abrasion was observed (data not shown). The samples of spores, $Mg_3(PO_4)_2$, and MPC with and without spores were analyzed using a photography camera and SEM. Figure 6a–d in the supporting document shows the appearance of spores, $Mg_3(PO_4)_2$.

MPC without spores, and MPC with spores in images captured by the photographic camera. Figure 7a–d show images of the same samples analyzed by SEM. Small circular structures in Figure 7a are spores of Paenibacillus sp. whose particle size ranges from 2–20 µm. Figure 7b shows irregular morphologies present in $Mg_3(PO_4)_2$ powder, for which the particles have a size between 0.05–0.75 µm. Figure 7c

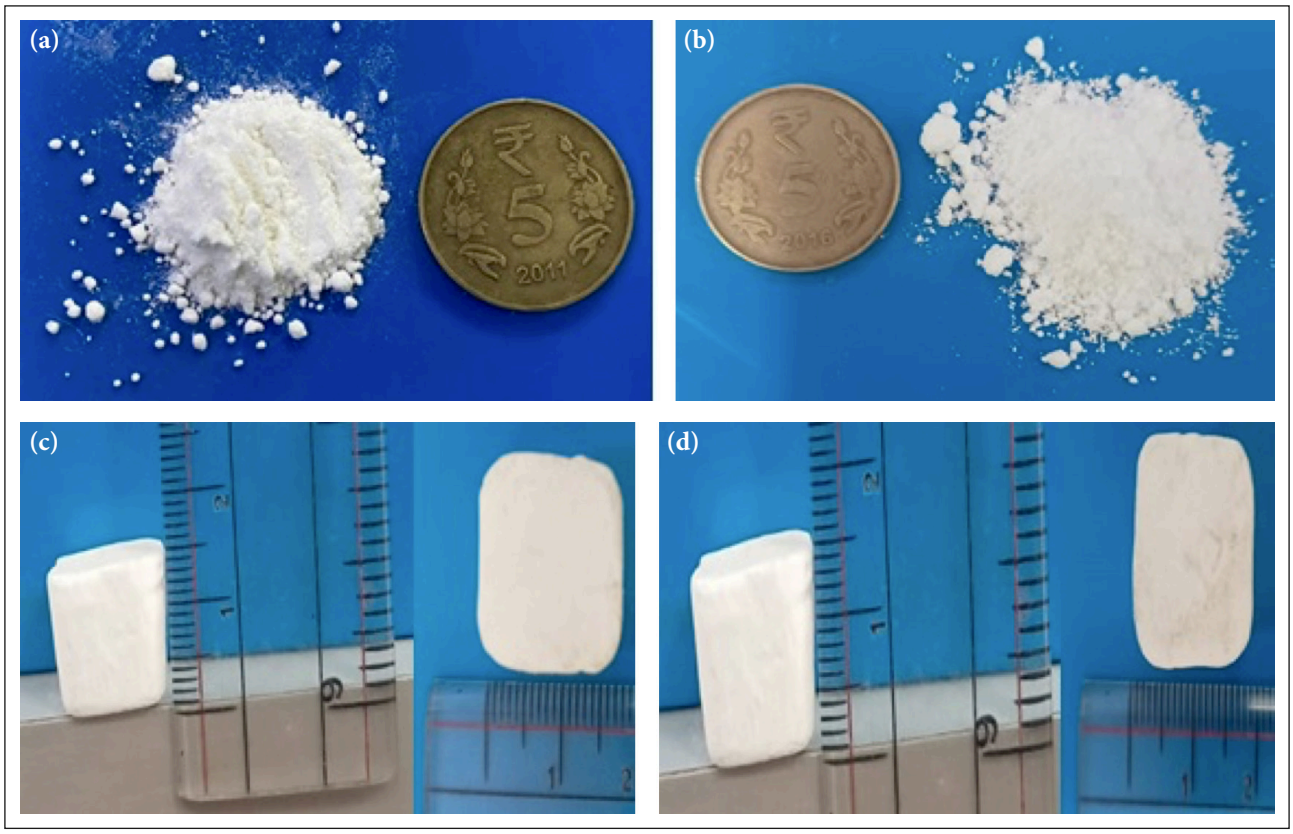

Figure 6. Appearance of various samples **(a)** photographic image of spore powder **(b)** photographic image of $Mg_3(PO_4)_2$ powder **(c)** photographic image of MPC cube without spores **(d)** photographic image of MPC cube with spores.

shows the presence of rod-shaped struvite in MPC having 1.5–9.5 µm particle size. Similar needle or rod-shaped morphologies were reported previously for MPC [31, 32]. MPC is formed due to a continuous dissolution and precipitation reaction, resulting in a stable ceramic product. It comprises equimolar concentrations of Mg, ammonium (NH^{4+}), and phosphate (PO_4^{3-}) combined with six water molecules. $Mg_3(PO_4)_2$ reacts with ammonium phosphate solution to form struvite ($MgNH_4PO_4 \bullet 6H_2O$). The most general reaction equation assumes that three kinds of free ions bind with 6 moles of water to form $MgNH_4PO_4 \bullet 6H_2O$ (Eq. 1) [28, 33, 34] Figure 7d shows that struvite particles of 11 µm size cover the spores.

$$Mg^{2+} + NH^{4+} + PO_4^{3-} + 6H_2O \quad MgNH_4PO_4 \bullet 6H_2O \quad (1)$$

Thermogravimetric analysis (TGA) and derivative thermogravimetry (DTG) were also conducted on the MPC samples; the results are shown in Figure 8. Only two prominent peaks were observed in the DTG of the sample, both below 200 °C. The peak at ~150 °C corresponds to a loss of physically and chemically bound water, while the peak at ~100 °C could correspond to the decomposition of struvite according to previous research [30, 35, 36].

3.3. Study of Leaching of Spores from MPC Matrix, Viability, and Crack Healing Phenomenon

A study was conducted to find the immobilization of spores in the MPC matrix. The results show no bacterial colonies on the plates for MPC with and without spores (Fig. 9).

4. DISCUSSION

It is evident from these results that the MPC matrix holds and protects the spores from external mechanical force. The viability of bacterial spores in the MPC matrix was determined by immersing the spore-containing MPC specimen in a containing medium. The amount of urea decomposed was studied. The control, urea-containing medium without spores, and the urea-containing medium containing MPC (without spores) showed negligible hydrolysis of urea. Free bacterial spores showed the highest urea hydrolysis. The bacteria-containing MPC decomposed around 70 (±0.48) % of urea (Fig. 10). These results suggest that the cementation process did not cause any damage to the bacterial spores.

The MPC provided a microenvironment for the germination and growth of bacterial spores, thus protecting the bacteria from the external environment. The crack was created in an MPC cube, and the self-healing of the crack was studied. The crack healing was observed in 7 days (data not shown). The samples were collected from the healed area and analyzed using SEM-EDS. The EDS analysis confirmed the presence of Ca in the healed product (Fig. 11). This shows the calcite-precipitating ability of Paenibacillus sp. NCIM 5410.

Wang et al. [37] found that the amount of urea decomposed by the free bacterial cells in the high pH cement slurry was significantly decreased, from 95% to less than 5%. However, they observed that the immobilization of bacterial cells increased the urea hydrolysis. In another study, Jad-

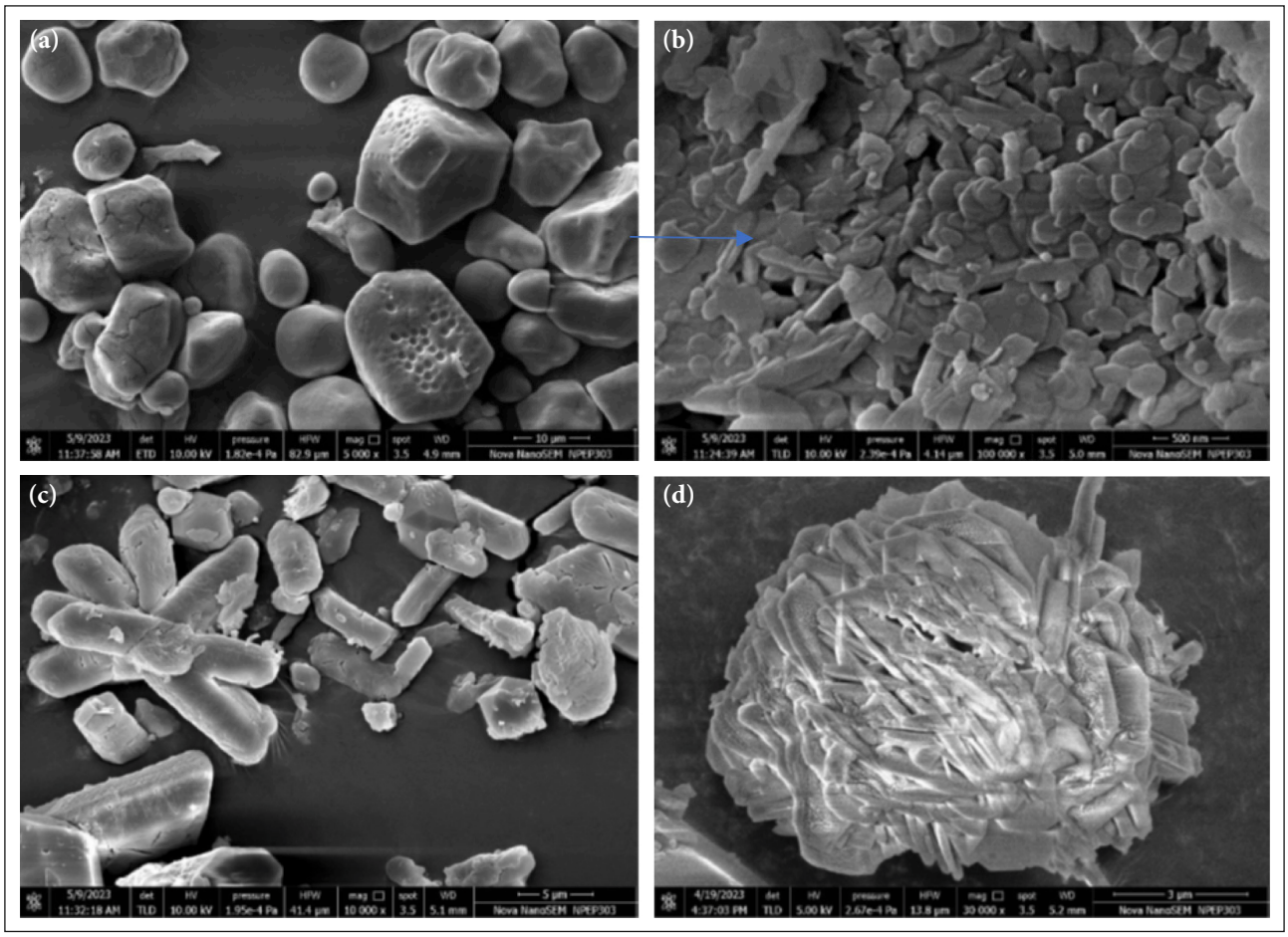

Figure 7. Appearance of various samples **(a)** SEM image of spore powder **(b)** SEM image of $Mg_3(PO_4)_2$ powder **(c)** SEM image of MPC cube without spore powder **(d)** SEM image of MPC cube with spore powder.

hav et al. [17] synthesized geopolymer to immobilize the bacterial cells. They found that the geopolymer reaction did not cause any damage to the bacterial spores, and the spores got activated when the bacteria-containing geopolymer specimen was immersed in a urea-based medium. These activated cells decomposed 98 (±0.20)% of urea was decomposed. The geopolymer provides interconnected pores and sufficient space to accommodate the bacterial spores and reactivated bacterial cells. A similar phenomenon happens with MPC synthesized in the present study. The viability of the spores after being immobilized into microcapsules was also reported by Wang et al. [38].

A study was conducted to examine the effect of calcite precipitation on the water absorption behavior of MPC cubes. The results show reduced water absorption for the specimens containing spores. The specimens without spores showed 5% water absorption, while those with spores showed 2.6% (Fig. 12). These specimens were immersed in a precipitation medium before the water absorption test. The precipitation medium might have provided the nutrients to spores, which helped them germinate. The germinated spores transformed into vegetative bacterial cells, and these cells might have produced calcite. The as-built calcite might have filled the pores of the MPC specimen, thereby reducing the water absorption.

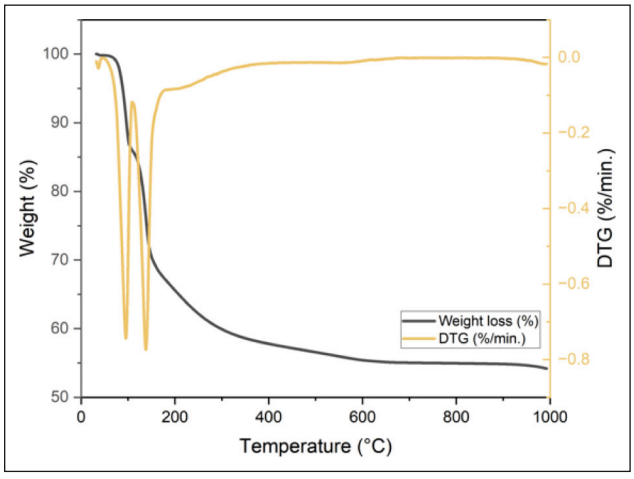

Figure 8. Thermogravimetric analysis of MPC.

5. CONCLUSION

This study successfully achieved the synthesis of MPC via an aqueous route. As a clinker-free binder characterized by rapid setting, high early compressive strength, excellent volume stability, robust bonding strength, minimal shrinkage, and superior abrasion resistance, MPC becomes an ideal material for immobilizing bacterial

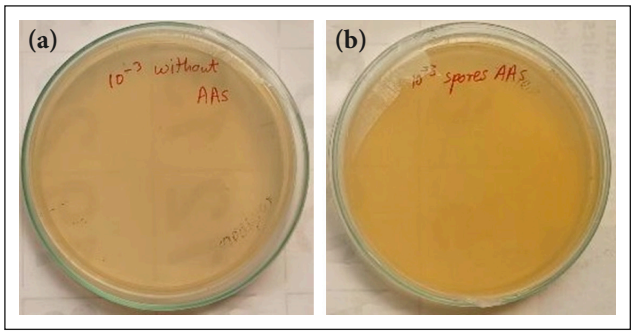

Figure 9. Study of leakage of spores from MPC **(a)** sample without spore **(b)** sample with spore.

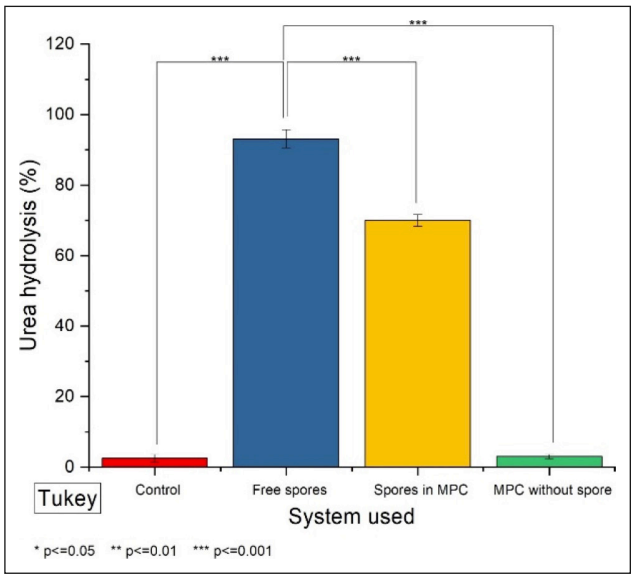

Figure 10. Viability testing by urea hydrolysis test.

spores. It prevents the compression of spores, a phenomenon commonly observed in concrete, conferring a durable self-healing attribute to MPC.

The aqueous route facilitated the effective immobilization of bacterial spores within MPC. Notably, MPC demonstrated its ability to retain bacterial spores, which is evident through urea hydrolysis and calcite precipitation. These findings indicate that MPC can safeguard spores for extended storage durations. However, it is essential to note that the present study did not assess spore viability over periods exceeding five months. The amalgamation of MPC matrix with bacteria holds promise in creating a bioactive material.

Considering the future applications of MPC-containing bacteria, particularly in scenarios requiring rapid repairs, is crucial. The harsh environmental conditions of concrete can be effectively countered by MPC, safeguarding bacteria from adverse conditions. MPC is already employed as a repair material for diverse concrete structures, and incorporating bacteria into MPC provides an additional advantage by imparting self-healing capabilities.

ACKNOWLEDGMENTS

The author, Deeksha Patil, would like to acknowledge DBT.

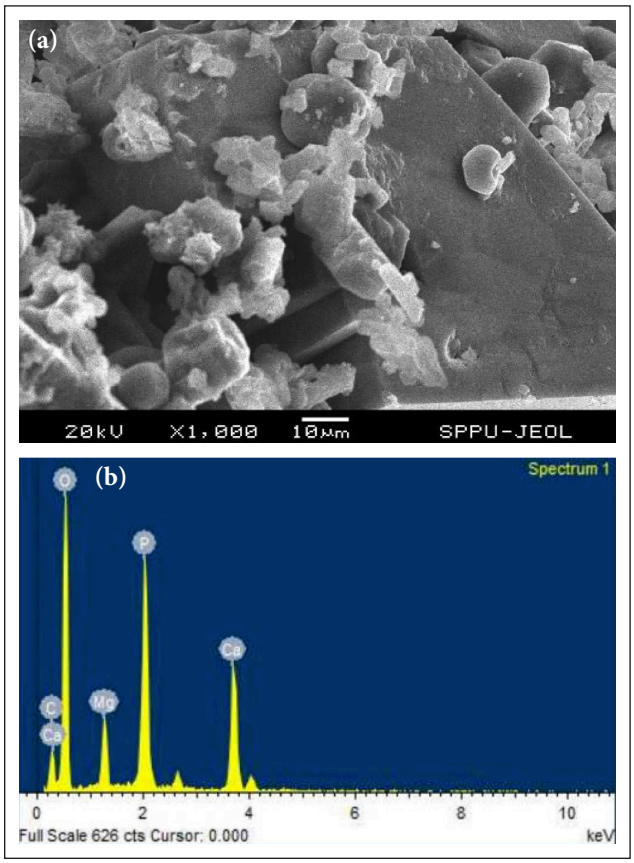

Figure 11. **(a)** SEM and **(b)** EDS analysis of the healed product.

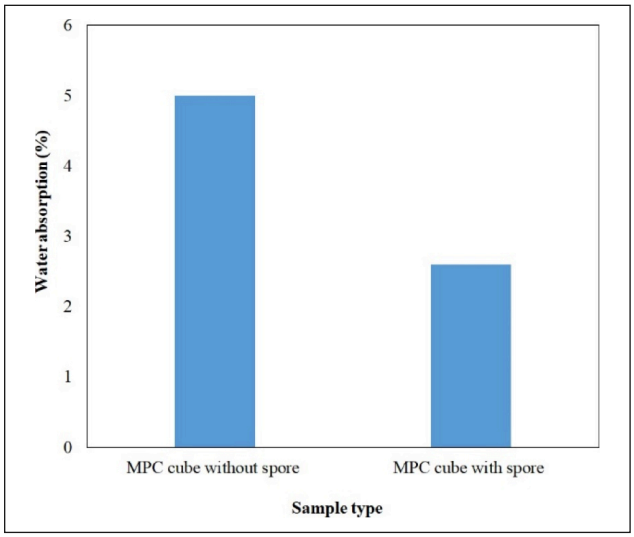

Figure 12. Water absorption **(a)** without spore and **(b)** with spore.

ETHICS

There are no ethical issues with the publication of this manuscript.

DATA AVAILABILITY STATEMENT

The authors confirm that the data that supports the findings of this study are available within the article. Raw data that support the finding of this study are available from the corresponding author, upon reasonable request.

CONFLICT OF INTEREST

The authors declare that they have no conflict of interest.

FINANCIAL DISCLOSURE

The authors declared that this study has received no financial support.

USE OF AI FOR WRITING ASSISTANCE

Not declared.

PEER-REVIEW

Externally peer-reviewed.

REFERENCES

[1] Walling, S. A., & Provis, J. L. (2016). Magnesia-based cements: A journey of 150 years, and cements for the future? *Chem Rev, 116*(7), 4170–4204. [CrossRef]

[2] Nasreen, S., & Suresh Babu, T. (2015). Effect of bacteria on 28 days split tensile strength of concrete and its stress-strain curves. *Int J Civ Struct Eng Res, 3*(2), 33–38.

[3] Wagh, A. S. (2004). Chemically bonded phosphate ceramic matrix composites. *In Chemically Bonded Phosphate Ceramics*. (pp. 157–176). Elsevier. [CrossRef]

[4] Mao, W., Cao, C., Li, X., Qian, J., & You, C. (2022). Preparation of magnesium ammonium phosphate mortar by manufactured limestone sand using compound defoaming agents for improved strength and impermeability. *Buildings, 12*(3), 267. [CrossRef]

[5] Qin, J., Qian, J., You, C., Fan, Y., Li, Z., & Wang, H. (2018). Bond behavior and interfacial micro-characteristics of magnesium phosphate cement onto old concrete substrate. *Constr Build Mater, 167*, 166–176. [CrossRef]

[6] Hong, S., Zhang, J., Liang, H., Xiao, J., Huang, C., Wang, G., Hu, H., Liu, Y., Xu, Y., Xing, F., & Dong, B. (2018). Investigation on early hydration features of magnesium potassium phosphate cementitious material with the electrodeless resistivity method. *Cement Concrete Compos, 90*, 235–240. [CrossRef]

[7] Jia, X., Li, J., Wang, P., Qian, J., & Tang, M. (2019). Preparation and mechanical properties of magnesium phosphate cement for rapid construction repair in ice and snow. *Constr Build Mater, 229*, 116927. [CrossRef]

[8] Haque, M. A., & Chen, B. (2019). Research progress on magnesium phosphate cement: A review. *Constr Build Mater, 211*, 885–898. [CrossRef]

[9] Zhou, H., Agarwal, A. K., Goel, V. K., & Bhaduri, S. B. (2013). Microwave assisted preparation of magnesium phosphate cement (MPC) for orthopedic applications: A novel solution to the exothermicity problem. *Mater Sci Eng C, 33*(7), 4288–4294. [CrossRef]

[10] Xing, S., & Wu, C. (2018). Preparation of magnesium phosphate cement and application in concrete repair. *MATEC Web Conf, 142*, 02007. [CrossRef]

[11] Li, Y., Bai, W., & Shi, T. (2017). A study of the bonding performance of magnesium phosphate cement on mortar and concrete. *Constr Build Mater, 142*, 459–468. [CrossRef]

[12] Jia, L., Zhao, F., Yao, K., & Du, H. (2021). Bond performance of repair mortar made with magnesium phosphate cement and ferroaluminate cement. *Constr Build Mater, 279*, 122398. [CrossRef]

[13] Li, Y., & Chen, B. (2013). Factors that affect the properties of magnesium phosphate cement. *Constr Build Mater, 47*, 977–983. [CrossRef]

[14] Gardner, L. J., Bernal, S. A., Walling, S. A., Corkhill, C. L., Provis, J. L., & Hyatt, N. C. (2015). Characterisation of magnesium potassium phosphate cements blended with fly ash and ground granulated blast furnace slag. *Cement Concrete Res, 74*, 78–87. [CrossRef]

[15] Ma, H., Xu, B., Liu, J., Pei, H., & Li, Z. (2014). Effects of water content, magnesia-to-phosphate molar ratio, and age on pore structure, strength, and permeability of magnesium potassium phosphate cement paste. *Mater Des, 64*, 497–502. [CrossRef]

[16] Jia, X., Luo, J., Zhang, W., Qian, J., Li, J., Wang, P., & Tang, M. (2020). Preparation and application of self-curing magnesium phosphate cement concrete with high early strength in severe cold environments. *Materials, 13*(23), 5587. [CrossRef]

[17] Jadhav, U. U., Lahoti, M., Chen, Z., Qiu, J., Cao, B., & Yang, E. H. (2018). Viability of bacterial spores and crack healing in bacteria-containing geopolymer. *Constr Build Mater, 169*, 716–723. [CrossRef]

[18] Doctolero, J. Z. S., Beltran, A. B., Uba, M. O., Tigue, A. A. S., & Promentilla, M. A. B. (2020). Self-healing biogeopolymers using biochar-immobilized spores of pure-and-co-cultures of bacteria. *Minerals, 10*(12), 1114. [CrossRef]

[19] Ekinci, E., Turkmen, İ., & Birhanli, E. (2022). Performance of self-healing geopolymer paste produced using Bacillus subtilis. *Constr Build Mater, 325*, 126837. [CrossRef]

[20] Soltmann, U., Nies, B., & Böttcher, H. (2011). Cements with embedded living microorganisms – a new class of biocatalytic composite materials for application in bioremediation, biotechnology. *Adv Eng Mater, 13*(1–2), B25–B31. [CrossRef]

[21] Liu, F., Cheng, X., Miu, J., Li, X., Yin, R., Wang, J., & Qu, Y. (2021). Application of different methods to determine urease activity in enzyme engineering experiment and production. *E3S Web Conf, 251*, 02057. [CrossRef]

[22] Brown, J. V., Wiles, R., & Prentice, G. A. (1979). The effect of a modified tyndallization process upon the sporeforming bacteria of milk and cream. *Int J Dairy Technol, 32*(2), 109–112. [CrossRef]

[23] Aliyu, A. D., Mustafa, M., Aziz, N. A. A., Kong, Y. C., & Hadi, N. S. (2023). Assessing indigenous soil ureolytic bacteria as potential agents for soil stabilization. *J Trop Biodivers Biotechnol, 8*(1), 75128. [CrossRef]

[24] Krajewska, B. (2018). Urease-aided calcium carbonate mineralization for engineering applications: A review. *J Adv Res, 13*, 59–67. [CrossRef]

[25] Singh, A. K., Singh, M., & Verma, N. (2017). Extraction, purification, kinetic characterization, and immobilization of urease from bacillus sphaericus MTCC 5100. *Biocatal Agric Biotechnol, 12*, 341–347. [CrossRef]

[26] Jiang, N. J., Yoshioka, H., Yamamoto, K., & Soga, K. (2016). Ureolytic activities of a urease-producing bacterium and purified urease enzyme in the anoxic condition: Implication for subseafloor sand production control by microbially induced carbonate precipitation (MICP). *Ecol Eng, 90*, 96–104. [CrossRef]

[27] Dhami, N. K., Mukherjee, A., & Reddy, M. S. (2016). Applicability of bacterial biocementation in sustainable construction materials. *Asia-Pac J Chem Eng, 11*(5), 795–802. [CrossRef]

[28] Christel, T., Christ, S., Barralet, J. E., Groll, J., & Gbureck, U. (2015). Chelate bonding mechanism in a novel magnesium phosphate bone cement. *J Am Ceram Soc, 98*(3), 694–697. [CrossRef]

[29] Britvin, S. N., Ferraris, G., Ivaldi, G., Bogdanova, A. N., & Chukanov, N. V. (2002). Cattiite, Mg3(PO4)2·22H2O, a new mineral from Zhelezny Mine (Kovdor Massif, Kola Peninsula, Russia). *Neues Jahrb Min Monatsh, 2002*(4), 160–168. [CrossRef]

[30] Leela, S., Ranishree, J. K., Perumal, R. K., & Ramasamy, R. (2019). Characterization of struvite produced by an algal associated agarolytic bacterium exiguobacterium aestuarii St. SR 101. *J Pure Appl Microbiol, 13*(2), 1227–1234. [CrossRef]

[31] Suguna, K., Thenmozhi, M., & Sekar, C. (2012). Growth, spectral, structural and mechanical properties of struvite crystal grown in presence of sodium fluoride. *Bull Mater Sci, 35*, 701–706. [CrossRef]

[32] Lahalle, H., Patapy, C., Glid, M., Renaudin, G., & Cyr, M. (2019). Microstructural evolution/durability of magnesium phosphate cement paste over time in neutral and basic environments. *Cement Concrete Res, 122*, 42–58. [CrossRef]

[33] Liu, Y., Kumar, S., Kwag, J. H., & Ra, C. (2013). Magnesium ammonium phosphate formation, recovery and its application as valuable resources: A review. *J Chem Technol Biotechnol, 88*(2), 181–189. [CrossRef]

[34] Tansel, B., Lunn, G., & Monje, O. (2018). Struvite formation and decomposition characteristics for ammonia and phosphorus recovery: A review of magnesium-ammonia-phosphate interactions. *Chemosphere, 194*, 504–514. [CrossRef]

[35] Yu, J., Qian, J., Wang, F., Li, Z., & Jia, X. (2020). Preparation and properties of a magnesium phosphate cement with dolomite. *Cement Concrete Res, 138*, 106235. [CrossRef]

[36] Hövelmann, J., Stawski, T. M., Besselink, R., Freeman, H. M., Dietmann, K. M., Mayanna, S., Pauw, B. R., & Benning, L. G. (2019). A template-free and low temperature method for the synthesis of mesoporous magnesium phosphate with uniform pore structure and high surface area. *Nanoscale, 11*(14), 6939–6951. [CrossRef]

[37] Wang, J. Y., De Belie, N., & Verstraete, W. (2012). Diatomaceous earth as a protective vehicle for bacteria applied for self-healing concrete. *J Ind Microbiol Biotechnol, 39*(4), 567–577. [CrossRef]

[38] Wang, J. Y., Soens, H., Verstraete, W., & De Belie, N. (2014). Self-healing concrete by use of microencapsulated bacterial spores. *Cement Concrete Res, 56*, 139–152. [CrossRef]

J Sustain Const Mater Technol, Vol. 9, Issue. 1, pp. 11–24, March 2024

Journal of Sustainable Construction Materials and Technologies
Web page info: https://jscmt.yildiz.edu.tr
DOI: 10.47481/jscmt.1406171

JSCMT
Journal of Sustainable Construction Materials and Technologies

Research Article

Research on the long-term strength development of Datça Pozzolan-based geopolymer

Kübra Ekiz BARIŞ*[1], Leyla TANAÇAN[2]

[1]*Department of Architecture and Design, Kocaeli University, İzmit, Türkiye*
[2]*Department of Architecture, İstanbul Technical University, İstanbul, Türkiye*

ARTICLE INFO

Article history
Received: 17 December 2023
Revised: 25 January 2024
Accepted: 02 February 2024

Key words:
Geopolymer, heat curing, long-term curing, natural pozzolan, strength, ultrasound pulse velocity

ABSTRACT

This study examined the influence of long-term curing duration on the properties of geopolymers produced through the geopolymerization reaction between Datça Pozzolan and sodium silicate and potassium hydroxide solutions. The specimens were heat cured at 90 °C, 95±5% RH for 24 h initially and then kept under ambient conditions until the tests were conducted at 7, 90, and 365 days. The results showed that applied initial heat curing was appropriate to achieve high early and long-term strength. Geopolymer mortars with 12.5 M and 2.5 activator ratios had the lowest porosity (20.90%) and the highest ultrasound pulse velocity (UPV) (3.10 km/s), compressive strength (10.57 MPa), and flexural strength (5.20 MPa) after seven days. While the porosity of the identical specimens decreased by up to 15.77%, the UPV, compressive strength and flexural strength increased by 3.37 km/s, 15.32 MPa, and 6.06 MPa, respectively, after 365 days. The physical and mechanical improvement in the first 90 days exceeded 90–365 days. A higher rate of improvement was obtained when the activator ratio was low, i.e., the improvement decreased inversely as the sodium silicate content of the mortar increased. An increasing trend was observed in the plot of compressive strength as a function of UPV, and the slope values presented a strongly related linear function relation.

Cite this article as: Barış, K. E., & Tanaçan, L. (2024). Research on the long-term strength development of Datça Pozzolan-based geopolymer. *J Sustain Const Mater Technol*, 9(1), 11–24.

1. INTRODUCTION

The cement industry is responsible for 5–7% of CO_2 emissions, and the global demand for OPC by 2030 is projected to increase by 216% [1]. In Türkiye, the housing sector consumes 32% of the total energy, and 8.,7% of the total CO_2 emissions originate from cement production [2]. Therefore, the search for low-embodied CO_2 materials is essential for Türkiye. Geopolymers can reduce CO_2 emissions compared with cement production [3]. The geopolymeric reactivity of Datça Pozzolan was investigated in the literature, and the results revealed that it could be used as an aluminosilicate source to produce geopolymer mortars [4]. However, the possibilities of using this material in the building industry should be further investigated toward a carbon-neutral building stock commitment.

The evolution of the geopolymer structure into a semi-crystalline amorphous material and the consequent strength properties of the final product is affected by the curing conditions (curing temperature, duration, humidity), mixture components (precursor and activator type), and mixture design parameters (water/solid ratio, molar ratios of Si/Al, Al/Na, and H_2O/Na_2O). Proper curing conditions prevent high porosity and permeability and, therefore, improve the strength gain of the material. Regardless of the type and dosage of alkali activators, curing below or

***Corresponding author.**
*E-mail address: kubra.ekizbaris@kocaeli.edu.tr

at room temperature (7–20 °C) is not convenient for geopolymers because the beginning of the setting is delayed, and the chemical reaction rate is prolonged [5–9]. Mineral phases in natural pozzolan dissolved in the first three days. The dissolved phases remained 7 and 14 days after the reaction, and the geopolymer matrix continued progressing. At 28 days, the morphology of dense plates, which is related to the polycondensation reaction, produced an interconnected structure, and it was predicted that it would improve over time due to the progress of the geopolymerization reaction [10]. For example, brick powder-based geopolymer cured at 28 and 90 days yielded strengths of 5.3 and 18.7 MPa, respectively [11]. The strength of the red mud and rice husk ash-based geopolymer became almost constant in 35 days (11.7 MPa), and the geopolymer could only gain strength after a certain curing period [12]. Haruna et al. [13] cured high calcium-fly ash-based one-part alkali-activated binders at 25 °C for 365 days. The maximum strength was found after 90 days, and the strength improvement at 180 and 365 days was negligible compared with that at 90 days. The increase in strength beyond 28 days was explained by the formation of fly ash reactions at later ages, which resulted in more calcium alumina silicate hydrate gel production.

Although curing at elevated temperatures is an energy-intensive process, it is particularly crucial in low-calcium aluminosilicate precursors to initiate geopolymerization reactions and enhance the mechanical properties of the final cured products [14]. Elevated temperature curing could overcome the obstacle to further reaction along with improved dissolution of reactive species [5]. An increase in the curing temperature up to 90 °C favors the dissolution of reactive species [15], substantially improves cross-linking in an amorphous structure [14], and increases the compressive strength of the product [6, 16]. According to Naghizadeh et al. [17], the strength development and durability performance of fly ash-based geopolymer concrete (Na_2O/FA>0.09–0.10) cured at 60 °C for 24 h were higher than those of the specimens cured under ambient conditions for 28 days. Another study determined that heat curing at 60 °C for a more extended curing period was beneficial for strength development [18]. According to Bing-hui et al. [19], who investigated the effects of curing temperature (within the range of 20 to 100 °C) on the properties of metakaolin-based geopolymers, elevating the curing temperature increases the activity of hydroxide ions and the dissolution rate of amorphous aluminosilicates; increases polycondensation, polymerization, and reprecipitation processes due to the dehydration of water in the early stage of the geopolymerization reaction; and finally, accelerates the hardening process and improves the physical properties of the geopolymer. However, a curing temperature higher than the appropriate one may negatively affect the properties. For example, Yılmaz et al. [20] determined that curing low-calcium fly ash-based geopolymer mortars above 60 °C for 24, 48, and 72 h decreased the strength of the material. In another study investigated by Yang et al. [21], the mechanical properties of the steel slag-based geopolymer mortar decreased above 60 °C because of the increased shrinkage cracks of the material. Curing temperatures above the optimum one caused rapid setting and restrained the transformation into a compact and tough structure due to the following reactions: The viscosity of the slurry increased rapidly at the initial polycondensation stage. Dissolved ions of aluminate precursors react quickly and increase the setting speed; therefore, the time between the initial and final setting is extremely short. With the rapid coagulation of the slurry, undissolved aluminosilicate particles are covered with this gel, and further dissolution of amorphous phases and solid-state transformation into dense structures is restrained [19]. Zeolite-like crystalline products are formed at higher temperatures (up to 200 °C) [22].

When metakaolin-based geopolymers are cured at temperatures lower than 50 °C, the dissolution and formation of hydroxy species are not complete and insufficient to form the oligomers, leading to lower compressive strength results [23]. However, when pre-cured at 75 °C for three hours, it exhibited improved mechanical properties without diminishing in the long-term curing up to 28 days. However, mixtures of metakaolin and slag cured at the same temperature produced microstructural defects through volume expansion [24]. Aygörmez et al. [25] cured colemanite and metakaolin-based geopolymer mortar at 60 °C for 72 h and allowed it to cure under ambient conditions for 365 days. The strength results were lower at day 365 than at day 14, and it was explained that curing at 60 °C for 72 h positively affected the strength in the early period. However, rapidly developing reaction products adversely affect the material's long-term microstructure and strength properties.

Numerous studies have been conducted on the humidity conditions during the curing of geopolymers. Both natural and artificial-based geopolymers, cured in an oven (RH≤10%) at 70–90 °C, showed visible cracks on the surface of the specimens caused by a substantial loss of moisture and drying shrinkage [10–13, 16, 24–27]. Likewise, the compressive strength of Datça pozzolan-based geopolymer binder was 9.36 MPa after curing at 90 °C under sealed conditions; however, its strength decreased to 5.60 MPa without sealed conditions at the same curing temperature [4]. Therefore, geopolymerization reactions require moisture during the first curing stage to produce a stronger crack-free product [16]. Bondar et al. [28] achieved higher early strength by curing alkali-activated Taftan pozzolan at 60 °C. However, by curing at 40 °C under sealed conditions, higher strength could be obtained in the long term (365 days). In addition, the tests conducted at 28, 90, and 120 days showed a good correlation between ultrasound pulse velocity (UPV) and compressive strength, suggesting that pulse velocity techniques could be successfully used for the estimation of geopolymer strength made with alkali-activated natural pozzolans. Indeed, non-destructive ultrasonic wave technology allows continuous monitoring of a material's reaction process. By the propagation speed of the ultrasound pulse in a material, early-age reaction processes and microstructure development, improvement in rheological properties, setting (due to initial gel formation), hardening and strength development (due to the gradual progression of polymerization/crystallization), and durability properties have been successfully measured [28–32].

Table 1. Chemical analysis of natural Datça Pozzolan

	SiO_2	Al_2O_3	Fe_2O_3	CaO	MgO	P_2O_5	K_2O	Na_2O	TiO_2	MnO_2	Cr_2O_3	NiO
Wt%	75.29	15.99	0.98	1.22	0.62	0.07	3.02	2.21	0.14	0.04	0.005	0.004
	CuO	ZnO	Rb	SrO	Y_2O_3	ZrO_2	Nb_2O_5	BaO	Cl	SO_3	LOI	Total
Wt%	0.002	0.002	0.006	0.015	0.002	0.01	0.001	0.097	0.092	0.1	0.15	100

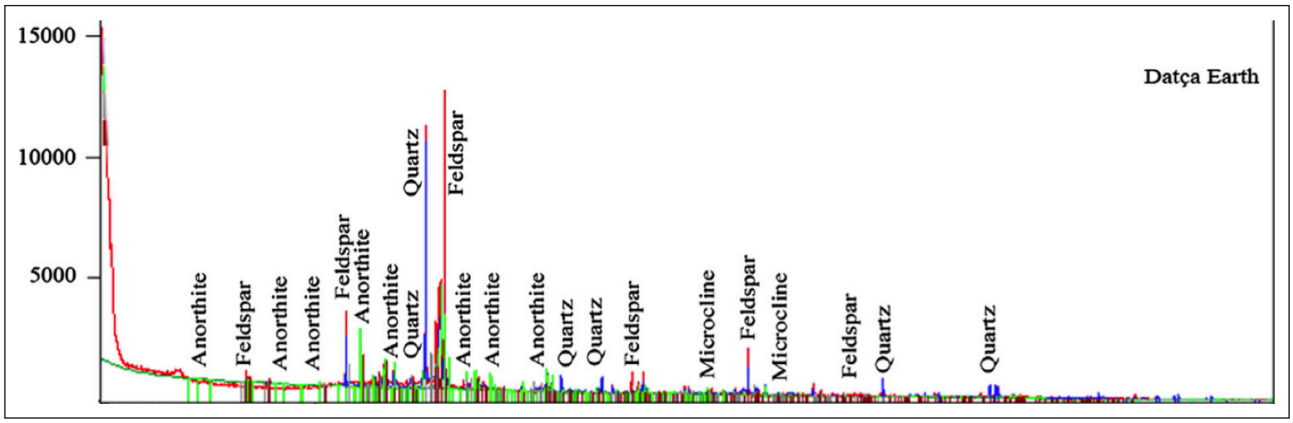

Figure 1. XRD analysis of natural Datça Pozzolan.

If the results are analyzed critically, the strength of the geopolymers cured under ambient conditions continues to increase for up to 90 days. On the other hand, in the geopolymers pre-cured at higher temperatures. However, the early strength increases because of the effect of the temperature. It may decrease in the long term depending on the source precursor. Strength development largely depends on the aluminosilicate precursor and alkali activator type, alkali concentration, activator ratio, curing type, temperature, and curing period. The novelty of this manuscript is that it investigates the development of the properties of natural pozzolan-based geopolymers over the long term by considering the effects of various alkali concentrations and activator ratios. Therefore, the effort to achieve the desired target strength must be determined experimentally for each mixture design. Thus, the objectives of this study are as follows: 1) to investigate the influence of long-term curing on the physical and mechanical properties of heat-cured Datça pozzolan-based geopolymers; 2) to determine the effect of alkali concentration and activator ratio on the long-term microstructural evolution of the geopolymer by evaluating the relationship between UPV and physical and mechanical properties, and 3) to predict the geopolymer strength from UPV.

2. MATERIALS AND METHODS

Natural pozzolan [33], extracted from the Datça Peninsula in Türkiye, was used as an aluminosilicate source to produce geopolymer mortar. It was dried at 55 °C for 24 h and pulverized until a particle size of 95% less than 90 µm was obtained. It has a significantly high specific surface area (5467 cm^2/g) and a specific gravity of 2.52 g/cm^3. The chemical characterization results obtained using an X-ray fluorescence spectrometer (XRF) are presented in Table 1.

As can be seen, the most abundant oxides are pozzolanic oxides (SiO_2 and Al_2O_3), followed by K_2O and Na_2O. It can be accepted as a low-calcium pozzolan (1.22% CaO ≤5%) and classified as a dacitic pozzolan (63–77% SiO_2) because of its 75.2% SiO_2 content [1]. The mineralogical composition (X-ray diffraction, XRD) analysis indicated that the pozzolan consisted mainly of anorthite, quartz, feldspar, microcline, and a compound with an amorphous structure, as shown in Figure 1.

Liquid sodium silicate (Na_2SiO_3) with a 3.24 modulus (SiO_2/Na_2O) and technical-grade potassium hydroxide (KOH) were used for alkaline activation. KOH solutions with 7.5, 10, and 12.5 molarities (M) were prepared by dissolving KOH pellets in distilled water and allowing them to cool before being added to the mixture.

Since this study is based on the previous research of the authors [4], the mixing ratios and initial curing conditions of the first seven days applied in the last study were taken as the basis. The sodium silicate (SS)-to-KOH ratios, termed "activator ratio," were 1.0, 1.5, 2.0, and 2.5. The total alkaline activator-to-binder ratio was kept constant at 0.30 by weight. Standard quartz sand was used with a maximum grain size of 2.0 mm in conformity with TS EN 196-1 [34]. The dry pozzolan/sand ratio was 1/3, and the mortar flow was maintained at 60.

The slurry was cast into prismatic molds with dimensions of 40x40x160 mm. The following curing method was applied: (i) first, curing at 20 °C and 95±5% RH for 24 h, and curing at 90 °C and 95±5% RH for 24 h; (ii) after demolding the specimens, curing at 20 °C and 55±5% RH until testing at 7, 90, and 365 days.

The specimens were coded in [XM-X-X] format: "XM" represents the molarity (M) of KOH, the second group indicates the activator ratio and the third group indicates the curing duration. To ensure reproducibility, three specimens

were prepared for each test; only the compressive strength test was applied to six specimens. The specimens were tested for unit weight (Δ) and specific gravity according to TS EN 1015-10 [35], water absorption under atmospheric pressure (Sa) according to TS EN 13755 [36], dynamic ultrasound velocity (UPV)/Young's modulus of elasticity (MoE) according to TS EN 14579 [37], and flexural (R_f) and compressive (R_c) strengths according to TS EN 196-1 [34].

3. RESULTS AND DISCUSSION

3.1. Effect of Heat Curing on the Properties of Mortars

All test results are given in Table 2, and the physical test results of the specimens cured for seven days are shown in Figure 2.

The porosity (P) and water absorption ratio (S_a) of the material decreased gradually, depending on the increase in the molarities from 7.5, 10 to 12.5 M, as well as the rise in activator ratios varying from 1, 1.5, 2 to 2.5 after seven days of curing. In parallel with these changes, unit weights gradually increased. According to the short error bars, no significant variations were observed in almost all physical properties. In the mortar series of 12.5 M, the water absorption ratio reduced at the fastest rate (0.86 times) on average. The water absorption ratio gives the pore volume ratio of the material to be larger than 0.1 microns that water could penetrate.

On the other hand, open porosity (S_h) is the ratio of open and interconnected pores that water can fill. If (P), (S_a), and (S_h) were analyzed concerning the effect of alkali molarity and activator ratios on pore structure, it could be determined that the micro and gel void ratios (≤0.1 μ) of the (7.5M-1.0–7) and (12.5M-2.5–7) mortars increased from 2% to 20%, respectively, 13 times. An increase in the alkali molarity and alkali activator ratio promoted the formation of a more stable geopolymer gel with lower porosity [38]. However, the pore structure and morphology of the mortars should be further analyzed using mercury intrusion porosimetry (MIP) and scanning electron microscopy equipped with energy-dispersive X-ray spectroscopy (SEM-EDX). The saturation coefficient (SC) denotes the quality of the material in terms of frost resistance and is recommended to be lower than 80% for porous ceramics. All samples produced in this study, even after 365 days, indicated that a frost-resistant material was produced, as shown in Table 2.

The mortars produced in this study were microstructurally monitored using the UPV method. In this method, the ultrasonic pulse is coupled into the material from a transducer and undergoes multiple reflections at the boundaries of the different material phases within the material. A complex system of stress waves is developed that includes both longitudinal and shear waves propagating through the material. The pulse velocity (V) (in km/s or m/s) is given by:

$$V = l / t \quad (1)$$

Where (l) is the path length and (t) is the pulse's time to transverse that length. The pulse velocity (V) of longitudinal stress waves in a material is related to its elastic properties and unit weight according to the following relationship:

$$E_d = 10^5 x V^2 x \Delta / g \quad (2)$$

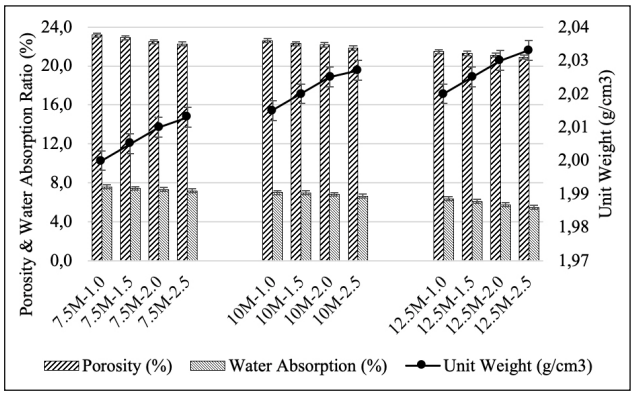

Figure 2. Comparison of the physical properties of mortars with different molarities (7.5, 10, and 12.5) and activator ratios (1, 1.5, 2, and 2.5) after seven days.

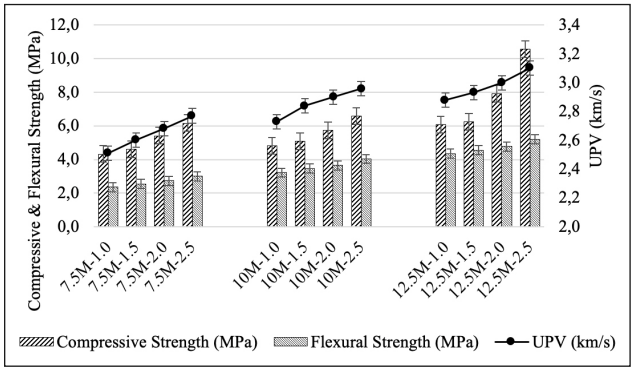

Figure 3. Comparison of the mechanical properties of mortars with different molarities (7.5, 10, and 12.5) and activator ratios (1, 1.5, 2, and 2.5) after seven days.

Where (E_d) is the dynamic modulus of elasticity (MoE), (V) is the pulse velocity, (Δ) is the unit weight of the material, and (g) is the gravitational acceleration (g:9.81m/s).

UPV values were measured on average at 2.64, 2. at 85, and 2.89 km/s, in parallel with the increase in molarity (7.5, 10, and 12.5 M) and activator ratio, UPV increased by 1.1 times on average, respectively. This indicates that the geopolymer evolved toward a more homogeneous structure without cracks or gaps that will reduce the ultrasound velocity by absorption or dispersion. The dynamic modulus of elasticity (MoE) of the material increased in parallel with (UPV) and unit weight (Table 2). MoE values increased by an average of 1.23 times as the molarity of the mortars increased and by an average of 1.20 times as the activator ratio increased.

Moreover, as the molarity concentration increased, the effectiveness of the activator ratio on all properties decreased. The elasticity modulus of cement-lime mortars (binder/sand ratio: 1:3) varies between 40% lime: 23 MPa and 80% lime: 11 MPa, depending on the lime content in the mortar. In this study, very close MoE values between 12.8 and 19.9 MPa were obtained in mortars in 7 days with the effect of heat cure at 90 °C [39]. With the same sand content, the MoE of cement mortars is given as 37.5 MPa. MoE is a measure of the stiffness of a material; in this sense, after seven days, more elastic mortars were produced than cement mortars.

Table 2. Test results of the specimens

Specimen codes of the series	Unit weight (Δ)	Porosity (P) (%)	Open porosity (S_h) (%) (S_a*Δ)	Water absorption (S_a) (%)	Saturation coefficient (SC) (%) (S_h/P)	Ultrasound pulse velocity (UPV) (km/s)	Modulus of elasticity (MoE) (GPa)	Compressive strength (R_c) (MPa)	Flexural strength (R_f) (MPa)
7.5M-1.0-7	2.00	23.18	15.22	7.61	66	2.51	12.84	4.32	2.35
7.5M-1.5-7	2.01	22.90	14.90	7.43	65	2.60	13.81	4.60	2.55
7.5M-2.0-7	2.01	22.50	14.69	7.31	65	2.68	14.71	5.41	2.73
7.5M-2.5-7	2.01	22.25	14.47	7.19	65	2.77	15.74	6.16	3.00
7.5M-1.0-90	2.02	21.40	14.13	7.00	62	2.71	15.12	6.30	3.02
7.5M-1.5-90	2.02	21.12	14.10	6.71	63	2.80	16.18	6.63	3.22
7.5M-2.0-90	2.03	19.91	13.81	6.48	62	2.89	17.30	7.66	3.39
7.5M-2.5-90	2.03	19.36	13.50	6.22	62	3.01	18.82	8.35	3.70
7.5M-1.0-365	2.02	20.90	12.89	6.59	60	2.75	15.78	7.21	3.11
7.5M-1.5-365	2.03	20.14	12.35	6.23	58	2.83	16.82	7.56	3.31
7.5M-2.0-365	2.03	19.27	11.69	6.00	55	2.92	17.95	8.53	3.52
7.5M-2.5-365	2.03	18.67	11.14	5.86	53	3.06	19.81	9.10	3.77
10M-1.0-7	2.02	22.62	14.14	7.01	66	2.73	15.31	4.82	3.21
10M-1.5-7	2,03	22.30	13.59	6.98	64	2.84	16.61	5.10	3.47
10M-2.0-7	2.03	22.17	13.17	6.82	66	2.90	17.36	5.74	3.65
10M-2.5-7	2.04	21.84	12.68	6.66	65	2.96	18.10	6.59	4.03
10M-1.0-90	2.03	20.47	12.24	6.03	60	2.97	18.25	7.03	3.91
10M-1.5-90	2.04	20.08	11.99	5.89	60	3.05	19.30	7.41	4.07
10M-2.0-90	2.04	19.23	11.67	5.71	61	3.10	20.01	8.02	4.32
10M-2.5-90	2.05	18.91	11,39	5.56	60	3.20	21.38	8.76	4.60
10M-1.0-365	2.04	19.82	11.02	5.75	57	3.00	18.85	7.90	3.97
10M-1.5-365	2.04	19.01	10.77	5.63	58	3.09	20.07	8.25	4.15
10M-2.0-365	2.05	18.28	9.92	5.49	56	3.15	20.96	8.78	4.44
10M-2.5-365	2.06	17.31	9.31	5.34	56	3.28	22.83	9.50	4.79
12.5M-1.0-7	2.05	21.47	13.49	6.38	65	2.88	17.08	6.07	4.35
12.5M-1.5-7	2.06	21.29	12.83	6.10	64	2.93	17.72	6.25	4.56
12.5M-2.0-7	2.07	21.10	12.39	5.76	64	3.00	18.62	7.90	4.77
12.5M-2.5-7	2.08	20.90	12.16	5.48	65	3.10	19.92	10.57	5.20
12.5M-1.0-90	2.06	19.50	11.82	5.41	60	3.12	20.21	9.25	5.20
12.5M-1.5-90	2.06	18.47	11.61	5.28	61	3.16	20.77	9.71	5.38
12.5M-2.0-90	2.07	17.62	11.38	4.84	62	3.25	22.07	11.35	5.57
12.5M-2.5-90	2.08	16.50	11.12	4.53	64	3.31	22.95	14.57	5.88
12.5M-1.0-365	2.06	18.90	10.40	5.05	55	3.21	21.64	10.13	5.38
12.5M-1.5-365	2.07	18.02	9.52	4.61	53	3.25	22.23	10.55	5.56
12.5M-2.0-365	2.08	16.93	9.17	4.42	54	3.32	23.31	12.00	5.75
12.5M-2.5-365	2.09	15.77	8.53	4.09	54	3.37	24.13	15.32	6.06

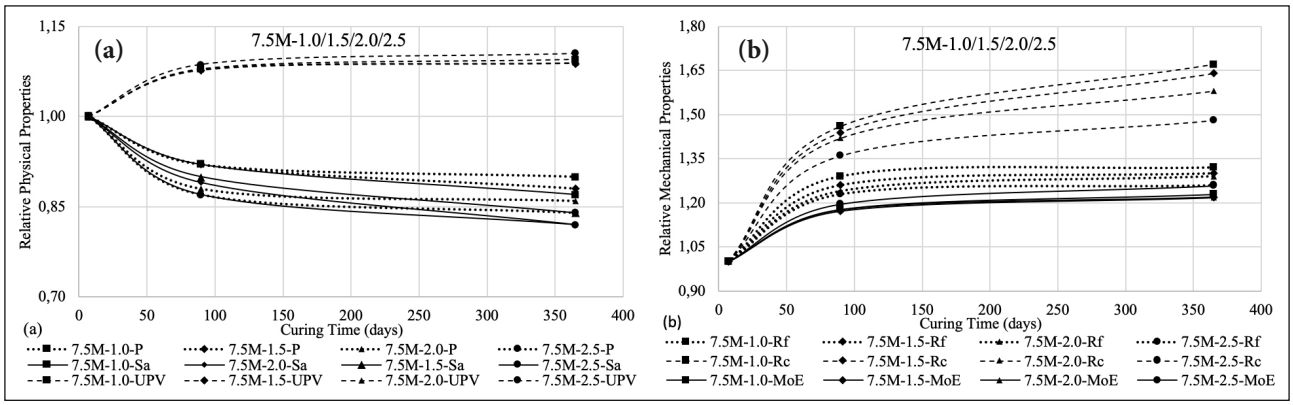

Figure 4. Graph of relative properties as a function of curing duration: **(a)** physical properties (P, S_a, Δ) at 7.5 M; **(b)** mechanical properties (R_c, R_f, UPV) at 7.5 M.

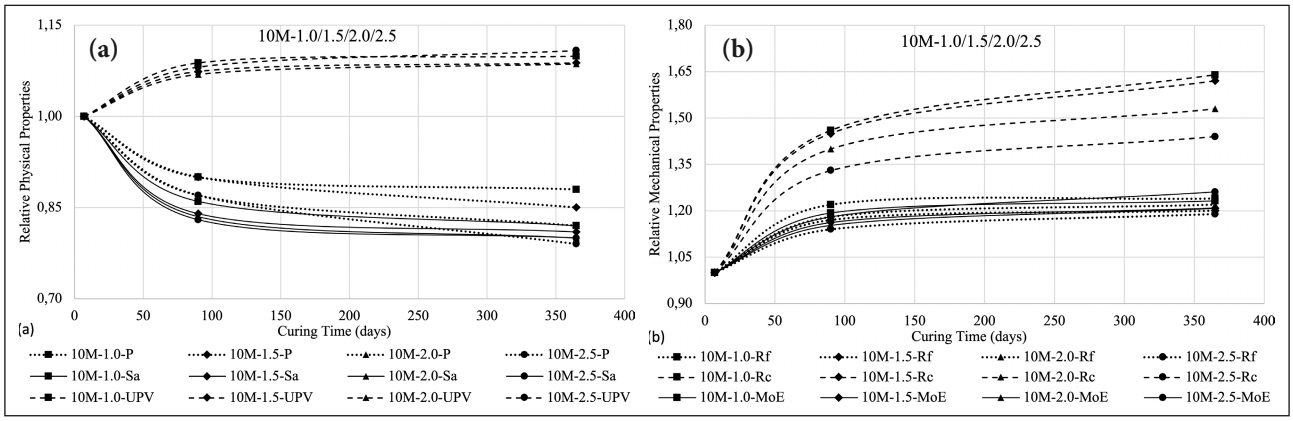

Figure 5. Graph of relative properties as a function of curing duration: **(a)** physical properties (P, S_a, Δ) at 10 M; **(b)** mechanical properties (R_c, R_f, UPV) at 10 M.

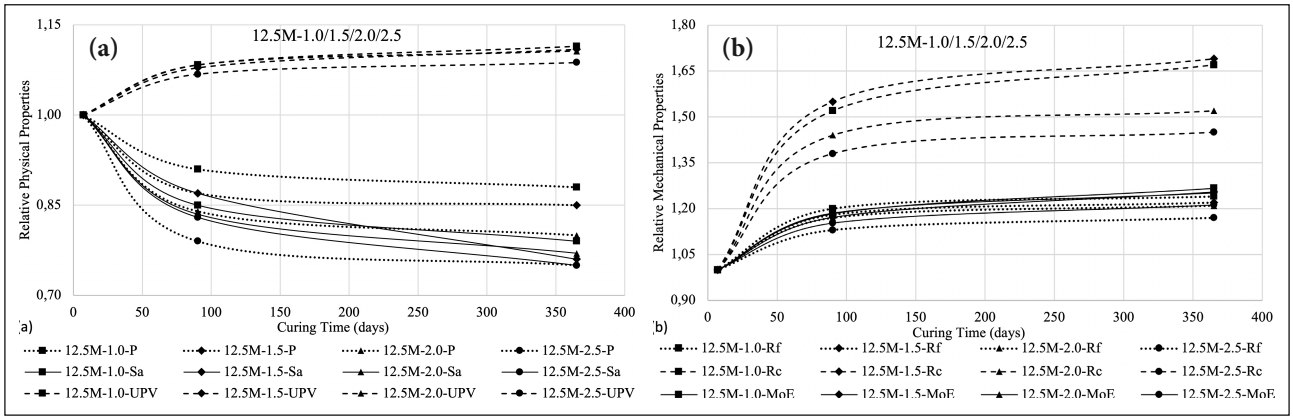

Figure 6. Graph of relative properties as a function of curing duration: **(a)** physical properties (P, S_a, Δ) at 12.5 M; **(b)** mechanical properties (R_c, R_f, UPV) at 12.5 M.

The rising trend observed in the material's mechanical strength after seven days of curing was parallel to its physical properties (Fig. 3). The shorter error bars in Figure 3 indicate less uncertainty in the test results. According to the 7-day compressive strength (R_c) results, an increase in (R_c) was determined depending on the rise in both molarities (7.5, 10, 12.5) and activator ratio (1.0, 1.5, 2.0, 2.5). On the 7-day, the (R_c) of 12.5 M was 1.50 and 1.38 times higher than R_c) values of 7.5 and 10 M, respectively. Therefore, the 12.5 M concentration resulted in mechanical properties at seven days. This improvement, which was detected by increasing the molarity of the activator, may be explained by the fact that higher concentrations of alkali hydroxides enhance the dissolution of Datça pozzolan as an aluminosilicate source. The higher amount of dissolved Si and Al in the reaction zone favors the development of a continuous polycondensation reaction [40] with a three-dimensional structure (NASH gel).

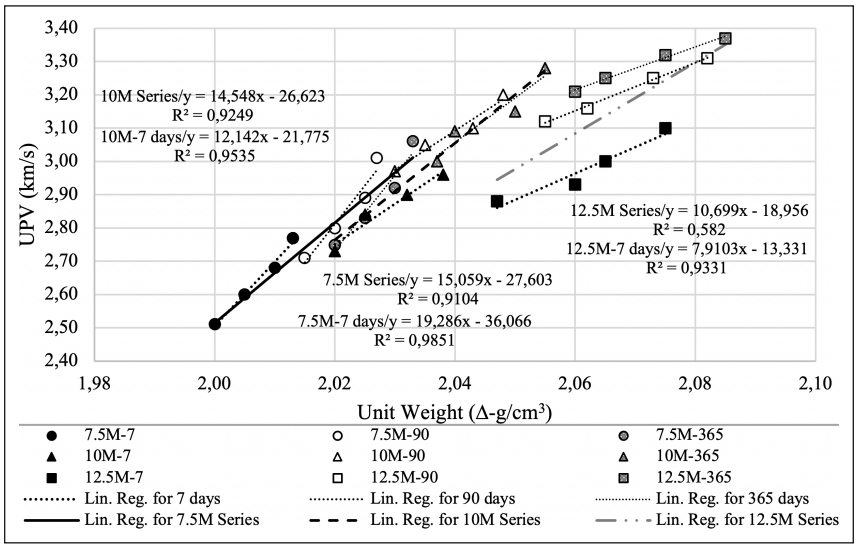

Figure 7. Ultrasound pulse velocities (UPV) of the mortar series (7.5, 10, and 12.5 M) as functions of unit weight (Δ).

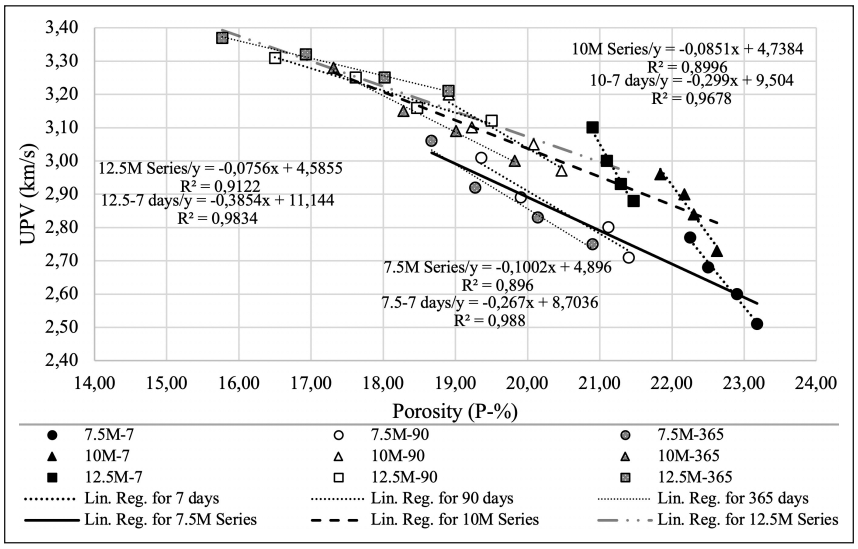

Figure 8. Ultrasound pulse velocities (UPV) of the mortar series (7.5, 10, and 12.5 M) as functions of porosity (P).

The increase in compressive strength (R_c) due to the higher activator ratio (SS/K), mainly when the activator ratio is 2 and 2.5, indicates a higher sodium silicate (SS) content in the mixture and can be explained as follows: (i) SS enhances the dissolution rate of Si and Al in the aluminosilicate source; (ii) Al ions dissolve quickly in the alkali medium because the Al–O bonds of the aluminosilicate source are weaker than the Si–O bonds. As a result, more Si ions in the reaction medium may increase the degree of geopolymerization [41]. In addition, more SS in the mixture also leads to stronger ion-pair formation, which leads to more long-chain silicate oligomers. The longer-chain silicate oligomers mean the NASH gel is more easily formed [42]. Furthermore, a geopolymer binder with a more homogeneous structure with high silica availability was obtained in the early stages [38]. Thus, a higher activator ratio of the geopolymer mixture is important to support the development of geopolymerization reactions on day 7. As a result, heat curing at 90 °C benefited the strength development by improving the physical properties of the mortars after seven days.

3.2. Effect of Curing Duration on the Properties of Mortars

The geopolymer mortars' relative physical and mechanical properties with 7.5, 10, and 12.5 molarities and activator ratios of 1, 1.5, 2, and 2.5 as functions of curing duration are shown in Figures 4–6.

Effect of Curing Duration on the Activator Ratio: As the curing time progressed, the improvement in the physical and mechanical properties of the mortars with lower activator ratios was greater in all mortars with 7.5, 10, and 12.5 M concentrations. Because the properties of the mortar with a high activator ratio already reached their highest value at the end of the 7-day cure, the increase in the long term slowed down. That is, the densification and continuous formation of the geopolymer matrix increased as the activator ratio decreased. While this improvement was more effective in the first 90 days, it lost its efficiency between 90 and 365 days. Despite the relatively low rate of improvement in the physical properties at all activator

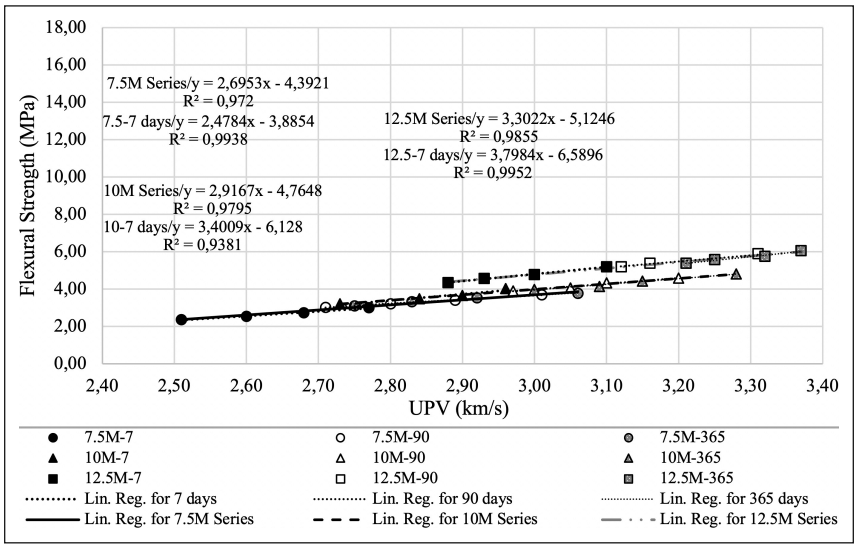

Figure 9. Flexural strengths (R_f) of the mortar series (7.5, 10, and 12.5 M) as functions of (UPV).

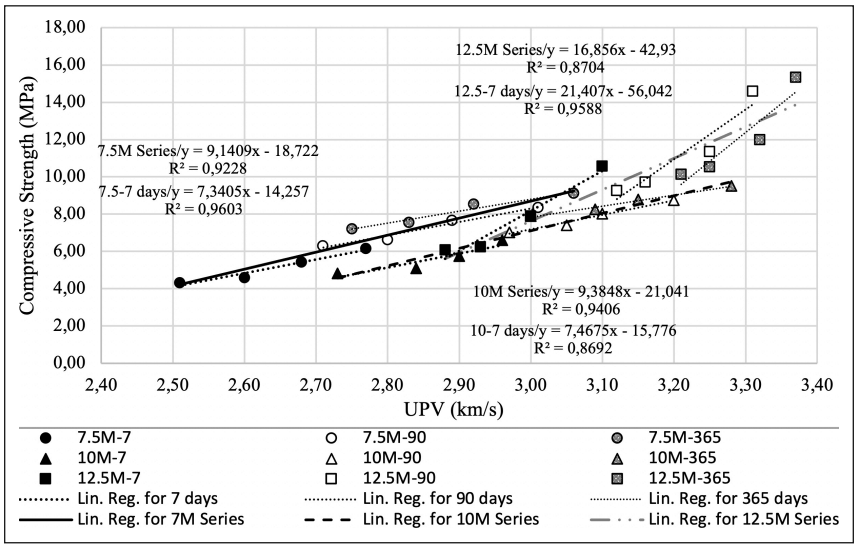

Figure 10. Compressive strengths (R_c) of the mortar series (7.5, 10, and 12.5 M) functions of (UPV).

ratios, a significant increase in the compressive strengths was observed. This increased rate, again, which was higher at lower activator ratios, took lower values in parallel with the increase in activator ratios. The strength of a material is closely related to its fine-grained microstructure and low porosity. The inverse relationship between the porosity, UPV, water absorption, and the strengths of all mortars was obtained accordingly.

Although the time-dependent increase rate in the 12.5 M and 2.5 activator ratio specimen, which gave the highest mechanical properties in 7-day curing, was at the lowest level, its mechanical properties at 90 and 365 days were still the highest. In other words, the increased efficiency in the first seven days in the development of geopolymerization reactions also positively reflected the results obtained in the later period.

Effect of Curing Duration on Alkali Concentration: The changes detected in the properties of the geopolymer mortars revealed that the material transformed into a more compact microstructure and improved structurally over time. However, the improvement rate in mortar properties was negligible between 90 and 365 days, compared with 7 to 90 days. These findings are incompatible with the research results of colemanite and metakaolin-based geopolymer mortar, which claim that rapidly developing reaction products by pre-curing at 60 °C for 72 h have a negative influence on the long-term microstructure and strength properties of the material [25]. This emphasizes that the aluminosilicate source, alkaline reactants, and their ratios play a role in developing the internal structure of geopolymers and the curing effect.

As expected from the decrease in porosity, the UPV values of 7.5, 10, and 12.5 M geopolymer mortars on the 365 days increased by an average of 1.09, 1.10, and 1.10 times compared with those obtained on day 7. While the average UPV values obtained in 7 days were 2.64, 2.86, and 2.98 km/s, respectively, these values increased to an average of 2.89, 3.13, and 3.29 km/s in 365 days. UPV values of less than three km/s indicate that the strength is very low due to excess voids [43]. UPV values within the scope of this

Table 3. Comparison of calculated and experimental results of compressive strengths (R_c)

Specimen code	R_c calc. (MPa)	R_c exp. (MPa)	Diff. (%)	Specimen code	R_c calc. (MPa)	R_c exp. (MPa)	Diff. (%)	Specimen code	R_c calc. (MPa)	R_c exp. (MPa)	Diff. (%)
7.5M-1.0-7	4.22	4.32	2.34	10M-1.0-7	4.57	4.82	5.55	12.5M-1.0-7	5.63	6.07	7.88
7.5M-1.5-7	5.04	4.60	8.80	10M-1.5-7	5.60	5.10	8.90	12.5M-1.5-7	6.47	6.25	3.40
7.5M-2.0-7	5.78	5.41	6.32	10M-2.0-7	6.16	5.74	6.83	12.5M-2.0-7	7.65	7.90	3.27
7.5M-2.5-7	6.60	6.16	6.64	10M-2.5-7	6.72	6.59	1.99	12.5M-2.5-7	9.34	10.57	13.22
7.5M-1.0-90	6.05	6.30	4.14	10M-1.0-90	6.82	7.03	3.12	12.5M-1.0-90	9.67	9.25	4.37
7.5M-1.5-90	6.87	6.63	3.52	10M-1.5-90	7.57	7.41	2.09	12.5M-1.5-90	10.35	9.71	6.16
7.5M-2.0-90	7.69	7.66	0.45	10M-2.0-90	8.04	8.02	0.21	12.5M-2.0-90	11.87	11.35	4.34
7.5M-2.5-90	8.79	8.35	5.02	10M-2.5-90	8.98	8.76	2.40	12.5M-2.5-90	12.88	14.57	13.15
7.5M-1.0-365	6.42	7.21	12.3	10M-1.0-365	7.10	7.90	11.2	12.5M-1.0-365	11.19	10.13	9.48
7.5M-1.5-365	7.15	7.56	5.79	10M-1.5-365	7.94	8.25	3.86	12.5M-1.5-365	11.87	10.55	11.08
7.5M-2.0-365	7.97	8.53	7.04	10M-2.0-365	8.51	8.78	3.22	12.5M-2.0-365	13.05	12.00	8.01
7.5M-2.5-365	9.25	9.10	1.60	10M-2.5-365	9.73	9.50	2.32	12.5M-2.5-365	13.89	15.32	10.31
Mean	6.82	6.82		Mean	7.31	7.33		Mean	10.32	10.31	
Standard deviation (s)	1.47	1.53		Standard deviation (s)	1.45	1.50		Standard deviation (s)	2.66	2.84	
Coefficient of variation (CV)	21.55	22.43		Coefficient of variation (CV)	19.83	20.46		Coefficient of variation (CV)	25.77	27.54	

study were determined to be in the range of 2.85–3.21 km/s even after 90 days of curing. The increase in UPV, MoE, and strength of the samples depending on the curing time may indicate the formation of a three-dimensional amorphous aluminosilicate structure (NASH gel) that fills the voids and bridges the unreacted pozzolan particles [13]. However, different morphologies were also detected, where a clear distinction was observed between the gel and unreacted particles, unlike the spherical shape of fly ash, which might cause the structure to become denser or more porous [9].

90% of the compressive strength could be obtained in one day in low-calcium FA-based geopolymers cured at 80–90 °C; however, when the same samples were cured under ambient conditions for a long time, the strength increased, similar to that of OPC cement. Therefore, long-term strength could be achieved under all curing conditions, and increasing the curing temperature only accelerates the change over time [44]. However, in our study, the compressive strength obtained in 365 days increased 1.56 times on average for all mortar series of 7.5, 10, and 12.5 M compared with the compressive strength obtained in the first seven days. Therefore, in the same mortars, with the triggering effect of curing at 90 °C (RH: 95%) for 24 h, the strengths obtained in the first seven days constituted only 64% on average of the strengths in 365 days. With the effect of the elapsed curing time, the highest strength development was obtained at the highest molar concentration ratio.

It is indicated for brittle materials that the flexural strength is often approximately 0.10 of the compressive strength [45]. The R_f/R_c ratios of 7.5, 10, and 12.5 M mortars were 0.51, 0.66, and 0.64 on average in 7 days, respectively, and decreased to an average of 0.42, 0.51, and 0.48 in 365 days, respectively. Over time, this decrease in the ratio indicates that the curing duration has a greater effect on the compressive strength and that the geopolymer has evolved into a more fragile structure. However, mortars still exhibit elastic behavior.

3.3. Effects of Alkali Concentration and Activator Ratio on the Long-Term Microstructural Evolution of Geopolymers

The non-destructive and continuous character of the investigations with ultrasound pulse velocity (UPV) makes it possible to take continuous measurements of the hydration kinetics, to indicate variations in the mix composition due to the mix formulation, and to assess the strength development of materials [46]. On the other hand, the compressive strength of a material is the most essential mechanical property and notably influences other properties, including density, porosity, flexural strength, and modulus of elasticity. However, the UPV technique cannot determine the strength of cementitious systems made of different materials consisting of various ingredients and proportions [47]. Therefore, to estimate the strengths of geopolymers from ultrasound velocity, the effects of alkali concentrations and activator ratios on long-term microstructural evolution were interpreted by correlating UPV with other macro properties such as porosity, unit weight, compressive strength, and flexural strength. The analysis was performed based on 7 and 365 days, as seven days represent the effect of heat curing on the geopolymerization of the mortar series, while 365 days represent the effect of the entire curing time.

Effect of Unit Weight and Porosity on the UPV: Ultrasound pulse velocities (UPV) of all mortar series, based on their different molarities (7.5, 10, and 12.5 M) as functions of unit weight (Δ) after 7, 90, and 365 days of curing, are depicted in Figure 7.

According to the (UPV) development observed after seven days of curing, as the molarities and activator ratios of the mortar series of 7.5, 10, and 12.5 M increased, (UPV) s increased as functions of unit weight (Δ). The slopes of the regression lines of each mortar series show how the changes influence the (UPV)s of the series in their (Δ)s. Accordingly, the mortar series of 7.5 M was the most affected, followed by the 10 and 12.5 M mortar series. The slopes of the regression lines reduced slowly toward higher molarities on the order of 7.5 M (m_7:19), 10 M (m_7:12), and 12.5 M (m_7:8).

Parallel to the increase in the activator ratio from 1 to 2.5, all properties, including (UPV) gradually improved. Initial heat curing accelerates hydroxide ions' activity and the amorphous aluminosilicates' dissolution rate. However, the initial release of Al is faster than that of Si, and the dissolved ions of aluminate precursors react with any silicate initially provided by the activating solution, leading to the formation of aluminosilicate gel phases. Therefore, sodium silicate solutions as activators have better mechanical properties than alkali hydroxide alone. However, as the molar concentrations gradually increased toward 10 and 12.5 M, the efficiency of the SS may decrease progressively. At low molar concentrations, the quantity of the alkali solution is the lowest, and the Si ions provided by SS become more efficient in the mixture. This might be why a higher rate of improvement was obtained in the long term when the activator ratio was low; that is, the improvement decreased inversely as the sodium silicate content of the mortar increased.

The same trend was also detected in the long-term curing results. The slopes of the mortar series of 7.5 and 10 M were almost the same (m_{365}:15), indicating similar (UPV) development as functions of (Δ) in time. On the other hand, the mortar series of 12.5 M had the lowest slope (12.5M m_{365}) in 365 days, indicating that their (UPV)s were least influenced by (Δ)s over time. Increasing the activator ratio from 1 to 2.5 increased the UPV at all molarities, but the most significant increase was in the 7.5 M series, which was 1.22-fold. Towards 10 and 12.5 M, the improvement rate decreased by 1.20 and 1.17 times, respectively. However, the unit weight increase at each molarity was only 1.02 times.

The rate of improvement in the (UPV)s of the mortar series of 7.5 M became 0.79 times slower at the longer curing duration of 365 days than that of the values obtained at seven days (m_7:19>m_{365}:15). On the other hand, both slopes of the mortar series of 10 M and 12.5 M increased 1.20 (m_7:12<m_{365}:14.5) and 1.35 times (m_7:7.9<m_{365}:10.6) respectively. Hence, in the long term, better structural improvements were detected for the mortar series of 10 and 12.5 M than in seven days. However, the (Δ) improvement was only in the 2.02–2.09 g range/cm^3, which can be considered negligible.

Although the regression lines of the mortar series of 7.5 and 10 M had strong correlation coefficients (R^2>0.90) between (UPV)s and (Δ)s at both 7 and 365 days, the mortar series of 12.5 M only had a strong correlation (R^2:0.93) at seven days; at later days of curing duration, the correlation coefficient between these properties dropped by 0.62 times (R^2:0.58) in 365 days. This significant decrease in the correlation coefficient may be because the 7-day UPV values of the 12.5 M series remain much lower than the 90 and 365-day values. For example, at the same unit weight value (2.06 g/cm^3), UPV values were obtained as 2.93 km/s in 7 days, 3.16 km/s in 90 days, and 3.21 km/h in 365 days. In other words, while the 90-day increase rate was 1.08 times the 7-day value, the increase rate between 90 and 365 days was lower, 1.01 times. Figure 8 shows the (UPV) values of all mortar series based on their different molarities (7.5, 10, and 12.5 M) as functions of porosity (P) after 7, 90, and 365 days.

There is an inverse relationship between these two properties, as expected. As the (P)s of the mortar series increased, the (UPV) values decreased in the descending order of 12.5, 10, and 7.5 M. The increment of activator ratios from 1 to 2.5 also positively influenced the reduction of P values. Again, in the 7.5 M mortars, the rate rose in porosity, and the rate rose in UPV was the highest. After seven days of curing, even the negative slopes of the regression lines for each mortar series were almost the same (m_7:-0.3) and strongly correlated with an average of R^2=0.97. The same inverse trend was observed for long-term curing. The slopes of all mortar series were almost the same (m_{365}:-0.08), indicating similar (UPV) development as functions of (P) over time. The regression lines of each molarity also define the existence of a strong correlation ($7.5M_{365}$ and $10M_{365}$: R^2=0.89 and 12.5 M_{365}: R^2=0.91) between the two properties.

The negative slopes of the regression lines of the (UPV) s of all mortar series as functions of (P) at seven days dropped by 0.27 times (m_7:-0.3> m_{365}:-0.08) on average in the long-term curing of 365 days. Although the decrease in the porosity of the mortars changed the UPV to a lower level, mortars continued to develop their geopolymerization at a slower rate. Densification of solid phases increased the ultrasound pulse velocity of the material; however, since the reaction rate declined gradually, the UPV increased at a slower rate in the long term.

Effect of UPV on the Mechanical Properties: The flexural strengths (R_f) of all mortar series, based on their different molarities (7.5, 10, and 12.5 M) as functions of (UPV) after 7, 90, and 365 days of curing, are depicted in Figure 9.

As the molarities and activator ratios of the mortar series increased, (R_f) increased as a function of (UPV). The slopes of the regression lines of all mortar series were almost identical and in strong correlation (7.5 M: m_7:2.4, R^2=0.99; 10 M: m_7:3.4, R^2=0.93; 12.5 M m_7:3.7, R^2=0.99) after seven days. The same trend was also detected in long-term curing. The slopes of the regression lines obtained for the 7.5 M (m_{365}:2.7), 10 M (m_{365}:2.9), and 12.5 M (m_{365}:3.3) mortar series were also close to each other with a strong correlation after 365 days (7.5M: R^2: 0.97, 10M: R^2: 0.98 and 12.5M: R^2: 0.99).

Compared with the change in UPV, the increase in flexural strength (R_f) at a lower rate than the compressive strength (R_c) may indicate that the material has turned into a more brittle structure.

The compressive strengths (R_c) of all mortar series (7.5, 10, and 12.5 M) as functions of (UPV) after 7, 90, and 365 days of curing are depicted in Figure 10. The compressive strength is a good indicator of the degree of geopolymerization.

According to the (R_c) development after seven days, as the molarities and activator ratios of the mortars increased, (R_c)s increased as functions of (UPV) for each of the mortar series of 7.5, 10, and 12.5 M. The slopes of the regression lines for the mortar series of 7.5 M and 10 M were almost identical (7.5M and 10M: m_7:7.4) but lower than the slope of the mortar series of 12.5 M (12.5M: m_7:21.4); the higher slope indicates a higher rate of initial strength development as a function of UPV. The same trend was observed in the long term. The slopes of the regression lines of the mortar series of 7.5 M and 10 M were compatible (7.5 M and 10 M: m_{365}: 9), indicating the existence of a similar solid-state development in (R_c). In addition, the magnitude of the correlation coefficients was relatively high (7.5 M36: R^2: 0.92 and 10 M_{365}: R^2: 0.94).

On the other hand, the mortar series of 12.5 M had the highest slope and the lowest (correlation coefficient 12.5 M: m_{365}: 16.8, R^2: 0.87) in the long term. The reason for this decrease was the sudden increase in the compressive strength of the sample coded (12.5 M-2.5) in 90 and 365 days. However, despite this decrease, it is still 0.87, and the relationship between the two variables is generally considered strong when the "R^2" value is larger than 0.7.

At the same speed as ultrasound, the 7.5 M series with the lowest molar concentration is higher than 10 M. At the end of the 365 days, the compressive strengths of 7.5 M and 10 M become almost equal, while 7.5 M remains more porous. In geopolymers, higher strength can be achieved with a more porous structure. Similarly, a study comparing natural pozzolan-based geopolymer and OPC concrete observed that the UPV values of both materials increased as the curing time increased. Still, the UPV of geopolymer mortars remained lower at the same or higher compressive strengths than concrete [28]. On the other hand, the 12.5 M series maintains its already high compressive strength and relatively tight pore structure in 365 days.

At 365 days, the correlation coefficients between UPV and other properties decreased slightly, except for the slight increase observed for the UPV-R_c and UPV-R_f relationship of the 10 M series. This may imply that the geopolymerization of the mortars occurred very quickly because of the curing effect at 90 °C, and a sufficiently dense structure was formed after seven days. The fact that this process took place in a closed environment and the subsequent curing at ambient temperature for a relatively short period may have improved the correlation between the mortar properties. The last stage of the reaction process, solid-state transformation, involves the continual arrangement of the gel toward three-dimensional geopolymer networks and requires long-term termination. It might have been affected by slight ambient humidity and temperature changes, causing the relationship between properties to change relatively.

The regression lines of the mortar series at 7.5 M (m_7: 7.3 and m_{365}: 9.1) and 10 M (m_7: 7.4 and m_{365}: 9.3) have almost the same slopes at both curing times. The slope of the regression line of 12.5 M drops by 0.79 times at their 365-day curing time (m_7: 21.4 and m_{365}: 16.8). This indicates the occurrence of a lower rate of geopolymerization reaction at curing times longer than seven days for the 12.5 M mortars. It may be concluded from the similar trends of the regression lines at both curing durations (at seven 365 days-day) of each mortar series of 7.5, 10, and 12.5 M that there is a mechanical and physical improvement with time. This may show that the material's compressive strength (R_c) could be estimated through its (UPV) for the mortars under consideration in this study.

When all mortar types at 365 days are considered, the linear correlation between compressive strength (R_c) and (UPV) (R_c= f(v)) can be expressed by the following equation:

$$R_c = a \times V + b \quad (3)$$

"a" gives the slope (m) of the regression lines, which change to 9.14 (for 7.5 M), 9.38 (for 10 M), and 16.86 (for 12.5). "b" is 18.7, 21.04, and 42.93 for 7.5, 10, and 12.5 M mortars, respectively, as expressed by the following formulas:

$$7.5M/R_c = 9.14 \times V - 18.72 \quad (4)$$

$$10M/R_c = 9.38 \times V - 21.04 \quad (5)$$

$$12.5M/R_c = 16.86 \times V - 42.93 \quad (6)$$

There is an inverse V (UPV) - porosity (P) relationship with a high level of correlation in all mortar series (m_{365}:-0.08, R^2=0.90); hence, not only the mechanical properties but also the pore structures improve.

By considering Equations 4, 5, and 6 given above as representative of the compressive strength (R_c)–(V) relationship of the mortar series of 7.5, 10, and 12.5 molarities, the experimental values of V (UPV) of all the specimens, as shown in Table 2, were used to estimate the compressive strength. The estimated strength values were compared with the measured experimental values (Table 3). The standard deviation (s) and coefficient of variation (CV) values for 7.5, 10, and 12.5 M series were found to be (1.47–21.55), (1.45–19.83), and (2.66–25.77) respectively. (CV) of the 10 M, which is 19.83%, indicates that the "fitting" is most satisfactory. According to the compressive strength (R_c) values calculated for each mortar type, there is an approximately two-fold increment in 365 days compared to 7 days: 7.5M=2.19, 10M=2.13, and 12.5M=2.46.

Suppose the (UPV) of 3 km/s, accepted as the quality limit in concrete, is also taken as a limit value for the geopolymer mortars produced in this study. The geopolymer mortars with different molarities and activator ratios can be selected based on their expected performance. Accordingly, the range of physical and mechanical properties above three km/s (UPV) may be given as follows:

- Unit weight (Δ) ranges from 2.03–2.09 g/cm^3
- Porosity (P) varies between 15.77 and 21.10% (9.01–25.84% for geopolymers)
- Open porosity (S_h) varies between 8.53 and 13.50%
- Water absorption (S_a) varies between 4.09 and 6.22% (8–18% for bricks)
- The saturation coefficient (SC) varies between 53 and 62% (<80%)
- Ultrasound pulse velocity (UPV) varies between 3.00 and 3.37 km/s
- The modulus of elasticity (MoE) varies between 18.1 and 24.13 GPa (11–23 GPa for cement-lime mortars (1:3)
- Compressive strength (R_c) varies between 7.41 and 15.32 MPa (≥10 MPa for hydraulic cement)
- Flexural strength (R_f) varies between 3.70 and 6.06 MPa (1.5–3.5 MPa for concrete) [48].

Geopolymer concrete has a high environmental impact on categories other than global warming due to the heavy effect of the production of sodium silicate solution [49]. Hence, selecting mortar types with lower molarities and activator ratios produced within the scope of the study that fulfill the required performance is possible because of the positive effect of curing duration on the properties of geopolymer mortars proven in this study.

4. CONCLUSION

In line with the results obtained throughout the study, the following remarks can be made:

- The Earth of Datça, as a natural pozzolan precursor, has promising characteristics for use as a geopolymer mortar and should be encouraged for practical use as a green building material.
- The initial heat curing regime (24 h at 90 °C) is appropriate for the natural pozzolan-based geopolymer considered in this study because it facilitates the early-age reaction process without restricting the transformation to a compact microstructure in the long term. Moreover, it provides some advantages for practical purposes, such as shortening of demoulding time and early development of strength.
- The initial heat-curing regime had a positive effect on strength development in the early period as well as in the long term. The microstructure and strength properties of the geopolymer continued to progress for up to 365 days. There was an almost twofold improvement after 365 days. The improvement rate between 90 and 365 days was negligible compared with the 7–90 days.
- The rate of increase in the physical and mechanical properties was higher when the activator ratio was low (1.0 and 1.5). In other words, the rate of improvement in the properties decreased inversely with increasing sodium silicate content of the mortar.
- Geopolymer mortars with 12.5 M and 2.5 activator ratios had the highest mechanical properties after 7 and 365 days. However, because of the heavy environmental impact of sodium silicate solution production, selecting geopolymer mortars with lower molarities and activator ratios became possible when considering the positive influence of curing duration on the microstructure of the geopolymers, as proven in this research.
- An increasing trend was observed in the plot of compressive strengths as functions of UPV parallel with the increase in the alkali content of the geopolymer, and the slope values presented a strongly related linear function relation. Finally, the outcomes of this study provide a possible method to assess the strength of natural pozzolan-based geopolymers from ultrasound pulse velocity measurements.
- In this study, the variations in the solid-state transformation of the mortars were monitored by ultrasound and evaluated along with the physical and mechanical properties. However, further research is recommended using advanced measurement techniques to examine mortars' morphology and microstructure development.

ACKNOWLEDGEMENTS

The authors gratefully acknowledge the assistance of İbrahim Öztürk from the Building Materials Laboratory, ITU, Faculty of Architecture.

ETHICS

There are no ethical issues with the publication of this manuscript.

DATA AVAILABILITY STATEMENT

The authors confirm that the data that supports the findings of this study are available within the article. Raw data that support the finding of this study are available from the corresponding author, upon reasonable request.

CONFLICT OF INTEREST

The authors declare that they have no conflict of interest.

FINANCIAL DISCLOSURE

The authors declared that this study has received no financial support.

USE OF AI FOR WRITING ASSISTANCE

Not declared.

PEER-REVIEW

Externally peer-reviewed.

REFERENCES

[1] Robayo-Salazar, R. A., & de Gutiérrez, R. M. (2018). Natural volcanic pozzolans as an available raw material for alkali-activated materials in the foreseeable future: A review. *Constr Build Mater, 189*, 109–118. [CrossRef]

[2] Tanaçan, L., Kaya, K., & Yıldırım, E. (2022). Sustainable building material and technology [Sürdürülebilir yapı malzemesi ve teknoloji]. *İTÜ Vakıf Derg, 90*, 14–23.

[3] Singh, N. B., & Middendorf, B. (2020). Geopolymers as an alternative to portland cement: An overview. *Constr Build Mater, 237*, 117455. [CrossRef]

[4] Barış, K. E., & Tanaçan, L. (2021). Improving the geopolymeric reactivity of Earth of Datça as a natural pozzolan in developing green binder. *J Build Eng, 41*, 102760. [CrossRef]

[5] Jiang, D., Shi, C., & Zhang, Z. (2022). Recent progress in understanding the setting and hardening of alkali-activated slag (AAS) materials. *Cem Concr Comp, 134*, 104795. [CrossRef]

[6] Wang, K., Shah, S. P., & Mishulovich, A. (2004). Effects of curing temperature and NaOH addition on hydration and strength development of clinker-free CKD-fly ash binders. *Cem Concr Res, 34*(2), 299–309. [CrossRef]

[7] Nath, P., & Sarker, P. K. (2015). Use of OPC to improve the setting and early strength properties of low calcium fly ash geopolymer concrete cured at room temperature. *Cem Concr Comp, 55*, 205–214. [CrossRef]

[8] Hardjito, D., Wallah, S. E., Sumajouw, D. M. J., & Rangan, B. V. (2004). On the development of fly ash-based geopolymer concrete. *ACI Mater J, 101*, 467–472. [CrossRef]

[9] Djobo, J. N. Y., Elimbi, A., Tchakouté, H. K., & Kumar, S. (2016). Volcanic ash-based geopolymer cements/concretes: The current state of the art and perspectives. *Environ Sci Pollut Res, 24*, 4433–4446. [CrossRef]

[10] González-García, D. M., Téllez-Jurado, L., Jiménez-Álvarez, F. J., Zarazua-Villalobos, L., & Balmori-Ramírez, H. (2022). Evolution of a natural pozzolan-based geopolymer alkalized in the presence of sodium or potassium silicate/hydroxide solution. *Constr Build Mater, 321*, 126305. [CrossRef]

[11] Tuyan, M., Andiç-Çakir, O., & Ramyar, K. (2018). Effect of alkali activator concentration and curing condition on strength and microstructure of waste clay brick powder-based geopolymer. *Compos Part B Eng, 135*, 242–252. [CrossRef]

[12] He, J., Jie, Y., Zhang, J., Yu, Y., & Zhang, G. (2013). Synthesis and characterization of red mud and rice husk ash-based geopolymer composites. *Cem Concr Comp, 37*, 108–118. [CrossRef]

[13] Haruna, S., Mohammed, B. S., Wahab, M., Kankia, M. U., Amran, M., & Gora, A. M. (2021). Long-term strength development of fly ash-based one-part alkali-activated binders. *Materials, 14*(15), 4160. [CrossRef]

[14] Athira, V. S., Bahurudeen, A., Saljas, M., & Jayachandran, K. (2021). Influence of different curing methods on mechanical and durability properties of alkali activated binders. *Constr Build Mater, 299*, 123963. [CrossRef]

[15] Heah, C. Y., Kamarudin, H., Mustafa Al Bakri, A. M., Binhussain, M., Luqman, M., Khairul Nizar, I., Ruzaidi, C. M., & Liew, Y. M. (2011). Effect of curing profile on kaolin-based geopolymers. *Phys Procedia, 22*, 305–311. [CrossRef]

[16] Chindaprasirt, P., Chareerat, T., & Sirivivatnanon, V. (2007). Workability and strength of coarse high calcium fly ash geopolymer. *Cem Concr Comp, 29*(3), 224–229. [CrossRef]

[17] Naghizadeh, A., Ekolu, S. O., Tchadjie, L. N., & Solomon, F. (2023). Long-term strength development and durability index quality of ambient-cured fly ash geopolymer concretes. *Constr Build Mater, 374*, 130899. [CrossRef]

[18] Raut, A. N., Murmu, A. L., & Alomayri, T. (2023). Physico-mechanical and thermal behavior of prolong heat cured geopolymer blocks. *Constr Build Mater, 370*, 130309. [CrossRef]

[19] Bing-hui, M., Zhu, H., Xue-min, C., Yan, H., & Si-yu, G. (2014). Effect of curing temperature on geopolymerization of metakaolin-based geopolymers. *Appl Clay Sci, 99*, 144–148. [CrossRef]

[20] Yılmaz, A., Degirmenci, F. N., & Aygörmez, Y. (2023). Effect of initial curing conditions on the durability performance of low-calcium fly ash-based geopolymer mortars. *Boletín de la Soc Española de Cerámica y Vidrio, 2023*, 398. [CrossRef]

[21] Yang, X., Wu, S., Xu, S., Chen, B., Chen, D., Wang, F., Jiang, J., Fan, L., & Tu, L. (2024). Effects of GBFS content and curing methods on the working performance and microstructure of ternary geopolymers based on high-content steel slag. *Constr Build Mater, 410*, 134128. [CrossRef]

[22] Ferone, C., Colangelo, F., Cioffi, R., Montagnaro, F., & Santoro, L. (2011). Mechanical performances of weathered coal fly ash based geopolymer bricks. *Procedia Eng, 21*, 745–752. [CrossRef]

[23] Muñiz-Villarreal, M. S., Manzano-Ramírez, A., Sampieri-Bulbarela, S., Ramón Gasca-Tirado, J., Reyes-Araiza, J. L., Rubio-Ávalos, J. C., Pérez-Bueno, J. J., Apatiga, L. M., Zaldivar-Cadena, A., & Amigó-Borrás, V. (2011). The effect of temperature on the geopolymerization process of a metakaolin-based geopolymer. *Mater Lett, 65*(6), 995–998. [CrossRef]

[24] Kim, H., & Kim, Y. (2013). Relationship between compressive strength of geo-polymers and pre-curing conditions. *Appl Microscopy, 43*(4), 155–163. [CrossRef]

[25] Aygörmez, Y., Canpolat, O., & Al-Mashhadani, M. M. (2020). A survey on one year strength performance of reinforced geopolymer composites. *Constr Build Mater, 264*, 120267. [CrossRef]

[26] Zuhua, Z., Xiao, Y., Huajun, Z., & Yue, C. (2009). Role of water in the synthesis of calcined kaolin-based geopolymer. *Appl Clay Sci, 43*(2), 218–223. [CrossRef]

[27] Perera, D. S., Uchida, O., Vance, E. R., & Finnie, K. S. (2006). Influence of curing schedule on the integrity of geopolymers. *J Mater Sci, 42*, 3099–3106. [CrossRef]

[28] Bondar, D., Lynsdale, C. J., Milestone, N. B., Hassani, N., & Ramezanianpour, A. A. (2011). Engineering properties of alkali-activated natural pozzolan concrete. *ACI Mater J, 108*(1), 1–9. [CrossRef]

[29] Dai, X., Ren, Q., Aydin, S., Yardimci, M. Y., & De Schutter, G. (2023). Accelerating the reaction process of sodium carbonate-activated slag mixtures with the incorporation of a small addition of sodium hydroxide/sodium silicate. *Cem Concr Comp, 141*, 105118. [CrossRef]

[30] Chen, W., Li, Y., Shen, P., & Shui, Z. (2013). Microstructural development of hydrating portland cement paste at early ages investigated with non-destructive methods and numerical simulation. *J Nondestruct Eval, 32*, 228–237. [CrossRef]

[31] Azarsa, P., & Gupta, R. (2017). Electrical resistivity of concrete for durability evaluation: A review. *Adv Mater Sci Eng*, 8453095, 1–30. [CrossRef]

[32] Dai, X., Aydin, S., Yardimci, M. Y., Lesage, K., & De Schutter, G. (2022). Early age reaction, rheological properties and pore solution chemistry of NaOH-activated slag mixtures. *Cem Concr Comp, 133*, 104715. [CrossRef]

[33] Barış, K. E., & Tanaçan, L. (2017). Earth of Datça: Development of pozzolanic activity with steam curing. *Constr Build Mater, 139*, 212–220. [CrossRef]

[34] TS EN 196-1. (2009). Standard Specification for Methods of Testing Cement – Part 1: Determination of Strength. Ankara, TC: Turkish Standard Institution.

[35] TS EN 1015-10. (2001). Standard Specification for Methods of Test for Mortar for Masonry – Part 10: Determination of Dry Bulk Density of Hardened Mortar. Ankara, TC: Turkish Standard Institution.

[36] TS EN 13755. (2014). Standard Specification for Natural Stone Test Methods – Determination of Water Absorption at Atmospheric Pressure. Ankara, TC: Turkish Standard Institution.

[37] TS EN 14579. (2015). Standard Specification for Natural Stone Test Methods – Determination of Sound Speed Propagation. Ankara, TC: Turkish Standard Institution.

[38] Tchadjie, L. N., & Ekolu, S. O. (2017). Enhancing the reactivity of aluminosilicate materials toward geopolymer synthesis. *J Mater Sci, 53*, 4709–4733. [CrossRef]

[39] Kubica, J., & Gasiorowski, S. A. (2010). Mortar selection in design practice - description of the problems, solutions and requirements. *Archit Civ Eng Environ, 3*, 53–61.

[40] Panagiotopoulou, C. H., Kontori, E., Perraki, T. H., & Kakali, G. (2006). Dissolution of aluminosilicate minerals and by-products in alkaline media. *J Mater Sci, 42*, 2967–2973. [CrossRef]

[41] Nadoushan, M. J., & Ramezanianpour, A. A. (2016). The effect of type and concentration of activators on flowability and compressive strength of natural pozzolan and slag-based geopolymers. *Constr Build Mater, 111*, 337–347. [CrossRef]

[42] Xu, H., & Van Deventer, J. S. J. (2000). The geopolymerisation of alumino-silicate minerals. *Int J Miner Process, 59*(3), 247–266. [CrossRef]

[43] Postacıoğlu, B. (1986). Beton - Bağlayıcı Maddeler - Agregalar-2. Cilt. Istanbul, TC: Teknik Kitaplar Yayınevi.

[44] Farooq, F., Jin, X., Javed, M. F., Akbar, A., Shah, M. I., Aslam, F., & Alyousef, R. (2021). Geopolymer concrete as sustainable material: A state of the art review. *Constr Build Mater, 306*, 124762. [CrossRef]

[45] Carter, G. W., Cannor, A. M., & Mansell, D. S. (1982). Properties of bricks incorporating underground rice husks. *Build Environ, 17*(4), 284–291. [CrossRef]

[46] Tanaçan, L., Kurugöl, S., & Ersoy, H. Y. (2009). Investigation of ultrasonic pulse velocity-strength relationship of lime-pozzolan mortars. Fourth International ECOMATERIALS Symposium, Bayamo, Cuba.

[47] Demirboğa, R., Türkmen, I., & Karakoç, M. B. (2004). Relationship between ultrasonic velocity and compressive strength for high-volume mineral-admixtured concrete. *Cem Concr Res, 34*(12), 2329–2336. [CrossRef]

[48] Akman, S. (1990). Yapı Malzemeleri, 2nd ed. İstanbul, TC: ITÜ Matbaası.

[49] Habert, G., d'Espinose de Lacaillerie, J. B., & Roussel, N. (2011). An environmental evaluation of geopolymer based concrete production: Reviewing current research trends. *J Clean Prod, 19*(11), 1229–1238. [CrossRef]

Journal of Sustainable Construction Materials and Technologies
Web page info: https://jscmt.yildiz.edu.tr
DOI: 10.47481/jscmt.1383493

JSCMT
Journal of Sustainable Construction Materials and Technologies

Research Article

Effect of mineral admixtures and curing regimes on properties of self-compacting concrete

Chava VENKATESH*, M. V. Seshagiri RAO, Munugala PRAVEEN KUMAR, Chereddy SONALI SRI DURGA

Department of Civil Engineering, CVR College of Engineering, Vastunagar, Mangalpalli, Ibrahimpatnam, Ranga Reddy, Telangana, India

ARTICLE INFO

Article history
Received: 30 October 2023
Accepted: 16 December 2023

Key words:
Compressive strength, curing conditions, metakaolin, scanning electron microscope, self-compacting concrete

ABSTRACT

This study investigated the influence of mineral admixtures (fly ash, silica fume, metakaolin) and curing conditions (water immersion, polyethylene glycol, gunny bags, accelerated curing) on the properties of self-compacting concrete (SCC). The rheological properties, compressive strength, chloride penetration resistance, and microstructure were evaluated. Incorporating mineral admixtures improved the workability, strength (up to 53% increase), and durability of SCC compared to plain mixes, with 20% metakaolin replacement optimal. Water immersion curing enhanced the compressive strength (3–15% increase) and chloride resistance (up to 30% decrease in migration coefficient) owing to improved hydration and microstructural refinement. Mineral admixtures reduced the sensitivity of SCC to the curing method. Microstructural analysis showed higher density and additional C-S-H phases with mineral admixtures under wet curing. The study demonstrates that optimized SCC containing appropriate supplementary cementitious materials and proper external curing can achieve high performance.

Cite this article as: Venkatesh, C., Rao. M. V. S., Kumar, M. P., & Sonali Sri Durga, C. (2024). Effect of mineral admixtures and curing regimes on properties of self-compacting concrete. *J Sustain Const Mater Technol*, 9(1), 25–35.

1. INTRODUCTION

Self-compacting concrete (SCC) represents a significant advancement in concrete technology that has revolutionized the construction industry over the past two decades. SCC is characterized by its ability to flow and compact under its weight without requiring external vibration, even in densely reinforced structural elements [1, 2]. Compared to conventional vibrated concrete, SCC offers several benefits, such as faster construction, reduced noise and labor, excellent surface finishes, and improved durability [3]. Eliminating vibration also enables the fabrication of complex architectural forms and intricate structural shapes that were previously not feasible [4].

The unique properties of SCC are achieved by careful mix design optimization to obtain the necessary rheological performance in the fresh state. This involves using chemical admixtures like superplasticizers coupled with proportioning powders, aggregates, water, and air content to achieve adequate flowability, passing ability, and resistance to segregation [5, 6]. However, SCC has some challenges, too. The high powder content needed to achieve robust self-compacting characteristics increases material costs. The reduction in coarse aggregate content also tends to lower the modulus of elasticity and creep resistance compared to traditional concrete [7]. Concerns about inadequate consolidation in highly congested members must be addressed through proper mix design and quality control [8].

***Corresponding author.**
*E-mail address: chvenky288@gmail.com

A popular approach to addressing the challenges of SCC has been the incorporation of mineral admixtures as partial replacements for cement. Materials like fly ash, silica fume, ground granulated blast furnace slag, metakaolin, and rice husk ash, among others, have been investigated as cementitious components of SCC [9–11]. Compared to single or binary binder systems, ternary and quaternary blends utilizing mineral admixtures have shown improved rheology and stability owing to their particle size distribution benefits while enhancing technical properties like strength and durability due to their pozzolanic reactivity [12, 13].

Fly ash has been one of the most commonly studied mineral admixtures for SCC due to its spherical shape, satisfactory size, and pozzolanic nature [14]. Replacement levels of 15–35% have shown good performance, with flowability, segregation resistance, and compressive strength improved compared to plain Portland cement mixes [15]. Silica fume has been utilized at 5–10% dosages to enhance particle packing density, cohesiveness, and later-age strength development in SCC. However, higher additions can impair workability [16]. Ground granulated blast furnace slag has demonstrated the ability to maintain good rheology at replacement levels up to 50–60% while enhancing strength and durability via its latent hydraulic behavior [17].

Metakaolin has emerged as an increasingly popular pozzolanic additive for high-performance and architectural concretes. Its ultrafine particle size, high purity, and pozzolanic reactivity make it attractive as a SCC ingredient. Metakaolin has been shown to improve the stability, strength, and transport properties of SCC at replacement levels of 10–20% [18, 19]. Multi-blend SCC incorporating fly ash, slag, limestone, and metakaolin has also offered advantages over single or binary systems [20]. Rice husk ash, an agro-industrial byproduct, has demonstrated promising results as a supplementary cementing material in SCC, along with metakaolin and other mineral admixtures [21]. While significant research exists on the influence of different mineral admixtures on various SCC properties, there is further scope to optimize multi-blends to develop high-performance self-compacting concrete [22].

In addition to suitable materials selection through optimal mix design, proper curing is essential to achieve the performance potential of any concrete. Curing impacts the cement hydration reactions and governs the microstructural development, which controls the long-term properties related to strength and durability [23]. While SCC has shown superior performance when properly cured by water immersion, the need for practical and efficient curing that can be applied in field conditions has led to growing interest in alternative curing techniques. Accelerated curing using steam or heat can provide an early strength boost but may lead to delayed effects over time [24]. Membrane curing blocks moisture loss with limited effectiveness based on the barrier material [25]. Self-curing strategies using saturated lightweight aggregates, superabsorbent polymers, and chemical additives provide internal water reservoirs to sustain hydration [26].

Recent studies have investigated the influence of various external and internal curing techniques on the properties of conventional concrete and SCC [27–29]. Water immersion is the optimal method, while polyethylene glycol showed promise as a self-curing agent for SCC [30]. However, limited studies compare different curing regimes for multi-blended SCC containing various mineral admixtures. There is also a need to correlate the curing effectiveness with the resultant microstructure of SCC using advanced characterization techniques. Therefore, this study aims to address some of the research gaps and make novel contributions by Systematically optimizing the design of high-performance self-compacting concrete utilizing multi-blends of fly ash, silica fume, and metakaolin as partial cement replacements and evaluating the influence of different practically relevant curing regimes, namely water immersion, membrane curing, accelerated curing, and self-curing on properties of the optimized SCC mixes and comparing the effectiveness of the various internal and external curing techniques based on the compressive strength as well as critical durability parameters like chloride migration coefficient and correlating the mechanical and durability performance to the resultant hydration and microstructure of SCC using sophisticated SEM-EDX analysis. The research outcomes are expected to guide the optimal selection of supplementary cementing materials and curing methods to develop durable and sustainable self-compacting concrete for advanced structural applications. The study will also generate predictive models relating curing conditions to SCC properties that can be applied for performance-based design and quality assurance.

Table 1. Physical properties of aggregates

	Specific gravity	% of water absorption	Fineness modulus	Bulk density
Fine aggregates	2.69	1.10	2.56	1.46
Coarse aggregates	2.72	0.75	7.25	1.51

Table 2. Physical properties of SCMs

Properties	Cement	Fly ash	Silica fume	Metakaolin
Specific gravity	3.10	2.41	2.20	2.55
Specific surface area (m^2/kg)	700	900	20000	11000
Color	Grey	Grey	Light grey	White
Average particle size (μm)	50	45	1	5

2. MATERIALS AND METHODS

2.1. Materials

The study utilized ordinary Portland cement (OPC) of grade 53 as per ASTM C150 [31]. The physical and chemical properties confirm the codal provisions. IS used fine and coarse aggregates 383 – 2016 [32], and their physical properties are enlisted in Table 1. Figure 1 represents the size distribution of coarse and fine aggregates. The fly ash was obtained from local coal-based thermal industries, with a specific gravity of 2.41 and an average particle size of 45 μm, as shown in Table 2.

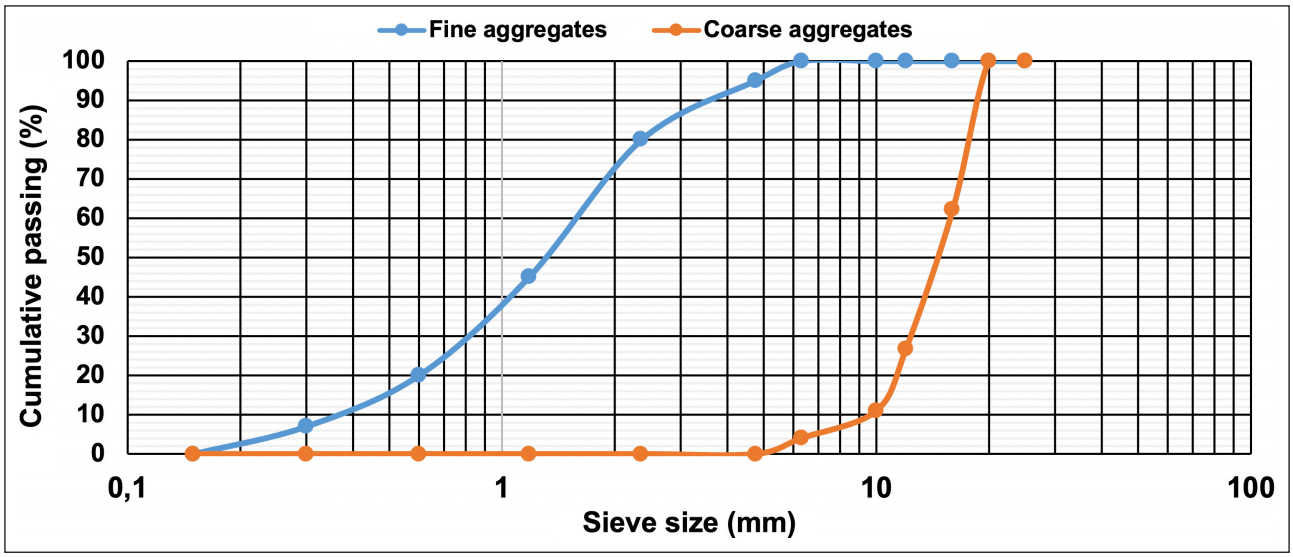

Figure 1. Aggregates size distribution.

Table 3. Chemical composition of binders (weight %)

Materials	CaO	SiO_2	Al_2O_3	Fe_2O_3	Na_2O	MgO	K_2O	TiO_2	Others
Cement	65.29	20.93	4.73	3.95	0.29	1.43	0.36	–	3.02
Fly ash	0.80	61	30.3	3.93	0.25	0.4	0.91	1.95	0.46
Silica fume	0.36	92	0.46	1.6	0.7	0.74	0.9	–	3.24
Metakaolin	0.1	52.1	36.1	4.3	–	0.84	1.38	–	5.18

Table 4. Physical properties of ROOF PLAST SP-455

Name of the chemical admixture	Appearance	Relative density (g/cm^3)	pH	Compatible
ROOF PLAST SP-455	Brown colour	1.02–1.05	<6	For all sorts of cement

Table 5. Physical properties PEG-400

Name of the self-curing agent	Molecular weight	Appearance	Moisture	pH	Specific gravity
PEG-400	400	Clear Fluid	0.2%	6	1.2

Similarly, silica fume and metakaolin were procured from the local markets. Their specific gravities are 2.20 and 2.55, with average particle sizes of 1 μm and 5 μm, respectively. Table 3 shows the chemical composition of the binder (or mineral admixtures). The ROOFPLAST SP-455 was used as a water reducer in this study, and its properties are illustrated in Table 4. Polyethylene glycol-400 was used as a self-curing agent at a proportional level of 1% to the weight of the binder. Its specifications are listed in Table 5.

2.2. Mix Proportions

In the present study, 40MPa strength concrete was used for all the experiments, and its mix calculations were finalized according to the IS 10262-2019 [33], as shown in Table 6.

2.3. Rheological Studies

In the present study, all the rheological properties (namely, Flow test, V-Funnel, and L-Box) were evaluated according to the European Federation of National Associations Representing Concrete (EFNARC) guidelines [34].

2.3.1. L-box Test

Figure 2a represents the L-box; it is used to assess the passing ability of self-compacting concrete through tight openings like spaces between reinforcing bars. A vertical section and a horizontal area with a movable gate in between. Fill the vertical section and open the gate to let the concrete flow into the flat section. Measure the height of the concrete at the end of the flat section. Calculate the passing ability ratio as the height of concrete in the flat section divided by the height in the vertical section. A ratio of 0.8–1.0 indicates good passing ability.

2.3.2. V-funnel Test

Figure 2b depicts the V-funnel; it measures self-compacting concrete's flowability and filling ability. A V-shaped

Table 6. Mix proportions (Kg/m^3)

Mix no	Mix designation	OPC	FA	SF	MK	Fine aggregate	Coarse aggregate	SP (lit)	Water (lit)	w/b
M1	C100	531	–	–	–	891	786	9.34	185	0.35
M2	C60+FA40	319	212	–	–	891	786	9.34	185	0.35
M3	C85+MS15	452	–	79	–	891	786	9.34	185	0.35
M4	C80+MK20	425	–	–	106	891	786	9.34	185	0.35
M5	C35+MK15+FA50	186	265	–	73	891	786	9.34	185	0.35

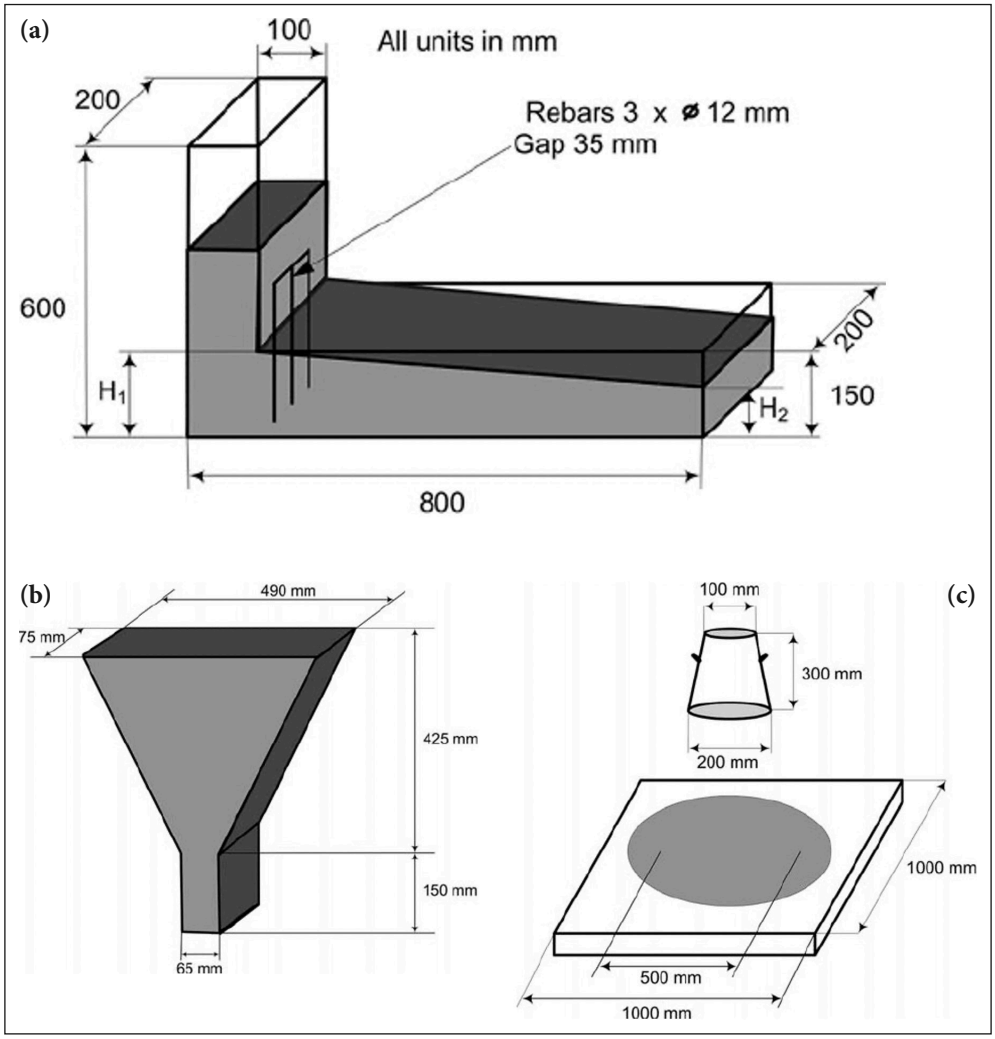

Figure 2. **(a)** L-box. **(b)** V-funnel. **(c)** Slume cone and flow.

funnel with the bottom gate closed. Fill the funnel with concrete and open the gate. Measure the time the concrete takes to ultimately flow out of the funnel. Typical values are 6–12 seconds. Lower times indicate greater flowability.

2.3.3. T50 Slump Flow Test

Used to assess the horizontal free flow and filling ability of self-compacting concrete. Concrete is poured into a cone placed on a flat surface and lifted vertically. Measure the time the concrete takes to reach a diameter of 50 cm. Typical T50 times are 2–5 seconds. Lower times indicate better flowability. Figure 2c shows the slump cone.

2.3.4. Slump Flow Test

It has the same test procedure as the T50 slump flow. Instead of measuring T50 time, the final diameter of the concrete circle is measured. Diameters of 650–800mm indicate good flowability. Figure 2c represents the slump flow.

2.4. Curing Conditions

2.4.1. Water Immersion Curing

By ASTM C192-15 [35], water immersion curing involves fully submerging the hardened concrete component. This technique is commonly employed in laboratories for curing concrete

Figure 3. **(a)** Water immersion curing. **(b)** Self-curing with PEG-400. **(c)** Gunny bag membrane curing. **(d)** Accelerated curing.

specimens. It fulfills all curing requirements, including promoting hydration, reducing shrinkage, and dissipating heat during hydration. Water immersion curing is depicted in Figure 3a.

2.4.2. Accelerated Curing

Concrete is provided an early boost in compressive strength using the accelerated curing method. This study subjected the concrete mixes to accelerated curing conditions by ASTM C684-99 [36]. Under these conditions, the concrete will achieve full maturity within 28 hours. Figure 3b illustrates the experimental setup.

2.4.3. Membrane Curing

According to IRC-015 [37], gunny bag membrane curing was performed in the present study, and its experimental photograph is shown in Figure 3c.

2.4.4. Self-curing

In the present study, Polyethylene glycol-400 was employed as a self-curing agent in the self-compacting concrete, following the method outlined by Madduru et al. [38]. Experimental images are shown in Figure 3d.

Table 7. Rheological properties of different SCC mixes

Tests	EFNARC limits	M1	M2	M3	M4	M5
Flow test						
Slump (mm)	650–800	732	705	712	719	695
T-50 (Sec)	2–5	3.45	4.26	4.05	4.07	4.95
V-funnel	6–12	6.85	9.28	7.56	8.08	10.8
L-box	0.8–1	0.98	0.92	0.95	0.94	0.90

2.5. Compressive Strength

The value of uniaxial compressive stress achieved when a material completely fails is referred to as the material's compressive strength. Cube specimens measuring 150 mm x 150 mm x 150 mm were employed in this study and examined following IS 516: 1959 [39]. 60 cubic samples were prepared and cured under the above-selected curing conditions for up to 28 days.

2.6. Durability Properties

2.6.1. Rapid Chloride Permeability Test

They were used to measure the electrical conductance of concrete to provide a rapid indication of its resistance to the penetration of chloride ions. A 100 mm diameter, 50 mm thick concrete specimen is vacuum saturated and sealed between two cells containing calcium hydroxide solution. A 60V DC voltage is applied across the cell for 6 hours. The amount of electrical current passed through the specimen over this period is used to evaluate the resistance of concrete to chloride ion penetration. Charge passed is based on the current flow and time, according to the ASTM C1202 [40]. A lower coulomb value indicates higher resistance to chloride ion penetration.

2.6.2. Rapid Chloride Migration Test

They were used to determine the resistance of concrete to chloride ion penetration. A 50mm thick slice of 100mm diameter core is vacuum saturated. One face is exposed to a 2.8M NaCl solution. The other face to a 0.3M NaOH solution. A 30V DC voltage is applied for 24 hours. After testing, the specimen is split and sprayed with silver nitrate to measure chloride penetration depth, according to NT BUILD 492 [41]. The non-steady state migration coefficient is then calculated using the applied voltage, temperature, penetration depth, and test duration. A lower migration coefficient indicates higher resistance to chloride ion ingress.

2.7. Microstructural Properties

In the present study, the concrete sample's surface morphology and elemental composition were assessed using "Scanning Electron Microscope (SEM) and Energy Dispersive X-ray Spectroscopy analyses (EDX) [42–52]." The microstructure and elemental composition of the samples were analyzed using an SEM (Model: VEGA 3 Generation, TESCAN, Brno, Czech Republic) equipped with EDX spectroscopy (Model: EDAX-EDS-SSD, EDAX Inc., USA). Small pieces of the samples were mounted on aluminum stubs using carbon tape. A thin layer of gold was coated on the illustrations by sputter coating for 120 seconds at 10 mA (Model: 108 auto sputter coater, TED PELLA, INC.) to enhance the conductivity.

The surface morphology of gold-coated samples was examined under the SEM at an accelerating voltage of 10 kV and a working distance of 10–20 mm. Micrographs were taken at various magnifications ranging from 2.00kx to 5.00kx. For EDX analysis, the SEM was coupled with an EDX spectrometer. EDX spectra were collected at three spots on each sample to determine the elemental composition.

3. RESULTS AND DISCUSSION

3.1. Rheological Properties

The rheological properties of the various self-compacting concrete (SCC) mixes are presented in Table 7. All the mixes satisfied the EFNARC limits for slump flow, T50 slump flow, V-funnel, and L-box tests, indicating adequate flowability, filling, and passing ability. Mix M1 with 100% cement had the highest slump flow of 732 mm, while Mix M5 with 20% metakaolin replacement had the lowest slump of 695 mm. The reduced slump in M5 can be attributed to the higher water demand and increased viscosity caused by metakaolin's fine particle size and high pozzolanic reactivity.

3.2. Compressive Strength

The compressive strength results under different curing conditions are shown in Figure 4. The 28-day strengths ranged from 42.12 MPa for M1 under accelerated curing to 53.73 MPa for M5 under water immersion curing. All mixes showed increased strength with prolonged curing duration, as expected. Among the curing methods, water immersion consistently resulted in the highest compressive strengths, followed by polyethylene glycol, accelerated curing, and gunny bag curing. Water immersion provided a saturated environment that promoted better hydration and microstructural development than the other techniques. The strength gain under self-curing using polyethylene glycol was slightly lower, potentially due to some moisture loss over time. Accelerated steam curing generated higher early strength, but longer normal curing was needed to achieve later-age strengths similar to water immersion. Gunny bag curing was the least effective likely because it allowed greater moisture evaporation.

The relative compressive strength under different curing conditions compared to water immersion curing; Self-curing with polyethylene glycol achieved 92–96% of the strength under water curing. Accelerated curing re-

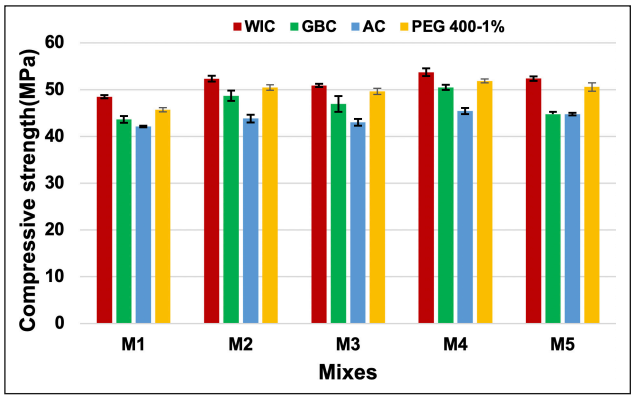

Figure 4. Compressive strength of concrete cured in various curing conditions.

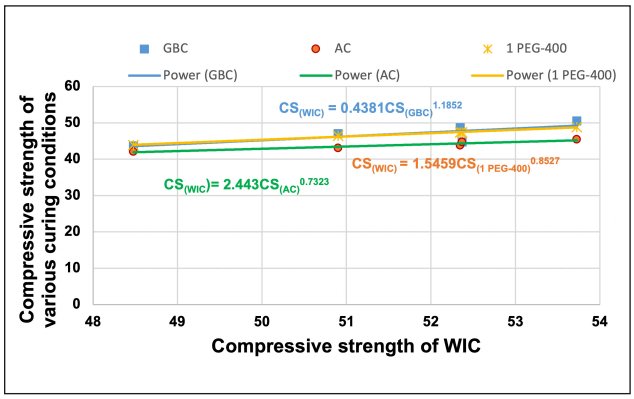

Figure 5. Relation between the compressive strength of WIC Vs other curing conditions.

Table 8. Chloride ions permeability and migration coefficient values

Mixes	Chloride ion migration coefficient ($\times 10^{-12}$ m^2/s)							
	WIC		GBC		AC		1 PEG-400	
	Coefficient values	Standard deviation	Coefficient values	Standard deviation	Coefficient values	Standard deviation	Coefficient values	Standard deviation
M1	7.23	0.0436	9.2	0.2646	10.17	0.0300	8.45	0.0400
M2	4.86	0.0346	7.15	0.0300	7.66	0.0458	6.23	0.0265
M3	4.02	0.0608	5.13	0.0265	5.95	0.0265	4.27	0.0265
M4	3.42	0.0265	4.38	0.0200	5.5	0.0173	3.41	0.0173
M5	5.31	0.0200	6.89	0.0985	7.57	0.0300	5.87	0.0300

sulted in 87–93%, while gunny bag curing gave the lowest strengths of 78–85% of water-cured samples. This reinforces water immersion as the optimal curing technique. Among the mixes, the metakaolin blend M5 showed the smallest differences between curing methods, suggesting it was less sensitive to external curing. Its high reactivity and pozzolanic nature meant sufficient internal curing occurred through ongoing hydration reactions.

Figure 5 represents the relationship between the compressive strength during water immersion curing and other selected curing conditions. Through observation, a good correlation was found between the experimental results and the predicted values from the following equations: Eq. 1–Eq. 3.

i. Relation between WIC and GBC is as follows

$$CS_{(WIC)}=0.4381CS_{(GBC)}^{1.1852} \quad \text{Eq.1}$$

ii. The relation between the WIC and AC is given below

$$CS_{(WIC)}=2.443CS_{(AC)}^{0.7323} \quad \text{Eq.2}$$

iii. The relation between the WIC and 1 PEG-400 is given below

$$CS_{(WIC)}=1.5459CS_{(1\ PEG\text{-}400)}^{0.8527} \quad \text{Eq.3}$$

3.3. Durability Studies

3.3.1. Rapid Chloride Migration Coefficient

The chloride ion migration coefficients in Table 8 indicate the resistance of the SCC mixes to chloride penetration. A lower migration coefficient represents lower permeability. Incorporating mineral admixtures reduced the permeability notably compared to plain cement mix M1, with the metakaolin blend M5 showing the best performance. The excellent chloride resistance with supplementary cementitious materials can be attributed to pore refinement and reduced porosity from the pozzolanic reactions. Among curing techniques, water immersion curing again led to the lowest permeability, followed by polyethylene glycol, accelerated, and gunny bag curing. The denser microstructure with improved hydration under wet curing restricted chloride ingress. The permeability trends matched the compressive strength trends, suggesting the microstructural changes influencing strength also governed transport properties.

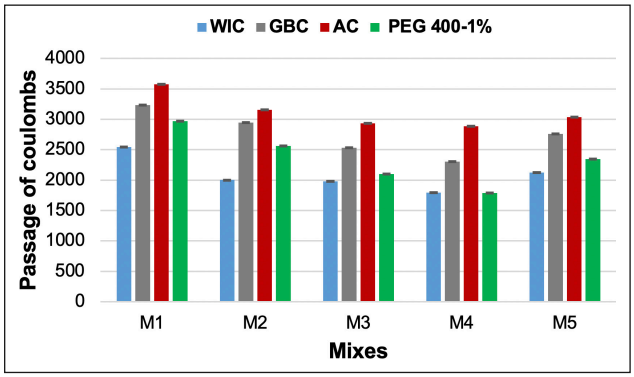

Figure 6. Rapid chloride permeability results.

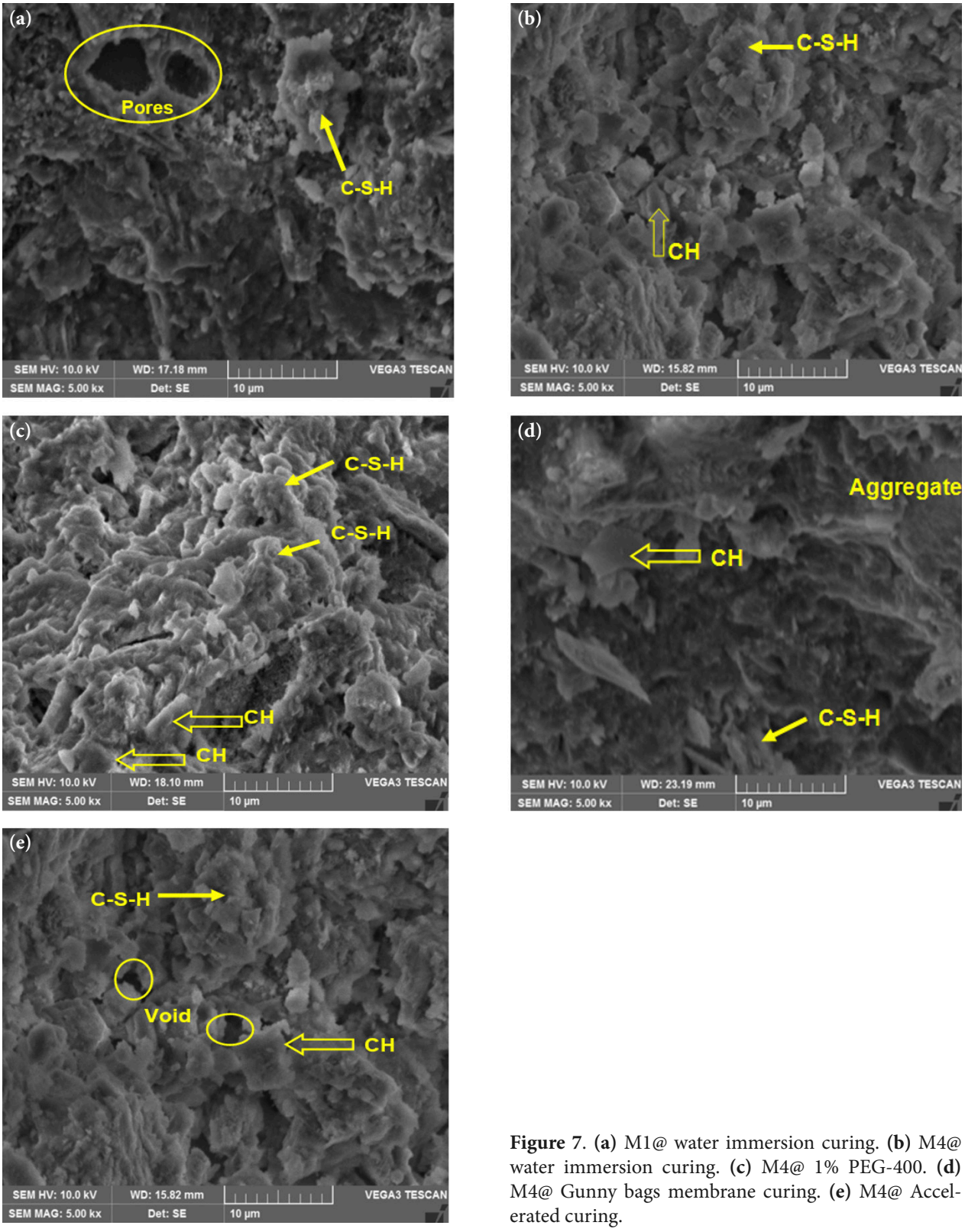

Figure 7. **(a)** M1@ water immersion curing. **(b)** M4@ water immersion curing. **(c)** M4@ 1% PEG-400. **(d)** M4@ Gunny bags membrane curing. **(e)** M4@ Accelerated curing.

3.3.2. Rapid Chloride Permeability Test

The rapid chloride permeability classification results in Figure 6 further demonstrate the reduced chloride penetrability with mineral admixtures and adequate external curing. Mix M1 had the highest permeability in the 'High' category under gunny bag curing, while metakaolin blends M5 achieved the 'Very Low' classification under water curing due to its low migration coefficient. The results indicate appropriate mix design and adequate external curing are essential to limiting chloride transport and achieving durable SCC.

Table 9. Elemental composition of optimum mixes

Mix designation	M1@WIC	M4@ WIC	M4@ 1% PEG-400	M4@ GBC	M4@ AC
Ca/Si	1.75	1.25	1.22	1.34	1.38

3.4. Scanning Electronic Microscope Analysis

The microstructure of selected optimized SCC mixes under different curing conditions was examined using scanning electron microscopy (SEM). The SEM images in Figure 7 show the morphology and hydration phases. In the plain cement mix, M1 cured by water immersion (Fig. 7a), abundant hydration products in the form of calcium silicate hydrate (C-S-H) gel and $Ca(OH)_2$ crystals can be observed filling voids and spaces between particles. The mix containing fly ash, silica fume, and metakaolin (M4) cured by water immersion (Fig. 7b) displays a denser microstructure with fewer voids owing to enhanced pozzolanic reactions and the filler effects of the mineral admixtures.

M4 cured with 1% polyethylene glycol (Fig. 7c) exhibits a reasonably dense structure, but some microcracks are visible, likely due to restrained shrinkage and moisture loss. In contrast, due to insufficient hydration and carbonation, the sample cured with gunny bags (Fig. 7d) shows a more porous structure with channels and cavities. M4 cured using accelerated techniques (Fig. 7e) displays some heterogeneity in the microstructure with regions of discontinuous hydration products.

The Ca/Si ratios in Table 9 indicate the C-S-H composition and hydration extent. The plain cement mix M1 had the highest Ca/Si ratio of 1.75 underwater curing due to $Ca(OH)_2$ and C-S-H formation. The blended mix M4 showed lower Ca/Si ratios between 1.22–1.38 owing to the pozzolanic consumption of $Ca(OH)_2$ and additional C-S-H from the reactions between silicates and the cement. Among curing regimes for M4, water immersion resulted in the lowest ratio of 1.25, suggesting the greatest hydration. The microstructural evidence correlates well with the improved mechanical and durability performance observed for the optimized metakaolin SCC blend under water curing.

4. CONCLUSION

This study demonstrated that incorporating fly ash, silica fume, and metakaolin as partial cement replacements in self-compacting concrete (SCC) improved rheological properties like flowability, passing ability, and filling ability. Metakaolin resulted in slightly higher viscosity and lower slump flow than other mixes, likely due to its finer particles and high reactivity requiring more water. However, all designed mixes satisfied EFNARC guidelines for SCC workability.

The compressive strength and chloride penetration resistance of SCC were enhanced by using mineral admixtures as cement replacements compared to plain cement mixes. Metakaolin at 20% replacement showed the best performance, increasing 28-day strength by up to 53% and reducing the chloride migration coefficient by up to 40% compared to the control. This is attributed to metakaolin's high pozzolanic reactivity, leading to refined pores and enhanced formation of secondary C-S-H.

Water immersion curing was the most effective method for curing SCC, improving 28-day compressive strength by 3–15% and reducing the chloride migration coefficient by up to 30% compared to other curing techniques. Wet curing provides an optimal hydration environment, allowing pozzolanic reactions to progress and increasing densification.

Mineral admixtures reduced the sensitivity of SCC to external curing conditions due to their ability to promote internal curing through ongoing pozzolanic reactions. Metakaolin SCC showed the least property variations between curing regimes due to its high reactivity.

Microstructural analysis revealed that mineral admixtures improved the interfacial transition zone in SCC by increasing particle packing density and enabling pozzolanic products like additional C-S-H to fill voids. Water curing produced the most refined pore structure with continuous hydration products.

ETHICS

There are no ethical issues with the publication of this manuscript.

DATA AVAILABILITY STATEMENT

The authors confirm that the data that supports the findings of this study are available within the article. Raw data that support the finding of this study are available from the corresponding author, upon reasonable request.

CONFLICT OF INTEREST

The authors declare that they have no conflict of interest.

FINANCIAL DISCLOSURE

The authors declared that this study has received no financial support.

PEER-REVIEW

Externally peer-reviewed.

REFERENCES

[1] de Souza, A. M., de Carvalho, J. M. F., Santos, C. F. R., Ferreira, F. A., Pedroti, L. G., & Peixoto, R. A. F. (2022). An analytical review of the strategies to improve the eco-efficiency of self-compacting concrete using industrial waste. *Constr Build Mater, 347*, 128634. [CrossRef]

[2] Faraj, R. H., Mohammed, A. A., & Omer, K. M. (2022). Self-compacting concrete composites modified with nanoparticles: A comprehensive review, analysis, and modeling. *J Build Eng, 50*, 104170. [CrossRef]

[3] Gupta, N., Siddique, R., & Belarbi, R. (2021). Sustainable and greener self-compacting concrete incorporating industrial by-products: A review. *J Clean Prod, 284*, 124803. [CrossRef]

[4] Dey, S., Kumar, V. P., Goud, K. R., & Basha, S. K. J. (2021). State of art review on self-compacting concrete using mineral admixtures. *J Build Pathol Rehabil, 6*(1), 18. [CrossRef]

[5] Madhavi, C., Reddy, V. S., Rao, M. S., Shrihari, S., Kadhim, S. I., & Sharma, S. (2023). The effect of elevated temperature on self-compacting concrete: Physical and mechanical properties. *E3S Web Conf, 391*, 01212. [CrossRef]

[6] Rao, T. V., Seshagiri Rao, M. V., & Rao, P. J. (2021, March 1). Strength properties of double blend and triple blend self-compacting concrete subjected to different curing methods. *IOP Conf Ser Mater Sci Eng, 1126*(1), 012085. [CrossRef]

[7] Klemczak, B., Gołaszewski, J., Smolana, A., Gołaszewska, M., & Cygan, G. (2023). Shrinkage behaviour of self-compacting concrete with a high volume of fly ash and slag experimental tests and analytical assessment. *Constr Build Mater, 400*, 132608. [CrossRef]

[8] Rao, M. D., Dey, S., & Rao, B. P. (2023). Characterization of fiber reinforced self-compacting concrete by fly ash and cement. *Chem Inorg Mater, 1*, 100010. [CrossRef]

[9] Karthiga, N., Siddharth, M. A., Kannan, V., & Dhanusree, C. (2023). Experimental investigation of self-compacting concrete (SCC) using fly ash. *Mater Today Proc, 2023*, 2023.04.582

[10] Luo, Y., Zhang, Q., Wang, D., Yang, L., Gao, X., Liu, Y., & Xue, G. (2023). Mechanical and microstructural properties of MK-FA-GGBFS-based self-compacting geopolymer concrete composites. *J Build Eng, 77*, 107452. [CrossRef]

[11] Singh, A., Mehta, P. K., & Kumar, R. (2022). Performance of binary admixtures (Fly ash and Silica fume) on self-compacting concrete. *Mater Today Proc, 58*, 970–977. [CrossRef]

[12] Jameel, G. S., İpek, S., Ahmed, A. D., Güneyisi, E., & Güneyisi, E. M. (2023). Rheological behavior and key properties of metakaolin and nano-SiO_2 blended fibrous self-compacting concretes. *Constr Build Mater, 368*, 130372. [CrossRef]

[13] Rojo-López, G., González-Fonteboa, B., Martínez-Abella, F., & González-Taboada, I. (2022). Rheology, durability, and mechanical performance of sustainable self-compacting concrete with metakaolin and limestone filler. *Case Stud Constr Mater, 17*, e01143. [CrossRef]

[14] Suprakash, A. S., Karthiyaini, S., & Shanmugasundaram, M. (2021). Future and scope for development of calcium and silica rich supplementary blends on properties of self-compacting concrete - a comparative review. *J Mater Res Technol, 15*, 5662–5681. [CrossRef]

[15] Devi, K., Aggarwal, P., & Saini, B. (2020). Admixtures used in self-compacting concrete: A review. *Iran J Sci Technol Trans Civ Eng, 44*, 377–403. [CrossRef]

[16] Frhaan, W. K. M., Bakar, H. B. A., Hilal, N., & Al-Hadithi, A. I. (2020). Effect of silica fume and super-plasticizer on mechanical properties of self-compacting concrete: A review. IOP Conf Ser Mater Sci Eng, 978(1), 012052. [CrossRef]

[17] Albiajawi, M. I., EMBONG, R., & Muthusamy, K. (2021). Influence of mineral admixtures on the properties of self-compacting concrete: An overview. *Constr, 1*(2), 62–75. [CrossRef]

[18] Danish, P., & Ganesh, G. M. (2021). Study on influence of metakaolin and waste marble powder on self-compacting concrete – a state of the art review. *Mater Today Proc, 44*, 1428–1436. [CrossRef]

[19] Venkatesh, C., Nerella, R., & Chand, M. S. R. (2020). Experimental investigation of strength, durability, and microstructure of red-mud concrete. *J Korean Ceram Soc, 57*(2), 167–174. [CrossRef]

[20] Ramkumar, K. B., Rajkumar, P. K., Ahmmad, S. N., & Jegan, M. (2020). A review on performance of self-compacting concrete – use of mineral admixtures and steel fibres with artificial neural network application. *Constr Build Mater, 261*, 120215. [CrossRef]

[21] Kumar, K. R., Shyamala, G., Awoyera, P. O., Vedhasakthi, K., & Olalusi, O. B. (2021). Cleaner production of self-compacting concrete with selected industrial rejects-an overview. *Silicon, 13*, 2809–2820. [CrossRef]

[22] Massana, J., Reyes, E., Bernal, J., León, N., & Sánchez-Espinosa, E. (2018). Influence of nano-and micro-silica additions on the durability of a high-performance self-compacting concrete. *Constr Build Mater, 165*, 93–103. [CrossRef]

[23] Güneyisi, E., Gesoğlu, M., & Algin, Z. (2013). Performance of self-compacting concrete (SCC) with high-volume supplementary cementitious materials (SCMs). *Eco-Eff Concr, 2023*, 198–217. [CrossRef]

[24] Devadass, T. (2019). Experimental study on replacement of fine aggregate in concrete with dissimilar curing conditions. *Case Stud Constr Mater, 11*, e00245. [CrossRef]

[25] Wang, Y., Wang, S., Wang, T., Song, T., Wu, X., Guo, L., Xie, W., Qiu, P., Dong, Q., & Li, Q. (2023). A green nanocomposite membrane for concrete moisturizing, with excellent barrier properties and aging resistance. *Mater Today Commun, 35*, 105553. [CrossRef]

[26] Saravanakumar, R., Elango, K. S., Piradheep, G., Rasswanth, S., & Siva, C. (2023). Effect of super absorbent polymers in properties of self-curing concrete - a state of art of review. *Mater Today Proc, 2023*, 05.117. [CrossRef]

[27] Hamada, H., Alattar, A., Tayeh, B., Yahaya, F., & Almeshal, I. (2022). Influence of different curing methods on the compressive strength of ultra-high-performance concrete: A comprehensive review. *Case Stud Constr Mater, 17*, e01390. [CrossRef]

[28] Athira, V. S., Bahurudeen, A., Saljas, M., & Jayachandran, K. (2021). Influence of different curing methods on mechanical and durability properties of alkali activated binders. *Constr Build Mater, 299*, 123963. [CrossRef]

[29] Ekolu, S. O. (2016). A review on effects of curing, sheltering, and CO_2 concentration upon natural carbonation of concrete. *Constr Build Mater, 127*, 306–320. [CrossRef]

[30] Sri Rama Chand, M., Rathish Kumar, P., Swamy Naga Ratna Giri, P., & Rajesh Kumar, G. (2018). Performance and microstructure characteristics of self-curing self-compacting concrete. *Adv Cem Res, 30*(10), 451–468. [CrossRef]

[31] ASTM C150/C150M-16e1. (2016). *Standard specification for Portland cement*. ASTM International, West Conshohocken, PA.

[32] BIS, IS 383-2016. (2016). *Specification for coarse and fine aggregates from natural sources for concrete*. Bureau of Indian Standards, New Delhi.

[33] BIS, IS 10262-2019 (2019) *Specification for concrete mix proportioning*. Bureau of Indian Standards, New Delhi.

[34] EFNARC. (2002). *Specification and guidelines for self-compacting concrete*. European Federation of Specialist Construction Chemicals and Concrete Systems, Syderstone, Norfolk, UK.

[35] ASTM C192/C192M-15. (2016). *Standard practice for making and curing concrete test specimens in the laboratory*. ASTM International, West Conshohocken, PA.

[36] ASTM C684-99. (2017). *Standard test method for making, accelerated curing, and testing concrete compression test specimens*. ASTM International, West Conshohocken, PA.

[37] IRC 15-2017. (2017). *Specification for gunny bag membrane curing for concrete pavement*. Bureau of Indian Standards, New Delhi.

[38] Madduru, S. R. C., Pancharathi, R. K., Giri, P. S. N. R., Kumar, G. R. (2018). Performance and microstructure characteristics of self-curing self-compacting concrete. *Adv Cem Res, 30*(10), 451–468. [CrossRef]

[39] BIS, IS 516: 1959. (1959). *Specification for determining compressive strength of concrete*. Bureau of Indian Standards, New Delhi.

[40] ASTM C 1202. (2012). *Standard test method for electrical indication of concrete's ability to resist chloride ion penetration*. ASTM International, West Conshohocken, PA.

[41] NT BUILD 492. (1999). *Concrete, mortar and cement-based repair materials: Chloride migration coefficient from non-steady-state migration experiments*. Nordtest, Finland.

[42] Chava, V., & Chereddy, S. S. D. (2023). Effect of calcination on the physical, chemical, morphological, and cementitious properties of red mud. *J Sustain Constr Mater Technol, 8*(4), 297–306. [CrossRef]

[43] Bellum, R. R., Al Khazaleh, M., Pilla, R. K., Choudhary, S., & Venkatesh, C. (2022). Effect of slag on strength, durability and microstructural characteristics of fly ash-based geopolymer concrete. *J Build Pathol Rehabil, 7*(1), 25. [CrossRef]

[44] Bellum, R. R., Venkatesh, C., & Madduru, S. R. C. (2021). Influence of red mud on performance enhancement of fly ash-based geopolymer concrete. *Innov Infrastruct Solut, 6*(4), 215. [CrossRef]

[45] Mukkala, P., Venkatesh, C., & Habibunnisa, S. (2022). Evaluation of mix ratios of light weight concrete using geopolymer as binder. *Mater Today Proc, 52*, 2053–2056. [CrossRef]

[46] Ruben, N., Venkatesh, C., Durga, C. S. S., & Chand, M. S. R. (2021). Comprehensive study on performance of glass fibers-based concrete. *Innov Infrastruct Solut, 6*(2), 112. [CrossRef]

[47] Venkatesh, C., Nerella, R., & Chand, M. S. R. (2021). Role of red mud as a cementing material in concrete: A comprehensive study on durability behavior. *Innov Infrastruct Solut, 6*(1), 13. [CrossRef]

[48] Anirudh, M., Rekha, K. S., Venkatesh, C., & Nerella, R. (2021). Characterization of red mud-based cement mortar; mechanical and microstructure studies. *Mater Today Proc, 43*, 1587-1591. [CrossRef]

[49] Rao, T. M., Mahesh, K., Venkatesh, C., Durga, C. S. S., Reddy, B. R., Tejaswi, P. S., & Charandeepneelesh, R. (2023). Influence of magnetization of water on mechanical and durability properties of fly ash concrete. *Mater Today Proc, 2023*, 194.

[50] Durga, C. S. S., Venkatesh, C., Muralidhararao, T., Bellum, R. R. (2023). Crack healing and flexural behavior of self-healing concrete influenced by different bacillus species. *Res Eng Struct Mater, 9*(4), 1477–1488. [CrossRef]

[51] Durga, C. S. S., Venkatesh, C., Muralidhararao, T., Bellum, R. R., Rao, B. N. M. (2023). Estimation of durability properties of self-healing concrete influenced by different bacillus species. *Res Eng Struct Mater, 9*(4), 1489–1505. [CrossRef]

[52] Venkatesh, C., Sri Rama Chand, M., Ruben, N., & Sonali Sri Durga, C. (2020). Strength characteristics of red mud and silica fume-based concrete. In Smart Technologies for Sustainable Development: Select Proceedings of SMTS 2019 (pp. 387-393). Springer Singapore. [CrossRef]

Journal of Sustainable Construction Materials and Technologies
Web page info: https://jscmt.yildiz.edu.tr
DOI: 10.47481/jscmt.1413471

JSCMT
Journal of Sustainable Construction Materials and Technologies

Research Article

Investigation of usability of recycled aggregate in SIFCON production

Adil GÜLTEKİN*

Department of Civil Engineering, Düzce University Faculty of Engineering, Düzce, Türkiye

ARTICLE INFO

Article history
Received: 02 January 2024
Revised: 08 February 2024
Accepted: 13 February 2024

Key words:
Fracture energy, high-temperature resistance, recycled aggregate, SIFCON, steel fiber

ABSTRACT

Using recycled aggregates is crucial for a more sustainable environment and economy. In this study, the properties of recycled aggregate-based SIFCONs were examined. In the scope of the study, compressive strength, high-temperature resistance, sorptivity, and fracture energy of SIFCONs produced with recycled aggregate were investigated. The results were compared with those of the limestone-bearing SIFCONs. It was determined that the compressive strength and fracture energy of SIFCONs produced with recycled aggregate were 61.2 MPa and 14.9 N/mm, respectively. Although these values are lower than those of SIFCONs produced with limestone, it has been determined that recycled aggregates are advantageous in high-temperature resistance. The results demonstrated that the recycled aggregate could be used to produce SIFCON.

Cite this article as: Gültekin, A. (2024). Investigation of usability of recycled aggregate in SIFCON production. *J Sustain Const Mater Technol*, 9(1), 36–44.

1. INTRODUCTION

Conventional concrete is a brittle building material and performs poorly under tensile stresses [1]. It is known that with the addition of fiber, some concrete properties like flexural and tensile strength [2], post-cracking behavior [3], first cracking strength, and impact resistance [4] improve. Steel fibers are widely used to reduce the brittleness of concrete and increase tensile strength and toughness. The amount of fiber is crucial in this regard [5]. However, fibers decrease the workability of concrete, and this reduction can also negatively affect mechanical and durability properties [6]. Thus, the amount of fiber used in producing fiber-reinforced and high-performance fiber-reinforced concrete is generally limited to around 1–3% by volume [7]. The limitation of fiber content in traditional fiber-reinforced concrete has led to a focus on new alternative composite materials with high fiber dosage [8]. Slurry infiltrated fiber concrete (SIFCON) is a type of high-volume fiber-bearing concrete produced with a special production method different from conventional concrete [9]. In SIFCON production, the fibers are first placed in the mold, then the phase prepared with cement, water, fine aggregate, and chemical and mineral additives (defined as slurry) is poured into the mold. In this way, the volume of fiber used in SIFCON increases by up to 30% [10]. SIFCON composites have superior properties like very high toughness and compressive and tensile strength [11]. The properties of the matrix phase and the fiber properties, like type, volume, and alignment, are critical for the mechanical properties of SIFCONs [12]. The highest fiber dosage that can be used in production depends on the length and diameter of the fiber, the fiber orientation, the dimensions of the mold, and the vibration [13]. SIFCON composites can be used in different application fields, such as strengthening, industrial floors [9], pavements [14], military complexes, and underground shelters [15] due to their advantages.

Today, sustainable constructions have significant importance on the concept of sustainability. Civil engineers also have essential duties and responsibilities in achieving sustainability goals [16]. For this reason, researchers have started investigating the recycling of different materials, the use of alternative materials to cement, and the use of

***Corresponding author.**
*E-mail address: adilgultekin@duzce.edu.tr

recycled materials in the production of building materials. Similar studies are carried out in SIFCON production. Al-Hadithi and Al-Hadithi [17] examined the usability of waste plastic fibers in SIFCON production. Celikten and Canbaz [18] and Drdlova et al. [19] investigated the properties of SIFCON composites produced using waste steel fibers obtained from waste automobile tires. Canbaz and Celikten [20] explored the effect of crumbed waste automobile tire rubbers on the properties of SIFCON composites. Tiwari et al. [21] examined the impact of replacing cement with waste glass powder on SIFCON properties. Khan and Selvaraju [22] investigated the effect of substituting various pozzolans with cement and replacing steel fibers with waste high-density polyethylene and waste plastic fibers on SIFCON properties. Altunci and Ocal [23] investigated the properties of SIFCON composites produced by using peanut shell ash partial replacement with cement.

The increase in the demand for construction causes an increase in the need for cement and aggregate. Recycling the construction and demolition wastes and using these recycled aggregates is essential for sustainability and reducing the demand for natural aggregates [24]. Also, most of the waste concrete obtained from the construction and demolition process is landfilled in open fields in nature, and this waste is one of the reasons for environmental pollution. Therefore, it is essential to obtain recycled aggregates from these wastes and use them as raw materials to produce new concrete [25]. However, recycled aggregates' properties differ from natural aggregates due to the mortar adhered to the aggregate of the old concrete. The transition zone between this mortar and aggregate significantly impacts recycled aggregate properties such as porosity and water absorption capacity [26]. Numerous studies have been conducted on concrete produced with only recycled aggregate or partially replacing recycled aggregate with traditional aggregate. It is mentioned that, in general, recycled aggregate negatively affects the concrete's strength and some of its durability properties [27]. The extent of the adverse effects of recycled aggregate on concrete properties depends on different factors like water/cement ratio, replacement ratio, and the quality of recycled aggregate [28]. The porosity and homogeneity determine the quality of recycled aggregate [29]. As recycled aggregate substitution increases, concrete properties such as workability, density, and strength decrease; meanwhile, the risk of bleeding and drying shrinkage increases [30]. Although studies show that utilization of 20–30% recycled aggregate can produce concrete of similar grade to conventional concrete, such low amounts cannot ensure the disposal of waste concrete [28].

Due to negative properties arising from the nature of recycled aggregate, early studies on recycled aggregate generally focused on non-structural concrete production. As the number of studies on recycled aggregate increases, different techniques like carbonation, exposure to different solutions, and coating with different materials have been examined to improve the properties of recycled aggregate. However, these improvements require an additional process before using [31]. Various factors, such as undesirable materials such as brick, wood, and plastic, inadequate standards, and quality control, raise concerns about using recycled aggregate [32]. Research continues for the characterization and more efficient use of recycled aggregate [33]. Countries like Belgium, Denmark, and Germany have developed different standards and acceptance criteria for recycled aggregates. It is possible to use these aggregates as fine or coarse aggregates in concrete [34].

There are many studies on recycled aggregate utilization in building materials production. Most of these studies used recycled aggregate as fine and coarse aggregate. However, the recycled aggregate has the potential to be used in the production of SIFCON slurry, and there is a lack of literature on this topic. This study investigated the usability of recycled aggregate powder produced from recycled aggregate in SIFCON production. This way, the usability of recycled aggregate powder generated in the facility during recycled aggregate production will also be examined. It was aimed to determine

Table 1. Chemical composition and some properties of cement

Compound	% (by weight)	Mechanical properties	
CaO	63.06	Compressive strength	
SiO_2	18.53	7 days	38.4 MPa
Al_2O_3	5.21	28 days	47.2 MPa
Fe_2O_3	3.65		
MgO	1.01	Physical properties	
Na_2O	0.48	Specific gravity	3.11
K_2O	0.64	Initial setting time	210 minutes
SO_3	3.20	Final setting time	315 minutes
Free CaO	0.91	Blaine's specific surface area	3420 cm^2/g
Loss on ignition	2.94		

Table 2. Chemical composition and some physical properties of kaolin and recycled aggregate

Compound	Kaolin % (by weight)	Recycled aggregate (<0.125 mm) % (by weight)
CaO	0.38	34.46
SiO_2	73.15	29.17
Al_2O_3	16.55	4.25
Fe_2O_3	0.69	1.97
MgO	0.31	2.06
Na_2O	0.10	4.81
K_2O	0.24	<0.10
Loss on ignition	6.90	21.08
Specific gravity	2.60	2.15

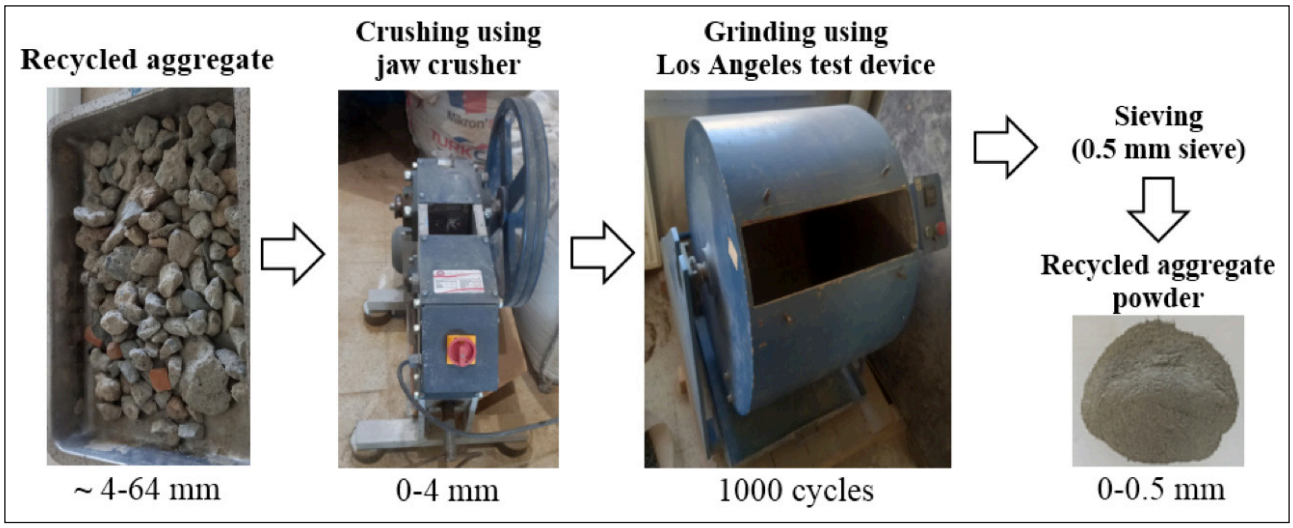

Figure 1. Preparation of RA powder.

whether reducing the particle size would enable both old concrete aggregate and old mortar to be used more effectively. The results were compared with the SIFCON composite produced using natural limestone powder. In the scope of the study, fracture energy, compressive strength, sorptivity, and high-temperature resistance tests were carried out.

2. MATERIALS AND METHODS

2.1. Materials

Hooked-end steel fiber 30 mm in length, 0.75 mm in diameter, and 1160 MPa in tensile strength, CEM I 42.5 R type Portland cement, crushed limestone aggregate (LA), and recycled aggregate (RA) were used to produce the specimens. The water absorption capacity of LA and RA were 1.1% and 10.4%, and the specific gravity of aggregates were 2.60 and 2.15, respectively. The water absorption of the RA was considerably higher than that of LA due to the adhered cement mortar.

Kaolin clay was utilized to adjust the viscosity of the slurry. Tables 1 and 2 show the chemical composition and some physical properties of cement and kaolin/recycled aggregate, respectively. In the production of the mixtures, tap water and polycarboxylate ether-based superplasticizer were also used.

2.2. Preparation of Recycled Aggregate Powder

The preparation of RA powder and the situation of aggregates at every step are summarized in Figure 1 and Figure 2, respectively. The RA was provided with a 4–64 mm size range (Fig. 2a). The aggregate also contained brick/roof tile, glazed wall tile, and many flat and elongated particles (Fig. 2b). This aggregate was crushed with a jaw crusher to 0–4 mm (Fig. 2d) and then ground with a Los Angeles test device for 1000 cycles. Afterward, the fine aggregate was sieved through a 0.5 mm sieve, and the fraction passing the sieve (Fig. 2e) was used to produce SIFCON.

The gradation of the aggregates used in the preparation of the slurries is given in Figure 3. LA and RA were screened through different sieves and remixed in definite proportions to obtain the specified gradation.

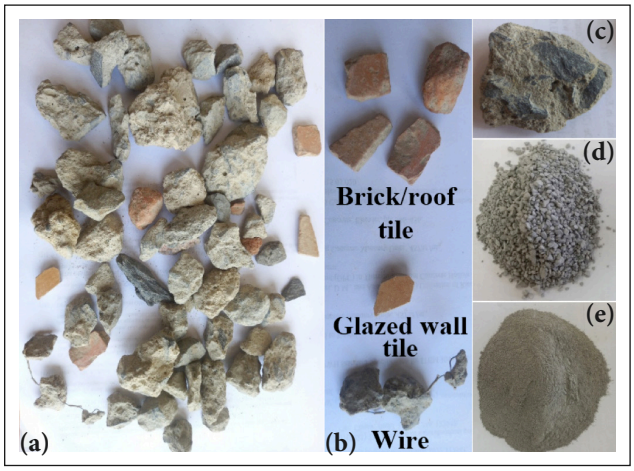

Figure 2. Obtaining RA powder **(a)** recycled aggregate as received; **(b)** different particles; **(c)** adhered mortar to the old concrete aggregate; **(d)** aggregate after crushing to 0–4 mm; **(e)** sieved RA powder after Los Angeles degradation.

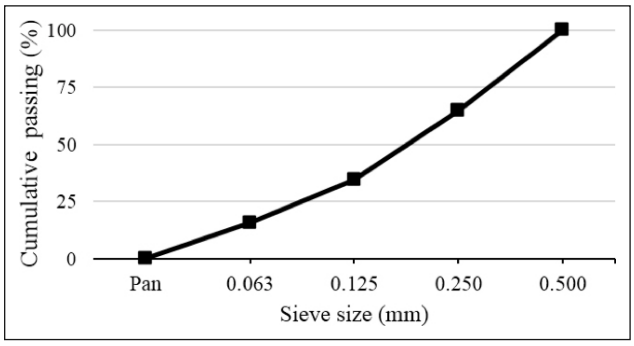

Figure 3. Gradation of aggregates.

2.3. Mixtures and Method

2.3.1. Sample Preparation

The ingredients and some properties of SIFCON mixtures are presented in Table 3. After the molds were lubricated, the fibers were put into the molds with the sprinkling

Table 3. Ingredients and some properties of SIFCONs

Ingredient (kg/m³)	LAS*	RAS**
Cement	640	605
Water	372	365
Limestone aggregate	780	–
Recycled aggregate	–	685
Kaolin	73	63
Steel fiber	620	620
Superplasticizer	7	12
Property		
Flow diameter of slurry (cm)	32.0	32.8
Fresh unit weight (kg/m³)	2441	2294

*: Limestone aggregate SIFCON; **: Recycled aggregate SIFCON.

method without any routing or vibration. At this stage, the fibers were only randomly distributed horizontally, and the position of the fibers in a vertical direction was prevented manually. Sand, kaolin, cement, water, and superplasticizer admixture were put into the mixer bowl during the slurry preparation. With the help of a spoon, the ingredients were mixed for approximately 15 seconds, and then the mixer was operated for 180 seconds at 62.5 rpm. The materials adhering to the wall of the container were removed in 15 seconds with a spoon, and the mixer was operated for another 180 seconds at 125 rpm.

For the sake of comparison, it was aimed to produce slurries with similar flow diameters. To determine the flow diameters of the slurry, a truncated cone with 7 cm top diameter, 10 cm bottom diameter, and 6 cm height

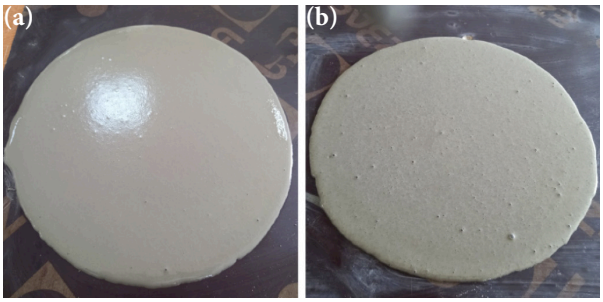

Figure 4. Photographs of slurries at the end of flow diameter tests **(a)** LAS; **(b)** RAS.

was filled with slurry without any compaction. The cone was pulled vertically, and the flow diameter was measured in two perpendicular directions after 30 seconds. The average of these two values was recorded as the flow diameter (Fig. 4). The SIFCONs prepared with limestone and recycled aggregate were coded as LAS (limestone aggregate SIFCON) and RAS (recycled aggregate SIFCON), respectively.

The slurry was poured into the molds with preplaced fibers, and a vibration table was used for 10 seconds to compact the specimens. The molds were kept in laboratory conditions for 24 hours before demoulding, and standard water curing was applied for 27 days (Fig. 5). 71 mm cube, 40×40×160 mm prism, and 50×50×240 mm notched prism specimens with 10 mm notch height and 3 mm notch width were used to determine the compressive strength, sorptivity, and fracture energy, respectively.

Figure 5. Sample preparation and curing.

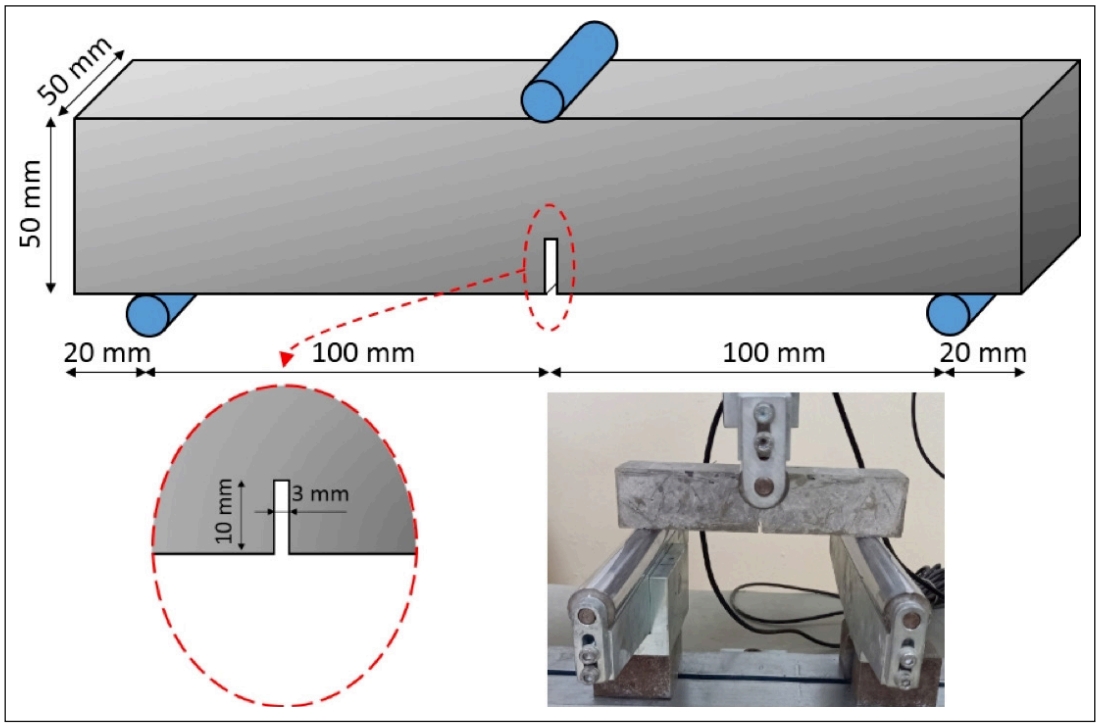

Figure 6. Details of specimen and test setup.

2.3.2. Tests

All hardened state tests were applied to the 28-day age samples. The compressive strengths were determined with 71 mm cube specimens using a mortar compression testing machine at a loading rate of 2.4 kN/s.

A muffle furnace was used to investigate the high-temperature resistance of SIFCONs. Samples were dried in an oven at 60 °C for 72 hours before the test. The temperature rise rate of the muffle furnace was 10 °C/minute. The samples were heated at 900 °C for 3 hours. Then, the specimens were allowed to cool gradually in the furnace. When the sample temperatures reached room temperature, the flexural test was applied, and the fracture energy losses were recorded.

ASTM C1585 Standard [35] was used to determine the rate of capillary water absorption. During the test, samples of 40×40×160 mm prism specimens were used. All parts of the samples, except the bottom surfaces (40×40 mm) that will come into contact with water, were covered with a waterproof insulation material, and experiments were carried out according to the relevant standard.

RILEM [36] defined fracture energy as the required energy for creating one unit area of a crack and stated that notched beam specimens can be used to calculate fracture energy. In this study, a fracture energy test was carried out using a 3-point flexural test setup with a displacement-controlled universal test machine at a 0.01 mm/minute rate. The test was ended when the peak load dropped by 95%. The fracture energy was calculated using Equation 1. considering the RILEM (50-FMC) [36]. The W_0, mg, δ_0 are the area under the load-displacement curve, the weight of the specimen between supports, and maximum displacement, respectively. The displacements were taken from the universal test device's measurement at the specimen's midspan. A is the midspan cross-sectional area without the notch. The details of the specimens used and the application of the test are shown in Figure 6.

$$G_F=(W_0+ mg\delta_0)/A \quad (1)$$

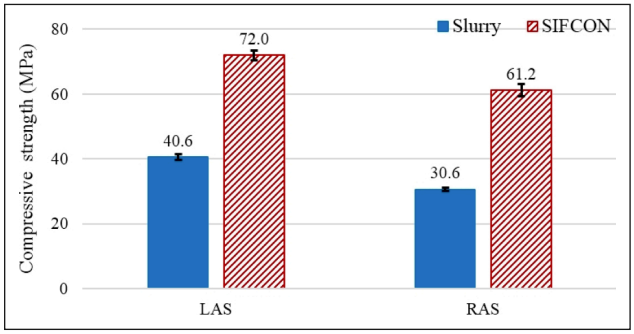

Figure 7. Compressive strengths of slurries and SIFCONs.

3. RESULTS AND DISCUSSION

3.1. Compressive Strength

The compressive strength of slurry and SIFCON specimens are shown in Figure 7. The compressive strengths of SIFCON samples produced with LA and RA are higher than those of fiber-free slurries by 77% and 100%, respectively. The compressive strength of slurry and SIFCON samples containing limestone aggregate was higher than those of specimens prepared with RA by 33% and 18%, respectively. Fan et al. [37] investigated the effect of fine recycled aggregate produced by two methods on the concrete properties produced with 0.35 and 0.55 w/c ratios. The researchers stated that the compressive strengths of the concretes produced with 100% recycled fine aggregate were up to 33% and 48%

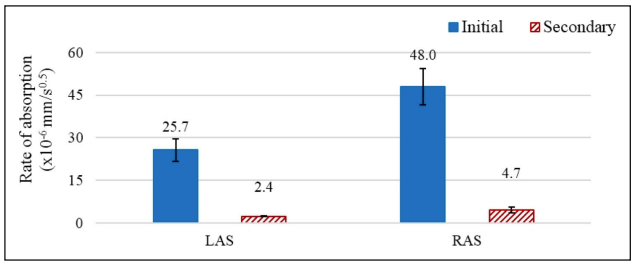

Figure 8. Rates of capillary absorption of LAS and RAS samples.

lower in the 0.35 and 0.55 w/c ratio concretes than those of the control samples (having the same water/cement ratios). In a similar study, Ju et al. [38] used fine recycled aggregate as a partial replacement for natural fine aggregate in normal- and high-strength concrete. It was determined that the compressive strengths in normal- and high-strength concrete mixtures decreased by 29% and 8%, respectively, using 100% recycled aggregate. The fact was attributed to the high porosity of the recycled aggregate arising from its adhered mortar, which was also the cause of the low density and high-water absorption capacity of recycled aggregate [39, 40].

3.2. Rate of Capillary Absorptions

The rate of capillary absorption values of the samples is shown in Figure 8. Initial and secondary rates of absorptions of SIFCON prepared with RA were 87% and 96% higher than those of the limestone aggregate SIFCON. It is thought that both the mortar still stuck to the aggregate particles after grinding in the Los Angeles testing device and the separated old mortar particles, which have a porous structure, are responsible for the high rate of sorptivity values. Ayub et al. [41] reported that the sorptivity of recycled aggregate concrete was higher than that of the reference mixture. In addition, it was stated that sorptivity gradually increases with the increase of the recycles aggregate substitution rate. Civioglu [42] also obtained similar results in his study. Algin [43] investigated the effects of recycled aggregates on self-compacting concrete. The researcher reported that using recycled aggregates increased the sorptivity. This situation was attributed to the high-water absorption capacity of the recycled aggregate [44].

3.3. Fracture Energy and the Effect of High Temperature on Fracture Energy

Load-midspan displacement graphs of the samples before and after exposure to high temperatures are given in Figure 9 and Figure 10, respectively. The peak load and maximum displacement values of the samples produced with limestone were higher than those containing RA before and after the high-temperature effect. Peak loads were reached quickly in the samples produced with both aggregate types. After the peak, the composite continued carrying the load until the maximum displacement values (end of test), but the load gradually decreased. After the effect of high temperature, both the peak loads and the maximum displacement values decreased compared to the samples not exposed to high temperature.

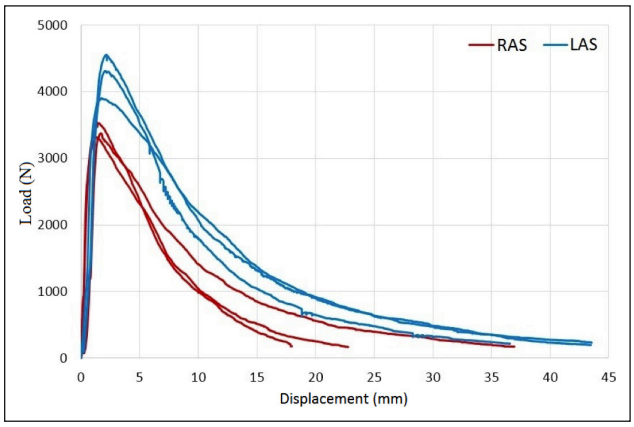

Figure 9. Load-displacement curves of samples before high-temperature effect.

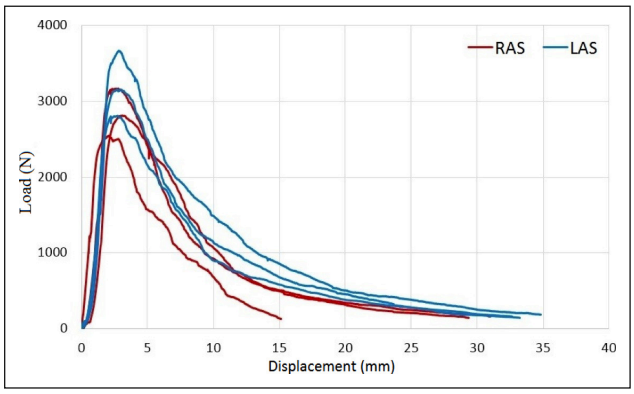

Figure 10. Load-displacement curves of samples after exposure to 900 °C.

The average peak load, fracture energy values, and displacement corresponding to the peak load of SIFCONs are shown in Figure 11. It was seen that the peak loads of LA SIFCONs either before or after the effect of 900 °C were higher than those of the SIFCONs produced with RA. The fact seems to be caused by the porous structure of the old mortar adhering to the recycled aggregate particles and the weak structure of the old mortar particles separated from the aggregate particles. In addition, new interfacial transition zones formed between the new and the old mortar and between aggregate and new paste are likely to impact this behavior of the mixtures significantly. While the peak loads of LASs were 25% higher than those of the RASs before the high temperature, this value decreased to 13% after the high-temperature effect.

Similarly, the displacement values corresponding to the peak loads of the LASs were 35% and 3% higher than those of the RASs before and after the high temperature, respectively. The higher displacement values corresponding to the peak loads of LASs indicated that these SIFCONs were more resistant to the initial crack formation than RAS and prevented the crack formation for a more extended period than RAS. Here, as in the peak loads, the difference between the displacement of two series decreased after exposure to high-temperature and even reached almost the same point.

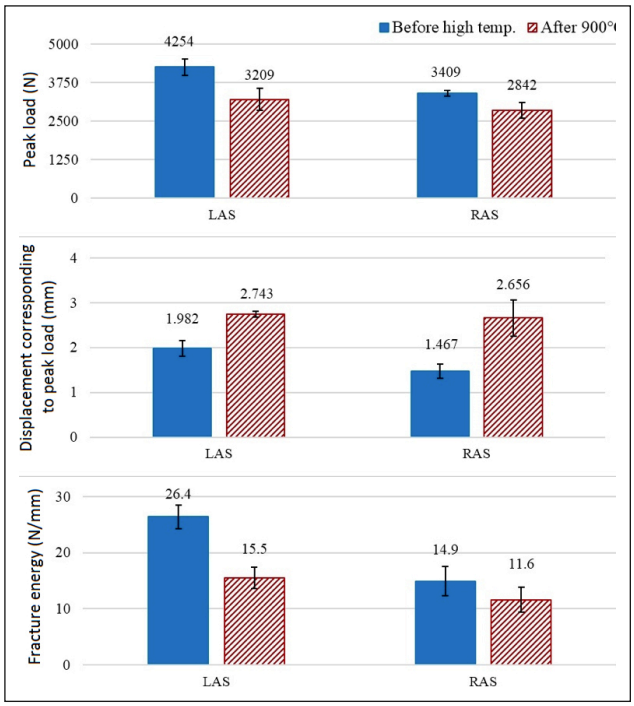

Figure 11. Peak loads, displacement corresponding to peak loads, and fracture energy of mixtures.

There are similar trends in fracture energies to peak load and displacement values corresponding to peak load. As expected, both before and after the high temperature, the fracture energies of LASs are higher than those of RASs. The fracture energies of LASs were 77% and 34% higher than RASs before and after the high-temperature effect. Like the other results, the fracture energy values became close after high temperature.

The losses in peak load and fracture energy with high temperature are shown in Figure 12. Samples produced using limestone suffered more than those produced with recycled aggregate. Although the peak loads and fracture energy values before the high-temperature effect are not the same, it is possible to say that SIFCONs produced with recycled aggregate are more resistant to high temperatures. The number of factors affecting this situation is relatively high. Kou et al. [45] investigated the effect of recycled aggregate substitution on the high-temperature resistance of concrete. They stated that with recycled aggregate, the compressive strength losses of concretes exposed to 800 °C were reduced compared to that of the control sample.

Similarly, in this study, with high temperatures, the SIFCON samples produced with recycled aggregate lost strength at lower rates than the LAS mixture. It has been stated that the thermal expansion coefficient of the old adhered mortar in the recycled aggregate is more compatible with the thermal expansion coefficient of the new mortar layer than that of the natural aggregate [46]. In addition, it is thought that the porous structure of the recycled aggregate facilitates the evacuation of the evaporated water. In this way, the internal stresses caused by the vapor pressure are reduced.

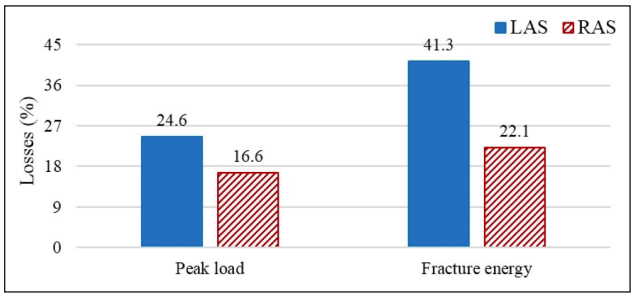

Figure 12. Peak load and fracture energy losses after high-temperature effect.

4. CONCLUSIONS

This study investigated the effects of recycled aggregate on compressive strength, sorptivity, fracture energy, and high-temperature resistance of SIFCONs. For this purpose, limestone and recycled aggregate under 0.5 mm were used. For the materials used and tests applied, the following conclusions may be drawn:

- The compressive strength of slurry and SIFCON prepared with recycled aggregate were 30.6 MPa and 61.2 MPa, respectively. The strength of limestone aggregate-bearing slurry and SIFCON were 33% and 18% higher than those of the recycled aggregate-bearing counterparts.
- The initial and secondary absorption rates of limestone aggregate SIFCON were 25.7×10^{-6} "mm/√s" and 2.4×10^{-6} "mm/√s", respectively. These values increased by 87% and 96% with using recycled aggregate.
- The fracture energy of recycled aggregate SIFCON was 14.9 N/mm, 44% lower than that of the SIFCON prepared with limestone aggregate. Additionally, the peak load and displacement corresponding to the peak load of limestone aggregate SIFCON were higher than those of the recycled aggregate SIFCON.
- After exposure to 900 °C temperature, the fracture energy of limestone and recycled aggregate SIFCON reduced to 15.5 N/mm and 11.6 N/mm, respectively. The relative reduction in fracture energy of the recycled aggregate SIFCON upon exposure to 900 °C (22%) was roughly half that of the SIFCON containing limestone aggregate (41%).

This study is a preliminary study examining the usability of recycled aggregate in SIFCON production. Increasing the number of studies on these materials' strength and durability properties will increase the cumulative knowledge on this subject.

ETHICS

There are no ethical issues with the publication of this manuscript.

DATA AVAILABILITY STATEMENT

The author confirm that the data that supports the findings of this study are available within the article. Raw data that support the finding of this study are available from the corresponding author, upon reasonable request.

CONFLICT OF INTEREST

The author declare that he have no conflict of interest.

FINANCIAL DISCLOSURE

The author declared that this study has received no financial support.

USE OF AI FOR WRITING ASSISTANCE

Not declared.

PEER-REVIEW

Externally peer-reviewed.

REFERENCES

[1] Bayraktar, O. Y., Kaplan, G., Shi, J., Benli, A., Bodur, B., & Turkoglu, M. (2023). The effect of steel fiber aspect-ratio and content on the fresh, flexural, and mechanical performance of concrete made with recycled fine aggregate. *Constr Build Mater*, *368*, 130497. [CrossRef]

[2] Madandoust, R., Kazemi, M., Talebi, P. K., & De Brito, J. (2019). Effect of the curing type on the mechanical properties of lightweight concrete with polypropylene and steel fibers. *Constr Build Mater, 223*, 1038–1052. [CrossRef]

[3] Watts, M. J., Amin, A., Gilbert, R. I., & Kaufmann, W. (2020). Behavior of fiber reinforced concrete members under sustained axial/flexural load. *Struct Concr, 21*(4), 1441–1457. [CrossRef]

[4] Wu, H., Lin, X., & Zhou, A. (2020). A review of mechanical properties of fibre reinforced concrete at elevated temperatures. *Cem Concr Res, 135*, 106117. [CrossRef]

[5] Shelorkar, A. P. (2021). Slurry infiltrated fibrous concrete (SIFCON) - A review. *Int J Res Publ Rev, 2*(8), 780–787.

[6] Wang, W., Shen, A., Lyu, Z., He, Z., & Nguyen, K. T. Q. (2021). Fresh and rheological characteristics of fiber reinforced concrete - A review. *Constr Build Mater, 296*, 123734.[CrossRef]

[7] Farnam, Y., Moosavi, M., Shekarchi, M., Babanajad, S. K., & Bagherzadeh, A. (2010). Behaviour of Slurry Infiltrated Fibre Concrete (SIFCON) under triaxial compression. *Cem Concr Res, 40*(11), 1571–1581. [CrossRef]

[8] Gok, S. G., & Sengul, O. (2023). Mechanical properties of alkali-activated slag based SIFCON incorporating waste steel fibers and waste glass. *Constr Build Mater, 408*, 133697. [CrossRef]

[9] Beglarigale, A., Yalçınkaya, Ç., Yiğiter, H., & Yazıcı, H. (2016). Flexural performance of SIFCON composites subjected to high temperature. *Constr Build Mater, 104*, 99–108. [CrossRef]

[10] Ipek, M., & Aksu, M. (2019). The effect of different types of fiber on flexure strength and fracture toughness in SIFCON. *Constr Build Mater, 214*, 207–218. [CrossRef]

[11] Yazıcı, H., Yiğiter, H., Aydın, S., & Baradan, B. (2006). Autoclaved SIFCON with high volume Class C fly ash binder phase. *Cem Concr Res, 36*(3), 481–486. [CrossRef]

[12] Ali, M. H., Atiş, C. D., & Al-Kamaki, Y. S. S. (2022). Mechanical properties and efficiency of SIFCON samples at elevated temperature cured with standard and accelerated method. *Case Stud Constr Mater, 17*, e01281. [CrossRef]

[13] Abbas, A. S., & Kadhum, M. M. (2020). Impact of fire on mechanical properties of Slurry Infiltrated Fiber Concrete (SIFCON). *Civil Eng J, 6*, 12–23. [CrossRef]

[14] Aygörmez, Y., Al-mashhadani, M. M., & Canpolat, O. (2020). High-temperature effects on white cement-based slurry infiltrated fiber concrete with metakaolin and fly ash additive. *Rev Constr, 19*(2), 324–333. [CrossRef]

[15] Tauma, W. K., & Balázs, G. L. (2023). Impact and blast resistance of slurry infiltrated fiber concrete (SIFCON): A comprehensive review. *Concr Struct*, 129–136. [CrossRef]

[16] Khan, M., & McNally, C. (2023). A holistic review on the contribution of civil engineers for driving sustainable concrete construction in the built environment. *Dev Built Environ, 16*, 100273. [CrossRef]

[17] Al-Hadithi, A. K. Y., & Al-Hadithi, A. I. (2022). Compressive and impact loads' effects on the behaviour of SIFCON made of plastic waste fibers. *Iraqi J Civil Eng, 16*(2), 44–54. [CrossRef]

[18] Celikten, S., & Canbaz, M. (2022). Influence of binder type on the mechanical properties of SIFCON composites made with waste steel fibers. *J Polytechnic, 25*(1), 251–256. [CrossRef]

[19] Drdlova, M., Prachar, V., Cechmanek, R., & Svitak, O. (2019, June 26–29). *Utilization of waste steel fibres from tires in slurry infiltrated fibre concrete for blast protective elements*. 7th International Conference on Sustainable Solid Waste Management, Heraklion, Crete Island, Greece/

[20] Canbaz, M., & Celikten, S. (2020). Utilization of crumbed waste tire rubbers for the production of SIFCON with different binders. *J Eng Archit Fac Eskisehir Osmangazi Univ, 28*(1), 9–15. [CrossRef]

[21] Tiwari, P., Kushwaha, Y., & Agrawal, A. (2019). SIFCON's behaviour on partial replacement of cement with waste glass powder. *Int J Res Advent Technol, 7*(9), 24–28. [CrossRef]

[22] Khan, S. A., & Selvaraju, G. (2019). Characteristic of slurry infiltrated fibrous concrete (SIFCON) produced by partially replacing cement by mineral admixtures and steel fibers by waste plastic fibers. *J Adv Res Eng Knowl, 7*(1), 1–15.

[23] Altunci, Y. T., & Ocal, C. (2022). The effect of peanut shell ash on some engineering features of SIFCON. *J Eng Sci Des, 10*(3), 869–877. [CrossRef]

[24] Riyar, R. L., Nazeer, M., Kapoor, K., Singh, R. B., & Singh, P. (2021). Hardened state behavior of beneficiated recycled aggregate concrete. *J Sustain Cem-Based Mater, 10*(6), 319–335. [CrossRef]

[25] Chang, C. Y., Huang, R., Lee, P. C., & Weng, T. L. (2014). Determining the optimal mixture for recycled aggregate concrete with multiple responses. *J Chin Inst Eng, 37*(2), 165–174. [CrossRef]

[26] Ouyang, K., Liu, J., Liu, S., Song, B., Guo, H., Li, G., & Shi, C. (2023). Influence of pre-treatment methods for recycled concrete aggregate on the performance of recycled concrete: A review. *Resour Conserv Recycl, 188*, 106717. [CrossRef]

[27] Nazarimofrad, E., Shaikh, F. U. A., & Nili, M. (2017). Effects of steel fibre and silica fume on impact behaviour of recycled aggregate concrete. *J Sustain Cem-Based Mater, 6*(1), 54–68. [CrossRef]

[28] Ataria, R. B., & Wang, Y. C. (2023). Improving the mechanical properties of recycled aggregate concrete with graphene. *Eur J Environ Civ Eng, 27*(4), 1747–1762. [CrossRef]

[29] Cakır, O., & Sofyanli, O. O. (2015). Influence of silica fume on mechanical and physical properties of recycled aggregate concrete. *HBRC J, 11*(2), 157–166. [CrossRef]

[30] Kim, J. (2022). Influence of quality of recycled aggregates on the mechanical properties of recycled aggregate concretes: An overview. *Constr Build Mater, 328*, 127071. [CrossRef]

[31] Danish, A., & Mosaberpanah, M. A. (2022). A review on recycled concrete aggregates (RCA) characteristics to promote RCA utilization in developing sustainable recycled aggregate concrete (RAC). *Eur J Environ Civ Eng, 26*(13), 6505–6539. [CrossRef]

[32] Hosseinnezhad, H., Tosun, E., Cakir, O., & Ramyar, K. (2022). Characterization of coarse recycled aggregates produced from concretes with different strength levels. *Nat Appl Sci J, 5*(1), 38–46. [CrossRef]

[33] Veriana, K. P., Ashraf, W., & Cao, Y. (2018). Properties of recycled concrete aggregate and their influence in new concrete production. *Resour Conserv Recycl, 133*, 30–49. [CrossRef]

[34] McNeil, K., & Kang, T. H. K. (2013). Recycled concrete aggregates: A review. *Int J Concr Struct Mater, 7*(1), 61–69. [CrossRef]

[35] ASTM International. (2021). ASTM C1585-Standard Test Method for Measurement of Rate of Absorption of Water by Hydraulic-Cement Concretes.

[36] RILEM (50-FMC). (1985). Determination of the fracture energy of mortar and concrete by means of three-point bend tests on notched beams. *Mater Struct, 18*(4), 287–290. [CrossRef]

[37] Fan, C. C., Huang, R., Hwang, H., & Chao, S. J. (2016). Properties of concrete incorporating fine recycled aggregates from crushed concrete wastes. *Constr Build Mater, 112*, 708–715. [CrossRef]

[38] Ju, M., Park, K., & Park, W. J. (2019). Mechanical behavior of recycled fine aggregate concrete with high slump property in normal- and high-strength. *Int J Concr Struct Mater, 13*(1), 61. [CrossRef]

[39] Pourghadrı Sefıdehkhan, H., & Şimşek, O. (2018). Investigation of some engineering properties of concrete made with recycled aggregate in different ratios. *J Polytechnic, 21*(1), 83–91.

[40] Saravanakumar, P., Abhiram, K., & Manoj, B. (2016). Properties of treated recycled aggregates and its influence on concrete strength characteristics. *Constr Build Mater, 111*, 611–617. [CrossRef]

[41] Ayub, T., Khan, A. R., & Mahmood, W. (2020). Effect of recycled concrete aggregates on compressive strength and water permeability of concrete. *Int J Energy Environ, 14*, 25–32. [CrossRef]

[42] Civioglu, F. S. (2020). *Investigation of physical, mechanical and durability properties of self-compacting concretes produced with recycled concrete aggregate*. [Master's Thesis, Afyon Kocatepe University].

[43] Algin, Z. (2020). The effect of recycled aggregate replacements on some hardened properties of self-compacting concrete [Geri kazanılmış agrega İkamesinin kendiliğinden yerleşen betonların bazı sertleşmiş özelliklerine etkisi]. *Harran Univ Eng J, 5*(3), 183–193. [CrossRef]

[44] Benito, E. K. D., Aragoncillo, A. M. M., Pascua, F. A. A., Juanites, J. M., Eneria, M. A., Zafra, R. G., & Madlangbayan, M. S. (2023). *Durability performance of concrete containing recycled coarse aggregates derived from laboratory-tested specimens. World J Eng.* https://www.emerald.com/insight/content/doi/10.1108/WJE-02-2023-0033/full/html [CrossRef]

[45] Kou, S. C., Poon, C. S., & Etxeberria, M. (2014). Residue strength, water absorption and pore size distributions of recycled aggregate concrete after exposure to elevated temperatures. *Cem Concr Compos, 53*, 73–82. [CrossRef]

[46] Zega, C. J., & Di Maio, A. A. (2006). Recycled concrete exposed to high temperatures. *Mag Concr Res, 58*(10), 675–682. [CrossRef]

J Sustain Const Mater Technol, Vol. 9, Issue. 1, pp. 45–59, March 2024

Journal of Sustainable Construction Materials and Technologies
Web page info: https://jscmt.yildiz.edu.tr
DOI: 10.47481/jscmt.1390474

JSCMT
Journal of Sustainable Construction Materials and Technologies

Research Article

Evaluating the factors influencing the sustainable refrigerant selection by fuzzy decision making approach

Mehmet SEYHAN[1], Ertuğrul AYYILDIZ[1], Melike ERDOĞAN[2]

[1]*Department of Mechanical Engineering, Karadeniz Technical University, Trabzon, Türkiye*
[2]*Department of Computer Engineering, Düzce University, Düzce, Türkiye*

ARTICLE INFO

Article history
Received: 14 November 2023
Revised: 20 February 2024
Accepted: 27 February 2024

Keywords:
AHP, energy efficiency, fuzzy logic, refrigerant, sustainability, type-2 fuzzy numbers

ABSTRACT

Considering that cooling in cooling systems is more costly than heating, the importance of refrigerant selection in cooling systems is even more obvious. Due to the complexity of the refrigerant selection problem, a multi-criteria decision approach must be used to implement a thorough and organized evaluation of the factors. The purpose of this study is to evaluate the criteria to be considered when choosing refrigerants using the interval type-2 trapezoidal fuzzy Analytic Hierarchy Process (AHP). As a result, the most important and least crucial refrigerant selection criteria are determined by calculating the weights and obtaining the ranking of the requirements. In this way, the refrigerant selection criteria are prioritized, and the most crucial factor in refrigerant selection has emerged as energy efficiency. In light of the results, it has become clear that it is now essential for everyone in the world to use environmentally friendly, highly effective refrigerants.

Cite this article as: Seyhan, M., Ayyıldız E., & Erdoğan, M. (2024). Evaluating the factors influencing the sustainable refrigerant selection by fuzzy decision making approach. *J Sustain Const Mater Technol*, 9(1), 45–59.

1. INTRODUCTION

The global energy consumption of refrigeration and air conditioning is approximately 20% [1]. For this reason, refrigeration systems, including heat pumps, pulsating heat pipes [24, 25], refrigerators, HVAC (heating, ventilation, and air conditioning), etc., have vital importance in our daily and business lives. They help cool dwelling places, business offices, and meat, vegetables, and fruit products [2, 3]. The main component of refrigeration systems is refrigerants, which are working fluids that change phase from gas to liquid regularly. In the literature, there are two different classifications of refrigerants. The first is related to chemical compositions [4], and the second is about the progression of refrigerants from the past to now [5]. Refrigerants can be divided into five groups that are natural refrigerants, chlorofluorocarbons (CFCs), hydrochlorofluorocarbons (HCFCs), refrigerant blends, and hydrofluorocarbons (HFCs) [3, 4] in terms of chemical compositions.

The evolution of refrigerants from their invention to the future is shown in Figure 1 by dividing into four generations [5]. These are the first generation from 1830 to the 1930s, the second generation from 1931 to 1990s, the third generation from 1991 to 2010s, and the fourth generation from 2010 to now in terms of development of refrigerants in the long run. The first generation of refrigerants

***Corresponding author.**
*E-mail address: ertgrulayyildiz@ktu.edu.tr

was used regardless of flammability, toxicity, and environmental impacts [1, 5]. In the second generation of refrigerants, the producer was taken into account the safety and durability of the refrigerants. HCFCs and CFCs are the refrigerant types commonly used in this generation. Third-generation refrigerants were developed to protect the ozone layer due to the requirement of the Montreal Protocol [6]. This protocol restricts the HCFCs and CFCs to achieve low ozone depletion potential (ODP). The fourth-generation refrigerants evolved because of concerns about the growing global warming after the Kyoto Protocol. According to this Protocol, countries must restrict or prohibit using the HFCs and PFCs types of refrigerants [3, 5]. In developing fourth-generation refrigerants, refrigerants with low/zero ODP, low global warming potential (GWP), and high efficiency have been developed and produced due to the increasing global warming concern.

The European Union (EU) Commission has restricted using HFC refrigerants due to their high global warming potential [7]. Hydrofluoroolefin refrigerants (HFO) present low/zero ODP and extremely low GWP due to the absence of no chlorine and a brief atmospheric period [8]. Hence, HFOs have great potential to be used as the fourth-generation refrigerant [9]. Along with developing or selecting the more eco-friendly refrigerant, other essential properties, such as sustainability, thermodynamic properties, flammability, etc., play an essential role in choosing a new refrigerant [10, 11]. Thermodynamic properties must be a high coefficient of performance (COP), thermal conductivity, vapor density, latent vaporization heat, low liquid viscosity, critical pressure, and liquid density to determine the suitable refrigerants in refrigeration systems. In selecting the appropriate refrigerant, it must have low/zero ODP [12], [13], low GWP [2, 3, 6, 10–12, 14–19], flammability [2, 3, 6, 10–12, 14, 15, 17–19], low secondary environmental impacts [2] and toxicity [2, 3, 10–12, 14, 15, 17, 19] in terms of environmental impacts. McLinden et al. [1] and Kaseeian et al. [2] prepared the required criteria list, including minimal flammability, low toxicity, GWP and secondary environmental impacts, zero ODP, long operational life, material compatibility, maximized recyclable content, maximum energy efficiency, reasonable cost, and stable for the life of the system for requirements for new refrigerants. In the study of Vuppaladadiyam et al. [3], they reviewed the development of refrigerants and their undesired environmental impacts. They mentioned ideal fourth-generation refrigerant properties such as zero ODP, low GWP, high efficiency, no toxicity, and no flammability. Abas et al. [4] researched the optimal refrigerant for low GWP and no ODP for the solar water heating system. Mohanraj and Abraham's review study [5] analyzed eco-friendly refrigerants for automobile air conditioners regarding thermophysical, thermodynamic, and chemical characteristics. Another review study by Bolaji and Huan [6] suggested natural refrigerants reduce the environmental impacts of the HFC, CFC, and HCFC refrigerants. Meng et al. [7] investigated the conditioning performance of a suggested R1234yf/R134a refrigerant having low GWP, no ODP, and no flammability for automobile air conditioner systems. Their suggested refrigerant helps to reduce the GWP impacts and eliminate the ODP and flammability. Direk et al. [8] experimentally investigated the performance of alternative refrigerants, R444A and R152a, in automobile air conditioner systems to reduce environmental impacts such as GWP and ODP. They found that R152a refrigerant significantly enhances the refrigeration performance compared to the R134a and R444A.

Table 1 summarizes the literature on refrigerant selection using different types of MCDM and machine learning methods. In the study of Poongavanam et al. [11], they found the optimum refrigerant for the automobile refrigeration system with the help of TOPSIS, MOORA, EDAS, and sensitivity analysis. Souayeh et al. [12] used MCDM methods like TOPSIS, EDAS, and MOORA to select environmentally friendly refrigerants in applying HVAC and renewable energy devices. Similarly, Ustaoğlu

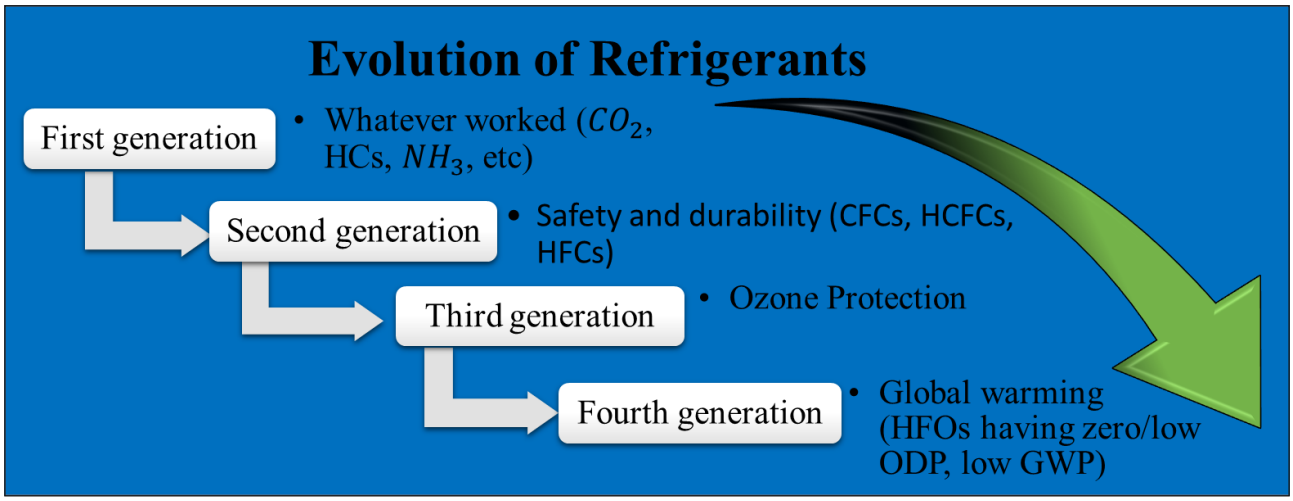

Figure 1. Evolution of refrigerants in time.

Table 1. Summary of literature related to refrigerant selection

Author(s)	Subject	Methods
Poongavanam et al. [11]	Refrigerant selection in the application of refrigeration systems for automobile	TOPSIS, MOORA, EDAS, and Sensitivity analysis
Devotta et al. [22]	Classification of refrigerant in terms of flammability	ANN, Random forest model
Souayeh et al. [12]	Eco-friend refrigerant selection in the application of HVAC and Renewable energy devices	TOPSIS, EDAS, MOORA
Prabakaran [23]	Optimization of future refrigerants for domestic refrigerant system	EDAS, Sensitivity analysis
Koundinya [21]	Selection of best refrigerant in terms of Environmental, Exergy, Economic, and Energy for heat pump	TOPSIS
Ustaoğlu et al. [20]	Refrigerant selection for vapor compression refrigeration cycle in terms of environmental, economic, safety, and cost	Taguchi, ANOVA, TOPSIS

et al. [20], for the vapor compression refrigeration cycle, and Koundinya and Seshadri [21] for the heat pump, selected the best refrigerant by using Taguchi, TOPSIS, and ANOVA and TOPSIS, respectively. On the other hand, Devotta et al. [22] performed a classification study for refrigerants regarding flammability with the help of ANN and the Random forest model.

Considering the sub-criteria mentioned above under main criteria such as thermodynamics, sustainability, and environmental, selecting the most suitable refrigerant for refrigeration systems is very challenging. At the same time, suitable refrigerants are determined using theoretical, simulation, and experimental methods, which take a long time and cost a lot of money [11]. Multi-criteria decision-making (MCDM) methods present a comprehensive selection and evaluation process considering different criteria for selecting eco-friendly, more efficient, and sustainable refrigerants. The need to consider many factors in the selection of refrigerants has made it possible to use the MCDM approach. Furthermore, it would be reasonable to use fuzzy logic to express the values that cannot be obtained numerically in the process and to model the uncertainty best. Based on all these important considerations, the problem of refrigerant selection is discussed in this paper, and a fuzzy MCDM approach is proposed to solve this problem. Besides, type-2 fuzzy sets, an extended version of fuzzy sets, handle uncertainty best and obtain results closest to the real world. As a result of detailed literature research, elements that should be considered in selecting the best refrigerant are determined, and then a prioritization analysis is performed to reveal the relative importance of these factors. For this purpose, the Analytic Hierarchy Process (AHP) method is utilized, which is an MCDM approach based on the pairwise comparison principle and is the most frequently used in the literature. As a result of this proposed fuzzy-based MCDM analysis, factors that should be considered first in selecting a refrigerant system have been successfully determined.

This study presents an innovative approach to addressing the complicated problem of refrigerant selection in cooling systems. This study introduces the interval type-2 trapezoidal fuzzy AHP for evaluating and ranking these criteria and factors. Previous research has emphasized the significance of considering various criteria and characteristics during selection. This study provides a more accurate representation of the decision-making process by employing type-2 fuzzy sets, which can effectively deal with uncertainty and model real-world scenarios. In addition, using the AHP method in conjunction with fuzzy logic is a novel combination that provides a systematic and exhaustive evaluation of refrigerant selection criteria. The results of this study not only list the factors that influence the selection of a sustainable refrigerant but also emphasize the importance of energy efficiency in this decision-making process. This research contributes to the field by introducing a novel methodology that improves the comprehension and application of sustainable refrigerant selection in cooling systems.

Section 2 presents the adopted methodology in detail. Section 3 includes the application for the refrigerant selection problem. While discussing the study's findings in Section 4 in Section 5, the study concludes with an evaluation of the results.

2. THE PROPOSED METHODOLOGY

MCDM approaches are valuable for handling comparison problems with diverse measurement units [24]. They enable the evaluation of qualitative and quantitative factors simultaneously, aiding in real-life problem-solving [25]. MCDM-based methodologies are widely used in different areas [26]. Concrete and abstract criteria pose challenges in decision-making, mainly when more abstract criteria exist. Fuzzy sets help represent data accurately and handle uncertainties and ambiguities [25].

The utilization of MCDM approaches in decision-making offers various benefits. Firstly, MCDM enables a structured and systematic evaluation and comparison of options based on multiple criteria. This approach provides a comprehensive framework for considering various factors and facilitates a thorough analysis of available alternatives. Secondly, MCDM allows for the explicit

consideration and weighing of the relative importance of criteria. Decision makers can assign weights to each criterion, ensuring the final decision reflects their priorities and values. Thirdly, MCDM approaches provide a clear and transparent decision rationale, fostering stakeholder support and consensus. The systematic nature of MCDM allows decision-makers to justify their choices based on a well-defined evaluation process.

Furthermore, MCDM facilitates the identification and evaluation of trade-offs between different criteria. In situations where it is impossible to optimize all criteria simultaneously, MCDM assists in understanding the compromises and trade-offs associated with other alternatives. Lastly, MCDM approaches enable the integration and synthesizing information from multiple sources, which is particularly beneficial in complex decision-making situations. By considering diverse perspectives and combining information from various stakeholders, MCDM enhances the quality and effectiveness of the decision-making process. Fuzzy MCDM methods utilize fuzzy logic to handle uncertain or imprecise information [27]. They are beneficial when evaluating multiple options with conflicting criteria and uncertain or inaccurate information. Fuzzy sets and membership functions allow flexible representation of criteria uncertainty and subjectivity. They are valuable in decision-making where classical methods fall short [28].

Fuzzy logic, suggested by Zadeh [29, 30] deals with approximate reasoning, representing uncertainty and fuzziness in real-world situations flexibly [31, 32]. It utilizes fuzzy sets with membership degrees from 0 to 1 [33]. Fuzzy logic finds applications in control systems, pattern recognition, and natural language processing, effectively handling uncertain or imprecise information. Fuzzy set theory quantifies linguistic variables to compare alternatives. Type-2 fuzzy sets take more uncertainty and are suitable for decision-making with subjective judgments [34]. They provide a more realistic conversion of information from decision-makers into numerical values [35]. Type-2 fuzzy sets offer more flexibility and expressiveness than type-1 fuzzy sets [36], thus enhancing the decision-making process in several ways. Firstly, type-2 fuzzy sets allow for the modeling of higher levels of uncertainty by accommodating varying degrees of fuzziness within the membership function [37]. This capability is particularly relevant in complex decision-making scenarios, such as refrigerant selection, where multiple factors and criteria may exhibit different levels of uncertainty. Secondly, type-2 fuzzy sets represent uncertainty in the membership function and the uncertainty bounds associated with the membership grades [38]. This additional layer of uncertainty modeling provides decision-makers with more nuanced information about each criterion's assessment's reliability and confidence level, contributing to a more robust decision-making process.

Furthermore, type-2 fuzzy sets offer flexibility in handling conflicting and ambiguous information, which is common in real-world decision-making contexts [39]. Type-2 fuzzy sets are used in this study based on their ability to address these specific challenges inherent in refrigerant selection [40]. Adopting type-2 fuzzy sets in this study facilitated a more comprehensive analysis of refrigerant selection criteria, enhancing the decision-making process compared to traditional type-1 fuzzy sets [41].

AHP is used to model MCDM problems with tangible and intangible criteria in a hierarchical structure [42] and developed by Saaty [43]. It calculates criteria weights through pairwise comparisons based on expert judgments. AHP is chosen due to its ability to handle qualitative and quantitative criteria, ensure consistency of judgments, and create a hierarchical structure. For the sustainable refrigerant selection problem, AHP is suitable because of its hierarchical structure [44] and linguistic evaluation of decision-makers. Type-2 fuzzy AHP is a promising approach that addresses high uncertainty from experts' subjective assessment of membership degrees. MCDM approaches, AHP based on type-2 fuzzy sets, offer valuable tools to improve decision-making in complex situations, enhancing the quality and effectiveness of the process [45].

The method adopted to solve the refrigerant selection problem in the paper is expressed in detail in the following sub-sections.

2.1. Interval type-2 fuzzy sets

The definitions of type-2 fuzzy sets and interval type-2 trapezoidal fuzzy sets are introduced in this sub-section [46–48]:

Definition 1. A type-2 fuzzy set $\tilde{\tilde{A}}$ is expressed with a type-2 membership function $\mu_{\tilde{\tilde{A}}}$ in the universe of discourse X, as shown:

$$\tilde{\tilde{A}} = \{((x,u),\mu_{\tilde{\tilde{A}}}(x,u))|\forall x \in X, \forall u \in J_X \subseteq [0,1], 0 \leq \mu_{\tilde{\tilde{A}}}(x,u) \leq 1\} \quad (1)$$

Where J_x denotes an interval in [0, 1]. Furthermore, the type-2 fuzzy set $\tilde{\tilde{A}}$ can be presented:

$$\tilde{\tilde{A}} = \int_{x\in X} \int_{u\in J_X} \mu_{\tilde{\tilde{A}}}(x,u)/(x,u) \quad (2)$$

where $J_x \subseteq [0,1]$ and $\iint$ show union over all admissible x and u.

Definition 2. $\tilde{\tilde{A}}$ is a type-2 fuzzy set and is presented by the type-2 membership function $\mu_{\tilde{\tilde{A}}}$ in the universe of discourse X. If all $\mu_{\tilde{\tilde{A}}}(x,u) = 1$, then $\tilde{\tilde{A}}$ is named an interval type-2 fuzzy set. An interval type-2 fuzzy set $\tilde{\tilde{A}}$ can be accepted as a specific case of a type-2 fuzzy set, presented as:

$$\tilde{\tilde{A}} = \int_{x\in X} \int_{u\in J_X} 1/(x,u) \quad (3)$$

where $J_x \subseteq [0,1]$

Definition 3. The upper and lower membership functions of interval type-2 fuzzy sets are defined as type-1 membership functions, accordingly. This study presents an approach for using interval type-2 fuzzy sets for fuzzy MCDM problems. Interval type-2 fuzzy sets are specialized using reference points and the heights of the upper and lower membership functions. Figure 2 denotes

a trapezoidal interval type-2 fuzzy set $\tilde{\tilde{A}}_i = (\tilde{A}_i^U, \tilde{A}_i^L) = \left(\begin{pmatrix} a_{i1}^U, a_{i2}^U, a_{i3}^U, a_{i4}^U; H_1(\tilde{A}_i^U), H_2(\tilde{A}_i^U) \end{pmatrix}, \begin{pmatrix} a_{i1}^L, a_{i2}^L, a_{i3}^L, a_{i4}^L; H_1(\tilde{A}_i^L), H_2(\tilde{A}_i^L) \end{pmatrix}\right)$ [47], where $\tilde{A}_i^U$ and $\tilde{A}_i^L$ are type-1 fuzzy sets, $a_{i1}^U, a_{i2}^U, a_{i3}^U, a_{i4}^U, a_{i1}^L, a_{i2}^L, a_{i3}^L$ and a_{i4}^L are the reference points of the interval type-2 fuzzy $\tilde{\tilde{A}}_i$; $H_j(\tilde{A}_i^U)$ presents the membership value of the element $a_{i(j+1)}^U$ in the upper trapezoidal membership function $\tilde{A}_i^U$; $1 \le j \le 2$, $H_j(\tilde{A}_i^L)$ presents the membership value of the element $a_{i(j+1)}^U$ in the lower trapezoidal membership function $\tilde{A}_i^L$; $1 \le j \le 2$, $H_j(\tilde{A}_i^L)$

$H_1(\tilde{A}_i^U) \in [0,1], H_2(\tilde{A}_i^U) \in [0,1], H_1(\tilde{A}_i^L) \in [0,1], H_2(\tilde{A}_i^L) \in [0,1]$ and $1 \le i \le n$.

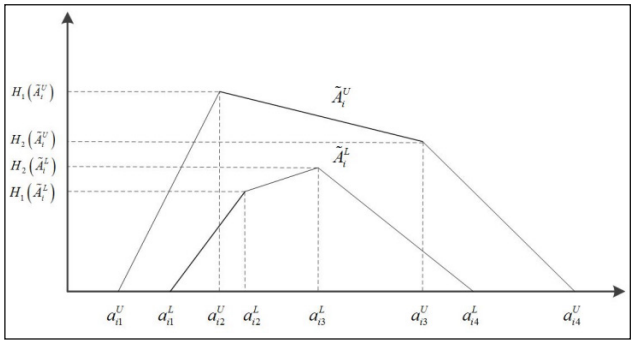

Figure 2. The membership functions of an interval type-2 fuzzy set.

Definition 4. The following equations describe the addition operation between trapezoidal interval type-2 fuzzy sets:

$$\tilde{\tilde{A}}_1 = (\tilde{A}_1^U, \tilde{A}_1^L) = \left(\begin{pmatrix} a_{11}^U, a_{12}^U, a_{13}^U, a_{14}^U; H_1(\tilde{A}_1^U), H_2(\tilde{A}_1^U) \end{pmatrix}, \begin{pmatrix} a_{11}^L, a_{12}^L, a_{13}^L, a_{14}^L; H_1(\tilde{A}_1^L), H_2(\tilde{A}_1^L) \end{pmatrix}\right) \quad (4)$$

$$\tilde{\tilde{A}}_2 = (\tilde{A}_2^U, \tilde{A}_2^L) = \left(\begin{pmatrix} a_{21}^U, a_{22}^U, a_{23}^U, a_{24}^U; H_1(\tilde{A}_2^U), H_2(\tilde{A}_2^U) \end{pmatrix}, \begin{pmatrix} a_{21}^L, a_{22}^L, a_{23}^L, a_{24}^L; H_1(\tilde{A}_2^L), H_2(\tilde{A}_2^L) \end{pmatrix}\right) \quad (5)$$

$$\tilde{A}_1 \oplus \tilde{A}_2 = (\tilde{A}_1^U, \tilde{A}_1^L) \oplus (\tilde{A}_2^U, \tilde{A}_2^L) = \left(\begin{pmatrix} a_{11}^U + a_{21}^U, a_{12}^U + a_{22}^U, a_{13}^U + a_{23}^U, a_{14}^U + a_{24}^U; \\ min\left(H_1(\tilde{A}_1^U), H_1(\tilde{A}_2^U)\right), min\left(H_2(\tilde{A}_1^U), H_2(\tilde{A}_2^U)\right) \end{pmatrix}, \begin{pmatrix} a_{11}^L + a_{21}^L, a_{12}^L + a_{22}^L, a_{13}^L + a_{23}^L, a_{14}^L + a_{24}^L; \\ min\left(H_1(\tilde{A}_1^L), H_1(\tilde{A}_2^L)\right), min\left(H_2(\tilde{A}_1^L), H_2(\tilde{A}_2^L)\right) \end{pmatrix}\right) \quad (6)$$

Definition 5. The following equations describe the subtraction operation between trapezoidal interval type-2 fuzzy sets:

$$\tilde{\tilde{A}}_1 = (\tilde{A}_1^U, \tilde{A}_1^L) = \left(\begin{pmatrix} a_{11}^U, a_{12}^U, a_{13}^U, a_{14}^U; H_1(\tilde{A}_1^U), H_2(\tilde{A}_1^U) \end{pmatrix}, \begin{pmatrix} a_{11}^L, a_{12}^L, a_{13}^L, a_{14}^L; H_1(\tilde{A}_1^L), H_2(\tilde{A}_1^L) \end{pmatrix}\right) \quad (7)$$

$$\tilde{\tilde{A}}_2 = (\tilde{A}_2^U, \tilde{A}_2^L) = \left(\begin{pmatrix} a_{21}^U, a_{22}^U, a_{23}^U, a_{24}^U; H_1(\tilde{A}_2^U), H_2(\tilde{A}_2^U) \end{pmatrix}, \begin{pmatrix} a_{21}^L, a_{22}^L, a_{23}^L, a_{24}^L; H_1(\tilde{A}_2^L), H_2(\tilde{A}_2^L) \end{pmatrix}\right) \quad (8)$$

$$\tilde{A}_1 \ominus \tilde{A}_2 = (\tilde{A}_1^U, \tilde{A}_1^L) \ominus (\tilde{A}_2^U, \tilde{A}_2^L) = \left(\begin{pmatrix} a_{11}^U - a_{21}^U, a_{12}^U - a_{22}^U, a_{13}^U - a_{23}^U, a_{14}^U - a_{24}^U; \\ min\left(H_1(\tilde{A}_1^U), H_1(\tilde{A}_2^U)\right), min\left(H_2(\tilde{A}_1^U), H_2(\tilde{A}_2^U)\right) \end{pmatrix}, \begin{pmatrix} a_{11}^L - a_{21}^L, a_{12}^L - a_{22}^L, a_{13}^L - a_{23}^L, a_{14}^L - a_{24}^L; \\ min\left(H_1(\tilde{A}_1^L), H_1(\tilde{A}_2^L)\right), min\left(H_2(\tilde{A}_1^L), H_2(\tilde{A}_2^L)\right) \end{pmatrix}\right) \quad (9)$$

Definition 6. The following equations describe the multiplication operation between trapezoidal interval type-2 fuzzy sets.:

$$\tilde{\tilde{A}}_1 = (\tilde{A}_1^U, \tilde{A}_1^L) = \left(\begin{pmatrix} a_{11}^U, a_{12}^U, a_{13}^U, a_{14}^U; H_1(\tilde{A}_1^U), H_2(\tilde{A}_1^U) \end{pmatrix}, \begin{pmatrix} a_{11}^L, a_{12}^L, a_{13}^L, a_{14}^L; H_1(\tilde{A}_1^L), H_2(\tilde{A}_1^L) \end{pmatrix}\right) \quad (10)$$

$$\tilde{\tilde{A}}_2 = (\tilde{A}_2^U, \tilde{A}_2^L) = \left(\begin{pmatrix} a_{21}^U, a_{22}^U, a_{23}^U, a_{24}^U; H_1(\tilde{A}_2^U), H_2(\tilde{A}_2^U) \end{pmatrix}, \begin{pmatrix} a_{21}^L, a_{22}^L, a_{23}^L, a_{24}^L; H_1(\tilde{A}_2^L), H_2(\tilde{A}_2^L) \end{pmatrix}\right) \quad (11)$$

$$\tilde{A}_1 \otimes \tilde{A}_2 = (\tilde{A}_1^U, \tilde{A}_1^L) \otimes (\tilde{A}_2^U, \tilde{A}_2^L) = \left(\begin{pmatrix} a_{11}^U \times a_{21}^U, a_{12}^U \times a_{22}^U, a_{13}^U \times a_{23}^U, a_{14}^U \times a_{24}^U; \\ min\left(H_1(\tilde{A}_1^U), H_1(\tilde{A}_2^U)\right), min\left(H_2(\tilde{A}_1^U), H_2(\tilde{A}_2^U)\right) \end{pmatrix}, \begin{pmatrix} a_{11}^L \times a_{21}^L, a_{12}^L \times a_{22}^L, a_{13}^L \times a_{23}^L, a_{14}^L \times a_{24}^L; \\ min\left(H_1(\tilde{A}_1^L), H_1(\tilde{A}_2^L)\right), min\left(H_2(\tilde{A}_1^L), H_2(\tilde{A}_2^L)\right) \end{pmatrix}\right) \quad (12)$$

Definition 7. Some basic arithmetic operations for trapezoidal interval type-2 fuzzy numbers are given:

$$\tilde{\tilde{A}}_1 = (\tilde{A}_1^U, \tilde{A}_1^L) = \left(\begin{pmatrix} a_{11}^U, a_{12}^U, a_{13}^U, a_{14}^U; H_1(\tilde{A}_1^U), H_2(\tilde{A}_1^U) \end{pmatrix}, \begin{pmatrix} a_{11}^L, a_{12}^L, a_{13}^L, a_{14}^L; H_1(\tilde{A}_1^L), H_2(\tilde{A}_1^L) \end{pmatrix}\right) \quad (13)$$

$$k\tilde{\tilde{A}}_1 = \left(\begin{pmatrix} k \times a_{11}^U, k \times a_{12}^U, k \times a_{13}^U, k \times a_{14}^U; H_1(\tilde{A}_1^U), H_2(\tilde{A}_1^U) \end{pmatrix}, \begin{pmatrix} k \times a_{11}^L, k \times a_{12}^L, k \times a_{13}^L, k \times a_{14}^L; H_1(\tilde{A}_1^L), H_2(\tilde{A}_1^L) \end{pmatrix}\right) \quad (14)$$

$$\frac{\tilde{\tilde{A}}_1}{k} = \left(\begin{pmatrix} \frac{1}{k} \times a_{11}^U, \frac{1}{k} \times a_{12}^U, \frac{1}{k} \times a_{13}^U, \frac{1}{k} \times a_{14}^U; H_1(\tilde{A}_1^U), H_2(\tilde{A}_1^U) \end{pmatrix}, \begin{pmatrix} \frac{1}{k} \times a_{11}^L, \frac{1}{k} \times a_{12}^L, \frac{1}{k} \times a_{13}^L, \frac{1}{k} \times a_{14}^L; H_1(\tilde{A}_1^L), H_2(\tilde{A}_1^L) \end{pmatrix}\right) \quad (15)$$

Definition 8. The following is a definition of the trapezoidal interval type-2 fuzzy set's ranking value:

$$Rank(\tilde{\tilde{A}}_i) = M_1(\tilde{A}_i^U) + M_1(\tilde{A}_i^L) + M_2(\tilde{A}_i^U) + M_2(\tilde{A}_i^L) + M_3(\tilde{A}_i^U) + M_3(\tilde{A}_i^L) - \frac{1}{4}\left(S_1(\tilde{A}_i^U) + S_1(\tilde{A}_i^L) + S_2(\tilde{A}_i^U) + S_2(\tilde{A}_i^L) + S_3(\tilde{A}_i^U) + S_3(\tilde{A}_i^L) + S_4(\tilde{A}_i^U) + S_4(\tilde{A}_i^L)\right) + H_1(\tilde{A}_i^U) + H_1(\tilde{A}_i^L) + H_2(\tilde{A}_i^U) + H_2(\tilde{A}_i^L) \quad (16)$$

where $M_p(\tilde{\tilde{A}}_i^j)$ shows the average of the factors a_{ip}^j and $a_{i(p+1)}^j$, $M_p(\tilde{\tilde{A}}_i^j) = \left(a_{ip}^j + a_{i(p+1)}^j\right)/2, 1 \le p \le 3$ shows the standard deviation of the factors a_{iq}^j and $a_{i(q+1)}^j$, $S_q(\tilde{A}_i^j) = \sqrt{\frac{1}{2}\sum_{k=q}^{q+1}\left(a_{ik}^j - \frac{1}{2}\sum_{k=q}^{q+1} a_{ik}^j\right)^2}$, $1 \le q \le 3$, $S_4(\tilde{A}_i^j)$ shows the standard deviation of the factors $a_{i1}^j, a_{i2}^j, a_{i3}^j, a_{i4}^j$, $S_4(\tilde{A}_i^j) = \sqrt{\frac{1}{4}\sum_{k=1}^{4}\left(a_{ik}^j - \frac{1}{4}\sum_{k=1}^{4} a_{ik}^j\right)^2} H_p(\tilde{A}_i^j)$ shows the membership value of the factor $a_{i(p+1)}^j$ in the trapezoidal membership function $\tilde{A}_i^j$, $1 \le p \le 3, j \in \{U, L\}$, and $1 \le i \le n$.

2.2. Trapezoidal Interval Type -2 fuzzy AHP

AHP is an MCDM method developed by Saaty [49, 50]. *The AHP method, widely recognized for determining criteria weights, is commonly employed to address complex problems involving multiple criteria [51]. AHP is adaptable, involves no complicated math, and utilizes a hierarchical structure to enhance focus and transparency in decision-making processes [52].* AHP is used. Triangular fuzzy numbers are employed in Laarhoven and Pedrycz's [53] hybridization of AHP with fuzzy logic to provide a method for usage in uncertain scenarios. The fuzzy comparison rates with the expanding

Table 2. Linguistic expressions

Linguistic Terms		Fuzzy Numbers											
Weak	**AW**	0.11	0.1	0.1	0.1	1	1	0.1	0.1	0.1	0.1	0.9	0.9
Very Veak	**VW**	0.11	0.1	0.2	0.2	1	1	0.1	0.1	0.2	0.2	0.9	0.9
Fairly Weak	**FW**	0.14	0.2	0.3	0.3	1	1	0.1	0.2	0.2	0.3	0.9	0.9
Slightly Weak	**SW**	0.2	0.3	0.5	1	1	1	0.2	0.3	0.5	0.9	0.9	0.9
Equal	**E**	1	1	1	1	1	1	1	1	1	1	0.9	0.9
Slightly Strong	**SS**	1	2	4	5	1	1	1.1	2.1	3.9	4.9	0.9	0.9
Fairly Strong	**FS**	3	4	6	7	1	1	3.1	4.1	5.9	6.9	0.9	0.9
Very Strong	**VS**	5	6	8	9	1	1	5.1	6.1	7.9	8.9	0.9	0.9
Strong	**AS**	7	8	9	9	1	1	7.1	8.1	8.9	8.9	0.9	0.9

approach were put forth by Buckley [54]. In his suggested method, the geometric mean method obtains fuzzy weights and performance scores. To more accurately depict the uncertainties in getting the criteria weights, interval type-2 fuzzy AHP—which also incorporates fuzzy membership functions—is employed in this study.

The interval type-2 trapezoidal fuzzy AHP method offers several advantages in accuracy, reliability, and computational efficiency compared to other MCDM methods, especially in complex decision-making scenarios such as sustainable refrigerant selection. First, the interval type-2 trapezoidal fuzzy AHP method provides a robust framework for capturing and managing the uncertainty and imprecision inherent in decision-making processes [55]. By allowing decision-makers to model varying degrees of uncertainty in criteria evaluations, this method provides a more accurate representation of real-world decision contexts than methods that rely solely on crisp values or type-1 fuzzy sets. Second, the interval type-2 trapezoidal fuzzy AHP method improves the reliability of the decision-making process by incorporating multiple sources of uncertainty and ambiguity into the analysis. By explicitly modeling uncertainty boundaries and considering different scenarios within the interval type-2 fuzzy framework, this method provides decision-makers with a more comprehensive understanding of potential outcomes and their associated risks. Although the interval type-2 trapezoidal fuzzy AHP method involves additional computational complexity compared to some traditional decision-making methods, advances in computational techniques and algorithms have made its application possible and efficient. In addition, the interval type-2 trapezoidal fuzzy AHP method is adaptable to specific decision contexts and problem structures, allowing efficient and scalable application in practical applications. In the context of this study, the Buckley AHP method is created using interval type-2 trapezoidal fuzzy sets. The proposed interval type-2 trapezoidal fuzzy AHP method is composed of the following steps:

Step 1. A decision hierarchy of main and sub-criteria is constructed.

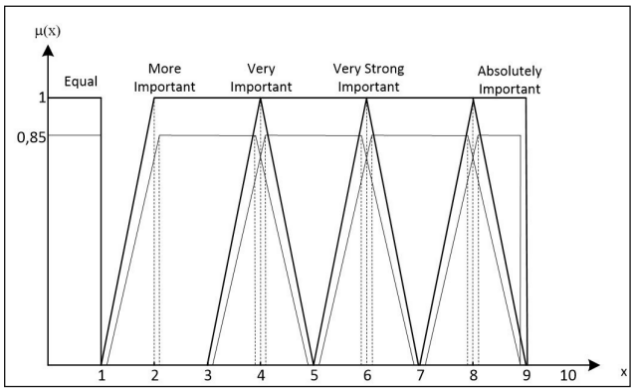

Figure 3. The membership functions of interval type-2 trapezoidal fuzzy numbers.

Step 2. It is decided on what scale will be used to evaluate the criterion. Table 2 lists the scale used in this study to transform linguistic expressions into interval type-2 trapezoidal fuzzy sets.

Figure 3 illustrates the scale's membership functions employed in this paper to guide decision-making.

Step 3. For main criteria and sub-criteria for each main criterion, pairwise comparison matrices are created in the hierarchy. The Equation 17 is a fuzzy pairwise comparison matrix:

$$\tilde{\tilde{A}} = \begin{bmatrix} 1 & \tilde{\tilde{a}}12 & \dots & \dots. & \tilde{\tilde{a}}1m \\ \tilde{\tilde{a}}21 & 1 & \dots & \dots & \tilde{\tilde{a}}2m \\ : & : & \dots & \dots & : \\ : & : & \dots & \dots & : \\ \tilde{\tilde{a}}1n & \tilde{\tilde{a}}2n & \dots & \dots & 1 \end{bmatrix} \quad (17)$$

$$\tilde{\tilde{a}}ij = \frac{1}{\tilde{\tilde{a}}ji} \quad (18)$$

e.g., $\tilde{\tilde{a}}31 = \frac{1}{\tilde{\tilde{a}}13}$

$$\tilde{\tilde{a}} = ((a_{11}^U; a_{12}^U; a_{13}^U; a_{14}^U; H_1(a^U); H2(a^U), (a_{11}^L; a_{12}^L; a_{13}^L; a_{14}^L; H_1(a^L); H2(a^L) \quad (19)$$

Therefore,

$$\frac{1}{\tilde{a}} = ((\frac{1}{a_{14}^U};\frac{1}{a_{13}^U};\frac{1}{a_{12}^U};\frac{1}{a_{11}^U};H_1(a_{12}^U);H2(a_{13}^U),\ (\frac{1}{a_{14}^L};\frac{1}{a_{13}^L};\frac{1}{a_{12}^L};\frac{1}{a_{11}^L};H_1(a_{12}^L);H2(a_{13}^L)) \quad (20)$$

Step 4. The defuzzification process is conducted to calculate consistency indexes. The following equations determine consistency ratio (CR) [56]. The pairwise comparison matrices are consistent when the CR is less than 0.1.

$$CI = \frac{\lambda_{max}}{n-1} \quad (21)$$

$$CR = \frac{CI}{RI} \quad (22)$$

The random index (RI) varies randomly about the number of criteria, where "n" is the number of criteria. Consistency Index (CI) is determined based on the table proposed by Saaty [49].

Step 5. Geometric means of all criteria are calculated:

$$\tilde{\tilde{r}}i = [\tilde{\tilde{a}}_{i1} \otimes \tilde{\tilde{a}}_{i2} \otimes \ldots \otimes \tilde{\tilde{a}}_{im}]^{1/n} \quad (23)$$

$$(\tilde{\tilde{a}}_{ij})^{1/n} = \begin{pmatrix} (\tilde{\tilde{a}}_{i1}^U)^{1/n}, (\tilde{\tilde{a}}_{i2}^U)^{1/n}, (\tilde{\tilde{a}}_{i3}^U)^{1/n}, (\tilde{\tilde{a}}_{i4}^U)^{1/n}, H_1(a_{i2}^U), H_2(a_{i3}^U) \\ (\tilde{\tilde{a}}_{i1}^L)^{1/n}, (\tilde{\tilde{a}}_{i2}^L)^{1/n}, (\tilde{\tilde{a}}_{i3}^L)^{1/n}, (\tilde{\tilde{a}}_{i4}^L)^{1/n}, H_1(a_{i2}^L), H_2(a_{i3}^L) \end{pmatrix} \quad (24)$$

Step 6. The weights are computed via normalization as follows:

$$wi = \tilde{\tilde{r}}i = [\tilde{\tilde{r}}1 \oplus \tilde{\tilde{r}}2 \oplus \ldots \oplus \tilde{\tilde{r}}n]^{-1} \quad (25)$$

Step 7. Finally, the fuzzy numbers are defuzzified using Eq. (26) to identify the degree of importance of each criterion.

$$w_i' = \frac{1}{2}\left(\frac{1}{2}\sum_{i=1}^{4}(a_i^L + a_i^L)\right) \otimes \frac{1}{4}\left(\sum_{i=1}^{2}\left(H_i(A^L) + H_i(A^U)\right)\right) \quad (26)$$

3. APPLICATION

Applications for air conditioning and refrigeration have become more crucial in recent years due to global warming and high energy consumption. The significance of refrigerant selection in refrigeration systems is even more apparent when considering that cooling costs more than heating. Incorrect material choice and improper application result in issues that are difficult to resolve after the system is operational and impose significant financial expenses on the user. In this situation, it is crucial to identify the criteria that affect the choice of the best refrigerant and to evaluate their significance methodically. This study aims to identify the requirements that should be considered for refrigeration and the most essential criteria in the evaluation process. For this aim, AHP, a well-known MCDM technique, is used by consulting experts in an interval type-2 trapezoidal fuzzy environment.

Table 2 indicates expert proficiencies as the decision makers in refrigerant selection. The criteria are determined and weighted using expert opinions and available literature about the problem. When selecting experts, their skills and expertise are considered in this field. In choosing the experts to be consulted for this study on sustainable refrigerant selection, several key aspects were crucial to ensure the credibility and relevance of their contributions. First, priority is given to experts with deep expertise in refrigerant selection, sustainable practices, environmental management, and multi-criteria decision making methodologies. Their reputation, experience, and publication record are thoroughly evaluated to ensure they have a track record of high-quality research and contributions to the field. It is critical to select experts who are available and accessible for consultation and have strong communication skills to facilitate fruitful collaboration. Careful consideration is also given to identifying and managing potential conflicts of interest to protect the integrity of the study. By carefully considering these factors, a panel of experts is assembled, ready to provide valuable insight and expertise and to validate the findings and conclusions of the study with the expert group. E-1, E-2, E-3, E-4, E-5, E-6, and E-7 are the abbreviations for seven decision-makers with a deep knowledge of the HVAC sector. Because each expert has a different experience level, as shown in Table 3, their weights (reputations) also differ. Although all experts are mechanical engineers, five have academic careers, and the remaining two work as engineers in the HVAC sector.

3.1. Evaluation criteria

Based on the literature review and expert opinions, a two-level criteria framework is created to prioritize the factors related to the refrigerant selection problem.

Table 3. Expert proficiencies as a decision-maker

Experts	Career	Title	Experience	Field	Reputation (Expert Weight)
E-1	Academician	Asst. Prof.	7	Mechanical Engineering	0.2
E-2	Academician	Res. Asst.	5	Mechanical Engineering	0.1
E-3	Academician	Prof. Dr.	15+	Mechanical Engineering	0.1
E-4	Engineer	HVAC specialist	3	Mechanical Engineering	0.1
E-5	Academician	Res. Asst.	7	Mechanical Engineering	0.1
E-6	Academician	Prof. Dr.	20+	Mechanical Engineering	0.2
E-7	Engineer	HVAC specialist	20+	Mechanical Engineering	0.2

Table 4. Main and sub-criteria

Main Criteria	Sub Criteria	References
C1. Environmental	C11. Ozone depletion potential	[2], [3], [6], [10]–[12], [14]–[19]
	C12. Global warming potential	[2]–[4], [6], [10]–[12], [14]–[19]
	C13. Secondary environmental impacts	[2]
	C14. Flammability	[2], [3], [6], [10]–[12], [14], [15], [17]–[19]
	C15.Toxicity	[2], [3], [10]–[12], [14], [15], [17], [19]
C2. Thermodynamic	C21. Latent heat of vaporization	[10]–[12], [15], [16], [19]
	C22. Thermal conductivity	[3], [11], [12], [16]
	C23. Vapor pressure	[6], [10]–[12], [14], [15]
	C24. Liquid density	[3], [6], [10]–[12], [15], [16]
	C25. Liquid viscosity	[3], [10]–[12], [16]
	C26. Normal boiling point	[3], [4], [6], [14], [16], [17], [19]
C3. Sustainability	C31. Operation life	[2], [6], [16], [17], [19]
	C32. Recyclable content	[2]
	C33. Material use	[2]
	C34.Energy efficiency	Expert view
	C35.Refrigerant cost	[2], [11], [12]
	C36.Materials compatibility	[2]

Table 5. Pairwise comparison matrices for main criteria

Expert		**1**			**2**			**3**			**4**	
Criteria	C1	C2	C3	C1	C2	C3	C1	C2	C3	C1	C2	C3
C1. Environmental	E	E	FW	E	SS	VS	E	VW	VS	E	AS	FS
C2. Thermodynamic	E	E	SW	SW	E	FS	VS	E	AS	AW	E	SW
C3. Sustainability	FS	SS	E	VW	FW	E	VW	AW	E	FW	SS	E
Expert		**5**			**6**			**7**				
Criteria	C1	C2	C3	C1	C2	C3	C1	C2	C3			
C1. Environmental	E	VW	SW	E	SS	SS	E	SW	AW			
C2. Thermodynamic	VS	E	E	SW	E	E	VS	E	VW			
C3. Sustainability	SS	E	E	SW	E	E	FS	VS	E			

Three main criteria—environmental, thermodynamic, and sustainable make up the first level. Table 4 presents the main and sub-criteria for refrigerant selection.

3.2 Determining the criteria weights for each level of the hierarchy

Seven experts are consulted, as explained before, and are required for criteria evaluation for each level through a questionnaire to determine the weights of the criteria. First, a pairwise comparison matrix is constructed for the main criteria by each expert based on linguistic variables in Table 2. Table 5 shows the matrices for the main criteria created by experts.

The consistency of the experts' opinions is examined; if the pairwise comparisons are inconsistent, the experts are asked to reassess. In response to inconsistencies identified by the CR, the revision process involves reviewing expert judgments and seeking consensus among experts. Re-evaluation of the relevance of the criteria further resolves inconsistencies and ensures robust decision outcomes. The weight calculation phase is initiated when the CR is less than 0.1 [57], indicating that the relevant matrix is consistent. The CR values for the pairwise comparisons of the main criteria for each expert are shown in Table 6. All matrices are determined to be consistent, as shown in Table 6.

Table 6. CR values for main criteria comparisons

Expert	**1**	**2**	**3**	**4**	**5**	**6**	**7**
CR	0.03	0.091	0.084	0.03	0.084	0	0.084

Table 7. Main criteria weights

Criteria/Expert	1	2	3	4	5	6	7
C1. Environmental	0.156	0.627	0.198	0.734	0.110	0.584	0.076
C2. Thermodynamic	0.197	0.301	0.751	0.080	0.511	0.208	0.152
C3. Sustainability	0.647	0.073	0.051	0.186	0.379	0.208	0.772

Table 8. Pairwise comparison of Expert-1 for sub-criteria of Environmental

Sub-Criteria	C11	C12	C13	C14	C15
C11. Ozone depletion potential	E	E	SS	AW	AW
C12. Global warming potential	E	E	SS	AW	AW
C13. Secondary environmental impacts	SW	SW	E	AW	AW
C14. Flammability	AS	AS	AS	E	SS
C15.Toxicity	AS	AS	AS	SW	E

Table 9. Pairwise comparison of Expert-3 for sub-criteria of Thermodynamic

Sub-Criteria	C21	C22	C23	C24	C25	C26
C21. Latent heat of vaporization	E	AW	AW	SS	E	VW
C22. Thermal conductivity	AS	E	E	AS	AS	SS
C23. Vapor pressure	AS	E	E	AS	FS	VS
C24. Liquid density	SW	AW	AW	E	E	FW
C25. Liquid viscosity	E	AW	FW	E	E	FW
C26. Normal boiling point	VS	SW	VW	FS	FS	E

Table 10. Consistency ratios for sub-criteria evaluations

Expert	1	2	3	4	5	6	7
For Sub-criteria of Environmental	0.078	0.091	0.066	0.087	0.084	0.063	0.099
For Sub-criteria of Thermodynamic	0.096	0.085	0.082	0.087	0.087	0.095	0.095
For Sub-criteria of Sustainability	0.096	0.095	0.089	0.09	0.087	0.099	0.096

The weights of the main criteria are computed by using the interval type-2 trapezoidal fuzzy AHP steps once all pairwise comparison matrices have been consistently obtained. Table 7 presents the main criteria weights based on expert opinions.

It can be noticed that Environmental (C1) is the most essential criterion for three experts (E-2, E-4, and E-6), and Thermodynamic (C2) is the most critical criterion for two experts (E-3 and E-5). Lastly, Sustainability (C3) is evaluated as the most crucial main criterion by two experts (E-1 and E-7). From this point of view, it can be said that experts have different opinions according to their knowledge and experience. Thus, making a more inclusive evaluation is possible by taking experts' opinions with other ideas.

The same experts are consulted to assess the second level of the criteria. For this reason, expert opinions are used to build pairwise comparison matrices for the sub-criteria. For instance, Table 8 displays the pairwise comparison matrix constructed using Expert-1's assessments of the sub-criteria under the Environmental main criterion. Additionally, Table 9 shows the pairwise comparison matrix constructed using Expert-3's judgments of the sub-criteria for the Thermodynamic main criterion.

The pairwise comparison matrices for the sub-criteria are first examined for consistency, and each is consistent. Table 10 displays the CR value for each matrix.

The criteria weights for the second level are computed by reapplying the interval type-2 trapezoidal fuzzy AHP steps after determining the consistency of all matrices. Table 11 lists the sub-criteria weights considering each expert.

The priority scores for each sub-criteria are determined, as shown in Figure 4, by multiplying the aggregated

Table 11. The weights of sub-criteria for each expert

Sub-Criteria/Expert	1	2	3	4	5	6	7
C11. Ozone depletion potential	0.060	0.196	0.075	0.287	0.044	0.285	0.093
C12. Global warming potential	0.060	0.379	0.322	0.360	0.081	0.176	0.086
C13. Secondary environmental impacts	0.036	0.040	0.039	0.031	0.048	0.059	0.025
C14. Flammability	0.500	0.193	0.195	0.099	0.260	0.195	0.412
C15. Toxicity	0.343	0.193	0.370	0.222	0.568	0.285	0.385
C21. Latent heat of vaporization	0.472	0.490	0.044	0.392	0.327	0.399	0.084
C22. Thermal conductivity	0.062	0.082	0.349	0.181	0.112	0.271	0.023
C23. Vapor pressure	0.201	0.109	0.373	0.215	0.169	0.121	0.149
C24. Liquid density	0.037	0.046	0.034	0.053	0.057	0.072	0.101
C25. Liquid viscosity	0.037	0.032	0.043	0.034	0.057	0.037	0.138
C26. Normal boiling point	0.190	0.242	0.156	0.124	0.278	0.100	0.506
C31. Operation life	0.098	0.220	0.229	0.202	0.283	0.225	0.267
C32. Recyclable content	0.063	0.159	0.116	0.160	0.120	0.068	0.064
C33. Material use	0.068	0.041	0.028	0.024	0.054	0.056	0.022
C34. Energy efficiency	0.362	0.470	0.508	0.484	0.409	0.249	0.427
C35. Refrigerant cost	0.165	0.047	0.051	0.067	0.072	0.342	0.100
C36. Materials compatibility	0.244	0.063	0.068	0.063	0.062	0.060	0.119

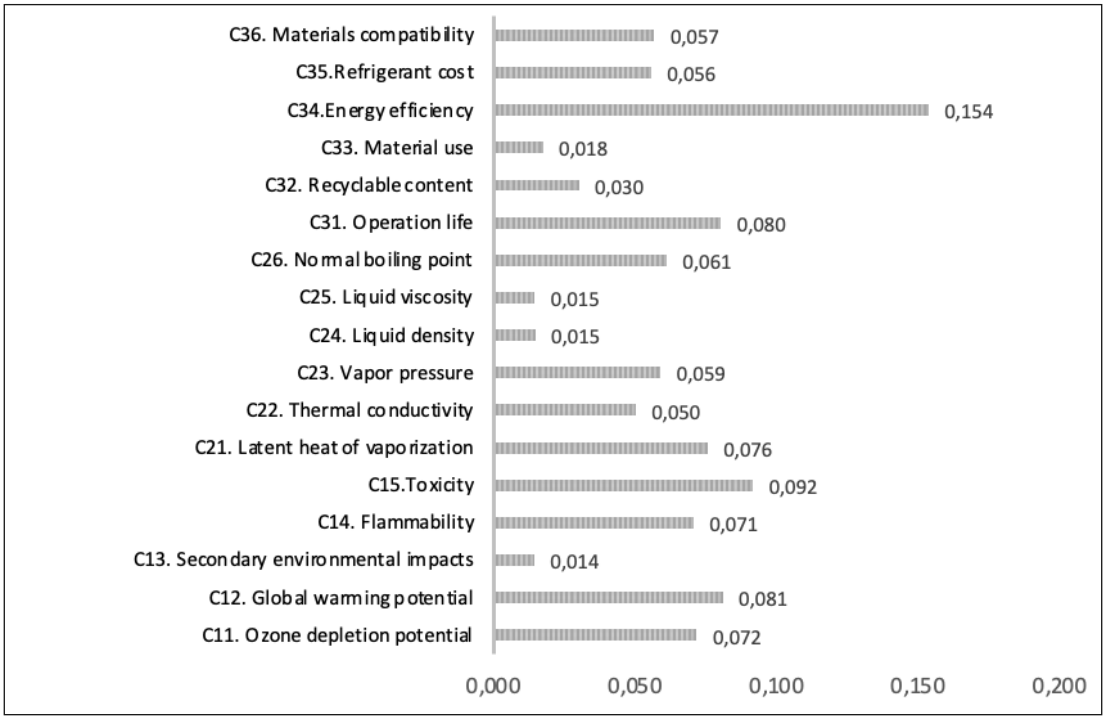

Figure 4. Sub-criteria weights.

sub-criteria weights by the corresponding main criterion weights. The criteria weights of 7 experts are compiled, considering the weights (reputations) of experts.

Energy efficiency (C34) is the most significant criterion among all sub-criteria. This outcome is expected because sustainability (C3) is the main criterion that matters the most to the two experts with the highest reputations. With final weights of 0.092 and 0.081, respectively, Toxicity (C15) and Global warming potential (C12) rank second and third. This rating illustrates that choosing a refrigerant is influenced by the Sustainability factor and the sub-criteria stated below, and decision-makers should consider this. The fourth ranking, Operation Life (C31), shows the significance of choosing a refrigerant with a

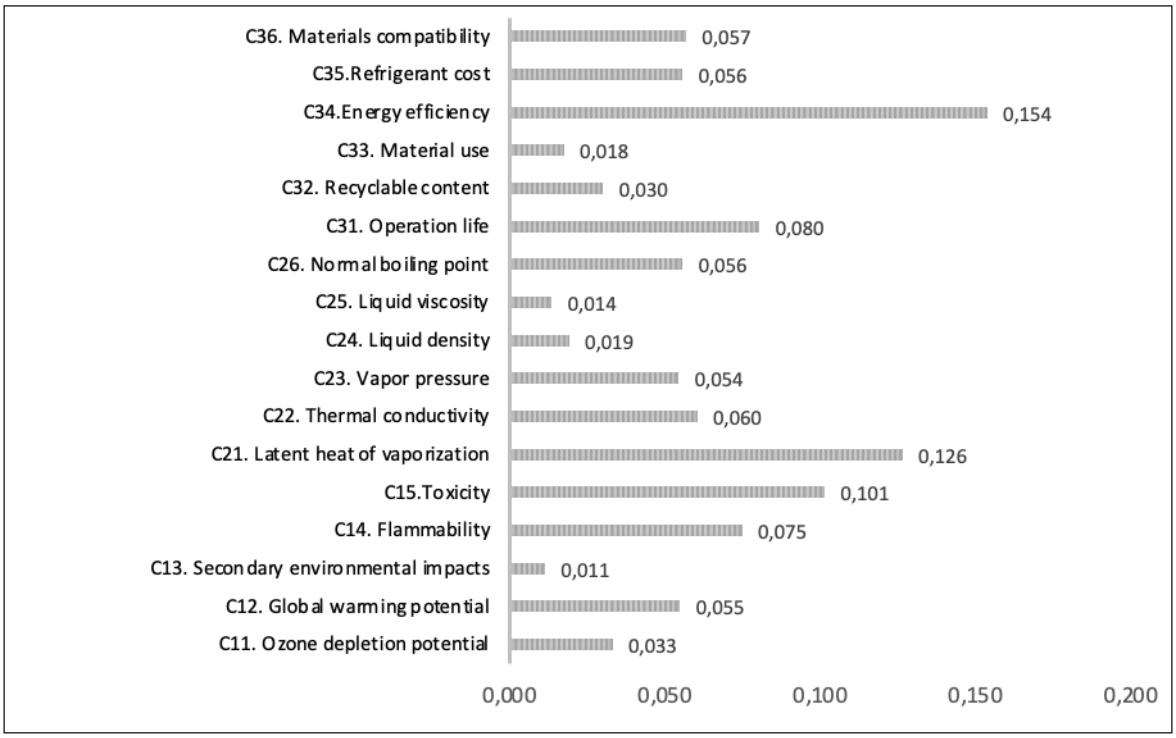

Figure 5. The weight changes of sub-criteria show that the proposed method is sensitive to small changes.

long lifetime. Secondary environmental effect (C13), one of the sub-criteria of the Environmental main criteria, is the least significant criterion. It implies that focusing on more essential criteria in the selection process would be more acceptable and that this criterion is not very important when choosing refrigerants.

3.3. Sensitivity Analysis

A sensitivity analysis is conducted to examine and evaluate the proposed methodology. In this process, the weights of the primary criteria derived from interval type-2 trapezoidal fuzzy AHP are modified between two main criteria while keeping the third constant. This involves sequentially replacing the weight of the first main criterion with those of the second and third criteria while maintaining the other constant. Subsequently, the sub-criteria weights are recalculated to assess the proposed methodology's behavior in response to weight changes. These results aid decision-makers in establishing priorities and facilitating the analysis process.

Moreover, as the weights of the main criteria change reciprocally, the overall weights of the sub-criteria also fluctuate. For instance, if we interchange the primary criteria "Environmental" and "Thermodynamic," the global weight of sub-criteria such as "Ozone depletion potential" decreases from 0.072 to 0.033. In contrast, the weight of "Latent heat of vaporization" increases from 0.076 to 0.126. The weights of sub-criteria are provided in Figure 5. The results show that the proposed method is sensitive to small changes.

4. DISCUSSION

This study initially identified criteria based on a comprehensive literature review and consultation with experts to ensure relevance to the decision-making context. Subsequently, the interval type-2 trapezoidal fuzzy AHP methodology is employed to assign weights to these criteria. Furthermore, to ensure the accuracy and validity of the results, the obtained criteria weights are verified through interviews with experts in the field. This approach ensured that the selected criteria accurately reflected the decision-making context. To reduce the impact of individual biases and limited perspectives, this study uses a variety of strategies, including diverse expert panels, rigorous validation processes, sensitivity analyses, and transparency in decision-making, ensuring that the final decision reflects a consensus-based, comprehensive assessment of all relevant factors.

As mentioned in the introduction, the energy consumption of refrigeration systems in domestic and industrial usage is approximately 20% worldwide [1]. Refrigeration and air conditioning are no longer considered luxuries because they are indispensable for food, health, and financial services but also for human comfort [58]. As a result of the ever-increasing number of refrigerators in all areas of our lives, there is a dramatic increase in energy demand and emissions, a growing contribution to global warming. Therefore, the energy efficiency of refrigerator systems is critical to postpone the global warming potential. Energy efficiency refers to the energy cost required to achieve a specific goal. The review study of McLinden et al. [2], it is indicated that the main aim is to achieve refrigeration

with new refrigerants while maximizing energy efficiency by minimizing environmental impact. In the study of Poongavanam et al. [9], they selected the best refrigerant by considering thermal properties, ecological impacts, and cost. When examined their selected R430A, which is the best refrigerant according to their criteria, it is seen that the thermodynamic properties of the refrigerant, i.e., its efficiency, are prioritized over environmental impacts such as GWP and ODP in the selection of refrigerant. This situation in Poongavanam et al. [9] study supports energy efficiency as the most influential criterion identified in the present study. Prabakaran et al. [10] selected the refrigerant among 14 alternatives by considering many criteria such as power construction, coefficient of performance, total environmental impacts, thermodynamic properties, cost, and lifetime. While R444B refrigerant was the best alternative regarding coefficient of performance, total environmental impacts, lifetime, and cost, R290 refrigerant was the best alternative regarding refrigerant charge and discharge pressure. While the selection of R444B refrigerant supports the results of the present study, while that of R290 refrigerant does not. The Natural Resources Defense Council (NRDC) proposed strategies for enhancing air conditioners (ACs) in India to rapidly expand the use of energy-efficient and low-GWP refrigerants [59]. As the studies above address, energy efficiency is the most valuable criterion in the selection of refrigerants. Studies on increasing the refrigerant energy efficiency of refrigerants also show the importance of energy efficiency in the selection of refrigerants, which is also emphasized in this study.

5. CONCLUSION

Refrigeration systems are crucial for home and commercial applications, including ice production, air conditioning, and air separation. Due to the wide applications of refrigeration systems in daily life, refrigerants are not a significant threat inside the system, but their leakage and discharge to the environment pose a significant threat to the environment by causing global warming and ozone depletion. On the other hand, the refrigeration system's performance is primarily based on the refrigerant performance, so developing highly efficient and environmentally friendly refrigerant is indispensable. The refrigerant choice for the refrigeration system is critical because it affects operating conditions and cycle performance. This study analyzes the refrigerant selection criteria by considering sustainability, environmental, and thermodynamics dimensions under ambiguous conditions. The interval type-2 trapezoidal fuzzy AHP approach, which allows multiple criteria to be evaluated simultaneously, solves the factors of the refrigerant selection problem. Three main criteria and 17 sub-criteria are determined in this study. The adoption of interval type-2 trapezoidal fuzzy AHP approach in the refrigerant selection is presented as a methodology to reveal the more suitable criteria. In this way, MCDM analysis is then carried out. The most significant criterion in the proposed multi-criteria analysis is "energy efficiency," the least considerable criterion is "secondary environmental impact." Although "vapor pressure," "latent heat of vaporization," and "material compatibility" are determined as other significant criteria, energy efficiency is almost twice as substantial as the second-most important criterion. Refrigerant and refrigeration systems developers can use the proposed methodology to improve their system performance by considering determined sub-criteria such as energy efficiency, GWP, vapor pressure, etc.

The main contributions of this study are as follows: (1) The Refrigerant selection problem is handled as an MCDM problem; (2) The most significant refrigerant selection criteria are identified and categorized in a hierarchical structure; (3) These main criteria and their sub-criteria are evaluated under uncertain conditions, and the weight of each criterion is determined; and (4) To the best of authors' knowledge, this study presents the first decision-making model for refrigerant selection problem. These contributions demonstrate how this fuzzy decision-making model incorporates several innovative elements in method and application domains, ensuring the study has novel characteristics for the pertinent literature.

Limitations of this study include potential biases in expert opinions, the complexity of integrating interval type-2 trapezoidal fuzzy AHP into decision-making processes, and the need for further validation of results in different contexts. Future research could use larger and more diverse expert panels to address these limitations, increase transparency in the decision-making process, and conduct comparative analyses to assess the robustness of this model. Additional criteria can be added, or the fuzzy AHP methodology can be developed better to capture the uncertainties and complexities in the decision-making process.

The proposed interval type-2 trapezoidal fuzzy AHP approach can efficiently handle larger and more complex decision problems by establishing hierarchical structures. Such problems can be decomposed into smaller, more manageable sub-problems, allowing faster and more scalable solutions. This hierarchical decomposition strategy makes it possible to effectively navigate the complexities of decision-making while optimizing the use of computational resources. Future recommendations include using various MCDM methods to verify the findings or probabilistic approaches to look at the issue from a probabilistic viewpoint. Different MCDM methods can extend this framework with different fuzzy environments, and heating and refrigeration materials can be evaluated for various cases. Integrating interval type-2 trapezoidal fuzzy AHP with other decision-making tools or software provides numerous advantages. For example, it combines different methodologies, enabling the selection of the most suitable refrigerant among alternatives. Furthermore, the integration allows the creation of various scenarios to validate results while taking advantage of advanced visualization and reporting tools for advanced analysis.

FUNDING

No funding information is available.

CONFLICT OF INTEREST

All authors certify that they have no affiliations with or involvement in any organization or entity with any financial or non-financial interest in the subject matter or materials discussed in this manuscript.

ETHICAL APPROVAL

Ethics committee approval is not required.

AVAILABILITY OF DATA AND MATERIAL

Not applicable

CODE AVAILABILITY

Not applicable

CONSENT TO PARTICIPATE

Not applicable

CONSENT TO PUBLISH

The author confirms that the final version of the manuscript has been reviewed, approved, and consented to for publication.

REFERENCES

[1] McLinden, M. O., & Huber, M. L. (2020). (R) Evolution of refrigerants. *J Chem Eng Data,* 65(9), 4176–4193. [CrossRef]

[2] Han, X., Wang, X., Zheng, H.,Xu, X., & Chen, G. (2016). Review of the development of pulsating heat pipe for heat dissipation. *Renew Sustain Energy Rev*, 59, 692–709. [CrossRef]

[3] Der, O., Alqahtani, A. A., Marengo, M., & Bertola, V. (2021). Characterization of polypropylene pulsating heat stripes: Effects of orientation, heat transfer fluid, and loop geometry. *Appl Therm Eng*, 184, 116304. [CrossRef]

[4] McLinden, M. O., Seeton, C. J., & Pearson, A. (2020). New refrigerants and system configurations for vapor-compression refrigeration. *Science*, 370(6518), 791–796. [CrossRef]

[5] Vuppaladadiyam, A. K., Antunes, E., Vuppaladadiyam, S. S. V., Baig, Z. T., Subiantoro, A., Lei, G., Leu, S. Y., Sarmah, A. K., Duan, H. (2022). Progress in the development and use of refrigerants and unintended environmental consequences. *Sci Total Environ*, 823, 153670. [CrossRef]

[6] Sánchez, D., Cabello, R., Llopis, R., Arauzo, I., Catalán-Gil, J., & Torrella, E. (2017). Energy performance evaluation of R1234yf, R1234ze(E), R600a, R290 and R152a as low-GWP R134a alternatives. *Int J Refrig*, 74, 267–280. [CrossRef]

[7] Calm, J. M. (2008). The next generation of refrigerants - historical review, considerations, and outlook. *Int J Refrig*, 31(7), 1123–1133. [CrossRef]

[8] Abas, N., Nawaz, R., & Khan, N. (2015). Parametric quantification of low GWP refrigerant for thermosyphon driven solar water heating system. *Procedia Comput Sci*, 52(1), 804–811. [CrossRef]

[9] European Commission. (2016). *Progress of the HFC Phase Down*. http://ec.europa.eu/clima/policies/f-gas/docs/phase-down_progress_en.pdf

[10] Wu, X., Dang, C., Xu, S., & Hihara, E. (2019). State of the art on the flammability of hydrofluoroolefin (HFO) refrigerants. *Int J Refrig*, 108, 209–223. [CrossRef]

[11] Mota-Babiloni, A., Makhnatch, P., & Khodabandeh, R. (2017). Recent investigations in HFCs substitution with lower GWP synthetic alternatives: Focus on energetic performance and environmental impact. *Int J Refrig*, 82, 288–301. [CrossRef]

[12] Mohanraj, M., & Abraham, J. D. A. P. (2022). Environment friendly refrigerant options for automobile air conditioners: a review. *J Therm Anal Calorim*, 147(1), 47–72. [CrossRef]

[13] Poongavanam, G., Sivalingam, V., Prabakaran, R., Salman, M., & Kim, S. C. (2021). Selection of the best refrigerant for replacing R134a in automobile air conditioning system using different MCDM methods: A comparative study. *Case Stud Therm Eng*, 27, 101344. [CrossRef]

[14] Souayeh, B., Bhattacharyya, S., Hdhiri, N., & Alam, M. W. (2022). Selection of best suitable eco-friendly refrigerants for HVAC sector and renewable energy devices. *Sustain*, 14(18), 11663. [CrossRef]

[15] Tripathi, A. K., Dubey, S., Pandey, V. K., & Tiwari, S. K. (2015, November 26-28). *Selection of refrigerant for air conditioning system using MCDM-TOPSIS approach*. Proc of 3rd International Conference on Industrial Engineering (ICIE-2015). SVNIT, Surat, India.

[16] Devecioğlu, A. G., & Oruç, V. (2015). Characteristics of some new generation refrigerants with low GWP. *Energy Procedia*, 75, 1452–1457. [CrossRef]

[17] Direk, M., Mert, M. S., Soylu, E., & Yüksel, F. (2019). Experimental investigation of an automotive air conditioning system using R444A and R152a refrigerants as alternatives of R134a. *J Mech Eng*, 65(4), 212–218. [CrossRef]

[18] Meng, Z., Zhang, H., Lei, M., Qin, Y., & Qiu, J. (2018). Performance of low GWP R1234yf/R134a mixture as a replacement for R134a in automotive air conditioning systems. *Int J Heat Mass Transf*, 116, 362–370. [CrossRef]

[19] de Paula, C. H., Duarte, W. M., Rocha, T. T. M., de Oliveira, R. N., & Maia, A. A. T. (2020). Optimal design and environmental, energy and exergy analysis of a vapor compression refrigeration system using R290, R1234yf, and R744 as alternatives to replace R134a. *Int J Refrig*, 113, 10–20. [CrossRef]

[20] Bolaji, B. O., & Huan, Z. (2013). Ozone depletion and global warming: Case for the use of natural refrigerant - A review. *Renew Sustain Energy Rev*, 18, 49–54. [CrossRef]

[21] Kasaeian, A., Hosseini, S. M., Sheikhpour, M., Mahian, O., Yan, W. M., & Wongwises, S. (2018). Applications of eco-friendly refrigerants and nano refrigerants: A review. *Renew Sustain Energy Rev*, 96(C), 91–99. [CrossRef]

[22] Ustaoglu, A., Kursuncu, B., Kaya, A. M., & Caliskan, H. (2022). Analysis of vapor compression refrigeration cycle using advanced exergetic approach with Taguchi and ANOVA optimization and refrigerant selection with enviroeconomic concerns by TOPSIS analysis. *Sustain Energy Technol Assessments*, 52, 102182. [CrossRef]

[23] Koundinya, S., & Seshadri, S. (2022). Energy, exergy, environmental, and economic (4E) analysis and selection of best refrigerant using TOPSIS method for industrial heat pumps. *Therm Sci Eng Prog*, 36, 101491. [CrossRef]

[24] Devotta, S., Chelani, A., & Vonsild, A. (2021). Prediction of flammability classifications of refrigerants by artificial neural network and random forest model. *Int J Refrig*, 131, 947–955. [CrossRef]

[25] Prabakaran, R., Sivalingam, V., Kim, S. C., Ganesh Kumar, P., & Praveen Kumar, G. (2022). Future refrigerants with low global warming potential for residential air conditioning system: A thermodynamic analysis and MCDM tool optimization. *Environ Sci Pollut Res* 2022;29(52):78414–78428. [CrossRef]

[26] Çalış Boyacı, A., Şişman, A., & Sarıcaoğlu, K. (2021). Site selection for waste vegetable oil and waste battery collection boxes: A GIS-based hybrid hesitant fuzzy decision-making approach. *Environ Sci Pollut Res*, 28(14), 17431–17444. [CrossRef]

[27] Alkan, N., & Kahraman, C. (2022). An intuitionistic fuzzy multi-distance based evaluation for aggregated dynamic decision analysis (IF-DEVADA): Its application to waste disposal location selection. *Eng Appl Artif Intell*, 111, 104809. [CrossRef]

[28] Thakkar, N., & Paliwal, P. (2022). Quad-level MCDM framework to analyse technology combinations for sustainable micro-grid planning in uncertainty domain. *Arab J Sci Eng*, 48(5), 5829–5858. [CrossRef]

[29] Ayyildiz, E. (2022). A novel pythagorean fuzzy multi-criteria decision-making methodology for e-scooter charging station location-selection. *Transp Res Part D Transp Environ*, 111, 103459. [CrossRef]

[30] Kiliç, M., & Kaya, I. (2015). Investment project evaluation by a decision-making methodology based on type-2 fuzzy sets. *Appl Soft Comput*, 27, 399–410. [CrossRef]

[31] Zadeh, L. A. (1965). Fuzzy sets. *Inf Control*, 8(3), 338–353. [CrossRef]

[32] Ayyildiz, E., & Taskin Gumus, A. (2021). A novel distance learning ergonomics checklist and risk evaluation methodology: A case of Covid-19 pandemic. *Hum Factors Ergon Manuf*, 31(4), 397–411. [CrossRef]

[33] Sinha, A. K., Narang, H. K., & Bhattacharya, S. (2020). A fuzzy logic approach for modelling and prediction of mechanical properties of hybrid abaca-reinforced polymer composite. *J Brazilian Soc Mech Sci Eng*, 42(6), 1–11. [CrossRef]

[34] Ayyildiz, E. (2022). Fermatean fuzzy step-wise Weight Assessment Ratio Analysis (SWARA) and its application to prioritizing indicators to achieve sustainable development goal-7. *Renew Energy*, 193, 136–148. [CrossRef]

[35] Görener, A., Ayvaz, B., Kuşakcı, A. O., & Altınok, E. (2017). A hybrid type-2 fuzzy based supplier performance evaluation methodology: The Turkish Airlines technic case. *Appl Soft Comput J*, 56, 436–445. [CrossRef]

[36] Ecer, F. (2022). Multi-criteria decision making for green supplier selection using interval type-2 fuzzy AHP: A case study of a home appliance manufacturer. *Oper Res*, 22(1), 199–233. [CrossRef]

[37] Coupland, S., & John, R. (2008). A fast geometric method for defuzzification of type-2 fuzzy sets. *IEEE Trans Fuzzy Syst*, 16(4), 929–941. [CrossRef]

[38] Paik, B., & Mondal, S. K. (2021). Representation and application of fuzzy soft sets in type-2 environment. *Complex Intell Syst*, 7(3), 1597–1617. [CrossRef]

[39] Mo, H., Wang, F. Y., Zhou, M., Li, R., & Xiao, Z. (2014). Footprint of uncertainty for type-2 fuzzy sets. *Inf Sci Ny*, 272, 96–110. [CrossRef]

[40] Yildiz, A., Ayyildiz, E., Taskin Gumus, A., & Ozkan, C. (2021). A framework to prioritize the public expectations from water treatment plants based on trapezoidal type-2 fuzzy Ahp Method. *Environ Manage*, 67(3), 439–448. [CrossRef]

[41] Karasan, A., Ilbahar, E., & Kahraman, C. (2019). A novel pythagorean fuzzy AHP and its application to landfill site selection problem. *Soft Comput*, 23(21), 10953–10968. [CrossRef]

[42] Ayyildiz, E., & Erdogan, M. (2023). A decision support mechanism in the determination of organic waste collection and recycling center location: A sample application for Turkiye. Appl Soft Comput, 147, 110752. [CrossRef]

[43] Saaty, T. L. T. L. (1980). *The Analytic Hierarchy Process*. New York: McGraw-Hill. [CrossRef]

[44] Li, L., & Tang, Y. (2023). A new method of human reliability analysis based on the correlation coefficient in the evidence theory and analytic hierarchy process method. *Arab J Sci Eng*, 48, 10713–10726. [CrossRef]

[45] Kusakci, S., Yilmaz, M. K., Kusakci, A. O., Sowe, S., & Nantembelele, F. A. (2022). Towards sustainable cities: A sustainability assessment study for metropolitan cities in Türkiye via a hybridized IT2F-AHP and COPRAS approach. *Sustain Cities Soc*, 78, 103655. [CrossRef]

[46] Mendel, J. M., John, R. I., & Liu, F. (2006). Interval type-2 fuzzy logic systems made simple. *IEEE Trans Fuzzy Syst*, 14(6), 808–821. [CrossRef]

[47] Lee, L. W., & Chen, S. M. (2008). *Fuzzy multiple attributes group decision-making based on the extension of TOPSIS method and interval type-2 fuzzy sets*. Proceedings of the 7th International Conference on Machine Learning and Cybernetics. ICMLC, vol. 6, pp. 3260–3265.

[48] Chen, S. M., & Lee, L. W. (2010). Fuzzy multiple attributes group decision-making based on the interval type-2 TOPSIS method. *Expert Syst Appl*, 37(4), 2790–2798. [CrossRef]

[49] Ordu, M., & Der, O. (2023). Polymeric materials selection for flexible pulsating heat pipe manufacturing using a comparative hybrid MCDM approach. *Polymers Basel*, 15(13), 2933. [CrossRef]

[50] Kumar, A., Sah, B., Singh, A. R., Deng, Y., He, X., Kumar, P., Bansal, R. C. (2017). A review of multi criteria decision making (MCDM) towards sustainable renewable energy development. *Renew Sustain Energy Rev*, 69, 596–609. [CrossRef]

[51] van Laarhoven, P. J. M., & Pedrycz, W. (1983). A fuzzy extension of Saaty's priority theory. *Fuzzy Sets Syst*, 11(1–3), 229–241. [CrossRef]

[52] Buckley, J. J. (1985). Fuzzy hierarchical analysis. *Fuzzy Sets Syst*, 17(3), 233–247. [CrossRef]

[53] Erdogan, M., & Kaya, I. (2019). Prioritizing failures by using hybrid multi criteria decision making methodology with a real case application. *Sustain Cities Soc*, 45, 117–130. [CrossRef]

[54] Singh, V., Chandrasekaran, M., Samanta, S., Devarasiddappa, D., & Arunachalam, R. (2021). Sustainability assessment of gas metal arc welding process of AISI 201LN using AHP-TLBO integrated optimization methodology. *J Brazilian Soc Mech Sci Eng*, 43(2), 1–20. [CrossRef]

[55] Ayyildiz, E., Erdogan, M., & Taskin Gumus, A. (2021). A pythagorean fuzzy number-based integration of AHP and WASPAS methods for refugee camp location selection problem: A real case study for İstanbul, Turkey. *Neural Comput Appl*, 33(22), 15751–15768. [CrossRef]

[56] Devotta, S. (2014). Refrigerant Selection – Global Environment, Thermodynamics, Safety and Efficiency. *Indian Chem Eng*, 56(3), 294–312. [CrossRef]

[57] NRDC International. (2018). *Cooling with less warming: Improving air conditioners in India*. https://www.nrdc.org/sites/default/files/cooling-india-air-conditioners-market-profile-2018-fs.pdf

Journal of Sustainable Construction Materials and Technologies
Web page info: https://jscmt.yildiz.edu.tr
DOI: 10.47481/jscmt.1338751

JSCMT
Journal of Sustainable Construction Materials and Technologies

Research Article

Rheology of superabsorbent polymer-modified and basalt fiber-reinforced cement paste with silica fume: Response surface methodology

Hasan DİLBAS*

Department of Civil Engineering, Van Yüzüncü Yıl University Faculty of Engineering, Van, Türkiye

ARTICLE INFO

Article history
Received: 07 August 2023
Revised: 25 September 2023
Accepted: 17 October 2023

Key words:
Basalt fiber, response surface methodology, rheology, silica fume, superabsorbent polymer

ABSTRACT

A composite's rheology can be changed by adding superabsorbent polymer (SAP) and basalt fibers and using silica fume. This study aimed to investigate the effects of these components on the viscosity and shear stress parameters of the paste. The proportions of the components were varied, with SAP content ranging from 0.01% to 0.03%, basalt fiber from 0% to 0.50%, silica fume (micro silica) at 15%, and water content from 0.40 to 0.50. Response surface methodology was used to optimize the mixture proportions, and the rheological properties of the resulting pastes were characterized using a rheometer. Results showed that the addition of SAP and basalt fiber had a significant impact on the rheological properties of the paste, with increasing amounts of both resulting in increased viscosity and shear stress. Overall, this study highlights the potential of SAP and basalt fiber in advances of the rheology of cement paste and provides insight into the optimal proportions of these components for achieving desired rheological properties. The findings of this study could be useful in developing high-performance concrete with enhanced rheological properties, which could have a wide range of applications in the construction industry. In addition, 0.50% BF, 0.01% SAP, and 0.445 water-to-cement were found as optimum proportions regarding the rheology of the cement paste.

Cite this article as: Dilbas, H. (2024). Rheology of superabsorbent polymer-modified and basalt fiber-reinforced cement paste with silica fume: Response surface methodology. *J Sustain Const Mater Technol*, 9(1), 60–71.

1. INTRODUCTION

Rheology studies the deformation and flow of materials under applied forces. It is essential to understand the rheological properties of cement pastes, significantly when they are modified with additives such as a superabsorbent polymer (SAP) and nano-silica (NS), because they affect the workability, pumpability, and performance of the cementitious materials. SAP is a type of hydrogel that can absorb and retain large amounts of water, up to several hundred times its weight. It has been used as an internal curing agent in cement pastes to mitigate autogenous shrinkage, a deformation caused by self-desiccation of the pores due to hydration progress. SAP can release water into the capillaries, thus maintaining a high relative humidity and reducing capillary tension. SAP can also improve cement pastes' durability and mechanical properties by reducing cracking and enhancing pore structure [1]. NS is a nanomaterial with a high specific surface area and reactivity. It has been used as a supplementary cementitious material (SCM) in cement pastes to improve the compressive strength, hydration rate, and microstructure. NS can fill the pores, reduce the porosity of cement pastes, participate in the pozzolanic reaction, and form additional calcium silicate hydrate (CSH) [2]. The rheological properties of cement pastes modified with SAP and NS depend on several factors, such as the dosage, parti-

***Corresponding author.**
*E-mail address: hasandilbas@yyu.edu.tr

cle size, dispersion, and interaction of the additives, as well as the water-to-cement ratio (w/c), temperature, and time. Several studies have investigated the effects of SAP and NS on the rheology of cement pastes using rotational rheometry, which can measure the viscosity and yield stress of the materials by applying a shear stress or strain [3]. The viscosity is a measure of the resistance to flow, while the yield stress is a measure of the minimum stress required to initiate flow. Both parameters are influenced by the amount and type of additives in cement pastes. Generally, increasing the dosage of SAP or NS increases the viscosity and yield stress of cement pastes because they consume more water and increase the solid content [4]. However, some studies have reported that low dosages of SAP or NS can reduce cement pastes' viscosity and yield stress because they act as lubricants or dispersants [5]. The particle size and distribution of SAP and NS also affect the rheology of cement pastes. Smaller particles increase viscosity and yield stress more than larger particles because they have a higher surface area and adsorption capacity [6]. The dispersion of SAP and NS in cement pastes is also important for achieving a homogeneous mixture and avoiding agglomeration or segregation [7]. The interaction between SAP and NS in cement pastes is another factor that influences their rheological properties. Some studies have suggested that SAP can reduce NS's negative effects on cement pastes' rheology by providing internal curing water and preventing excessive water consumption by NS [8]. However, other studies have indicated that SAP can interfere with the dispersion and hydration of NS in cement pastes by competing for water or forming a coating layer around NS particles [9]. Therefore, the optimal dosage and ratio of SAP and NS in cement pastes must be determined based on their rheological requirements.

Due to hydration and swelling processes, the rheological properties of cement pastes modified with SAP and NS vary with time. Hydration causes an increase in viscosity and yield stress over time because it consumes water and forms CSH gel [10]. Swelling causes a decrease in viscosity and yield stress over time because it releases water and reduces capillary tension [11]. The rate and extent of hydration and swelling depend on the w/c ratio, temperature, type and dosage of additives, and curing conditions [12]. Basalt fiber-reinforced cement paste (BFRC) is a composite material that consists of a cement paste matrix and basalt fibers dispersed randomly or aligned in a certain direction. Basalt fibers are natural fibers derived from volcanic rocks that have high tensile strength, modulus of elasticity, thermal stability, and chemical resistance [13]. BFRC has been used for various applications such as structural repair, fire protection, thermal insulation, and noise reduction [14]. The rheological properties of BFRC are influenced by several factors, such as the dosage, length, diameter, aspect ratio, surface treatment, and orientation of basalt fibers, as well as the water-to-cement ratio (w/c), admixtures, and curing conditions of the cement paste matrix [13–15]. The rheological properties of BFRC are important for its workability, pumpability, flowability, and stability during mixing, placing, and hardening. Adding basalt fibers to cement paste generally increases its viscosity and yield stress, decreasing its slump and flow [13–15]. However, a higher w/c ratio can also reduce the mechanical properties and durability of BFRC. Therefore, an optimum w/c ratio should be selected to balance the rheological and mechanical performance of BFRC. Admixtures such as superplasticizers or air-entraining agents can enhance the workability and stability of BFRC by reducing the water demand, increasing the fluidity, decreasing the segregation, and improving the air entrainment of the mixture [13–15]. Superplasticizers can also enhance the dispersion and alignment of basalt fibers by reducing their agglomeration and flocculation [14]. Air-entraining agents can create air bubbles that act as lubricants and spacers among basalt fibers and cement paste matrix, which reduce the frictional forces and increase the deformability of BFRC [15].

The surface treatment of basalt fibers can affect their adhesion and compatibility with the cement paste matrix, affecting their dispersion and rheological properties. The surface treatment can be physical (such as heat treatment or plasma treatment) or chemical (such as silane coupling agents or alkali treatment) [13, 14]. The surface treatment can modify basalt fibers' surface morphology, roughness, hydrophilicity/hydrophobicity, polarity, charge density, functional groups, and bond strength. The surface treatment can improve the wetting and bonding of basalt fibers with cement paste matrix, and this leads to a reduction in their pull-out resistance and an increase in their load transfer efficiency. The surface treatment can also reduce basalt fibers' water absorption and alkali reactivity, improving their durability in an alkaline environment. The surface treatment can also affect the dispersion and orientation of basalt fibers by changing their surface energy and electrostatic forces.

The mechanical properties of BFRC can be affected by the w/c ratio, admixtures, and curing conditions of the cement paste matrix [13–15]. The w/c ratio influences the porosity and hydration degree of the cement paste matrix, affecting its strength and durability. A lower w/c ratio can increase the compressive strength, tensile strength, flexural strength, modulus of elasticity, and fracture toughness of BFRC [13–15]. Superplasticizers can reduce the water demand and increase the hydration degree and strength of BFRC. Air-entraining agents can increase the air content and reduce the density and strength of BFRC [15]. However, air-entraining agents can also improve the durability and crack resistance of BFRC by creating air voids that act as stress relievers and crack arresters [15]. The surface treatment of basalt fibers can affect their mechanical properties by changing their adhesion and compatibility with the cement paste matrix [13, 14]. The surface treatment can also reduce the pull-out and slippage of basalt fibers, which improves their fracture toughness and crack resistance of BFRC [13, 14].

In conclusion, rheology is a valuable tool for characterizing the flow behavior of cement pastes modified with SAP and NS. These additives can affect cement pastes' viscosity

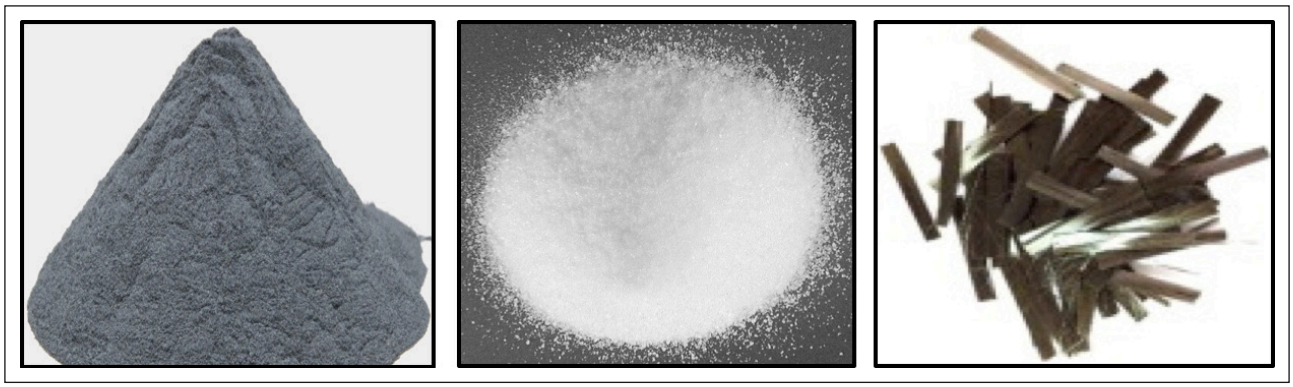

Figure 1. View of silica fume, super absorbent polymer, and basalt fiber (from left to right, respectively).

Table 1. Physical properties of the materials used in the study

Material	Specific gravity	Fineness (cm^2/g)	Blaine's surface area (cm^2/g)	Chemical properties
OPC	3.15	3,200	402	SiO_2: 21.1%, Al_2O_3: 4.8%, Fe_2O_3: 3.2%, CaO: 63.1%
Silica fume	2.2	20,000	28,800	SiO_2: 90–97%, Al_2O_3: 1–2%, Fe_2O_3: 0.5–2%, CaO: 0.5–2%
SAP	1.2	N/A	N/A	Na: 6.5%, K: 1.5%, Cl: 0.7%, SO_4: 1.2%
Basalt fiber	2.7	N/A	N/A	SiO_2: 46.1%, Al_2O_3: 10.4%, Fe_2O_3: 7.8%, CaO: 9.3%
Water	1.0	N/A	N/A	H_2O:100%

and yield stress differently depending on their dosage, size, dispersion, interaction, time, etc. Therefore, optimizing their use based on their desired effects on both fresh and hardened properties of cementitious materials is essential. Basalt fiber-reinforced cement paste (BFRC) is a composite material with superior rheological and mechanical properties compared to plain cement paste. The rheological and mechanical properties of BFRC are influenced by several factors related to the basalt fibers and the cement paste matrix. These factors should be considered carefully to optimize the performance and application of BFRC.

Response Surface Methodology (RSM) is a statistical tool that can investigate the relationship between multiple variables and their impact on a response, such as the rheological properties of cement paste [5]. RSM involves using mathematical models to describe the relationship between the input variables and the response variables, and the models are used to optimize the input variables to achieve the desired response. RSM is a useful tool for investigating complex systems with multiple variables, and it can help to identify the optimum conditions for achieving the desired response. The proportions of SAP, basalt fiber, silica fume, and water in cement paste can be optimized using RSM. The proportions of these components can be varied within a specific range, and the rheological properties of the paste can be measured using standard methods such as the slump test, the flow table test, and the rheometer test. The results of these tests can be used to develop mathematical models to describe the relationship between the input variables and the rheological properties of the paste. The models can be used to identify the optimum proportions of the components for achieving the desired rheological properties of the paste.

Table 2. Mix proportions of the cement paste

Component	Mix proportions (by weight)
OPC	1
Silica fume	0.15
SAP	0.01–0.03
Basalt fiber	0–0.50
Water	0.40–0.50

In this study, the impact of SAPs, basalt fibers, silica fume (micro silica), and water on the rheological properties of cement paste was investigated using response surface methodology (RSM) based on central composite design (CCD). The rheological properties of the cement paste, including viscosity and shear stress parameters, were analyzed using a rheometer.

2. MATERIALS AND METHODS

2.1. Materials

The materials used in the study include ordinary Portland cement CEM I 42.5R (OPC), silica fume, superabsorbent polymer (SAP), basalt fiber, and water (Fig. 1). OPC was obtained from a local supplier. Elkem Materials Inc., USA, provided silica fume. SAP was purchased from BASF Corporation, USA. Basalt fiber was obtained from Mafic USA, USA. The physical properties of the materials used in the study are presented in Table 1. SAP had a particle size distribution between 0.5 and 2 mm. The median is 1.1 mm. Basalt fiber had a 9–13 μm diameter and 2 mm length.

Table 3. Testing procedure

Shear rate, rpm	100*	100	50	25	10	5	1	0.10	0.05	0.01
Time, second	75	15	15	15	15	15	15	15	15	15

*Pre-shearing.

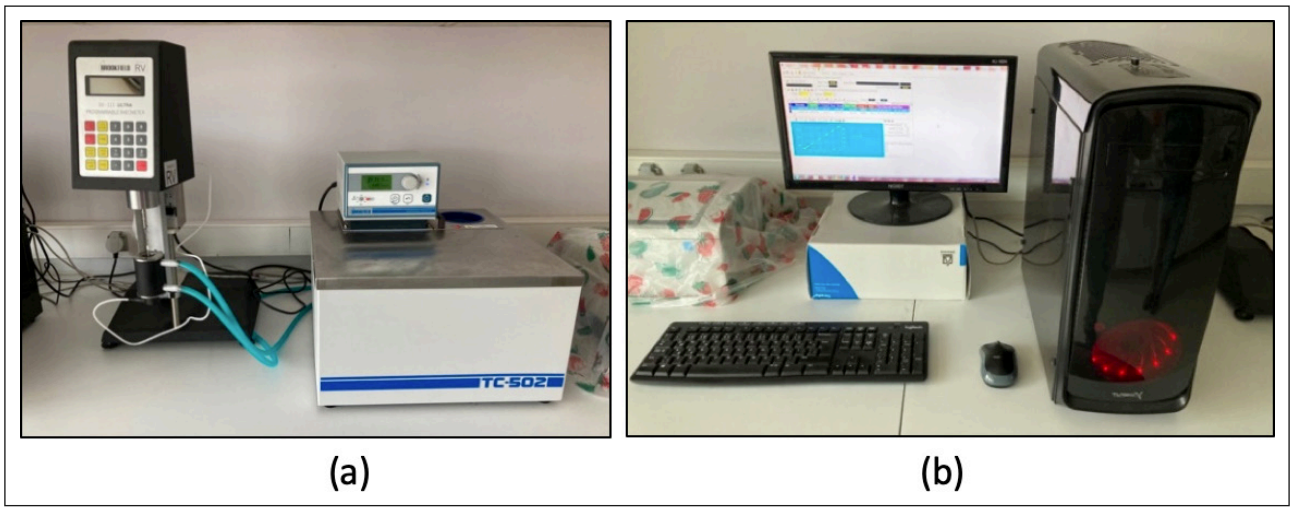

Figure 2. Rheology test setup **(a)** and data curation in computer with software **(b)**.

2.2. Methods

2.2.1. Preparation of Cement Paste

The cement paste was prepared according to ASTM C305-14. The OPC was mixed with silica fume, SAP, basalt fiber, and water in a mixer for 5 minutes at 1400 rpm. The mixture was then poured into a mold and placed in a curing chamber at 25°C and 95% relative humidity for 28 days. The mix proportions used in the study are presented in Table 2.

2.2.2. Rheological Testing

The rheological properties of the cement paste, including viscosity and shear stress parameters, were analyzed using a rheometer (Brookfield RV) (Fig. 2). The test was conducted according to ASTM C1437-15. The sample was placed in a cylindrical container with a diameter of 25 mm and a height of 20 mm. The rheometer had a concentric cylinder measuring system with a SC4-29 spindle. The test was conducted at a shear rate of 0.01–100 s^{-1} at 25°C (Table 3).

2.2.3. Response Surface Methodology

Response Surface Methodology (RSM) is a statistical technique used to optimize and improve the response of a system to various inputs or factors. RSM involves designing experiments to study the effects of different input variables on the output response and then using mathematical models to analyze the data and optimize the response. RSM has been widely used in various fields, such as engineering, chemistry, and agriculture, to optimize and improve the performance of complex systems.

In cement-based composites, RSM has been used to optimize the properties of the composites by studying the effects of various input factors such as cement type, aggregate type, water-cement ratio, and curing conditions. RSM has been used to study the impact of these factors on various properties such as compressive strength, flexural strength, and durability of the composites. RSM is an effective tool for optimizing the properties of cement-based composites as it can help identify the most significant factors affecting the properties and provide optimal conditions for achieving the desired properties.

RSM has been used in several studies to optimize the properties of cement-based composites [16, 17]. For example, RSM was used to optimize high-strength concrete's compressive strength and water absorption by studying the effects of different factors such as water-cement ratio, superplasticizer dosage, and curing temperature. Another study used RSM to optimize the flexural strength of cement-based composites by studying the effects of factors such as fiber type, fiber volume fraction, and curing conditions. In both studies, RSM was found to be an effective tool for optimizing the properties of cement-based composites and providing optimal conditions for achieving the desired properties.

RSM is a powerful statistical technique that can optimize cement-based composites' properties by studying the effects of various input factors on the response.

Central Composite Design (CCD) is a commonly used experimental design in RSM. CCD involves designing a set of experiments that allows for evaluating the curvature and interactions of the input variables. It includes a set of factorial, axial, and center points, allowing for the quadratic response surface model estimation. CCD is an efficient and cost-effective way to optimize the response of a system by studying the effects of various input variables on the output response. CCD is a widely used experimental design method in engineering and applied sciences for modeling and optimizing the response of a system or process under study.

Table 4. Range and levels of the variables used in the study

Variable	Level -1	Level 0	Level 1
X1 (SAP content, %)	0.01	0.02	0.03
X2 (Basalt fiber content, %)	0	0.25	0.50
X3 (Water-to-cement ratio)	0.40	0.45	0.50

Table 5. Rheological properties of the cement paste

Run#	X1	X2	X3	Viscosity (Pa·s)	Yield stress (Pa)	Shear stress (Pa)
1	0.01	0.50	0.50	0.0035	0.033	0.13
2	0.01	0.50	0.40	0.0032	0.031	0.12
3	0.01	0	0.40	0.0030	0.031	0.12
4	0.01	0.25	0.45	0.0034	0.032	0.13
5	0.01	0	0.50	0.0026	0.028	0.11
6	0.02	0.25	0.45	0.0030	0.031	0.12
7	0.02	0.25	0.50	0.0035	0.034	0.14
8	0.02	0.25	0.45	0.0033	0.033	0.13
9	0.02	0.50	0.45	0.0031	0.033	0.13
10	0.02	0.25	0.45	0.0033	0.033	0.13
11	0.02	0	0.45	0.0030	0.031	0.12
12	0.02	0.25	0.45	0.0032	0.033	0.13
13	0.02	0.25	0.45	0.0029	0.032	0.13
14	0.02	0.25	0.40	0.0031	0.033	0.13
15	0.02	0.25	0.45	0.0033	0.033	0.13
16	0.03	0	0.40	0.0028	0.030	0.12
17	0.03	0.25	0.45	0.0033	0.033	0.13
18	0.03	0.50	0.50	0.0034	0.032	0.13
19	0.03	0	0.50	0.0036	0.034	0.14
20	0.03	0.50	0.40	0.0031	0.032	0.13

The design involves creating a set of experimental runs that vary in levels of the input variables to obtain a quadratic response surface that can be used to model the system's behavior and predict optimal input settings. CCD is beneficial in cases where the relationship between input variables and response is complex and can be used to identify optimal input settings for a desired output response [18].

CCD has been applied in various fields, including materials science [19], chemical engineering [18], and environmental science [20, 21], among others. The method has been used for optimizing a range of parameters, including mechanical properties [19], chemical reactions [18], and process parameters [20]. CCD has also been combined with other techniques, such as artificial neural networks and fuzzy logic, for improved optimization and modeling [22, 23].

One of the advantages of CCD is that it allows for the estimation of the input variables' primary effects, quadratic effects, and interaction effects, which can help identify essential factors and their relative contributions to the response. Furthermore, the design is efficient regarding the number of experimental runs required, with a minimum number of runs needed to estimate the response surface [21]. Despite its usefulness, CCD has some limitations, including the assumption of linearity of the response surface and the need for a sufficient number of runs to achieve accurate results [22].

In conclusion, CCD is a powerful experimental design method that can be used to model and optimize the response of a system or process. Its application in various fields has demonstrated its effectiveness in identifying optimal input settings for a desired output response. However, it is essential to carefully consider the limitations and assumptions of the method to obtain accurate results.

The CCD was used to investigate the components' impact on the cement paste's rheological properties. The CCD is a statistical experimental design method used to optimize

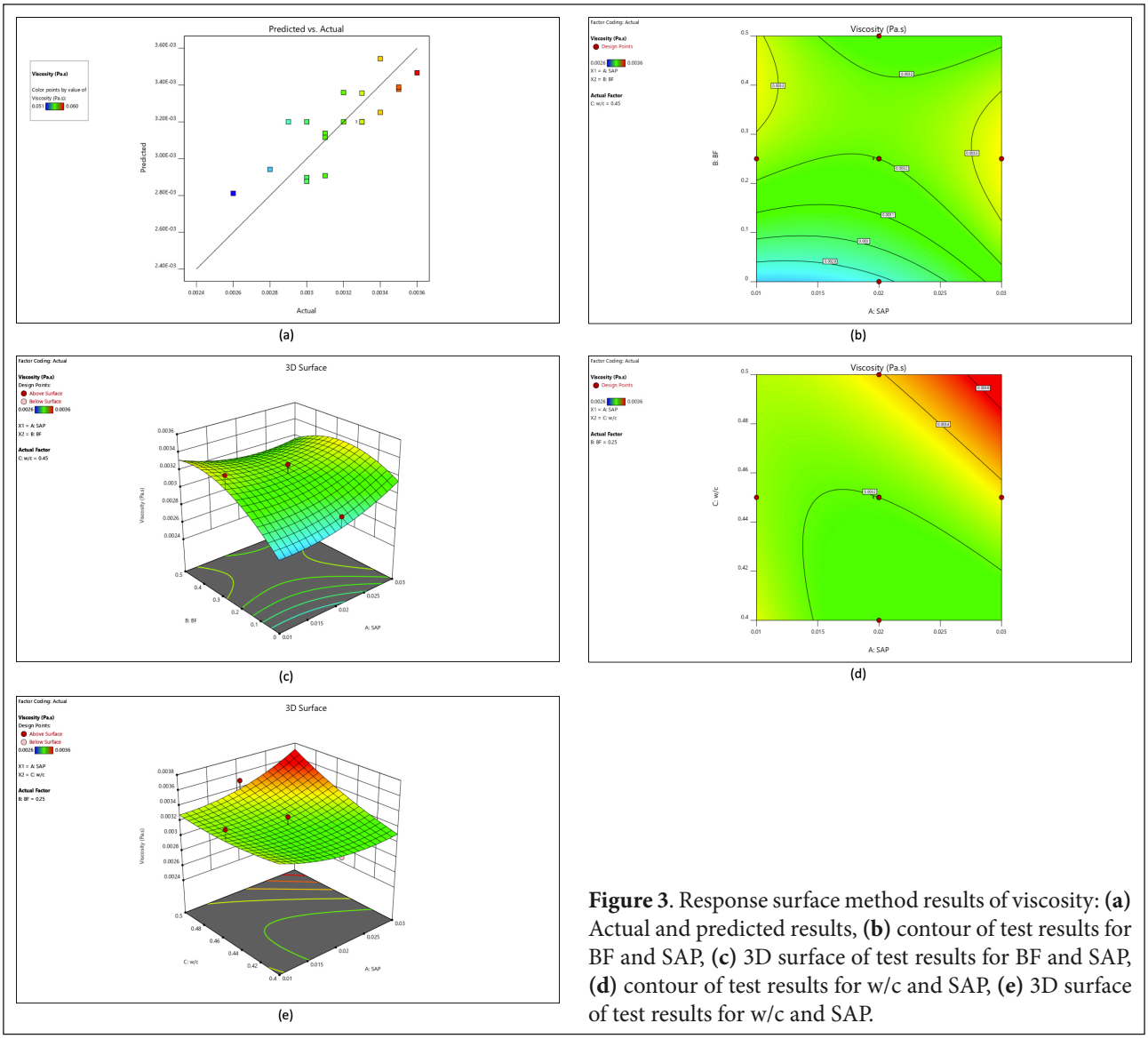

Figure 3. Response surface method results of viscosity: **(a)** Actual and predicted results, **(b)** contour of test results for BF and SAP, **(c)** 3D surface of test results for BF and SAP, **(d)** contour of test results for w/c and SAP, **(e)** 3D surface of test results for w/c and SAP.

a system's response by varying the input parameters. The CCD is a type of second-order design used to model the response surface of the system as a quadratic equation. The CCD requires fewer experimental runs than a complete factorial design and provides a better understanding of the relationship between the input and output variables.

The experimental design for the CCD involved three independent variables, namely SAP content (X1), basalt fiber content (X2), and water-to-cement ratio (X3). The range and levels of the variables used in the study are presented in Table 4.

In this paper, all experimental designs and analyses were examined with the help of the Design Expert software. The experimental design involved 20 runs, including one axial point, one factorial point, and six center points. The experimental runs were randomized to minimize the effect of extraneous variables. The experimental data were analyzed using the response surface methodology, and the quadratic model was developed to predict the rheological properties of the cement paste.

3. RESULTS AND DISCUSSION

The rheological properties of the cement paste, including viscosity and shear stress parameters, were analyzed using a rheometer. The results of the rheological testing are presented in Table 5. The components' impact on the cement paste's rheological properties is discussed below.

The viscosity of the cement paste increased with increasing SAP content and basalt fiber content and decreased with increasing water-to-cement ratio (Fig. 3). The quadratic model developed to predict the viscosity of the cement paste is presented in Equation 1 with R=0.8146.

$$(\text{Viscosity})^{0.5}=0.0565 + 0.0005X_1 + 0.0012X_2 + 0.0012X_3 + 0.0009X_1^2 - 0.0017X_2^2 + 0.0005X_3^2 - 0.0011X_1X_2 + 0.0014X_1X_3 + 0.0002X_2X^3 \quad (1)$$

Where X1, X2, and X3 are SAP content, basalt fiber content, and water-to-cement ratio, respectively.

The yield stress of the cement paste increased with increasing SAP content and basalt fiber ratio and decreased with increasing water-to-cement range (Fig. 4). The qua-

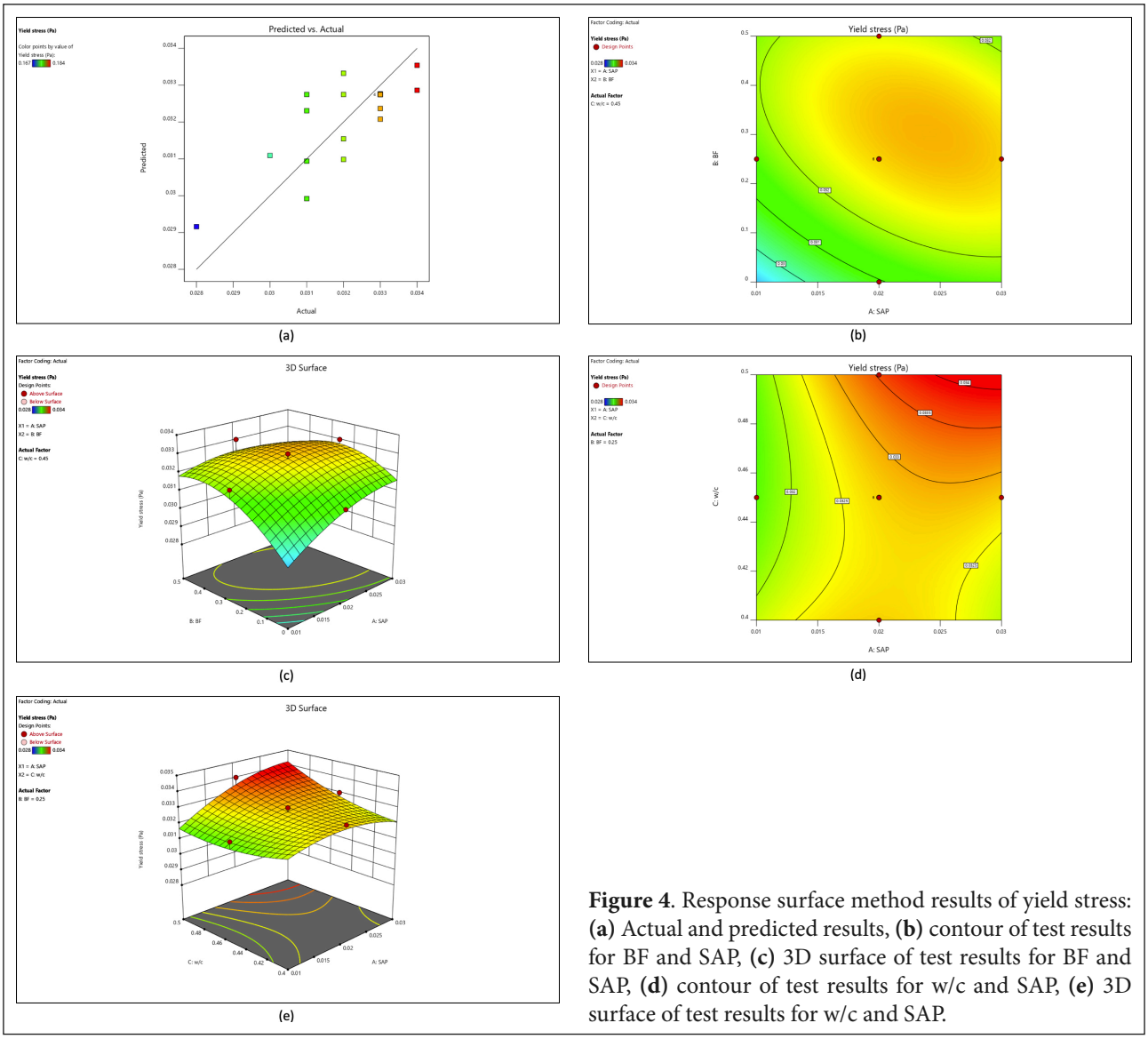

Figure 4. Response surface method results of yield stress: **(a)** Actual and predicted results, **(b)** contour of test results for BF and SAP, **(c)** 3D surface of test results for BF and SAP, **(d)** contour of test results for w/c and SAP, **(e)** 3D surface of test results for w/c and SAP.

dratic model developed to predict the yield stress of the cement paste is presented in Equation 2 with R=0.7899.

$$(\text{Yield Stress})^{0.5}=0.1809 + 0.0017X_1 + 0.0020X_2 + 0.0011X_3 - 0.0017X_1^2 - 0.0031X_2^2 + 0.0011X_3^2 - 0.0018X_1X_2 + 0.0018X_1X_3 + 0.0004X_2X_3 \quad (2)$$

Where X1, X2, and X3 are SAP content, basalt fiber content, and water-to-cement ratio, respectively.

The shear stress of the cement paste increased with increasing SAP content and basalt fiber ratio and decreased with increasing water-to-cement range (Fig. 5). The quadratic model developed to predict the shear stress of the cement paste is presented in Equation 3 with R=0.7855.

$$(\text{Shear Stress})^{0.5}=0.3599 + 0.0057X_1 + 0.0044X_2 + 0.0041X_3 - 0.0019X_1^2 - 0.0090X_2^2 + 0.0049X_3^2 - 0.0035X_1X_2 + 0.0035X_1X_3 + 0.0001X_2X_3 \quad (3)$$

Where X1, X2, and X3 are SAP content, basalt fiber content, and water-to-cement ratio, respectively.

The study found that the viscosity of the paste increases with an increase in SAP content and basalt fiber content while decreasing with an increase in the water-to-cement ratio. In contrast, the shear stress increases with an increase in SAP content and a decrease in water-to-cement ratio while decreasing with an increase in basalt fiber content. The study also developed quadratic models to predict the viscosity and shear stress of the paste. The models considered the interaction between SAP and basalt fiber content and showed that the exchange positively affects yield and shear stresses. The comments are supported by Table 4, which presents the rheological properties of the paste for different runs, including viscosity, yield stress, and shear stress.

Using the Response Surface Methodology (RSM) with Central Composite Design (CCD) in the study is an appropriate statistical technique to optimize the experimental design and analyze the effects of independent variables on the response variables. CCD is a widely used practical design approach that helps to explore the complex relationships between variables by modeling second-order polynomial equations. The study utilized CCD to design and conduct experiments by varying the proportions of paste components within a specified range. The study re-

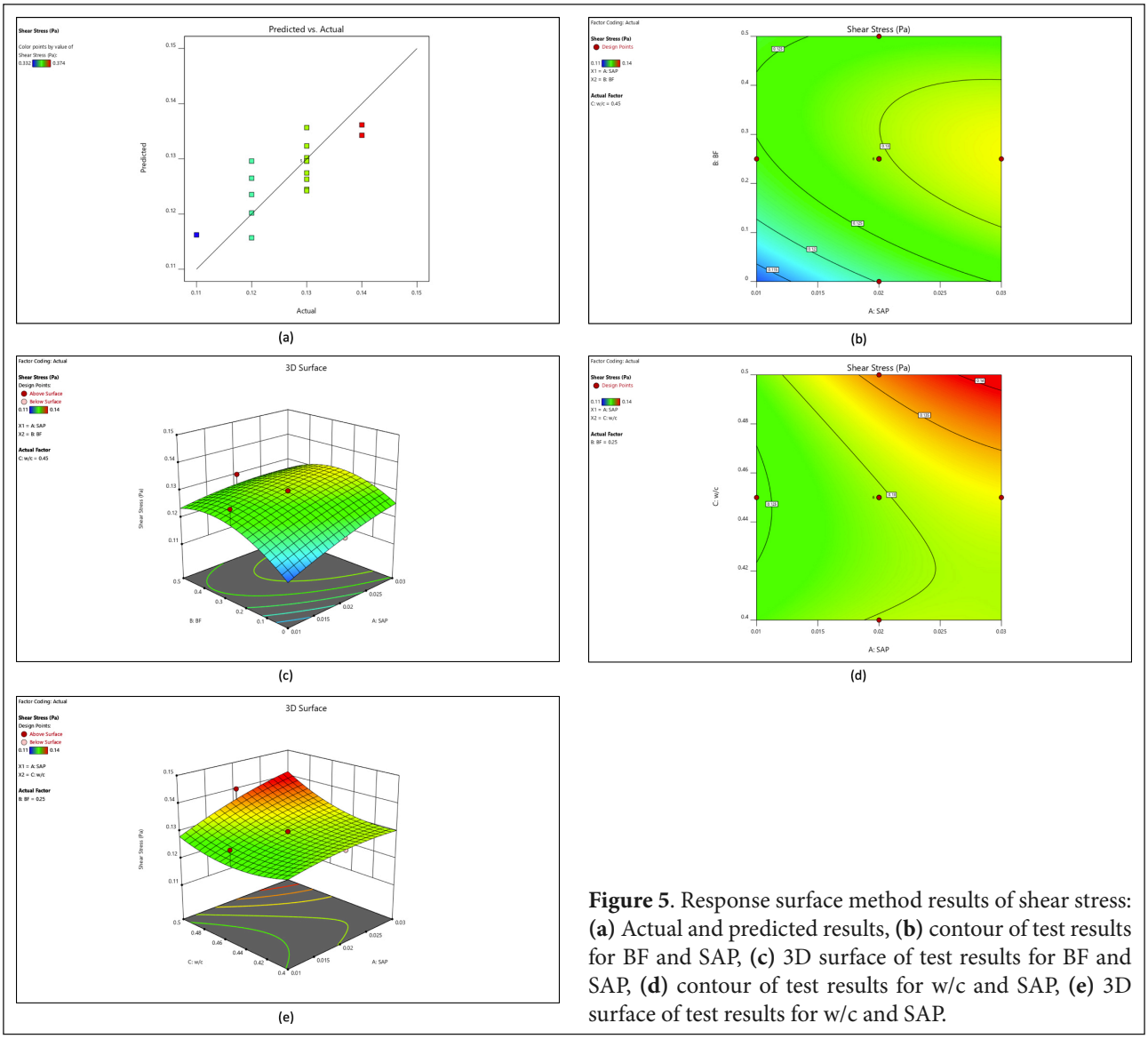

Figure 5. Response surface method results of shear stress: **(a)** Actual and predicted results, **(b)** contour of test results for BF and SAP, **(c)** 3D surface of test results for BF and SAP, **(d)** contour of test results for w/c and SAP, **(e)** 3D surface of test results for w/c and SAP.

sults could be useful in designing cementitious materials with improved rheological properties for various applications. Table 5 provides data on the effect of SAP content, basalt fiber content, and water-to-cement ratio on the cementitious composites' viscosity, yield stress, and shear stress. The data from the table can be analyzed using various statistical techniques to gain insights into the inter-relationships between the variables.

The statistical analysis of the data reveals that the water-to-cement ratio significantly affects the viscosity of the cementitious composites. According to the results of Runs, the composites with a higher water-to-cement ratio have a lower viscosity. This observation is consistent with the findings of previous studies that have shown that an increase in the water-to-cement ratio leads to a decrease in the viscosity of the cement paste [6]. On the other hand, the yield stress of the composites is influenced by the SAP and basalt fiber content. As seen from the data in Runs, the composites with a higher SAP content and basalt fiber content exhibit a higher yield stress. This result is in line with the previous studies that have demonstrated the reinforcing effect of SAP and basalt fiber on the mechanical properties of cementitious composites [6, 14]. The data in Table 5 also suggest that the shear stress of the composites is affected by the interaction between the SAP content, basalt fiber content, and water-to-cement ratio. For instance, the composites in Runs, which have the same SAP and basalt fiber content but different water-to-cement ratios, show different shear stress values. This finding is consistent with the research highlighting the complex interplay between multiple variables in determining the rheological properties of cementitious composites [6, 7, 9, 24].

In conclusion, the data in Table 5 and Figures 3–5 demonstrate the significant influence of SAP content, basalt fiber content, and water-to-cement ratio on the rheological properties of cementitious composites. The findings highlight the importance of carefully selecting the material components and optimizing their proportions to achieve the desired rheological behavior of the composites. The optimization of the test results is given in the next section.

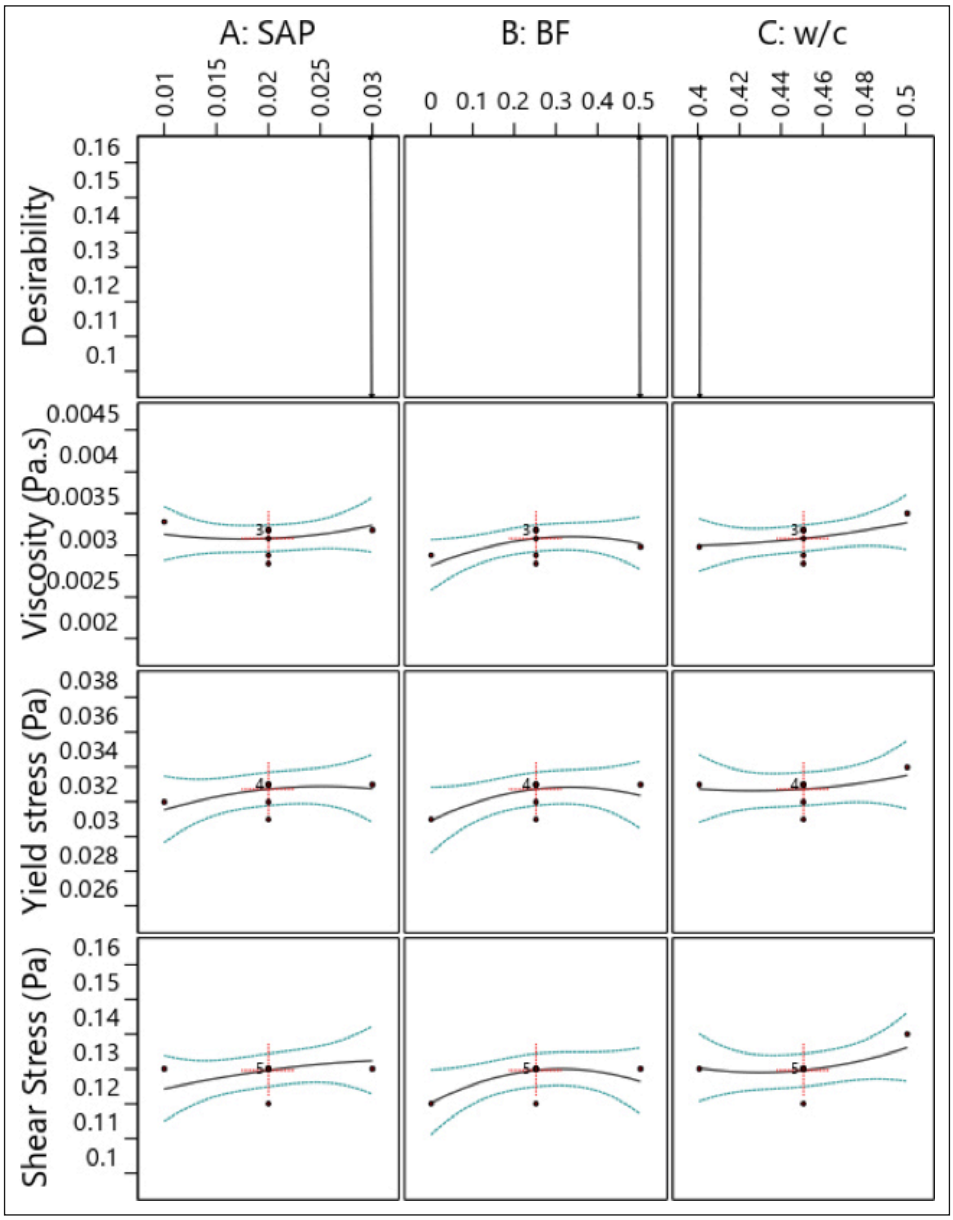

Figure 6. All factors impact on the test results.

Cement-based fresh paste has colloidal properties, and flow properties are essential during placement in the mold. Being in a fluid consistency like water is the most essential feature that is generally desired. For this reason, it is necessary to have a viscosity close to water, a low yield stress for it to flow, and a low shear stress between the particles. Considering the mentioned situations, the obtained test results have been optimized. Accordingly, the viscosity, yield stress, and shear stress are required to be minimum in the optimization. In addition, it is thought that the minimum SAP content, minimum basalt fiber content, and maximum water/cement content of the materials used will contribute positively to the results. Finally, the results shown in the figures below were obtained (Fig. 6, 7).

According to Figure 6, the relationship between the components and rheological parameters was given. The change in the rheology due to the use of SAP, BF, and w/c were observed. It was understood from Figure 6 that the increasing SAP and BF content in the mixture increased the yield and shear stress. Although the mixtures' components changed the mixtures' rheology, the mixtures' expected optimum behavior was evaluated below, as stated/argued in Figure 7.

In this comprehensive study, the viscosity, yield, and shear stress are required to be minimum in the optimization. In addition, it is thought that the minimum SAP content, minimum basalt fiber content, and maximum water/cement content of the materials used will contribute positively to the results. This leads to a high desirability of 0.887636, suitable up to 1.00. At this point, the proportions of components were BF=0%, SAP=0.01%, w/c=0.50, and the predicted rheological properties were approximately viscosity=0.0028 Pa.s, yield stress=0.029 Pa, and shear stress=0.116 Pa (Fig. 7). However, if the desirability level was set to 0.80 and the high is suitable up to 1.00, the proportions of components were BF=0.50%, SAP=0.01%, w/c=0.445, and the predict-

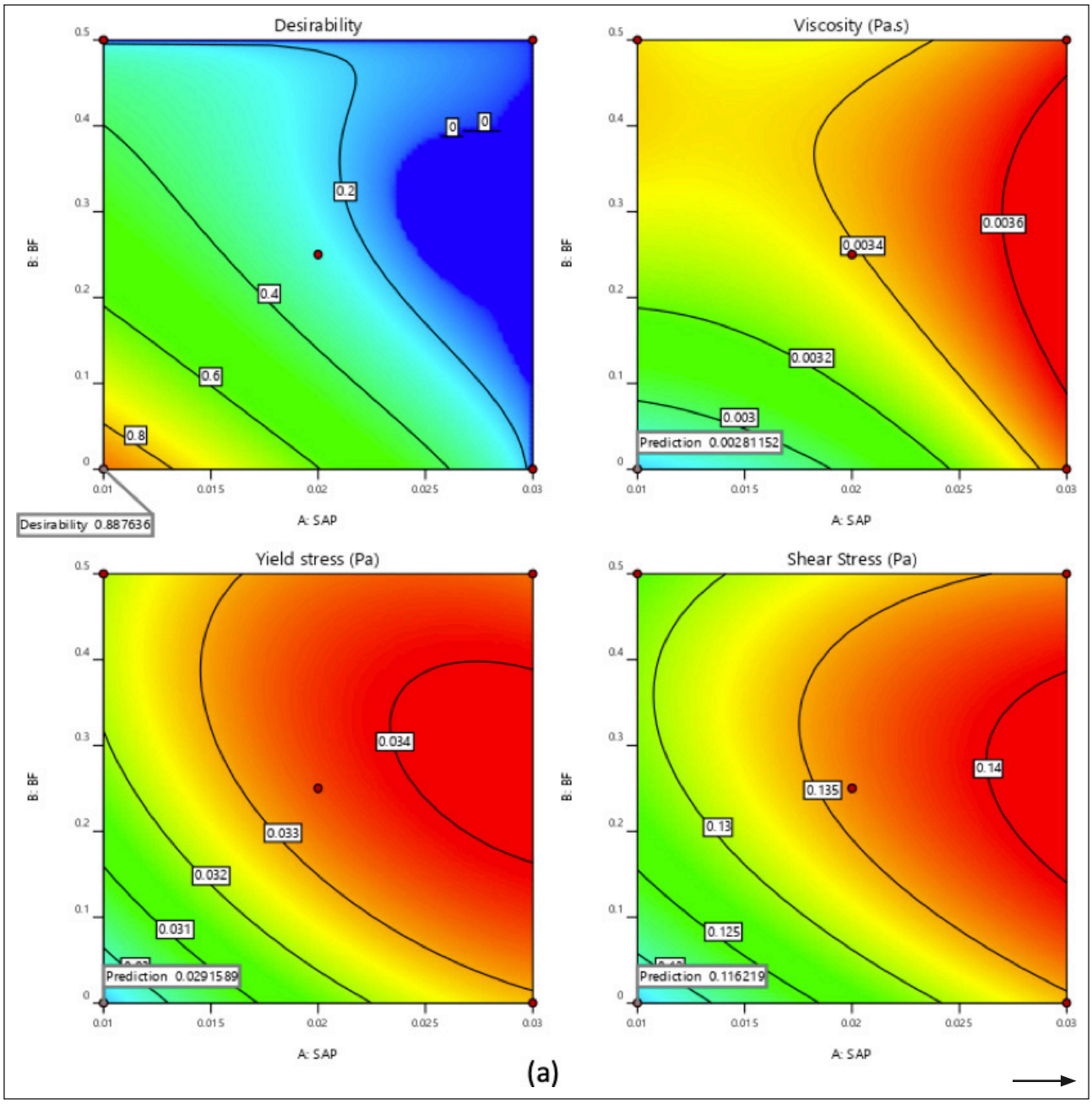

ed rheological properties were viscosity between 0.0028–0.0030 Pa.s, yield stress between 0.029–0.030 Pa, and shear stress between 0.114–0.115 Pa (Fig. 7).

4. CONCLUSIONS

In conclusion, the rheology of superabsorbent polymer-modified and basalt fiber-reinforced cement paste with silica fume was investigated using response surface methodology. The study demonstrated that adding superabsorbent polymer and basalt fibers significantly changed the rheological properties of the cement paste. The response surface methodology effectively optimized the mix design parameters to achieve the desired rheological properties. Some of the key findings of the study are commented on below.

Rheological properties: Adding superabsorbent polymer changed the cement paste's workability, yield stress, and plastic viscosity. The increase of water-to-cement proportion in the mixture increased workability, decreasing viscosity, yield/shear stress, super absorbent polymer, and basalt fiber's impact was the opposite of this. Basalt fibers enhanced the shear-thinning behavior of the cement paste, leading to a more stable and pumpable mixture.

Mixture design based on rheology: The optimum mix design parameters for achieving desired rheological properties were identified using the response surface methodology. Accordingly, the proportions of components such as BF=0.05%, SAP=0.01%, and w/c=0.445 can be offered for achieving desired rheological properties (low viscosity, yield stress, and shear stress).

The study highlights the potential of superabsorbent polymer and basalt fibers as effective additives for improv-

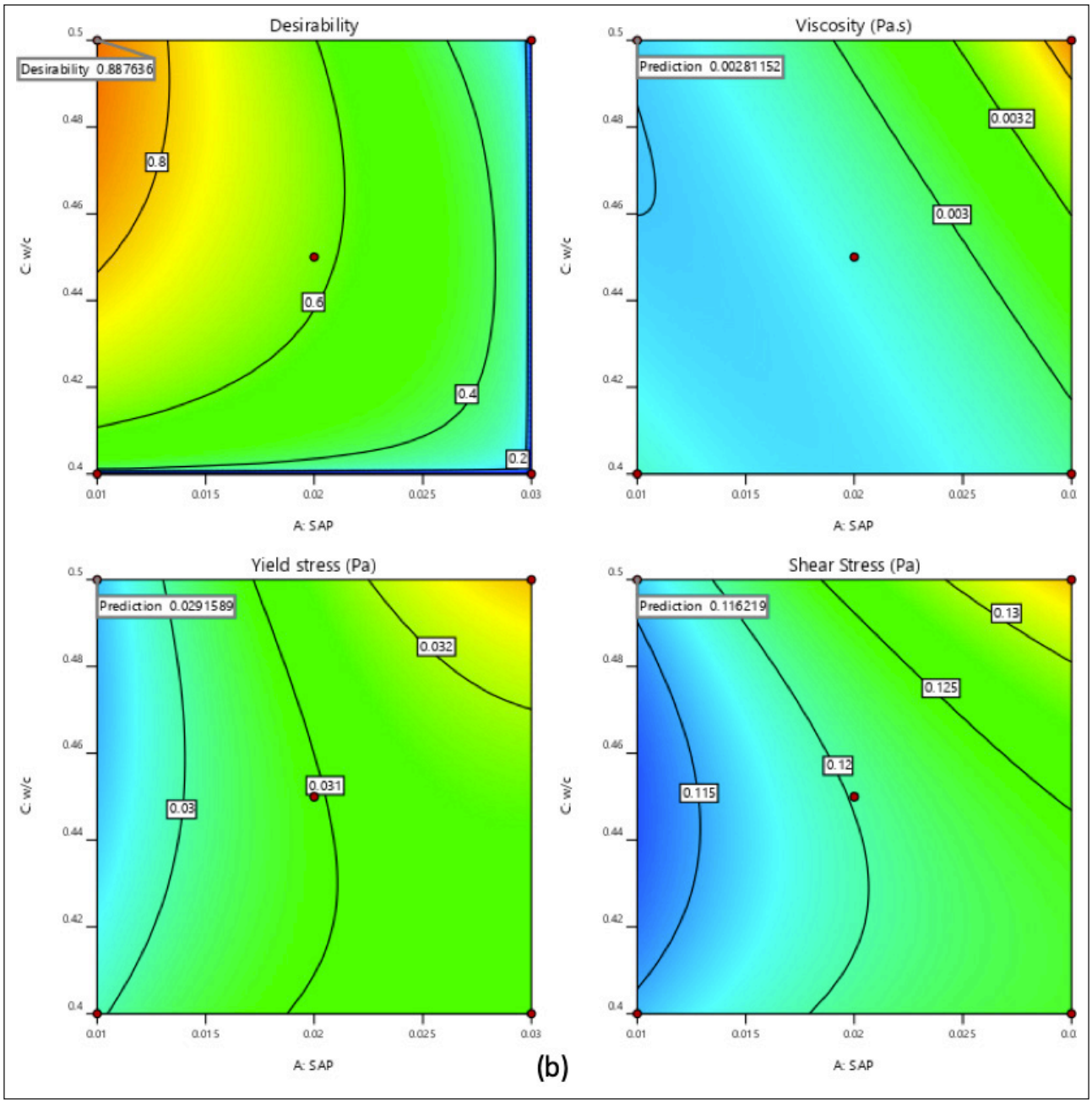

Figure 7. Desirability results: **(a)** rheological properties-BF-SAP, **(b)** rheological properties-SAP-w/c.

ing the rheological properties of cementitious materials. Further research is needed to explore the use of these materials in other cement-based applications, such as concrete and mortar. Additionally, the study focused on the effects of individual mix design parameters on the rheological behavior of the cement paste. Future research could investigate the interactions between multiple mixed design parameters and their combined impact on the material's rheological properties. This would provide a more comprehensive understanding of the factors influencing the rheology of cement-based materials and enable the development of more advanced mix designs that meet specific application requirements. Overall, the study demonstrates the potential of response surface methodology as a valuable tool in optimizing the mix design of cementitious materials for desired rheological behavior.

ETHICS

There are no ethical issues with the publication of this manuscript.

DATA AVAILABILITY STATEMENT

The authors confirm that the data that supports the findings of this study are available within the article. Raw data that support the finding of this study are available from the corresponding author, upon reasonable request.

CONFLICT OF INTEREST

The authors declare that they have no conflict of interest.

FINANCIAL DISCLOSURE

The authors declared that this study has received no financial support.

PEER-REVIEW

Externally peer-reviewed.

REFERENCES

[1] Ma, X., Liu, J., Wu, Z. & Shi, C. (2017) Effects of SAP on the properties and pore structure of high-performance cement-based materials. *Constr Build Mat* 131, 476–484. [CrossRef]

[2] Björnström, J., Martinelli, A., Matic, A., Börjesson, L., & Panas, I. (2004) Accelerating effects of colloidal nano-silica for beneficial calcium–silicate–hydrate formation in cement. *Chem Phys Lett*, 392(1), 242–248. [CrossRef]

[3] Jensen, O. M. & Hansen, P. F. (2001). Water-entrained cement-based materials: I. Principles and theoretical background. *Cem Concr Res*, 31(4), 647–654. [CrossRef]

[4] Kong, D. Y., Du, X., Wei, S., Zhang, H., Yang, Y., & Shah, S. P. (2012). Influence of nano-silica agglomeration on microstructure and properties of the hardened cement-based materials. *Constr Build Mater*, 37, 707–715. [CrossRef]

[5] Lura, P., Jensen, O. M., & van Breugel, K. (2003). Autogenous shrinkage in high-performance cement paste: An evaluation of basic mechanisms. *Cem Concr Res*, 33(2), 223–232. [CrossRef]

[6] Mechtcherine, V., & Reinhardt, H. W. (2012). *Application of superabsorbent polymers (SAP) in concrete construction*. State-of-the-Art Report Prepared by Technical Committee 225-SAP. Springer. [CrossRef]

[7] Mechtcherin, V., Secrieru, E., & Schröfl, C. (2015). Effect of superabsorbent polymers (SAPs) on rheological properties of fresh cement-based mortars – Development of yield stress and plastic viscosity over time. *Cem Concr Res*, 67, 52–65. [CrossRef]

[8] Agostinho, L. B., Alexandre D. C. P., Silva, E. F., & Filho, R. D. T. (2021). Rheological study of Portland cement pastes modified with superabsorbent polymer and nanosilica. *J Build Eng*, 34, 102024. [CrossRef]

[9] Manzano, M. A. R., Fraga, Y. S. B., da Silva, E. F., de Oliveira, R. B., Caicedo Hormaza, B., & Toledo Filho, R. D. (2021). Internal curing water effect of superabsorbent polymer on microstructure of high-performance fine-grained concrete. *ACI Mater J*, 118(5), 125–135. [CrossRef]

[10] Roussel, N. (2006). A thixotropy model for fresh fluid concretes: Theory, validation and applications. *Cem Concr Res*, 36(10), 1797–1806. [CrossRef]

[11] Snoeck, D., Pel, L., & De Belie, N. (2018). Superabsorbent polymers to mitigate plastic drying shrinkage in a cement paste as studied by NMR. *Cem Concr Compos*, 93, 54–62.

[12] Zhang, M.H., & Islam, J. (2012). Use of nano-silica to reduce setting time and increase early strength of concretes with high volumes of fly ash or slag. *Constr Build Mater*, 29, 573–580. [CrossRef]

[13] Bheel, N. (2021). Basalt fibre-reinforced concrete: Review of fresh and mechanical properties. *J Build Rehab*, 6(1), 12. [CrossRef]

[14] Hanafi, M., Aydin, E., & Ekinci, A. (2020). Engineering properties of basalt fiber-reinforced bottom ash cement paste composites. *Mater*, 13(8), 1952. [CrossRef]

[15] Zhou, X., Zeng, Y., Chen, P., Jiao, Z., & Zheng, W. (2021). Mechanical properties of basalt and polypropylene fiber-reinforced alkali-activated slag concrete. *Constr Build Mater*, 269, 121284. [CrossRef]

[16] Sridhar, J., Jegatheeswaran, D., & Gobinath, R. (2022). A DOE (Response Surface Methodology) Approach to predict the strength properties of concrete incorporated with jute and bamboo fibres and silica fumes. *Adv Civ Eng*, 2022, 1150837. [CrossRef]

[17] Luan, C., Zhou, M., Zhou, T., Wang, J., Yuan, L., Zhang, K., Ren, Z., Liu, Y., & Zhou, Z. (2022). Optimizing the design proportion of high-performance concrete via using response surface method. *Iranian J Sci Technol Trans Civ Eng*, 46, 2907–2921. [CrossRef]

[18] Soldatkina, L., & Yanar, M. (2023). Optimization of adsorption parameters for removal of cationic dyes on lignocellulosic agricultural waste modified by citric acid: Central composite design. *Chem Eng*, 7(1), 6. [CrossRef]

[19] Ali, M., Kumar, A., Yvaz, A., & Salah, B. (2023). Central composite design application in the optimization of the effect of pumice stone on lightweight concrete properties using RSM. *Case Stud Constr Mater*, 18, e01958. [CrossRef]

[20] Taşdemir, T., & Taşdemir, A. (2023). Optimization of floc-flotation process in the removal of suspended particles from wastewater in a Jameson cell using central composite design. *J Water Process Eng*, 52, 103552. [CrossRef]

[21] Montes Dorantes, P. N., & Mendez, G. M. (2023). *Non-iterative Wagner-Hagras general type-2 Mamdani singleton fuzzy logic system optimized by central composite design in quality assurance by image processing*. Recent Trends on Type-2 Fuzzy Logic Systems: Theory, Methodology and Applications. Springer. [CrossRef]

[22] Khan, M. Z., Yousuf, R. I., Shoaib, M. H., Ahmed, F. R., Saleem, M. T., Siddiqui, F., & Rizvi, S. A. (2023). A hybrid framework of artificial intelligence-based neural network model (ANN) and central composite design (CCD) in quality by design formulation development of orodispersible moxifloxacin tablets: Physicochemical evaluation, compaction analysis, and its in-silico PBPK modeling. *J Drug Deliv Sci Technol*, 82, 104323. [CrossRef]

[23] Hafez, H. M., Barghash, S. S., Soliman, M. M., Soltan, M. K., Elrahman, M. A., & Katamesh, N. S. (2023). Central composite design driven optimization of sustainable stability indicating HPLC method for the determination of Tigecycline and greenness assessment. *F1000Research*, 12, 341. [CrossRef]

[24] Dilbas, H. (2023). Effect of cement type and water-to-cement ratio on fresh properties of superabsorbent polymer-modified cement paste. *Mater*, 16(7), 2614. [CrossRef]

J Sustain Const Mater Technol, Vol. 9, Issue. 1, pp. 72–83, March 2024

Journal of Sustainable Construction Materials and Technologies
Web page info: https://jscmt.yildiz.edu.tr
DOI: 10.47481/jscmt.1384935

JSCMT
Journal of Sustainable Construction Materials and Technologies

Research Article

Dewatering process for reuse of seabed dredging material and time and cost optimization of the process by value engineering method

Cansu KAYABAŞI AKSU, Şenay ATABAY*

Department of Civil Engineering, Yıldız Technical University, İstanbul, Türkiye

ARTICLE INFO

Article history
Received: 02 November 2023
Revised: 28 November 2023
Accepted: 03 December 2023

Key words:
Dewatering process, geotextile tube, seabed dredging material, time and cost optimization, value engineering

ABSTRACT

The decrease in resources in the world has led people to produce new solutions for the more efficient use of resources and to use various management techniques. One of the techniques used is Value Engineering. Value Engineering strives to increase the value of structures by optimally organizing each component that makes up the structure. Increasing the value of a structure is possible by eliminating all the unnecessary costs in line with specific criteria and by providing the optimal solution between the owner, the user, and the contractor's objectives, that is, the duration, cost, and quality. This study includes the changes the Value Engineering team made to increase the value of the materials extracted from the submarine in a Container Port Terminal project without harming the environment and making them reusable. While expanding the project value, it also aimed to reduce the project duration and cost by considering the sustainability criteria. The original project was to create a clay pool while dewatering, separating the material, filling the loose sand into the reclamation area, and removing the sludge material by sea. With the recommendation of the value engineering team, the dewatering process was transformed into a method of directly pressing the dredged loose sand into the breeding area, filtering the material with geotextile tubes, and removing the material by loading it on the pontoons. With this change in the project, 42% savings were obtained from the cost and 21% from the project duration.

Cite this article as: Kayabaşı Aksu, C., & Atabay, Ş. (2024). Dewatering process for reuse of seabed dredging material and time and cost optimization of the process by value engineering method. *J Sustain Const Mater Technol*, 9(1), 72–83.

1. INTRODUCTION

The perception that the concept of value creates in most people is the price, which is the monetary equivalent of the product. However, value is not a concept that can only be measured by cost and price. The highest value is the value that can safely perform the desired functions at the desired time and place and meet the basic quality requirement with the minimum possible total cost. The true value of a product is only revealed by comparing its quality, cost, or other characteristics with another product that performs the same functions [1]. Value, used in many different ways in many fields, such as philosophy, sociology, and mathematics, has also found a place in engineering. "Value Engineering (VE)" can be defined as a systematic approach to improving projects, processes, services, products, and organizations [2]. According to a different definition of VE, it is by customer requests, functions determined by the value engineering team through in-depth analyses of products and business processes, eliminating unnecessary ones from the process, and concentrating on the functions of utmost importance via the criteria determined by the value engineering team and customers; additionally, using a variety of idea generation techniques, carrying out the work in the form of choosing and implementing the least expensive among the alternatives that can solve the problem in its entirety.

***Corresponding author.**
*E-mail address: satabay@yildiz.edu.tr

Maritime transportation has been essential to the sustainability of the countries' economies worldwide for centuries. With the spread of marine transport, there has been a significant daily increase in ship sizes and maritime traffic. This requires an increase in the size of ports and other marine structures. While building a larger navigational structure, dredging and removing the materials under the sea is necessary. Although most of these materials dredged from the seabed are wanted to be disposed of due to economic, logistical, legal, or environmental factors, it is possible to consider them a vital resource.

The widespread use of maritime transportation in trade makes ports the center of a country's economy [3]. The spread of marine transportation causes an increase in ship traffic and ship sizes. This situation reveals the necessity of dredging in port basins, transportation channels, and maneuvering areas. Dredging is essential for maintaining and developing ports and waterways for maritime transport, reclamation, and flood control [4]. As a result of dredging the channels, large amounts of dredging material are released. While most of this material is currently wanted to be disposed of for reasons related to the economy, logistics, law, or the environment, it can be viewed as a valuable resource. Some areas of use for this material have been defined in the literature. These areas of service are classified into three main categories.

- Engineering Applications: Coastal protection, flood control, coastal embankment, etc.
- Environmental Development Practices: Coastal embankment, creation and development of habitat, conservation of material resources, aquaculture and recreation, use as an agricultural product, etc.
- Manufacturing or Agricultural Products: Concrete material, brick, agricultural soil, etc. [5].

In the study conducted by Karadoğan et al. [6], it is shown that the materials obtained from the seabed dredging activities carried out in Türkiye can be used as filling materials on highways. In their study, Özer Erdoğan and Başar investigated the recovery of seabed dredging material, coal fly ash, and waste-cast sand as light aggregate [7]. There are studies in which the solidification and removal of the seabed dredging material by the dewatering method are applied, and the results are evaluated from various opinions [8-12]. In his study, McCafferty conducted a cost-benefit analysis of the dewatering process using geotextile tubes [13]. In a study by Pu et al. [14], they proposed an integrated method for rapid dewatering and solidification of dredged contaminated deposits with high water content. Noe and Kim proposed the sustainable and beneficial use of dredged materials in the Yangon River in Myanmar [15]. Karadoğan et al. [16] conducted a study on the dewatering of mine wastes with the help of geotextile tubes.

Value engineering has been applied to various construction projects for many purposes, such as increasing value, improving quality, shortening time, reducing cost, increasing project efficiency, and ensuring sustainability [17-22]. Value engineering has also been used to increase the value of marine structures for various purposes. Karkee et al. [23]'s study focused on different design concepts defined and evaluated through interactive collaboration between structural and geotechnical engineering disciplines before selecting design solutions that are ultimately considered for constructing a ferry terminal. Caspe et al. [24] conducted a study in which they benefited from value engineering in the environmental planning project of the Massachusetts Water Resources Authority for the MetroWest water supply tunnel.

This research delves into the application of Value Engineering within a Container Port Terminal project. Specifically, it examines the changes the Value Engineering team implemented to enhance the value of materials extracted from the sea. The primary aim of these changes is to streamline the project, reducing both time and costs. Notably, the modifications are designed to ensure the environmentally safe removal of these materials. The Container Port Terminal project serves as a practical example where the principles of Value Engineering are employed to optimize processes and resource utilization.

2. MATERIALS AND METHODS

2.1. Value Engineering Method

Value engineering seeks to avoid unnecessary costs when creating any product by examining its functions, designing it, creating a production process, organizing and managing the project, and eliminating components that are neither technically necessary nor desired by the customer, which drives up costs. It is a technique that aims to obtain the most valuable solution by analyzing the designs, processes, and specifications that can be obtained at the lowest cost in a way that provides the optimum benefit for the customer, removing the functions that are not needed from the process, as well as adding the necessary ones to the process if necessary [25].

The following is a list of the goals of value engineering, which refers to all of the research done by a multidisciplinary/stakeholder team made up of individuals not on the design team during the project's concept and design phases [26]:

- Providing the necessary functions safely, reliably, efficiently, and at the lowest cost.
- Increasing the value of the project.
- Reducing project completion time by using time effectively.
- Ensuring that the structure has a longer life.
- Eliminate unnecessary costs.
- To use existing materials, human resources, and money effectively and efficiently.
- Improve the quality of the project.
- Ensuring that the structure is more secure.
- Minimizing or even eliminating the mistakes and deficiencies in the project's drawing.
- By analyzing the project processes, removing the functions that do not contain value for the customer from the process, determining the necessary functions, and adding them to the process [27].

- Revealing staff skills with teamwork, creativity, adaptation, and psychological techniques.
- Apart from these, to produce value-based solutions to any problem encountered by using various creativity techniques.

To achieve these goals in Value Engineering, the processes are carried out in a certain systematic way. It is clear which techniques will be applied and the order in which they will be used. All operations are carried out in an application system called "Job Plan."

The concept of "value" expressed in value engineering can be expressed with the following formulas [28]:

Value=Merit/Cost (1)

Value=Customer Satisfaction/Cost (2)

Value=(Initial Impact of User+Benefit from Goods) (Initial Cost+Subsequent Pricing) (3)

Value=Functionality/Cost (4)

Value=Benefit (Function)/Cost (5)

In Value Engineering, the problem must first be clearly defined. Once the problem is identified, a Value Engineering Team is created. If necessary, consultants can also be used, depending on the size of the problem. This team decides what criteria they should consider when solving the problem. In other words, each stakeholder specifies their expectations of the solution. Then, using various methods of generating ideas, it is tried to produce as many alternative solutions as possible in a way that can meet these criteria. These proposed solutions are evaluated in detail regarding their advantages, disadvantages, technical feasibility, and applicability. These evaluations are based on "value" through the abovementioned formulas. As a result, the most valuable alternative ideas that can be a solution are selected and implemented.

2.2. Dewatering and Reuse of Seabed Dredging Material

There are variations in needs and capacity increases due to the growing global population and globalization. Like in every other profession, transportation is one area where these shifting needs are evident. Every day, not only land transportation but also sea transportation evolves and expands. Maritime transportation is the method of moving vast amounts of semi-finished, finished, and raw commodities. In addition to freight transportation, it is also used in passenger transportation, albeit limited. The sea route is preferred when speed is not a factor because it can deliver significant quantities of goods over great distances and has a high degree of reliability while being slow [29]. This increase in the reasons for preference causes an increase in both the size and number of ships. As a result, all these needs also affect marine structures, and building systems large enough to meet the requirements is necessary. Large marine systems require dredging the sea bottoms and excavating and landing the materials there.

In addition, increasing urbanization and industrial activities worldwide bring many environmental problems. One of the most critical problems is the pollution caused by waste sludge with high water content. To solve the pollution of seas and streams, waste sludge is extracted by bottom dredging. Uncontrolled discharge of dredging sludge with high water content obtained due to the dredging activity in the oceans is the most common. It has been reported that this situation harms the marine ecosystem [30]. In Türkiye, bottom sludge has been dredged to clean seas and streams in recent years, and the materials with high water content obtained are stored in predetermined areas or discharged back to the sea [31]. It is of great importance that dredging sludge and waste sludge are dewatered for transportation, storage, and use in functional areas after extraction [32-34]. It will contribute positively to the country's economy and environmental health by applying dewatering effectively quickly and minimizing the harmful chemicals in its content.

The use of geosynthetic and polyacrylamide in the dewatering of waste materials with high water content is seen by researchers as an effective and economical option [35-37]. Geotextile tubes are tubular elements formed by assembling and sewing geotextile rolls and have the strength to hold relatively large amounts of water-saturated material. Geotextile tubes are porous, and when filled with a water-saturated material or slurry, the solid part is retained, and the water is filtered out of the pores of the geotextile, forming the tube [38].

Dewatering seabed dredging material is critical for environmental preservation and sustainability. It is essential to carefully consider both the application of the method and the subsequent evaluation of the materials obtained. In addition to all these, of course, the method to be chosen should also be economical, provided that it meets specific criteria. This study includes the changes the Value Engineering team made to increase the value of the materials extracted from the submarine in a Container Port Terminal project without harming the environment and making them reusable. By considering sustainability principles and ensuring that the activities to be carried out do not negatively impact the environment, the goal is to increase the project value while reducing its duration and cost.

2.3. Time And Cost Optimization of Dewatering Process in Container Port Terminal Project Using Value Engineering Method

In this study, the value engineering studies for the time and cost optimization of the Yarımca Container Terminal Project, which was built in the Gulf of Izmit, and the dewatering project of the seabed dredging material were analyzed, and Kayabaşı Aksu [39] explained this study in detail in her master's thesis.

The project was built on an old porcelain factory site, 20 km from Izmit and 80 km from Istanbul. In addition, the project is adjacent to Tüpraş, Türkiye's largest refinery. The total construction area is 504,883 m^2 and consists of 212,718 m^2 of land, 257,165 m^2 of sea (to be rehabilitated), and 35,000 m^2 of previously rehabilitated areas.

Project: Separation of silt for re-filling the material dredged from the sea.

Original Idea: Creating a clay pond, separating the material, filling the loose sand into the reclamation area, and removing the sludge material by sea.

Value Engineering Recommendation: Pressing the dredged loose sand directly into the breeding area, filtering the material with geotextile tubes, and removing the material by loading it on the pontoons.

2.3.1. Methodology

In project management, the anticipated and forecasted durations of activities often experience extensions, mainly when dealing with critical path activities. Such extensions can subsequently impact the overall project completion time. Beyond duration challenges, there are instances where the allocated budget for specific activities proves inadequate for their successful execution. To address these issues and ensure both timeline adherence and budgetary compliance, the application of the value engineering method emerges as a highly suitable solution. This approach allows for strategic modifications to the project to prevent delays and maintain financial constraints within the defined budget limits.

One of the essential activities to be carried out in the Yarımca Container Terminal Project, which is being built in Izmit Bay, is the dredging and deepening the seabed to increase the port capacity. Along with the issue of where and how the material obtained from dredging the seabed will be utilized, it is also essential to determine how long and how costly this process will be carried out. In this project, time and cost plans were made for each activity before the construction started and then the construction started.

In the original project prepared for the separation of the silt to use the material dredged from the sea in filling again, there was the idea of "creating a clay pool, separating the material, filling the loose sand into the breeding area, and removing the sludge material by sea." This idea made the time plan for the container port terminal project. It was observed that the initially anticipated budget and the originally scheduled time for silt separation had been exceeded one month after this method began to be implemented to solve the silt separation problem. It has been established that the silt separation activity is one of the crucial tasks in the container port terminal project, so extending its duration will also lengthen the project's overall duration. When there was a need to implement a different method to reduce the project's cost and shorten the time, a value engineering team was formed, and this team started to produce new ideas to achieve the specified goals. Among these ideas, "Pressing the dredged loose sand directly into the breeding area, filtering the material with geotextile tubes, loading the barges and removing the material" was chosen as the most appropriate method and decided to be applied.

In this project, when it was foreseen that the total project completion time and the total budget would be exceeded one month after the start of construction, it was decided to conduct a value engineering study for the activity "separation of silt in the dredged material from the sea and reuse or removal of the material obtained" on the critical path. For this purpose, the first thing to be done to apply the value engineering method is to decide which professional group should work together to realize the relevant activity. Value engineering can only be done with a team of stakeholders who can find the most optimum solution according to the applicable criteria to produce an appropriate solution to the relevant problem. In this study, for this purpose, a team of people from many professional groups who can make cost and time planning, who have developed themselves in the selection of materials that will not harm the environment and can be used in the solution of the problem, and who can produce ideas were formed and a time was set for this team to work. They were asked to produce as many ideas as possible. The aim expected from the solution is to produce ideas that can be used for recycling the materials extracted from the seabed without harming the environment as much as possible and to obtain a solution with a lower cost and duration than the original project. Among the suitable solution ideas produced during this period, with the help of various selection processes, the idea of "Pressing the dredged loose sand directly to the reclamation area, filtering the material with geotextile tubes, removing the material by loading it on pontoons" was determined as the most suitable solution and it was decided to implement it.

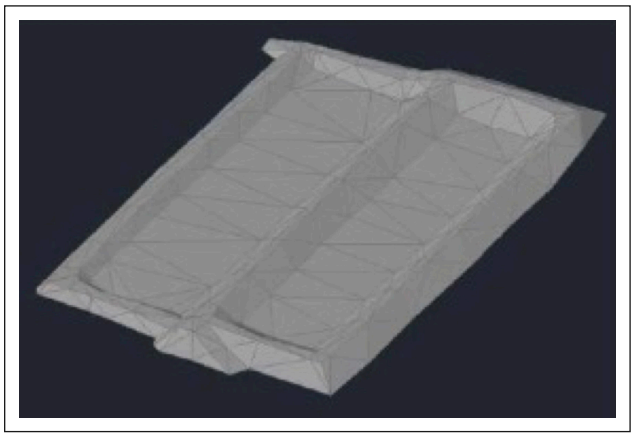

Figure 1. 3D view of the pools.

2.3.2. Analysis of the Original Design

By dredging the loose sand at a depth of 2-3 m on the surface of the sea area where the breeding area filling will be made;

- No soil improvement is needed in most of the reclamation areas.
- With the sand obtained from the dredge, the area created as the second area was filled, and thus, the dredged sand did not need to be removed and used in the filling by bringing materials from the outside.

Before the dredging activities started, two temporary pools were constructed on the Izmit side of the sea area. The purpose of making these pools is to take the silty material under the reclamation area before "Reclamation Area 2" is made and to minimize the possible settling of the reclamation area in the future. Thanks to these two pools, separating the dredged material and using the sand and gravel materials in the filling as recycling is planned.

The largest of the two pools to be created is 35,000 m^3, and the smallest has a capacity of 20,000 m^3 (Fig. 1).

Figure 2. Overview of application 1.

Before the construction of the small pool was completed, 12 pipes were placed at three different elevations to provide a connection between the two pools. The upper width of the area, which is 620 m in length, was manufactured as 7 meters. The total material dredged from the floor of this area was 35888 m^3. An overview of Application 1 can be seen in Figure 2.

It has been calculated that the material accumulated in the temporary pool was 6137 m^3 waste silt. Due to the mud consistency of the material, the material that could not be sent to the dump site was mixed with the excavation from another area in the project, and some of it was sent to the dump site. However, 138.95 tons of unquenched limestone were thrown into the material with high viscosity to reduce this rate and placed on hold. The leftover lime dried the material in the pool. It wasn't, however, sent to casting just yet. The channels for drying and resting the material were opened due to its high fluidity. The collected water was then released from the surface. After blending the slime silt that was still within with the reclamation area material again, it was made dense enough to be hauled by trucks using material gathered from nearby excavations and then transferred to the excavation. The embankment between the two pools was demolished, channels were opened in the pool, and the accumulated water was discharged. The delivery of the material, whose fluidity decreased with the effect of the season, took 132 days.

The materials, equipment, and manpower used in the dismantling stages of the temporary reclamation area are as follows (h: hour) (Table 1):

2.3.3. Cost Analysis of Original Design

The costs for separating the sludge material by creating a 55,000.00 m^3 clay pond and removing it by sea are given in Table 2. While calculating the total costs of the workers and machines in the tables, it is accepted that they work 8 hours a day, and subcontractor costs are given in lump sums.

Table 1. Materials, equipment, and labor used in the dismantling of the temporary reclamation area

Source	Quantity	Type
Tipper truck	894,48 h	Machine
Hyundai 290 excavator	637,44 h	Machine
Volvo 290 excavator	497,60 h	Machine
Hidromek 370 excavator	554.00 h	Machine
Short-sleeved JCB	162,00 h	Machine
Long-sleeved JCB	150,00 h	Machine
Disposal on land	46418,63 m^3	Transporting
Operator	150,00 h	Employee
Hitachi excavator	22,00 h	Machine
CAT 330 excavator	105,04 h	Machine
CAT 96F loader	28,08 h	Machine

The cost of transferring the separated loose sand to the reclamation area is given in Table 3.

The cost of pressing the sludge material into the clay pool with a pump, drying the pool with lime, and transporting it to the dumping site by sea is given in Table 4.

The total cost summary of Application 1 is given in Table 5.

2.4. Analysis of Value Engineering Proposal

The value engineering team proposed several changes to the original project to reduce the cost and duration of the project. It was decided that the suggestion of "pressing the dredged loose sand directly into the breeding area, filtering the material dredged under the sea with a geotextile tube, and removing it by loading it on the pontoons" was the most appropriate among these solutions. The silt within must be removed and returned to the seabed without endangering the environment for components like sand and gravel from the material taken from the seabed to be utilized once more

Table 2. The clay pool cost of Application 1

Resource name	Type	Quantity	Unit	Unit price ($/h)	Total price ($)
Plain worker	Workmanship	57	Day	2.8	1276.8
Foreman	Craft	19	Day	10,2	1550.4
Hitachi rental excavator	Machine	5,84	Day	44.54	2080,91
Hitachi rental excavator diesel	Machine	5,84	Day	33.13	1547,83
CAT 330 excavator rent and diesel	Machine	7.19	Day	118	6787,36
Dozer D7 rent	Machine	4,94	Day	28,35	1120,39
Dump truck rent	Machine	30	Day	23	5520
Filling of suitable material	Sub-contractor	39370,67	m^3	2	78741,34
Excavation of suitable material	Sub-contractor	39370,67	m^3	2.3	90552,54
CAT 533 cylinder rent and diesel	Machine	1	Day	56.6	452,80
Total					**193085,83**

Table 3. Cost of transferring loose sand to the reclamation area in Exercise 1

Resource name	Type	Quantity	Unit	Unit price ($)	Total price ($)
Master	Workmanship	389,24	Day	10.2/h	31761,98
Operator	Workmanship	778,48	Day	3.5/h	21797,44
Hidromek 370 excavator rental	Machine	170,95	Day	52/h	71115,20
Hidromek 370 excavator diesel	Machine	170,95	Day	69,61 /h	95198,64
CAT 330 excavator	Machine	104,36	Day	118 /h	98514,33
JCB loader 467 ZX depreciation	Machine	2.95	m^3	17 /m^3	50,08
JCB loader 467 ZX oil	Machine	2.95	Day	31,37 /h	739,23
Dozer-D6 rent	Machine	63.44	Day	28,35 /h	14387,19
Dozer-D6 oil	Machine	63.44	Day	42.80 /h	21720,35
Total					**355284,44**

in areas that require filling and in port development. Thus, while increasing the sea depth where the port will be built by removing material from the seabed, the material extracted from it will be used again in the areas where it is needed. The silt in the material extracted from the sea will be separated from other materials, poured back into the sea, and disposed of without harming the environment.

Figure 3 shows the preparations made so that the slurry material accumulated in the part indicated by the red line can be dewatered and thrown out. The parts shown with white arrows show the drilling work carried out.

To clean the sludge pool, the materials (toyo pump, 10" and 6" hose, trailer, mineral, polymer, and sludge tubes) required for the dewatering process recommended by the value engineering team were brought to the site. The sequence of operations of the dewatering method was as follows:

- Pulling the sludge from the pool with the toyo pump
- Transferring the sludge to the trailer with the help of 10" and 6" hoses
- Mixing sludge with minerals and polymers in trailers
- Transferring the mixture to geotextile tubes with 6" hoses
- Filtration of water separated from the sludge precipitated in the tubes
- Removing the sludge from the site by opening the tubes

The materials brought to the site to clean the sludge pool were prepared for dewatering. As the first process step, the material was withdrawn from the pool at a flow rate of 350 m^3/h with the help of a 110 kW toyo pump crane. For the removed material to provide the desired decomposition, the content of the material must be 90% water and 10% solid (clay and silt). This ratio was obtained as a result of tests performed in the laboratory. To adjust this ratio during material pulling with the pump, the crane operator has a monitor showing the amount and ratio of material pulled. Thanks to this dredge, the operator has achieved the desired ratio by moving the pump up and down in the water. The material pulled in the desired proportions was transferred to the trailer with 10" and 6" hoses. Tests were performed in the laboratory to remove water from the sludge and allow the solid material to precipitate. As a result of these tests, two different materials were determined as minerals and polymers that provide optimum decomposition. The

Table 4. In Application 1, the cost of pressing the sludge material into the clay pool and transporting the lime to the marine dumping area

Resource name	Type	Quantity	Unit	Unit price ($)	Total price ($)
Dump truck rental	Machine	93,92	Day	23/h	17281,35
Hyundai 290 excavator rental	Machine	66.93	Day	37/h	19811,64
Volvo 290 excavator rental	Machine	52,25	Day	37/h	15465,41
Hidromek 370 excavator rental	Machine	58,17	Day	52/h	24198,72
JCB short-sleeve excavator depreciation	Machine	17,01	Day	20/h	2721,60
JCB long-sleeve excavator depreciation	Machine	15,75	Day	20/h	2520
Disposal on land	Machine	39370,67	m^3	11,14/m^3	438589,26
Operator	Workmanship	32.76	Day	3.5/h	917,28
Dump truck diesel	Machine	93,92	Day	7,35/h	5522,52
Hyundai 290 excavator diesel	Machine	66.93	Day	44.54/h	23848,93
Volvo 290 excavator diesel	Machine	52,25	Day	33,13/h	13847,81
Hidromek 370 excavator diesel	Machine	58,17	Day	69,61/h	32393,71
JCB short arm excavator diesel	Machine	17,01	Day	50,82/h	6915,59
JCB long-arm excavator diesel	Machine	15,75	Day	51.47/h	6485,22
Hitachi excavator rental	Machine	2,31	Day	44.54/h	823.1
Hitachi excavator diesel	Machine	2,31	Day	33,13/h	612,24
CAT 330 excavator rent and diesel	Machine	11,03	Day	118/h	10411,56
Mud pump	Machine	56	Day	36.12/h	16181,76
Quicklime	Machine	627,52	Day	59,10/h	37086,43
CAT 966F loader rent and diesel	Machine	2.95	Day	76.39/h	1801,83
Transportation to the marine dumping area	Transporting	28000	Hour	5,69/h	159320
Total					**836755,96**

Table 5. Total cost of application 1

	Cost ($)
Cost of the clay pond	193085,83
The cost of pressing the sludge material into the clay pool and transporting the lime to the marine dumping area	836755,96
Cost of transferring loose sand to the reclamation area	355284,44
Total	**1385126,23**

formation of flocculation in the material transferred to the trailer was constantly controlled, and the mineral ratio used accordingly was adjusted between 2 and 4 kg/ton DS (Solid Matter). In addition, 0.5 to 1 kg/ton of polymer was used.

A sample assembly was installed in the system to control the flocculation results instantly. This system consists of one transparent tube and two valves (Fig. 4). The valve under the transparent tube is opened to see the mixture coming from the trailer, and the material is taken into the transparent tube. If the desired flocculation is achieved, the solid material collapses to the bottom of the transparent tube in small lumps while the water decomposes on the collapsed solid. To see this separation again, the process can be repeated by emptying the tube from the valve on the transparent tube.

Geotextile sludge tubes coming to the site in rolls are rolled and laid to the places determined by the length of the supply hoses coming out of the trailer with manpower. When the material is pressed into the laid tubes, the tubes are tied with rope from the binding ears on the tube to the vaults until the tubes reach a certain height to prevent the tubes from tilting to the right and left while displacing and inflating. There are four filling chimneys on each sludge tube. These chimneys have a diameter of 0.3 m and a length of 1.0 m. The supply pipe is fixed to one of the filling chimneys with a suitable belt. The treated slurry was filled into the tube utilizing 6" supply hoses using these chimneys. From the moment the material is pressed into the tubes, the solid (clay, silt) settles at the bottom of the tube in the flocculated material, while the water remaining on the surface drains out of the sludge tubes designed to provide filtration. Drainage channels with a width of 60 cm and a depth of 50 cm were opened around the sludge tubes to prevent the drained water from dispersing into the field. The channels are surrounded by a safety strip so that the opened channels do not cause any accidents. With these channels, water discharge is controlled without dispersing to the site.

Figure 3. Reclamation area ground improvement – overview.

Figure 4. Flocculation instantaneous control.

Given that the volume of solids in the tubes rose once they reached a height of one meter, compaction was performed on the sludge tubes with a compactor to prevent the clogging of the pores where the sludge filtering took place and to ensure better water drainage. The filling and compaction process of the tubes was continued until the maximum height reached 2.10 m. When the height of the sludge tube reached the maximum level, the process of pressing material into the tubes was terminated, and the tubes were left to wait for 10 days for final filtration. During the final waiting period, samples were taken daily from the filling chimneys in the tubes and checked. When the samples taken at the end of 10 days were examined, it was seen that the material in the tubes was suitable for transportation. When the tubes became suitable for transportation, they were cut and opened, controlled with a snap blade. The removal of the resulting material from the site took place in 4 stages:

- Loading the material into the truck with an excavator
- Unloading into the loading pond by trucks
- Uploading from the upload pool to split dump barge
- Discharging by ship to the previously designated site

After the tubes were opened, 600 m^3 of material came out of each tube. The material coming out of the tubes was loaded into the trucks with the help of an excavator. The trucks unloaded the material into the loading pond. From here, it was loaded onto the split dump barge with a long boom excavator. Each sludge tube fills a split dump barge. When the loading of the split dump barges was completed, the ship went to the discharge site and discharged the material, and thus, the dewatered silt material was safely removed from the site.

Table 6. Cost of application 2

Resource name	Type	Quantity	Unit price	Total price ($)
Dump truck rental	Workmanship	98,08	23/h	18046,72
JCB short-sleeve excavator depreciation	Workmanship	49,04	20/h	7846.4
Hitachi Zaxis Long arm excavator	Machine	49,04	35,83/h	14056,83
Destruction at sea	Transporting	28000	5,69/h	159320
Geotextile subcontractor cost	Sub-contractor	1	550000/ls	550000
Operator	Workmanship	98,08	3.5/h	2746,24
Dump truck diesel	Machine	98,08	7,35/h	5767.1
JCB short arm excavator diesel	Machine	49,04	50,82/h	19937.7
Hitachi Zaxis Long arm excavator	Machine	49,04	49,36/h	19364,92
Mud pump	Machine	68,66	36.12/h	19838,84
Total				**816924,75**

Figure 5. Completed Yarımca container terminal project.

Since geotextile dewatering tubes are "disposable" materials, the remaining tube residues were disposed of according to local regulations after the processed sludge was transported in a way that would not pollute the environment.

2.4.1. Cost Analysis of Exercise 2

As a result of the change proposed by the value engineering team in the project, the cost of the application stages of the method of dewatering and separating the sludge material with geotextile tubes and removing the material by sea is given in Table 6 (ls: Lump Sum).

The completed version of the Yarımca Container Terminal Project can be seen in Figure 5.

3. RESULTS

The benefits/results obtained as a result of the applications in the projects proposed by the original and value engineering team are shown below:

The cost impact of:

- The total cost in Application 1 is 1,385,126.23 USD,
- The total cost of Application 2 is 816,924.75 USD,

The total cost difference between the two applications was calculated as 568,201.48 USD. Hence, 42% savings were made in terms of cost.

Time effect:

- In Application 1, creating a clay pool, separating the material, filling the loose sand into the reclamation area, and removing the sludge material by sea were calculated as a total of 451 working days.
- In Application 2, it was planned to press the dredged loose sand directly into the breeding area, filter it with geotextile material, load it on the pontoons, and remove the material for 359 days.

The time difference between the two applications was 92 days. 21% savings were made in terms of time.

Sustainability impact:

- With this application, the material dredged from the seabed was cleaned from silts and used in backfilling and other necessary construction activities at the port in the project.

4. CONCLUSION

Because shipping is one of the most significant ways to move vast quantities of semi-finished, finished, and raw goods, both the size and number of ships in use have grown, necessitating the construction of marine buildings that are big enough to satisfy demand. Dredging the seabed and excavating and landing materials are additional requirements for large marine buildings.

In this study, one of the stages of the Yarımca Container Terminal Project built in the Gulf of İzmit, the studies carried out to separate the silt for refilling the material dredged from the sea were examined. The value engineering studies carried out for the time and cost optimization of the dewatering project of the seabed dredging material were explained. During the port construction process, after the material is extracted from the sea, these materials must be separated and removed from the area for reuse without harming the environment. In this project, the idea was "creating a clay pool, separating the material, filling the loose sand into the reclamation area, and removing the sludge material by sea" during the project's design phase to separate the silt existing in the extracted materials. The time and budget planning of the project were also based on this idea. One month after the implementation of this idea, it was understood that the initially estimated budget and time limits were exceeded, and the total project duration was prolonged since the activity containing this idea was also critical. Therefore, in this process, a value engineering study has been carried out on the project, and the need to shorten the cost and duration has become indispensable.

As a result of their work, the value engineering team concluded that the idea of "pressing the dredged loose sand directly into the breeding area, filtering the material with geotextile tubes, and removing the material by loading it on the pontoons" is an appropriate method to both reduce the cost and shorten the time within the framework of sustainability principles without harming the environment. With this method, it was ensured that the elements such as sand and gravel in the material extracted from the seabed were separated from the silt to be used again in places where filling is needed and in port construction, and this silt was transported to the seabed again without harming the environment. Thus, while increasing the sea depth in the area where the port will be built by removing material from the seabed, the material extracted from the seabed was used again where it was needed. The silt extracted from the sea was separated from other materials, poured back into the sea, and disposed of without harming the environment.

Although not implemented in this project, silt material, which is subjected to dewatering by means of geotextile tubes in similar project applications, can be evaluated in the cosmetics sector according to its content by performing the necessary tests (silt can be used in the production of various cosmetic products, including creams, lotions, gels, make-up materials, and other).

ETHICS

There are no ethical issues with the publication of this manuscript.

DATA AVAILABILITY STATEMENT

The authors confirm that the data that supports the findings of this study are available within the article. Raw data that support the finding of this study are available from the corresponding author, upon reasonable request.

CONFLICT OF INTEREST

The authors declare that they have no conflict of interest.

FINANCIAL DISCLOSURE

The authors declared that this study has received no financial support.

PEER-REVIEW

Externally peer-reviewed.

REFERENCES

[1] Atabay, Ş. (2023). Value Engineering in construction projects. In Cengiz, M. S., & Ozkaya, U. (Eds.), *Küreselleşen Dünyada Mühendislik ve Mimarlık* (pp. 107–139). Duvar Yayınları.

[2] SAVE International. (2023). About the value methodology. https://www.value-eng.org/page/About-VM

[3] European Environment Agency. (2023). *News: EU maritime transport*. https://www.eea.europa.eu/highlights/eu-maritime-transport-first-environmental

[4] International Association of Dredging Companies (IADC). (2023). The importance of dredging. https://www.iadc-dredging.com/subject/what-is-dredging/the-importance-of-dredging/

[5] Demirbaş, N. (2016). *Assessment and beneficial use of the material from seabed dredging operations* [Master's thesis, Istanbul Technical University].

[6] Karadoğan, Ü., Çevikbilen, G., & Teymür, B. (2020). Use of dredge materials as road embankment. *Uludağ Univ J Fac Eng, 25*(2), 1059–1070. [CrossRef]

[7] Özer Erdoğan, P. & Başar, H. M. (2019). Recycling of marine dredged materials, coal fly ash and waste foundry sand as lightweight aggregates. *J Fac Eng Archit Gazi Univ, 34*(3), 1377–1394.

[8] Karadoğan Ü., Korkut, S., Çevikbilen, G., Teymur, B., & Koyuncu, İ. (2021). Evaluation of beneficial of polyacrylamide use dewatering of dredged sludge obtained from Golden Horn. *Mar Georesour Geotechnol, 39*(8), 919–928. [CrossRef]

[9] Cao, B., Zhang, T., Zhang, W., & Wang, D. (2021). Enhanced technology based for sewage sludge deep dewatering: A critical review. *Water Res, 189*, 1–19. [CrossRef]

[10] Karadoğan, Ü., Çevikbilen, G., Korkut, S., Pasaoglu, M. E., & Teymur, B. (2022). Dewatering of Golden Horn sludge with geotextile tube and determination of optimum operating conditions: A novel approach. *Mar Georesour Geotechnol, 40*(7), 782–794. [CrossRef]

[11] Zhang, H., Sun, H. L., Liu, S. J., Chu, J., Shi, L., Geng, X. Y., Deng, Y., & Cai, Y. Q. (2023). Large-strain consolidation of sludge in multiple-drainage geotextile tubes. *J Geotech Geoenviron Eng, 149*(6), 04023037. [CrossRef]

[12] Li, C., Song, Z., Zhang, W., Li, L., Liao, G., & Wang, D. (2022). Impact of hydroxyl aluminum speciation on dewaterability and pollutants release of dredged sludge using polymeric aluminum chloride. *J Water Process Eng, 49*, 103051. [CrossRef]

[13] McCafferty, C. M. (2021). A cost-benefit analysis for geotextile tube dewatering with and without a spacer product [Doctoral Thesis, Drexel University].

[14] Pu, H., Mastoi, A. K., Chen, X., Song, D., Qiu, J., & Yang, P. (2021). An integrated method for the rapid dewatering and solidification/stabilization of dredged contaminated sediment with a high water content. *Front Environ Sci Eng, 15*, 1–12. [CrossRef]

[15] Noe, K. M., & Kim, K. (2020). Preliminary framework for sustainable beneficial use of dredged materials in Yangon River, Myanmar. *J Water Chem Technol, 42*, 514–521. [CrossRef]

[16] Karadoğan, Ü., Çevikbilen, G., Korkut, S., & Teymur, B. (2022). Dewatering of mine waste using geotextile tubes. *Min Metall Explor, 39*(6), 2477–2490. [CrossRef]

[17] Atabay, Ş. (2021). Value engineering for the selection of the filler material between shoring wall and the structure. *Tehnički vjesnik, 28*(6), 2164–2172. [CrossRef]

[18] Albarbary, M. M., Tahwia, A. M., & Elmasoudi, I. (2023). Integration between sustainability and value engineering in the production of eco-friendly concrete. *Sustainability, 15*(4), 3565. [CrossRef]

[19] Taher, A. H., & Elbeltagi, E. E. (2023). Integrating building information modeling with value engineering to facilitate the selection of building design alternatives considering sustainability. *Int J Constr Manag, 23*(11), 1886–1901. [CrossRef]

[20] Gunarathne, A. S., Zainudeen, N., Perera, C. S. R., & Perera, B. A. K. S. (2022). A framework of an integrated sustainability and value engineering concepts for construction projects. *Int J Constr Manag, 22*(11), 2178–2190. [CrossRef]

[21] Alsanabani, N. M., Al-Gahtani, K. S., Bin Mahmoud, A. A., & Aljadhai, S. I. (2023). Integrated methods for selecting construction foundation type based on using a value engineering principle. *Sustainability, 15*(11), 8547. [CrossRef]

[22] Atabay, Ş. (2023). Determination of exterior material in sustainable buildings by value engineering method according to LEED criteria. *J Sustain Constr Mater Technol, 8*(1), 1–11. [CrossRef]

[23] Karkee, M. B., Horvitz, G. E., Chamberlain, M. B., Gastineau, A. J., Bennett, A. K., & Mooney, T. (2022). Geotechnical and structural adaptations for the seismic design of a new ferry terminal in Washington. *Ports, 2022*, 848–858. [CrossRef]

[24] Caspe, H. P., Kim, A. Y., Bergen, L. J., & Araujo, J. R. (1994). *Environmental planning for the Massachusetts Water Resources Authority's MetroWest water supply tunnel*. In Tunnelling '94. Springer, Boston, MA. [CrossRef]

[25] Gupta, V. K. (2009). Flexible strategic framework for managing forces of continuity and change in value engineering processes: Study in Indian context. *Glob J Flex Syst Manag, 10*(4), 55–65. [CrossRef]

[26] U.S. Department of Transportation Federal Highway Administration. (2017, June 27). *The value engineering (VE) process and job plan*. https://www.fhwa.dot.gov/ve/veproc.cfm

[27] Kazanç, D. (2000). *Value engineering in construction* [Master's thesis, Istanbul Technical University].

[28] Fowler, T. C. (1990). *Value analysis design (Competitive manufacturing series)*. John Wiley & Sons, USA.

[29] Deniz, T. (2016). Türkiye'de ulaşım sektöründe yaşanan değişimler ve mevcut durum. *Doğu Coğrafya Derg, 21*(36), 135–156. [CrossRef]

[30] Sheehan, C., & Harrington, J. J. W. M. (2012). Management of dredge material in the Republic of Ireland - a review. *Waste Manag, 32*(5), 1031–1044. [CrossRef]

[31] Çevikbilen, G., Başar, H. M., Karadoğan, Ü., Teymur, B., Dağlı, S., & Tolun, L. (2020). Assessment of the use of dredged marine materials in sanitary landfills: A case study from the Marmara sea. *Waste Manag, 113*, 70–79. [CrossRef]

[32] Moo-Young, H. K., Gaffney, D. A., & Mo, X. (2002). Testing procedures to assess the viability of dewater-

ing with geotextile tubes. *Geotext Geomembr, 20*(5), 289–303. [CrossRef]

[33] Liao, K., & Bhatia, S. K. (2005). *Geotextile tube: Filtration performance of woven geotextiles under pressure*. Proceedings of NAGS 2005/GRI – 19 Cooperative Conference, Las Vegas, NV, USA.

[34] Lawson, C. R. (2008). Geotextile containment for hydraulic and environmental engineering. *Geosynth Int, 15*(6), 384–427. [CrossRef]

[35] Ratnayesuraj, C. R., & Bhatia, S. K. (2018). Testing and analytical modeling of two-dimensional geotextile tube dewatering process. *Geosynth Int, 25*(2), 132–149. [CrossRef]

[36] Müller, M., & Vidal, D. (2019). Comparison between open and closed system for dewatering with geotextile: Field and comparative study. *Int J Civ Environ Eng, 13*, 634–639.

[37] Aparicio Ardila, M. A., Souza, S. T. D., Silva, J. L. D., Valentin, C. A., & Dantas, A. D. B. (2020). Geotextile tube dewatering performance assessment: An experimental study of sludge dewatering generated at a water treatment plant. *Sustainability, 12*(19), 8129. [CrossRef]

[38] E Silva, R. A., Negri, R. G., & de Mattos Vidal, D. (2019). A new image-based technique for measuring pore size distribution of nonwoven geotextiles. *Geosynth Int, 26*(3), 261–272. [CrossRef]

[39] Kayabaşı Aksu C. (2019). *Research on value engineering with applications in marineconstruction* [Master's thesis, Yildiz Technical University].

J Sustain Const Mater Technol, Vol. 9, Issue. 1, pp. 84–92, March 2024

Journal of Sustainable Construction Materials and Technologies
Web page info: https://jscmt.yildiz.edu.tr
DOI: 10.47481/jscmt.1166150

JSCMT
Journal of Sustainable Construction Materials and Technologies

Case Report

A comparative evaluation of the mechanical properties of PET and polystyrene modified asphaltic concrete containing rice husk ash filler

Desmond E. EWA*, Joseph O. UKPATA, Anderson A. ETIKA, Enang A. EGBE, Alorye O. IDUKU

Department of Civil Engineering, Cross River University of Technology, Calabar, Nigeria

ARTICLE INFO

Article history
Received: 24 August 2022
Revised: 27 November 2023
Accepted: 21 January 2024

Key words:
Asphalt, binder, Marshall stability, PET, polystyrene

ABSTRACT

The study evaluated and compared the influence of bitumen modification for sustainable asphalt using waste plastic (Polyethylene Terephthalate, PET) and waste Polystyrene (PS) at 5–50% modification levels. Rice husk ash (RHA) and desilted sand were used as filler and fine aggregate with crushed granite as coarse aggregate. Tests conducted include; penetration, viscosity, flash point, fire point, specific gravity, ductility and marshal stability test on asphalt. For PET modified-binder a decrease in penetration and ductility was observed while the specific gravity, viscosity, flash and fire points of the binder increased. For the PS modified-binder, the penetration, ductility, viscosity and specific gravity decreased with an increase in PS while the flash and fire point increased. Marshall Stability results showed an optimal of 20% PET modification was adequate for medium traffic surfaing with stability, flow, density, air void, void in mineral aggregates (VMA), and Void filled with binder (VFB) of 4875N, 3.53 mm, 2.460 g/cm^3, 3.30%, 18.20%, and 81.87% respectively. For 10% PS modification content, the stability, flow, density, air void, void in mineral aggregates (VMA), and Void filled with binder (VFB) were found to be 6825N, 3.33 mm, 2.362 g/cm^3, 4.52%, 18.21%, and 75.18% respectively which was found to be adequate for heavy traffic surfacing. Hence, it was concluded that the investigated waste plastics could be used in Asphalt pavement courses. If applied, these results could provide low-cost materials for paving roads while also reducing waste-related pollution and environmental issues.

Cite this article as: Ewa, D. E., Ukpata, J. O., Etika, A. A., Egbe, E. A., & Iduku, A. O. (2024). A comparative evaluation of the mechanical properties of PET and polystyrene modified asphaltic concrete containing rice husk ash filler. *J Sustain Const Mater Technol*, 9(1), 84–92.

1. INTRODUCTION

The world has avoided paying close attention to the consequences of rapid increases in plastic consumption for decades. As a result, the ecosystem has been inundated by unprecedented amounts of uncontrolled mixed plastic waste. Plastics used in packaging make up nearly half of all plastic waste globally Nchube et al. [1]. Plastic is a waste stream with recycling and recovery potential, Babayemi et al. [2], however, the recycling rates for plastic in African countries are low. Furthermore, use and production of virgin plastics are increasing. Therefore, a high proportion of plastic waste is being disposed of in landfills and dumpsites. Plastic serves as fuel for open burning at landfills/dumpsites with associated releases and constitutes a large fraction of marine litter, making it a major and growing global pollution concern.

Plastics consumption increased globally from about 330 million tons in 2016 to over 367 million tons in 2020 [3], these figures have increased over the past years. Combating the threat of plastic trash pollution has turned into a global en-

*Corresponding author.
*E-mail address: desmondewa@crutech.edu.ng

vironmental issue. Plastic pollution has the potential to harm land, waterways, and oceans since a vast number of marine and land organisms have died as a result of plastic's non-biodegradability and soil danger. Plastic wastes are also hazardous to human health since they may contain toxic acids that can cause death Kehinde et al. [4]. It is not uncommon to encounter haze and poor air quality because of the burning of solid wastes (mostly plastic products) as a waste management method. It has been found that the emissions of CO_2 from incinerators are higher than those for coal, oil, or gas-propelled power plants. Incinerators produce 210 different types of toxic compounds, including mercury, fluorides, sulfuric acid, nitrous oxide, hydrogen chloride, and cadmium Bolden et al. [5].

The management of plastic waste in developing countries such as Nigeria is even more acute, where the infrastructures for collection, reuse, and recycling is often insufficient or lacking. For these countries, the development of effective plastic waste management strategies is imperative, and with such strategies geared towards addressing the technological, economic, environmental, and political challenges, Kehinde et al. [4].

Considering the enormous amount of construction work done annually and the quantity of waste produced each year, the concept of reusing and processing waste into raw materials in the construction industry is gaining traction among engineers, researchers, and government bodies. Past studies have tested the efficacy of different (Agro, Industrial, Mining, etc) waste as partial or full replacement of conventional construction materials. Results from such studies have shown great potentials. For example, Rice Husk (RH) is an abundantly available agricultural waste material in all rice-producing countries containing about 30%–50% of organic carbon Habeeb, and Mahmud [6]. When Rice Husk is burnt in the ambient atmosphere to any temperature within the range of 225–500 °C, Rice Husk Ash (RHA) is produced Kapur et al. [7]. The RHA has been researched as a partial replacement of cement in concrete with results showing it acted as a micro filler and enhancing cement paste pore structure Beagle [8]. Arabani et al. [9] studied the effects of RHA as an asphalt modifier on HMA using bitumen blends containing 5%, 10%, 15%, and 20% RHA modifier. The addition of RHA improved the rheological properties of bitumen, according to the findings. The MS, stiffness modulus, rutting strength, and fatigue performance of asphalt mixes were also improved by RHA modification. In an another study by Ewa et al. [10] the suitability of rice mill wastes in asphaltic concrete was reported. Quarry dust was partially and wholly replaced by rice husk and rice husk ash as filler up to 100% replacement levels. It was concluded that while, asphalt specimens with RH filler meets the requirement for binder course, samples with RHA filler met the requirement for both binder and waering courses.

One effective remedy to the problem of how to deal with plastic waste is to recycle it as an alternative road construction material since it can be used as a binder extender in asphalt binder Jamshidi and White [11]. Zoorob and Suparma [12] revealed that using recycled waste plastics materials mainly composed of Low-Density Polyethylene (LDPE) in

Figure 1. PET/PS blocked drains.

bituminous mixtures resulted in a significant enhancement of its stability i.e. approximately 2.5 times greater than the stability of the control mixtures and durability while decreasing in density. In addition, the outcomes of the study showed that the asphalt fatigue life of the modified mixtures was longer than the control Casey et al. [13] studied the potential of recycled polymer to modify binder. The results of the experiments showed that 4% of recycled High-Density Polyethylene (HDPE) in a pen grader binder can result in the most promising outcome and improve the properties of the binder.

Polystyrene is a type of plastic that has long been used in packaging. Chemical recycling of discarded polystyrene into the equivalent monomers or hydrocarbons has been used in a number of studies Sato et al. [14]. The process is inefficient, however, because the cost of hydrocarbons and monomers is minimal when compared to the cost of recycling Nassar et al. [15]. As a result, finding an effective way to recycle waste polystyrene is beneficial Imene et al. [16].

Mousa et al. [17] reported on the production of sustainable asphalt mixes using recycled Polystyrene with the objectives of studying the effects of polystyrene on properties of bitumen and to investigate the feasibility of using the polystyrene as an additive to asphalt pavements. While penetration and ductility decreased, viscosity and softening point increased. The binder met the safety specifications for flash and fire points. It was concluded that the PS-modified binder had the potential of performing under hot climate conditions and can be used for playgrounds, parking lots, sidewalk pavements. Polystyrene in disposable food pack was recycled by Murana et al. [18] as a modifier for Bitumen in Hot Mix Asphalt. DFP derived from home trash was added to the bitumen in percentages of 2%, 4%, 6%, 8%, and 10%. DFP modified bitumen had lower penetration, ductility, and specific gravity, while its softening point increased. According to the Marshal Stability data, the DFP treated bitumen improved the stability value. It is recommended that the DFP content of the Optimum Bitumen Content (OBC) be 6.7 percent by weight.

A huge amount of plastic has infiltrated the Nigerian technosphere, Babayemi et al. [19] with only about 12% of the waste ending up in the recycling stream. This critical waste and resource category requires long-term management. Nigeria as a developing nation is currently faced with the challenge of handling plastic waste disposal and management, see Figure 1. This current study seeks to evaluate the comparative properties of eco-friendly and sustainable

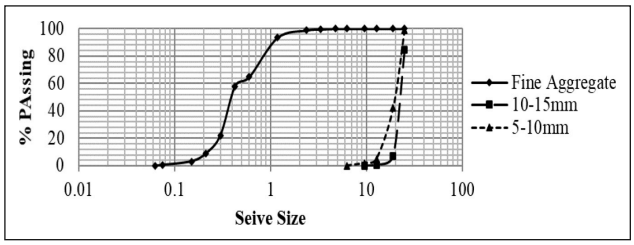

Figure 2. Particle Size Distribution curve of aggregate used.

asphalt having waste PET and PS as binder modifiifiers, rice husk ash as filler and de-silted sand (sediment sand blocking drain channels) as fine aggregate. Utilizing these waste will enhance cleaner engineering production of asphalt for road surfacing. The objectives of the study includes:

- To investigate the influence of waste PET and waste PS on the properties of modified binder.
- To investigate the influence of waste PET and waste PS on the properties of modified asphalt.
- Compare the influence of the modified-binder on asphalt properties.
- Determination of optimal PET and PS content on modified Binder

2. MATERIALS AND METHODS

2.1. Materials

Materials used in this study were bitumen grade 60 /70 penetration, waste plastic bottles (PET) and waste polystyrene (PS) as binder modifiers. Crushed granite with a size range of 5–15 mm was used as coarse aggregate, de-silted sand (sediment sand from gutters) was used as fine aggregate with a size range of 0–2 mm and Rice Husk Ash (ASH) as filler.

2.2. Methods

The aggregates were subjected to sieve analysis, specific gravity, and aggregate impact value (AIV) in accordance [20–22]. Figure 2 shows the particle size distribution curve of the aggregate while Table 1 is comparison of test results on aggregates with standards. The modified asphalt binders had partial replacement of bitumen with PET and PS at 5%, 10%, 15%, 20%, 25%, 30%, 35%, 40%, 45%, 50%. Penetration, viscosity, flash point, fire point, specific gravity, and ductility

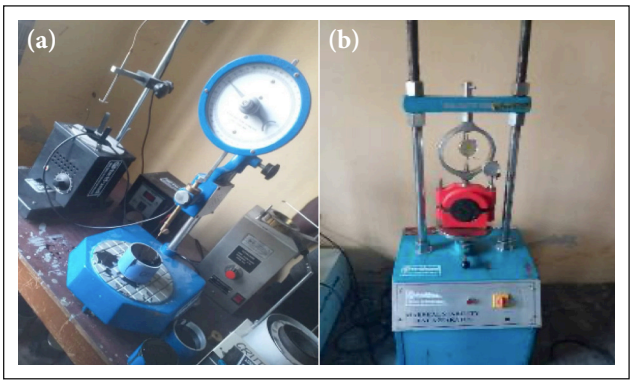

Figure 3. **(a, b)** Experimental set-ups.

tests were carried out on the bitumen and the modified binders in accordance [23–27], see Figure 3a for experimental set-up. In Table 2, the mix proportion for binder modification is presented, while Table 3 shows the bitumen characterization against Standards. The propotion for asphalt mix design is shown in Table 4. Asphalt samples were prepared in accordance with ASTM D6927-15 [28] and IRC: 111 [29]. To determine the optimal bitumen content, a Marshall Stability test using the set-up of Figure 3b, was performed for each sample. The flow, bulk density, air void, void in mineral aggregate (VMA), and void filled by bitumen (VFB) were measured and compared to Table 5's typical Marshall mix design criteria. Equation 1 was used to estimate the Rigidity Ratio (RR) or Marshall Quotient (MQ), which measures a mix's resistance to permanent deformations and rutting.

$$RR = \frac{Stability}{Flow} \qquad \left(\frac{KN}{mm^2}\right) \qquad \text{Eqn. 1}$$

3. RESULTS AND DISCUSSIONS

3.1. Modified Binder Properties

3.1.1. Penetration

The penetration behaviour of the modified binder is presented in Figure 4. The test result shows that the penetration values of the PET-modified binder increased up to 5% PET addition and thereafter, decreases as the polymer modifier

Table 1. Comparison of test results on aggregates with standards

Property	Limit	Result obtained	Code used	Code specification
AIR	%	14.7	BSEN 2620:2002	<30
Specific gravity (fine)	–	2.74	ASTM C128:2015	2.6–2.9
Specific gravity (coarse)	–	2.84	ASTM C128:2015	2.6–2.9
RHA	–	2.11	ASTM C136	–

Table 2. Mix proportions for asphalt binder modification

Bitumen	100	95	90	85	80	75	70	65	60	55	50
% PET	0	5	10	15	20	25	30	35	40	45	50
% PS	0	5	10	15	20	25	30	35	40	45	50

Table 3. Comparison of test results on pure bitumen with code specification

Test	Unit	Test method (ASTM)	Code specification for 60/70 penetration grade	Results obtained
Penetration@ 25 °C	mm	D5	60/70	69
Specific gravity@25 °C	–	D70	1.01–1.06	1.02
Flash and fire point	°C	D92	>250	262 and 285
Ductility@ 25 °C	cm	D113	>100	110
Viscosity@ 60 °C	Seconds	D4402	140–250	157

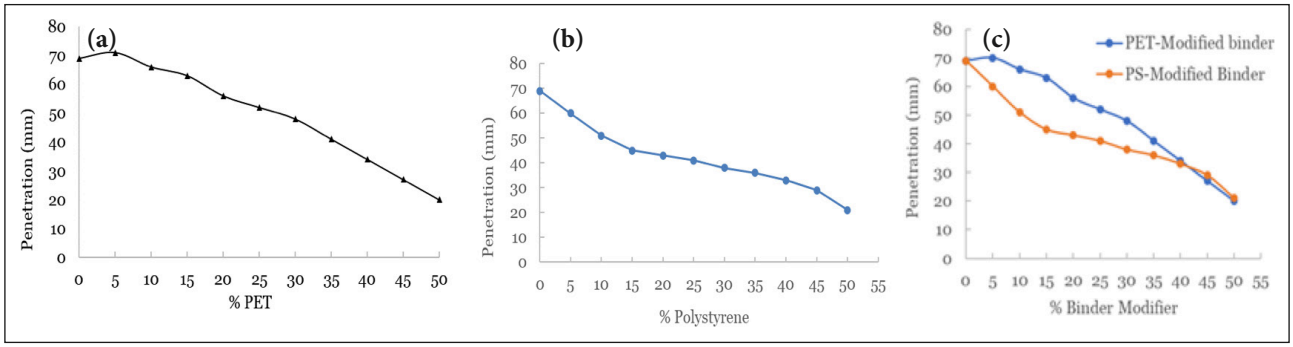

Figure 4. **(a)** Influence of PET on modified binder Penetration, **(b)** influence of PS on modified binder Penetration, **(c)** Comparative penetration curve.

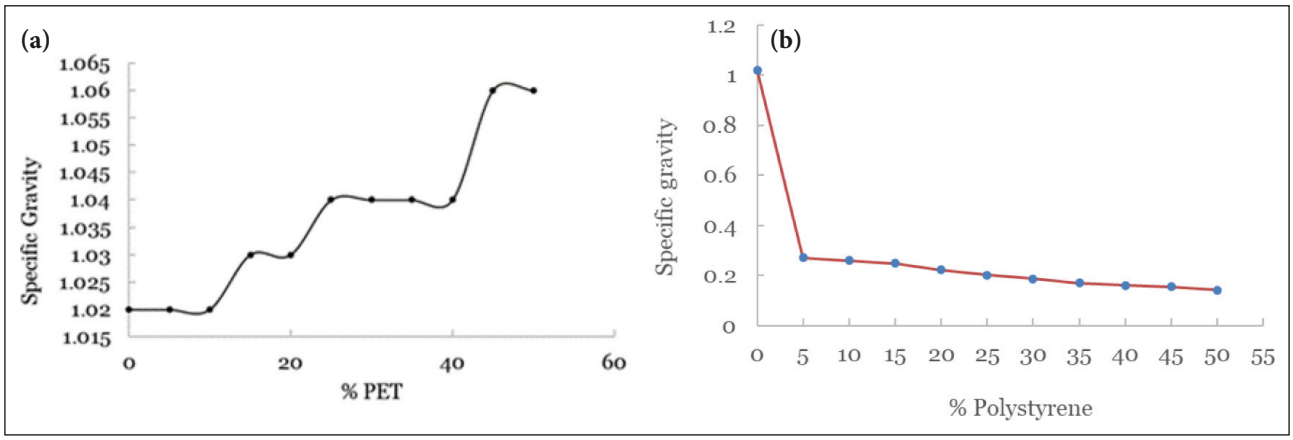

Figure 5. **(a)** Specific gravity of PET-Modified binder, **(b)** Specific gravity of PS-Modified binder.

increases. While the penetration of the PS-modified binder decreased with the increase in PS content as observed by Murana [18]. PET inclusion up to 15% gave acceptable penetration values in line with [23], while PS up to 5% gave acceptable value. It was observed that the addition of PET up to 5% makes the modified binder harder and more consistent which can lead to the improvement of rutting resistance of the mix, Esmaeil et al. [30] and Ramesh et al. [31]. From Figure 4c, PET-modified binder is stiffer than PS-modified binder within 0–40% binder addition, beyond this range, both modifiers behaved in similar ways. It is common for the consistency of modified asphalts to increase as a result of the inclusion of polymers, which implies a high resistance to deformation. This is most likely caused by swelling of maltenes (the oil fraction of bitumen) diffusing into the polymeric phase, as well as interactions between polar asphaltene molecules and polymer modifiers.

Table 4. Mix proportion used for asphalt

Type	Size in mm	% of constituents
Crushed sand	0–2 mm	59%
Crushed stone	5–10 mm	20%
Crushed stone	10–15 mm	10%
Filler	0–0.075 mm	5%
Bitumen	–	6%

3.1.2. Specific Gravity

The specific gravity of the PET-modified binder increases with the increase in the addition of the polymer as shown in Figure 5, while, the specific gravity of the PS-modified binder decreased with the inclusion of polystyrene Murana [18]. PS is a lighter weight waste compared to PET. Up to

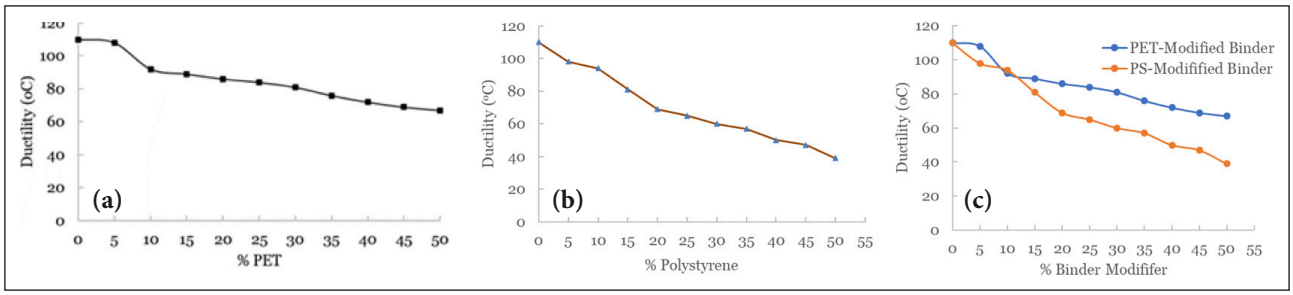

Figure 6. **(a)** Influence of PET on modified binder ductility **(b)** influence of PS on binder modified binder **(c)** Comparative ductility curve.

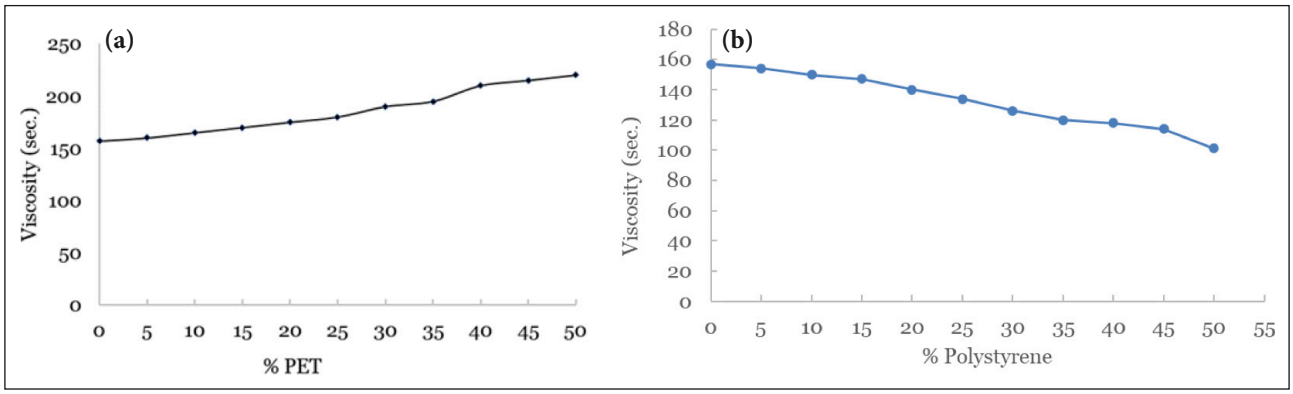

Figure 7. **(a)** Influence of PET on Viscosity **(b)** influence of PS on Viscosity.

Table 5. Typical Marshall mix design criteria [28]

Description	Base course		Binder course		Wearing course	
	Min.	Max.	Min.	Max.	Min.	Max.
Marshall specimens (ASTM D6927) No. of comp. Blows on each end of the specimen	75		75		75	
Stability (N)	2224		3336		6672	–
Flow (0.25 mm)	2	14	2	14	2	14
VMA (%)	13		14		15	–
Air voids (%)	3	8	3	8	4	6
VFB (%)	70		70		70	–

50% inclusion of PET gave acceptable values as required by [24]. Similar results were reported by Rahman et al. [32] and Akinleye et al. [33].

3.1.3. Ductility

Ductility is responsible for the internal cohesion of the binder. As seen in Figure 6, ductility decreased with the addition of the PET and PS. At 5% binder modification, PET-modified binder yielded acceptable ductility in line with [27] while PS-modified binder did not. Modified binder has reduced internal cohesion, resulting in lesser binder content and causing less ability for aggregates to adhere during asphalt mix. This mixture is suitable for usage in hotter climates, particularly in areas where temperature differentials are significant Akinleye et al. [33].

3.1.4. Viscosity

Figure 7 presents the influence of the PET on binder viscosity. The viscosity of the PET-modified binder increased as PET was added, indicating improvement in the adhesiveness of the modified binder. Up to 50% PET inclusion, viscosity values were within the specified limit in ASTM D4402 [26]. It can be concluded that PET-modified binder has higher workability than plain bitumen Akinleye et al [33]. On the other hand, the inclusion of polystyrene decreased viscosity as seen in Figure 5b. The optimal level of PS modification of binder is 20% while up to 50% PET addition, gave acceptable viscosity values as specified by [26].

3.1.5. Fire and Flash Point

The influence of polymer modification on the fire and flashpoints of the modified binder is shown in Fig-

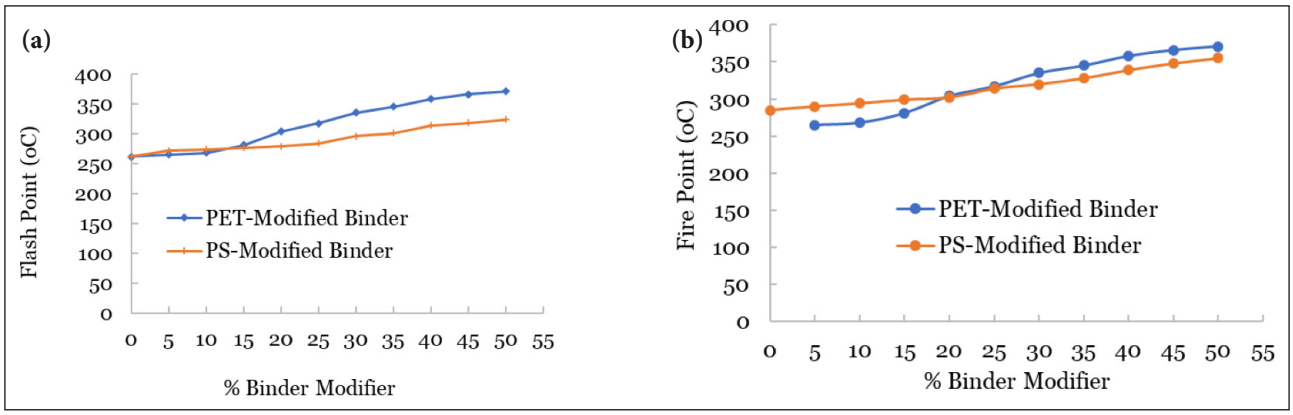

Figure 8. **(a)** Flash point, **(b)** fire point.

ure 8. Fire and flashpoints increased with the increased addition of both PET and PS with values failing within ASTM D 92 [25]. This implies a reduction in the risk of catching fire when the modified asphalt is being produced, with PET-modified binder having a better safety in terms of fire.

3.2. Influence of PET and PS on Asphalt Properties

3.2.1. Marshal Stability

As seen in Figure 9, the stability of the modified asphalt increased with percentage of the modifiers up to 20% optimal replacement level. The stabilities for PET and PS modified specimens at optimal modifier content were found to be 4525N and 6215N respectively. Beyond 20% inclusion of the modifiers, stability declined to 2238N and 3005N at 50% replacement level for PET and PS modified specimen respectively. While the stability value for PS-modified asphalt satisfied the requirement for wearing course (heavy traffic), PET-modified asphalt meet the requirement for binder course (medium traffic) [28]. The increased in stability of the modified asphalt mixture can be explained as a result of better adhesion development between asphalt binder and aggregate particles due to the addition of waste modifiers, Rasool et al. [34]. Due to the high rigidity of the modified PET and PS binder, the toughness and stability of the modified asphalt improved Jegatheesan et al. [35].This results in increased asphalt mixture strength, which helps to improve the asphalt mixture's stability.

3.2.2. Marshal Flow Values

The marshal flow value indicate asphalt deformation at the point when maximum load occurs. From Figure 10, the maximum flow value for both PET and PS modofied asphalt were 3.53 mm and 3.62 mm respectively, at 20% optimal modifier conetent. These values are within acceptabe flow values specified in [28]. Aliyu et al. [36] noted that a reduction in flow suggests that the polymer content has increased effects on the internal friction of the mix.

3.2.3. Bulk Density

Bulk density of the modified asphalt mixes increase with the addition of modifiers as seen in Figure 11. PET-

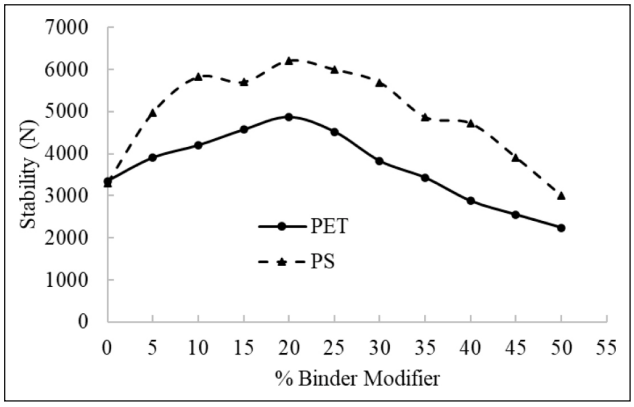

Figure 9. Stability of PET and PS modified asphalt.

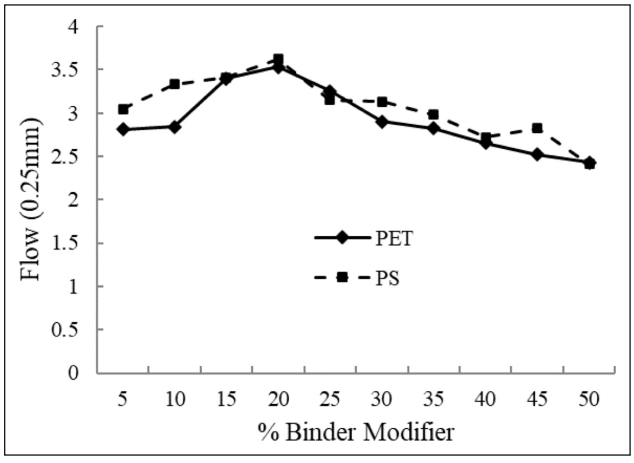

Figure 10. Inflence of modifiers on Marshal flow values.

modified asphalt increased in density from 2.205 g/cm^3 at 0% modifier content to 2.46 g/cm^3 at 20%. Bulk desmity of PS-modified asphalt increased from 2.205 g/cm^3 at 0% to 2.374 g/cm^3 at 15%.

3.2.4. Air Voids

The air void for the PET and PS modified asphalt decreased with increased in the modifier content (MC) as seen in Figure 12. At 50% modifier conetent, airvoid for PET and PS-modified mixes were found to be 3.15% and 2.45% repectively. The value for PET-modified asphalt

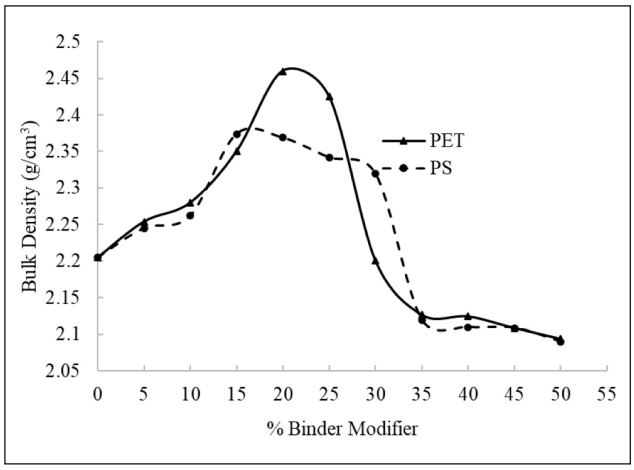

Figure 11. Inflence of modifiers on bulk density.

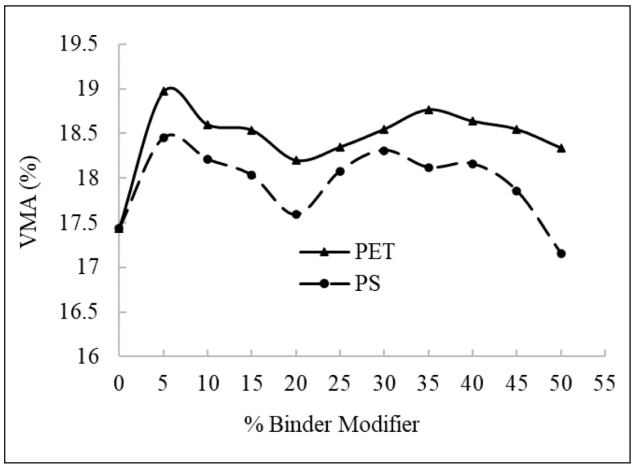

Figure 13. Inflence of modifiers on voids in mineral aggregate.

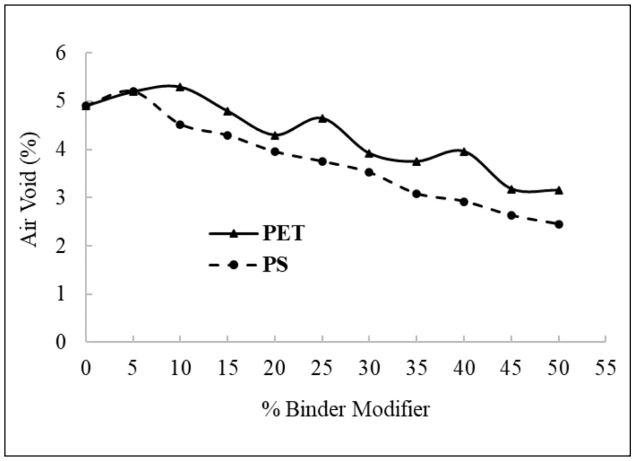

Figure 12. Inflence of modifiers on air voids.

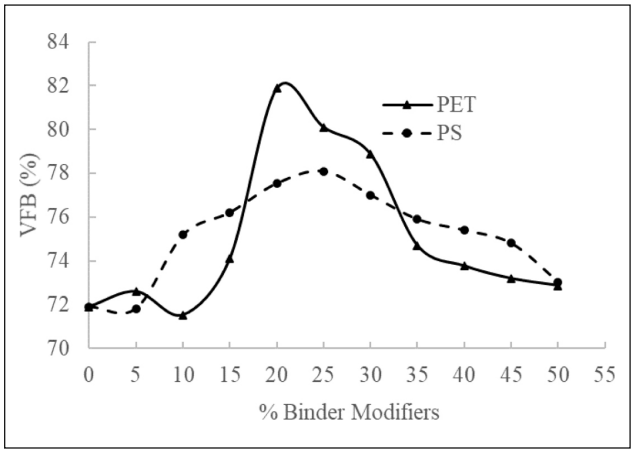

Figure 14. Inflence of modifiers on voids filled with binder.

is within the acceptable range for binder course while PS-modified asphalt did not meet the air void requirement at 50% replacement level. At 20% optimal modifier content, air void values were 4.3% and 3.95% for PET and PS modified asphalt respectively. These air void values are within acceptable range for binder and wearing course [28].

3.2.5. Voids in Mineral Aggregates (VMA)

In Figure 13, the influence of the modifiers on voids in mineral aggregate is presented. The amount of void space between the aggregate particles of compacted asphalt (VMA) increased first to maximum values at 10% OMC, then decreased sharply as the modifier content increased to 20% MC for both PET and PS samples. VMA values for both asphalt mixes satisfied the minimum requirements of 14% and 15% for binder and wearing courses respectively [28].

3.2.6. Voids Filled with Binder (VFB)

The result of VFB variation with PET and PS addition can be seen in Figure 14. The maximum VFB values obtained for PET and PS modified asphalt are 81.87% and 78.10% respectively both of which are greater than the minimum value of 70% recommended by [28].

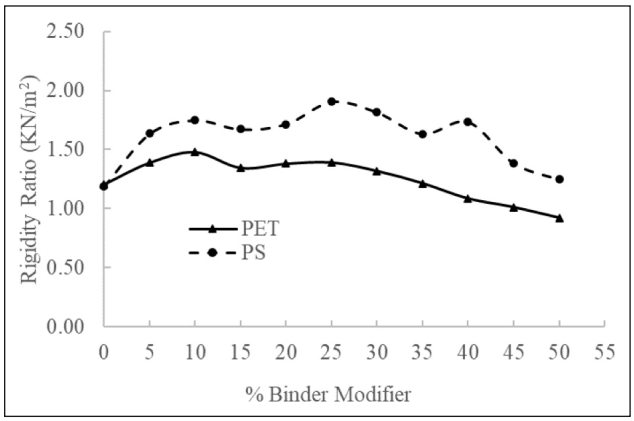

Figure 15. Influence of binder modificstion of rigity ratio.

3.2.7. Rigidity Ratio (RR)

Figure 15 depicts the mix's resistance to permanent deformations as evaluated by the Rigidity Ratio (RR) or Marshall quotient. The highest RR of 1.48 KN/m^2 for PET modified asphalt occurred at 10% MC while that of PS modified asphalt was 1.91 KN/m^2 at 25% MC. Rigidity ratio of PS modified asphalt is higher than PET modified asphalt. In service, RR values can be used to assess a material's resistance to shear stress, permanent deformation, and rutting Aliyu [36].

4. CONCLUSION

Waste management is a serious challenge in Nigeria and other developing countries. Plastic bottles and waste polystyrene being a major non-biodegradable waste. The modification of bituminous binder for asphalt purposes using waste plastic bottles (PET), waste Polystyrene and waste rice husk ash was studied. De-silted sand (sediment sand from gutters) was utilized as fine aggregate, reducing the menance of flood innblocked concrete channels. Waste rice husk ash served as asphalt filler. After comparing the results, the following conclusion was made:

1. Both polymers modified binders fell within acceptable ASTM Standards for use as asphalt paving materials. Waste plastic bottle inclusion up to 15% gave acceptable penetration values in line with ASTM Standard, while polystyrene up 5% gave acceptable value.
2. While PET increases the specific gravity of the modified binder, PS decreases the specific gravity of the modified binder. At 5% binder modification, PET-modified binder yielded acceptable ductility while PS-modified binder did not.
3. Viscosity increased with the PET modifier while it decreased with the PS modifier. The optimal level of PS modification of binder is 20% while up to 50% PET addition, gave acceptable results. PET-modified binder has a better safety in terms of fire due to higher flash/fire point temperatures.
4. Marshall Stability results showed an optimal of 20% PET modification was adequate for medium traffic surfaing with stability, flow, density, air void, void in mineral aggregates (VMA), and Void filled with binder (VFB) of 4875N, 3.53 mm, 2.460 g/cm^3, 3.30%, 18.20%, and 81.87% respectively.
5. For 10% PS modification content, the stability, flow, density, air void, void in mineral aggregates (VMA), and Void filled with binder (VFB) were found to be 6825N, 3.33 mm, 2.362 g/cm^3, 4.52%, 18.21%, and 75.18% respectively which was found to be adequate for heavy traffic surfacing.

ETHICS

There are no ethical issues with the publication of this manuscript.

DATA AVAILABILITY STATEMENT

The authors confirm that the data that supports the findings of this study are available within the article. Raw data that support the finding of this study are available from the corresponding author, upon reasonable request.

CONFLICT OF INTEREST

The authors declare that they have no conflict of interest.

FINANCIAL DISCLOSURE

The authors declared that this study has received no financial support.

USE OF AI FOR WRITING ASSISTANCE

Not declared.

PEER-REVIEW

Externally peer-reviewed.

REFERENCES

[1] Nchube, L. K., Ude, A. U., Ogunmuyiwa, E. N., Zulkifli, R., & Beas, I. N. (2021). An overview of plastic waste generation and management in food packaging industries. *Recycling, 6*, 12. [CrossRef]

[2] Babayemi, J. O., Nnorom, I. C., Osibanjo, O., Weber, R. (2019). Ensuring sustainability in plastics use in Africa: Consumption, waste generation, and projections. *Environ Sci Eur, 31*, 60. [CrossRef]

[3] Plastics Europe. (2021). Plastics – the Facts 2021. Plastics Europe Market Research Group (PEMRG) and Conversio Market & Strategy GmbH Estimated data. https://plasticseurope.org/knowledge-hub/plastics-the-facts-2021/

[4] Kehinde, O., Ramonu, O. J., Babaremu, K. O., & Justin, L. D. (2020). Plastic wastes: Environmental hazard and instrument for wealth creation in Nigeria. *Heliyon, 6*(10), e05131. [CrossRef]

[5] Bolden, J., Abu-Lebdeh, T., & Fini, E. (2013). Utilization of recycled and waste materials in various construction applications. *Am J Environ Sci, 9*, 14–24. [CrossRef]

[6] Habeeb, G., & Mahmud, H. (2010). Study on properties of rice husk ash and its use as cement replacement material. *Mat Res, 13*(2), 185–190. [CrossRef]

[7] Kapur, P. C., Singh, R., & Srinivasan, J. (1984). Tube-in-basket burner for rice husk. *Sādhanā, 7*(4), 291–300. [CrossRef]

[8] Beagle, E. C. (1978). Rice husk conversion to energy. Rome: FAO. *Agricultural Services Bulletin* No. 31.

[9] Arabani, M., & Tahami, S. A. (2017). Assessment of mechanical properties of rice husk ash modified asphalt mixture. *Constr Build Mater, 149*, 350–358. [CrossRef]

[10] Ewa, D. E., Ukpata, J. O., Ukam, G. S., & Ogar, A. I. (2020). Suitability of rice mill wastes in asphaltic concrete. *J Sci Eng Technol, 7*(1), 26–34.

[11] Jamshidi, A., & White, G. W. (2019). Evaluation of performance and challenges of use of waste materials in pavement construction: A critical review. *Appl Sci, 10*, 226. [CrossRef]

[12] Zoorob, S. E., & Suparma, L. B. (2000). Laboratory design and investigation of the properties of continuously graded asphalt concrete containing recycled plastics aggregate replacement (plastiphalt). *Cement Concrete Comp, 22*(4), 233–242. [CrossRef]

[13] Casey, D., McNally, C., Gibney, A. D., & Gilchrist, M. (2008). Development of a recycled polymer modified binder for use in stone mastic asphalt. *J Resour Conserv Recycl, 52*(10), 1167–1174. [CrossRef]

[14] Sato, Y., Kodera, Y., Goto, J., & Matsui, Y. (2002). Effect of polystyrene addition on the monomer recycling of phenol novolac. *Polym Degrad Stab, 78*(2), 315–322. [CrossRef]

[15] Nassar, I. M., Kabel, K. I., & Ibrahim, I. M. (2012). Evaluation of the effect of waste polystyrene on performance of asphalt binder. *ARPN J Sci Technol, 2*(10), 927–935.

[16] Imene, B., Sami, B., & Mohamed, B. (2007). A technique for purifying wastewater with polymeric flocculent produced from waste plastic. *Desalination, 204*, 198–203. [CrossRef]

[17] Mousa, B. B., Raed, A., Taisir, K., & Zaydoun, A. (2016). Production of sustainable asphalt mixes using recycled polystyrene. *Int J Appl Environ Sci, 11*(1), 183–192.

[18] Murana, A. A., Akilu, K., & Olowosulu, A. T. (2020). Use of expanded polystyrene from disposable food pack as a modifier for bitumen in hot mix asphalt. *Niger J Technol, 39*(4), 1021–1028. [CrossRef]

[19] Babayemi, J. O., Ogundiran, M. B., Weber, R., & Osibanjo, O. (2018). Initial inventory of plastics imports in Nigeria as a basis for more sustainable management policies. *J Health Pollut, 8*(18), 180601. [CrossRef]

[20] ASTM C136 / C136M-19. (2019). Standard test method for sieve analysis of fine and coarse aggregates. ASTM International, West Conshohocken, PA.

[21] ASTM C128-15. (2015). Standard test method for relative density (specific gravity) and absorption of fine aggregate. ASTM International, West Conshohocken, PA.

[22] ASTM D5874-16. (2016). Standard test methods for determination of the impact value (IV) of a soil. ASTM International, West Conshohocken, PA.

[23] ASTM D5. (2006). Standard test method for determining penetration grade of bituminous materials. American Society for Testing and Material (ASTM), Philadelphia, USA.

[24] ASTM D70. (2001). Standard test method for determining specific gravity of bituminous materials. American Society for Testing and Material (ASTM), Philadelphia, USA.

[25] ASTM D92. (2018). Standard test method for flash and fire points by Cleveland open cup tester. ASTM International, West Conshohocken, PA.

[26] ASTM D4402 / D4402M-15. (2015). Standard test method for viscosity determination of asphalt at elevated temperatures using a rotational viscometer. ASTM International, West Conshohocken, PA.

[27] ASTM D113. (2017). Standard test method for ductility of asphalt materials. ASTM International, West Conshohocken, PA.

[28] ASTM D6927-15. (2015). Standard test method for Marshall stability and flow of asphalt mixtures. ASTM International, West Conshohocken, PA.

[29] IRC:111-2009. Specifications for dense graded bituminous mixes. Indian Road Congress.

[30] Ahmadinia, E., Zargar, M., Karim, M. R., Abdelaziz, M., & Ahmadinia, E. (2012). Performance evaluation of utilization of waste polyethylene terephthalate (PET) in stone mastic asphalt. *Constr Build Mater, 36*, 984–989. [CrossRef]

[31] Ramesh, K. G., Bharani, S., & Sujith Kumar, R. S. (2017). Partial replacement of bitumen by waste plastic and polypropylene in road construction. *Int J Current Eng Sci Res, 4*(11), 57–64.

[32] Rahman, M. N., Ahmeduzzaman, M., Sobhan, M. A., & Ahmed, T. U. (2013). Performance evaluation of waste polyethylene and PVC on hot asphalt mixtures. *Am J Civ Eng Archit, 1*(5), 97–102. [CrossRef]

[33] Akinleye, M. T., Jimoh, Y. A., & Laoye, A. A. (2020). Performance characteristics models of properties of dissolved plastic bottles modified bitumen for hot mix asphalt. *Glob J Eng Technol Adv, 2020, 3*(2), 19–27. [CrossRef]

[34] Rasool, D. A., Fahad, B. M., & Awaeed, K. M. (2015). Utilization of waste plastic water bottle as a modifier for asphalt mixture properties. https://www.iasj.net/iasj?func=fulltext&aId=9919

[35] Jegatheesan, N., Rengarasu, T. M., & Wasala Bandara, W. M. K. R. T. (2018). Effect of polyethylene terephthalate (PET) fibres as binder additive in hot mix asphalt concrete. Annual Sessions of IESL. The Institution of Engineers, Sri Lanka.

[36] Aliyu, A., Usman, J., Kaura, M., Ashiru, M., & Kingsley, I. (2015). Polyethylene from water sachet as a modifier in hot asphalt mixture. Department of Civil Engineering, Ahmadu Bello University, Zaria, Nigeria.

[37] Elmohr, A. I., Radwan, L. S., El Refaey, M., & Zakaria, M. (2018). Laboratory performance of stone matrix asphalt mixtures containing recycled asphalt pavements. *Life Sci J, 15*(8), 1–9.